Partial Discharge Ageing of Polymer Insulation under Combined AC and DC Stress at Elevated Temperatures

Thesis presented for the degree of

Doctor of Philosophy

in the

Department of Electronic & Electrical Engineering

University of Strathclyde

2017

Weijia Zhao, BEng (Hons)

Department of Electronic & Electrical Engineering

University of Strathclyde

Glasgow, U.K.

Declaration of Authorship

The thesis is the result of the author's original research. It has been composed by the author and has not been previously submitted for examination which has led to the award of a degree.

Signed:

Date:

Acknowledgements

I would like to give my first appreciation to my supervisors Dr W. H. Siew and Dr Martin J. Given, for their continued support and guidance throughout the course of this research. Thanks for their kindness to provide me with the opportunity to pursue a PhD degree in the University of Strathclyde and moreover always being supportive and patient in supervision of my study.

I would also like to acknowledge my host supervisors Prof Jinlinag He in Tsinghua University and Prof Qingmin Li in North China Electric Power University. Thanks for their kindness in providing the relevant equipment, allowing me to carry on my research and their supervision.

Special thanks to Dr Leung Tang and Dr John Liggat in the Department of Pure and Applied Chemistry, University of Strathclyde for showing me FTIR-ATR technology and analysing the results.

Many thanks to all colleagues in both Tsinghua University and North China Electric Power University for their kindness and assistance in my project. Thanks to Francis Cox for his kind support. Thanks to my colleagues in the High Voltage Technologies Group for providing a convivial working environment.

Finally, thanks to my family and relatives, especially my parents, who have always supported me in my study and everything I have done.

Abstract

Cable termination is the weakest part in any HV underground cable system, as defects may be left in the main insulation during the installation process. In HVDC systems, the converters produce the intended DC voltage for transmission but there may also be AC harmonics superimposed. The frequency of the AC harmonics could be in kHz range. The superimposed harmonics on the HVDC may have synergistic effects on cable insulation and may lead to further degradation in the cable insulation. In addition, for the sake of environmental protection, XLPE is no longer the suitable choice for underground cable insulation as it cannot be recycled. Thermoplastic material may be a candidate. There is little published information on the behaviour of thermoplastic materials under combined AC and DC voltages.

In thermoplastic materials, HDPE film and PP film were selected as the target material to study in this project. As the properties of HDPE are similar to those of XLPE, the data obtained from HDPE was regarded as a bench-mark. It was decided to use the thermo-electrical stress to age the samples. For thermal stress, 90°C was chosen as the aging temperature for HDPE, while 90°C and 110°C were chosen for PP. For the electrical stress, AC & DC combined voltage was used to age the samples. DC voltage was 6 kV. The superimposed frequency of AC voltage was 1 kHz, 1.5 kHz, 2 kHz and 2.5 kHz. The AC/DC voltage ratio is from 10%, 30% and 50%. In this project, the effect of frequency and voltage ratio on HDPE and PP degradation under superimposed stresses was studied using the following approaches: Equivalent Phase Resolved Partial Discharge (PRPD) plots, Fourier Transform Infrared - Attenuated Total Reflection (FTIR-ATR) Spectroscopy and Dielectric Spectroscopy (DS) measurements were carried out. The performance of HDPE and PP were compared.

List of Acronyms

AC	Alternating Current
AC%	Voltage Ratio
aPP	Atactic Polypropylene
CI	Carbonyl Index
CT	Current Transformer
DC	Direct Current
DS	Dielectric Spectroscopy
DSC	Differential Scanning Calorimetry
ET	Electrical Treeing
FTIR-ATR	Fourier Transform Infrared Spectroscopy - Attenuated Total Reflection
GIS	Gas Insulated Substations
HDPE	High-density Polyethylene
HFCT	High Frequency Current Transformer
HVDC	High Voltage Direct Current
iPP	Isotactic Polypropylene
KBS	Knowledge-Based System
LDPE	Low-density Polyethylene
NO	Nitric Oxide

PD	Partial Discharge
PDIV	Partial Discharge Inception Voltage
PE	Polyethylene
PES	Poly(Ether Sulphone)
PET	Poly(Ethylene Terephthalate)
PP	Polypropylene
PRPD	Phase Resolved Partial Discharge
sPP	Syndiotactic Polypropylene
UHF	Ultra-High Frequency
WT	Water Treeing
XLPE	Cross-linked Polyethylene

List of Figures

List of Tables

List of Publications

Journal Papers:

1. Hongxin Ji, Chengrong Li, Zhikai Pang, Guoming Ma, Xiwang Cui, Weijia Zhao and Jian Wang, “Influence of Tip Corona of Free Particle on PD Patterns in GIS”, IEEE Transactions on Dielectrics and Electrical Insulation, Vol.24, Issue 1, pp.259-267, 2017.
2. Weijia Zhao, Wah Hoon Siew, Martin J Given, Qingmin Li and Jinliang He, “Assessment of HDPE Aged under DC Voltage Combined with AC Harmonic Stresses of Various Frequencies”, IEEE Transactions on Dielectrics and Electrical Insulation, Vol.24, Issue 2, pp.1189-1196, 2017.

Conference Papers:

3. Weijia Zhao, Wah Hoon Siew and Martin J Given, 2013, The Electrical Performance of Thermoplastic Polymers When Used As Insulation in Cables, 48th International Universities' Power Engineering Conference (UPEC), pp:1-4
4. Weijia Zhao, Wah Hoon Siew, Martin J Given, Qingmin Li, Jinliang He and Edward Corr, “Thermoplastic Materials Aging under Various Stresses”, IEEE Electr. Insul. Conf., Montreal, Canada, June 2016.
5. Weijia Zhao, Wah Hoon Siew, Martin J Given, Qingmin Li, Jinliang He and Edward Corr, “Aging Behaviour of Polypropylene under Various Voltage Stresses”, IEEE Conference on Electrical Insulation and Dielectric Phenomenon (CEIDP), Toronto, Canada, Oct 2016.

Contents

1. Introduction

1.1 Project Background

1.1.1 HVDC Power System with AC Components

With the steadily increasing demand for electric energy, the high voltage direct current (HVDC) transmission system will be enlarged to satisfy the demand of electric energy. HVDC transmission lines can be classified as over-head lines and underground/submarine cable systems. The latter one is much more suitable for somewhere like cities and underwater where over-head lines are hard to install.

In addition, as environmental protection and sustainable development issues attract more and more attention nowadays, more power generation methods are being used. In history, coal was the major source for thermal power generation in the electrical energy industry. When coal is burned, CO_2 will be created which is not environmental friendly. With the decrease of coal resources and increase of CO_2 emission, it is required to produce electric power in sustainable ways. Sun, wind and hydro are sustainable sources, which could be used as the substitutes for coal. Among the renewable sources, wind energy attracts more and more attention [1-3]. As these sources are remote from users, HVDC transmission provides an efficient way to transmit power from such remote sources with converters rectifying the power at the sending end of transmission line and invertors converting the DC power to AC power for consumers at the receiving end.

The converter is a key component in HVDC system, which is used to rectify alternating voltages. Classic HVDC systems are based on Line Commutated Converters (LCC), while modern HVDC systems use voltage source converters (VSC) [4-5].

However, as the switching of the power electronics in the converters cannot be

ignored, the output DC voltage of both converter types is normally superimposed with transients [6-8]. The switching frequency can go to the kHz range [6-7].

1.1.2 Cable Termination and Its Problems

As cable terminations are the weakest part in cable systems, it is of interest to investigate the performance of insulation in cable terminations. Cable termination is a kind of cable accessory, which is installed at the end of the cable to connect with the power system or other electrical facilities. Although most reports are for high voltage alternating current (HVAC) terminations, the manufacture process of DC cable termination is similar to that of AC cable termination. Therefore, the reports can still be used to predict potential problems in DC systems. Cable terminations need to be sealed and insulated very well. The manufacturers normally provide the components, including premoulded rubber stress cone, stress cone stopper, clamping ring and stress cone compression kit. The components are assembled with the end of cable and become a cable termination.

Typical cable consists of core, main insulation, semi-conducting layer and shield layer. Air gap may occur on the main insulation as shown in Figure 1.1.

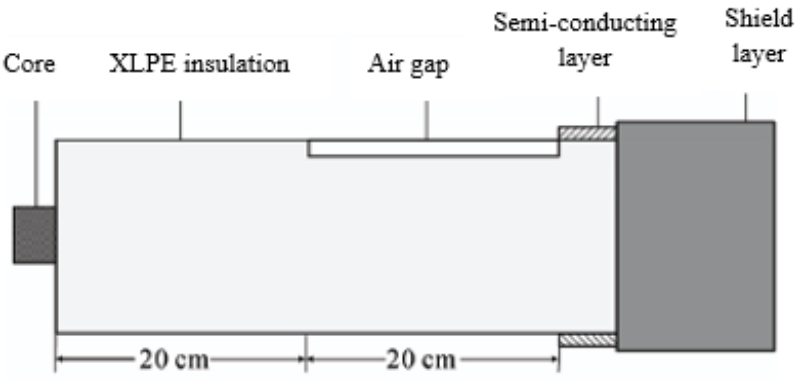

Figure 1.1. Air-gap on insulation in cable termination [9].

For underground/subsea cable termination installation, the semi-conducting layer and

shield layer of the cable need to be removed. The way to strip both layers is ring-cutting around the outer semi-conductive layer truncation, then cutting the semiconducting layer along the axial and finally strip away the cut part. However, as it is hard to control the depth of the tool, damage can occur to the cable insulation. The ring-cutting defect and slitting defect remain on the outer surface of the cable insulation and introduce air filled gaps between the cable surface and the joint assembly. When electric strength is high, partial discharge may occur in the airgaps present in these areas of defects and may cause breakdown eventually. As manufacturing processes have improved the number of defects in the bulk of the cable insulation is reducing. Therefore, the ring-cutting defects and slitting defects are the most significant cause of partial discharge sites in cable insulation [10-11].

In many cases, although cable terminations would pass an on-site voltage test, after some time, failures occurred. In most cases, these failures were caused by ring-cutting defects and slitting defects around the semiconducting layer truncation. Examples of defects and damage are shown in Figure 1.2 and Figure 1.3.

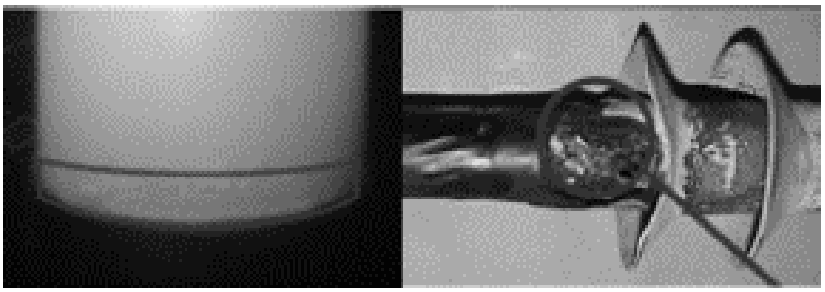

Figure 1.2. Ring-cutting defect and the corresponding breakdown phenomenon [12].

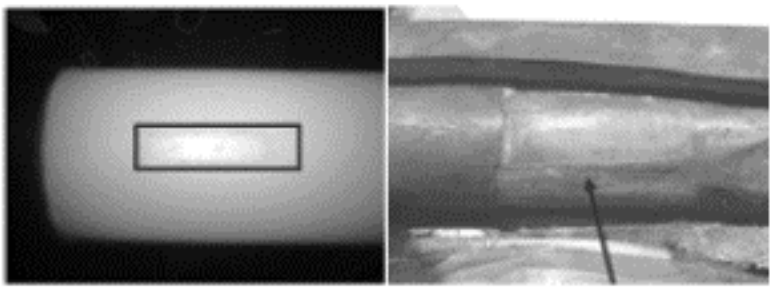

Figure 1.3. Slitting defect and the corresponding breakdown phenomenon [12].

In addition to these defects in cable terminations, the IEEE C-19W group [13] believes that in extruded-insulation cable system, typical insulation defects will including cavity defects and other air gaps

- inside cable main insulation
- on the interface between insulation and the semiconducting layers
- on the interface between cable main body and terminations

When electric field is high, partial discharge (PD) will happen in the air-gaps. In solid dielectrics, PD could cause irreversible mechanical, thermal and chemical degradation of the insulation material. PD event could make insulation material deteriorate, lead to decline of insulation properties and to electrical breakdown [14].

Water treeing may occur under superimposed voltages [7]. Therefore, the superimposed voltages generated by converters may further age the main insulation in termination. It is of interest to have an investigation about the impact of superimposed voltages on the properties of cable insulation.

The impact of DC stresses and the combined DC and periodic transients associated with converters on partial discharge activity and the subsequent aging of the insulation is of interest due to the increasing use of HVDC transmission systems. This project investigates possible effects by considering discharges similar to those expected in an air gap on the surface of cable insulation. The discharges are driven by a combination of DC and sinusoidal voltages which will give an indication of the possible impact of converter waveforms on cable terminations.

1.2 The Objectives of the Project

To investigate the changes in aging in polymer insulation caused by partial discharges in an airgap stressed with combinations of DC and AC voltages.

To achieve this aim:

- To investigate the effects of differing magnitudes and frequency of the superimposed AC stress on the performance of the polymer. This has been performed at elevated temperatures to accelerate the aging of the polymer to allow experimental tests to be performed in a reasonable timescale.
- To monitor the partial discharge activity during the aging of the samples and to derive parameters such as the cumulative energy per second associated with the discharge activity.
- To develop a novel parameter apparent cumulative energy per second ($E_{CA}^{\cdot}$) which will be linked to the apparent cumulative energy which is based on the real energy delivered to quantify partial discharge.
- To assess the changes in the material properties through the use of FTIR-ATR which has allowed values of the Carbonyl Index to be derived. In addition changes in the conductivity and susceptibility as a result of aging have been derived using dielectric spectroscopy.
- To study the correlation of Carbonyl Index, conductivity and susceptibility with $E_{CA}^{\cdot}$ and to analyse the aging process.
- To investigate and compare the aging behaviour of two polymers: high-density polyethylene (HDPE) which is similar in its properties to XLPE a standard cable insulation and polypropylene (PP) which is an alternative insulation with lower environmental impact.

The results obtained allow comparisons to be made between the behaviour of the polymers under different stress combinations and a possible explanation for the behaviour of the aging process has been developed.

1.3 Structure of the Thesis

The subsequent chapters of the thesis are as follow:

Chapter 2 is the literature review chapter.

- Section 2.1 summarizes the stresses which cause degradation in cable insulation and introduces relevant aging mechanisms and models.
- Section 2.2 introduces the fundamentals of dielectric spectroscopy (DS) measurement.
- Section 2.3 introduces the fundamentals of Fourier transform infrared spectroscopy-attenuated total reflection (FTIR-ATR) measurement.
- Section 2.4 introduces the fundamentals of phase resolved partial discharge (PRPD) measurement and reviews relevant experimental data and methods from the literature. This helps to build a basic understanding for this project.

Chapter 3 describes the project design process.

- Section 3.1 shows the criteria used for material selection and the introduction of the two materials investigated in this project.
- Section 3.2 introduces the thermo-electrical aging system. In this section, information of the aging electrodes, temperature selection, AC & DC combined voltages production, the voltage ratio selection, superimposed frequency selection and aging duration selection. The set-up of the thermo-electrical aging system is also introduced. The phase resolved partial discharge (PRPD) measurement set-up and the method to collect PD data are described in detail.
- Section 3.3 describes the Fourier transform infrared spectroscopy - attenuated total reflection (FTIR-ATR) measurement equipment.
- Section 3.4 describes the dielectric spectroscopy (DS) measurement equipment and the way to undertake this measurement.

Chapter 4 reports the results of HDPE samples aged at 90°C with various superimposed frequencies and voltage ratios.

- Section 4.1 describes the PRPD results. Mean with standard deviation of PD voltage, number of discharges and PD apparent cumulative energy per second are

three indexes used to demonstrate the PRPD results. How these three indexes change with superimposed frequency and voltage ratio is demonstrated.

- Section 4.2 describes a proposed mechanism for the partial discharge generation.
- Section 4.3 describes the FTIR-ATR results and discusses how the Carbonyl Index (CI) of HDPE samples change with superimposed frequency and voltage ratio.
- Section 4.4 describes the DS results. Values for the conductivity and a dielectric susceptibility index are calculated and their variation with frequency and voltage ratio are summarized.
- Section 4.5 summarizes the relationship of PD apparent cumulative energy per second, Carbonyl Index, conductivity and dielectric susceptibility index.

Chapter 5 reports the results of PP samples aged at 90°C using the same superimposed frequencies and voltage ratios as for the HDPE.

- Section 5.1 describes the PRPD results. The data is analysed in the same way as in section 4.1 to derive the mean with standard deviation of PD voltage, number of discharges and PD apparent cumulative energy per second for the different aging conditions.
- Section 5.2 describes the FTIR-ATR results. As in section 4.3 this data is used to derive the behaviour of CI as a function of the aging conditions.
- Section 5.3 describes the DS results with derivation of the conductivity and susceptibility indexes for the various aging conditions in the same way as in section 4.4.
- Section 5.4 summarizes the results in Section 5.1- Section 5.3.

Chapter 6 reports the results of PP samples aged at 110°C using the same superimposed frequencies and voltage ratios as in Chapters 4 and 5.

- Section 6.1 describes the PRPD results. The data is analysed in the same way as in section 4.1 and 5.1 to derive the mean with standard deviation of PD voltage,

number of discharges and PD apparent cumulative energy per second for the different ageing conditions.

- Section 6.2 describes the FTIR-ATR results. As in section 4.3 and 5.2 this data is used to derive the behaviour of CI as a function of the aging conditions.
- Section 6.3 describes the DS results, with derivation of the conductivity and susceptibility indexes for the various aging conditions in the same way as in section 4.4.
- Section 6.4 summarizes the results in Section 6.1- Section 6.3.

Chapter 7 is a discussion chapter. In this section, the results in Chapter 4 to Chapter 6 are discussed and comparisons are made between the behaviours of HDPE at 90°C, PP at 90°C and PP at 110°C.

- Section 7.1 examines how apparent cumulative energy per second ($\dot{E}_{CA}$), changes with superimposed frequency and voltage ratio. The temperature effect on $\dot{E}_{CA}$ is also discussed.
- Section 7.2 summarizes conductivity (σ) changes with superimposed frequency and voltage ratio. The temperature effect on σ is also discussed.
- Section 7.3 summarizes dielectric susceptibility index (χI) and number of carbonyl group ($N_{1(C=O)}$) change with superimposed frequency and voltage ratio.
- Section 7.4 summarizes Carbonyl Index (CI) change with superimposed frequency and voltage ratio. The relationship between CI and is $N_{1(C=O)}$ is also discussed.
- Section 7.5 compares measured indices change with apparent cumulative energy per second of each material according to the data in Section 7.1-7.4.

Chapter 8 shows the achievement of this project in detail, draws conclusions and makes suggestions for future work in this area.

1.4 References

[1] N. M. Kirby, M. J. Luckett, L. Xu and W. Siepmann, “HVDC TRANSMISSION FOR LARGE OFFSHORE WINDFARMS”, IEEE AC-DC Power Transmission Conference, pp.162-168, 2001.

[2] P Bresesti, W L. Kling, R L. Hendriks and R Vailati, “HVDC Connection of Offshore Wind Farms to the Transmission System”, IEEE Transactions on Energy Conversion, Vol.22, pp.37–43, 2007.

[3] L Xu, L Yao and C Sasse, “Grid Integration of Large DFIG-Based Wind Farms Using VSC Transmission”, IEEE Transactions on Power Systems, Vol.22, pp.976-984, 2007.

[4] C H Chien and R W. G. Bucknall, “Analysis of Harmonics in Subsea Power Transmission Cables Used in VSC–HVDC Transmission Systems Operating Under Steady-State Conditions”, IEEE Transactions on Power Delivery, Vol.22, pp.2489-2497, 2007.

[5] C Guo, Y Zhang, A M. Gole and C Zhao, “Analysis of Dual-Infeed HVDC with LCC–HVDC and VSC–HVDC”, IEEE Transactions on Power Delivery, Vol.27, pp.1529-1537, 2012.

[6] L Ming, F Sahlen, S Haled, G Brosig and L Palmqvis, “Impacts of High-frequency Voltage on Cable-terminations with Resistive Stress grading”, IEEE Solid Dielectrics Conference, Vol.1, pp.300–303, 2004.

[7] H H. Sæternes, J Aakervik and S Hvidsten, “Water Treeing in XLPE Insulation at a Combined DC and High Frequency AC Stress”, IEEE Electrical Insulation Conference, pp.494-498, 2013.

[8] Frank Mauseth, Martin Amundsen and Hallvard Faremo, “Water Tree Growth of Wet XLPE Cables Stressed with DC and High Frequency AC Voltage Superimposed”, IEEE Electrical Insulation (ISEI) Conference, pp.266–269, 2012.

[9] Wan Li, Zhou Kai, Li Xutao and Wu Ke, 2014, “Toward Understanding Development Mechanism of Partial Discharge in Air Gap Defects in Cable Termination by Analysis of Electric Field Characteristics”, High Voltage Engineering, Vol.40, No.1, pp.3709-3716. Chinese version.

[10] W. Vahlstrom, “Strategies for field testing medium voltage cables”, IEEE Electrical Insulation Magazine, Vol.25, pp.1–17, 2009.

[11] H. E. Orton, “Diagnostic testing of in-situ power cables—An overview,” IEEE/PES Transmission and Distribution Conference and Exhibition, Vol.2, pp. 1420–1425, 2002.

[12] Zhou Kai, Li Xutao, Huang Huayong, Wei Changming and Yang Ke, “Analysis of partial discharge characteristics for installing cutting defects in cable terminations”, Power System Protection and Control, Vol.41, No.10, pp.104-110.

[13] Liao Yanqun, Hui Baojun, Xia Rong and Xu Yang, “Partial Discharge Characteristics Analysis of Typical Defects for 110 kV Cable and Joint”, Insulating Materials, Issue 47, no.5, pp. 60-67, 2014. Chinese version.

[14] T. Tanaka, "Internal partial discharge and material degradation", IEEE Transactions on Electrical Insulation, Vol.EI-21, Issue 6, pp.899-905, 1986.

2. Literature Review

This project required knowledge of engineering and chemistry. This chapter will introduce some background information involved in this project. The experimental data for this project is shown in Chapter 4-6 in detail. The results will be discussed in Chapter 7.

In Section 2.1, the stresses which cause degradation in cable insulation are summarized and relevant aging mechanisms and models will be introduced.

In Section 2.2, the fundamentals of DS measurement are introduced.

In Section 2.3, the fundamentals of FTIR-ATR measurement are introduced.

In Section 2.4, the fundamentals of PRPD measurement are introduced. Relevant experimental data and methods from the literature are reviewed.

Section 2.5 is a summary.

This helps to build a basic understanding for this project.

2.1 Stresses Faced by Cable Insulation and Their Models

The life of high voltage cable systems are highly dependent on the life of the main insulation. In this section, stresses faced by cable insulation and the aging mechanisms will be summarized.

2.1.1 Aging Stresses

After a period of operation, the stresses discussed below will lead to degradation in the cable insulation. On the macro-scale, degradation of dielectric materials leads to: insulation resistance reduction; surface cracking; hardness increase; dielectric loss increase and insulation breakdown. On the micro-scale, degradation of dielectric materials occurs as electric trees or water trees [1]. The mechanism of insulation degradation is a complicated topic and it varies with different external factors. According to different external factors, the aging stress can be classified into electrical aging, thermal aging, mechanical aging and environmental aging (including factors such as moisture, contamination and radiation). The mechanism of each aging stress is summarized as follows:

a) **Electrical aging:** Electrical stress is the main cause for insulation degradation. During the manufacturing process or installation process, defects will occur on a cable is main insulation [2]. As the insulation is exposed to high external electrical strength conditions for a long time, partial discharges can occur in the defect areas, leading to partial degradation and finally developed breakdown to destroy the dielectric properties of the insulation [3, 4].

b) **Thermal aging:** When operating, cables can be in a high temperature condition. High external temperatures, the internal dielectric load current and short-circuit currents could lead to heating of the cable insulation and temperature increases [5]. Thermal aging is a kind of chemical aging that

makes chemical properties of material change in high temperature conditions. Under high temperature conditions, chemical reactions such as oxidation and thermal decomposition, would take place and degrade the material. In chemical reactions, temperature is an important factor which affects the reaction rate. A chemical reaction usually occurs more rapidly as the temperature increases. In particular, oxidation reactions degrade the material and affect the electrical and mechanical performance of the insulation. Degradation also leads to change of mechanical properties, such as elongation at break and tensile strength, of the material [6].

c) **Mechanical aging:** Micro-defects [7] may occur in cable insulation during manufacture, installation and operation. If the insulation is exposed to mechanical stress for a long time, micro-defects could be enlarged leading to breakdown and damage to the insulation.

d) **Environmental aging:** Environmental aging includes factors such as moisture [8], contamination [9] and irradiation [10]. During the installation process and in service, moisture and other contaminants can be introduced to the cable and affect cable performance. The presence of moisture and other contaminants could affect dielectric losses and capacitance of the material, lead to electrical tracking, water treeing and corrode elements of the cable. Cables may also be used in irradiated environments: the radiation may initiate chemical processes that degrade the insulation.

All aging stresses mentioned above, plus the aging mechanisms and effects produced, are summarized in Table 2.1.

Table 2.1. Summary of aging causes and effects [11].

Aging factor	Aging mechanisms	Effects
Thermal		
• High temperature • Temperature cycling	• Chemical reaction • Incompatibility of materials • Thermal expansion • Diffusion • Anneal lock-in mechanical stresses • Melting / flow of insulation	• Hardening, softening, loss of mechanical strength, embrittlement • Increased tan delta • Shrinkage, loss of adhesion, separation, delamination at interfaces • Swelling • Loss of liquids, gases • Conductor penetration • Rotation of cable • Formation of soft spots, wrinkles • Increased migration of components
Low temperature	• Cracking • Thermal contraction	• Shrinkage, loss of adhesion, separation, delamination at interfaces • Loss / ingress of liquids, gases • Movement of joints, terminations
Electrical		
Voltage, ac, dc, impulse	• Partial discharge (PD) • Electrical treeing (ET) • Water treeing (WT) • Dielectric losses and capacitance • Charge injection • Intrinsic breakdown	• Erosion of insulation: ET • PD • Increased losses and ET • Increased temperature, thermal aging, thermal runaway • Immediate failure
Current	• Overheating	• Increased temperature, thermal aging, thermal runaway
Mechanical		
Tensile, compressive, shear stresses, fatigue, cyclic bending, vibration	• Yielding of materials • Cracking • Rupture	• Mechanical rupture • Loss of adhesion, sepatation, delamination at interfaces • Loss / ingress of liquids, gases
Environmental		
Water / humidity Liquids / gases Contamination	• Dielectric losses and capacitance • Electrical tracking • Water treeing • Corrosion	• Increased temperature, thermal aging, thermal runaway • Increased losses and ET • Flashover
Radiation	• Increased chemical reaction rate	• Hardening, softening, loss of mechanical strength, embrittlement

2.1.2 Aging Models

As thermo-electrical aging was applied in this project, the aging models summarized mainly focus on electrical aging, thermal aging and combined aging.

2.1.2.1Electrical Aging Model

Electrical stress is a major cause of insulation degradation. For aging due to electrical stressing only, the widely used empirical models are the inverse power model and exponential model [12].

Inverse power model is shown as follows:

$$L = kE^{-n} \tag{2.1}$$

where, L is the lifetime of a material, E is the electrical field strength, k and n are constants that are determined experimentally. The inverse power model is in agreement with the behaviour expected from Weibull statistics [13]. A problem with the power model, as shown in equation 2.1, is that the expected lifetime approaches infinity as the field approaches zero [12]. To address this problem the equation can be modified into the form:

$$L(E) = \begin{cases} L_0, & E < E_0 \\ L_0\left(\frac{E}{E_0}\right), & E \geq E_0 \end{cases}$$

Where it is assumed that the electric field has no impact on the lifetime of the material for electric fields below a threshold E_0 and L_0 is the lifetime under these conditions.

Exponential model is shown as follows:

$$L = a \times exp(-bE) \tag{2.2}$$

where, L is the lifetime of a material, E is the electrical field strength, a and b are constants that are determined experimentally.

2.1.2.2Thermal Aging Model

As lifetime of most electrical equipment depends on thermal properties of insulation [14], thermal stress is another important factor that affects electrical insulation life. The well-known Arrhenius equation [15] describes chemical reaction rate changes with temperature, which is shown as follows:

$$R_t = Aexp\left(-\frac{B}{T}\right) \tag{2.3}$$

Where, R_t is thermal aging rate, A and B are constants (B is the ratio of the activation energy to Boltzman's constant), T is the absolute temperature.

Dakin adopted this relationship to describe the thermal aging of materials. According to Dakin's theory, by assuming that the lifetime is inversely related to the aging rate, the thermal life model [16] was established as below:

$$L = \frac{1}{A}\exp\left(\frac{B}{T}\right) \tag{2.4}$$

Where, L is the lifetime of the insulation at absolute temperature T, the value of A can be established if the lifetime of the insulation L_0 is known at ambient temperature T_0. Equation 2.4 can be rewritten as:

$$\frac{1}{A} = L_0 \exp\left(-\frac{B}{T_0}\right) \tag{2.5}$$

Substituting the value of *1/A* into equation 2.4 leads to the expression:

$$L_T = L_0 \exp\left(-\frac{B}{T_0}\right)\exp\left(\frac{B}{T}\right) \tag{2.6}$$

Which can be rewritten in the form:

$$L_T = L_0 \exp\left(-B\Delta\left(\frac{1}{T}\right)\right) \tag{2.7}$$

Where:

$$\Delta\left(\frac{1}{T}\right)=\frac{1}{T_0}-\frac{1}{T}$$

Plots of the log of lifetime against $\Delta(1/T)$ allows the value of the constant *B* to be determined.

2.1.2.3Thermo-electrical Aging Model

The investigation of thermo-electrical aging of materials can be traced to 1948. Dakin proposed that degradation rate would be affected by thermal activation when partial discharge took place [16]. P. Cygan et al. [17] reviewed single factor aging models and thermo-electrical multifactor aging models. The basis of the competing theories of Simoni, Ramu, Fallou, Crine and Montinari are presented in appendix A.

2.2 Dielectric Spectroscopy Measurement

2.2.1 Permittivity and Dissipation Factor

Real permittivity (also called dielectric constant) and dissipation factor [18-19] are two essential factors to evaluate the dielectric properties of material. When a dielectric layer is placed within a parallel-plate capacitor, the current *I* as a result of an AC sinusoid voltage *U* with angular frequency ω applied across the capacitor is:

$$\boldsymbol{I}=j\omega\varepsilon^{*}C_0\boldsymbol{U} \tag{2.8}$$

Where, ε^{*} is the complex permittivity of the dielectric material $\varepsilon^{*}=\varepsilon'-j\varepsilon''$, C_0 is the capacitance when a vacuum exists between the parallel-plates of the capacitor. The equivalent circuit of the dielectric material and the relevant phase diagram can be seen in Figure 2.1.

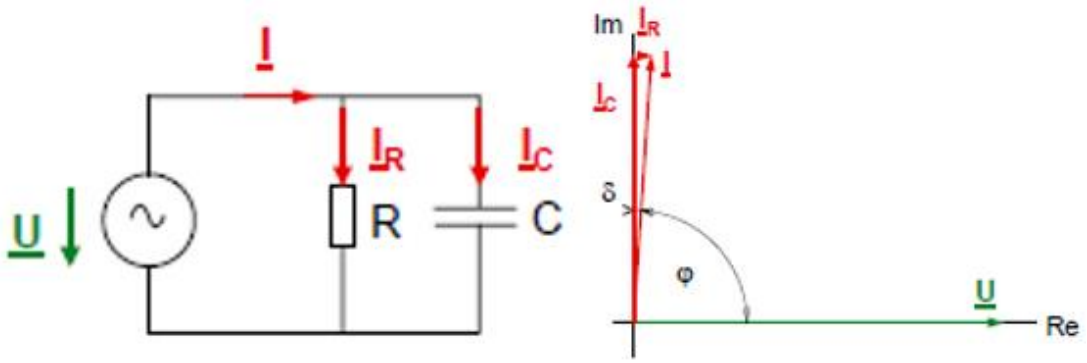

(a) (b)

Figure 2.1. (a) Circuit model for dielectric material; (b) The relative vector diagram [20].

Assume that voltage $\boldsymbol{U}$ is in the real axis (x axis) in Figure 2.1(b) and has no component in the imaginary axis (y axis). The current $\boldsymbol{I}$ could be described as having real axis component $\omega\varepsilon''C_0\boldsymbol{U}$ and imaginary axis component $j\omega\varepsilon'C_0\boldsymbol{U}$. Equation (2.9) could be expanded as below:

$$\boldsymbol{I}= j\omega\varepsilon'C_0\boldsymbol{U}+ \omega\varepsilon''C_0\boldsymbol{U}=j\omega(\varepsilon'-j\varepsilon'')\ C_0\boldsymbol{U} \tag{2.9}$$

Which shows that the definition of the complex permittivity written below is consistent:

$$\varepsilon^*=\varepsilon'-j\varepsilon'' \tag{2.10}$$

where, ε' is the real permittivity representing the capacitive polarization of the material and ε'' is the imaginary permittivity representing loss processes as a result of conductivity and polarization losses. $\varepsilon''=\sigma/\omega$ where σ is the conductivity. The tangent of dielectric loss angle $tan\delta$ (also called dissipation factor) can be written as [21]:

$$tan\delta = \frac{\varepsilon''}{\varepsilon'} \tag{2.11}$$

Complex permittivity and dissipation factor vary with the external frequency because each polymer polarization process corresponds to a certain frequency range. Different types of polarization will be introduced and summarized in detail in the Section 2.2.2.

2.2.2 Types of Polarization

When an external AC voltage applied, the polarization process of polymer may occur. Polarization is the process when charge redistributes within a material under the influence of an external electric field. The polarization acts to reduce the internal field within the material and leads either to changes in the voltage across the material or a flow of current in the external circuit if a constant voltage is applied across the system. As the polymer polarization is not an instantaneous process the change in polarization will not appear simultaneously with the shift of external voltage. This gives rise to a relaxation phenomenon. Dielectric relaxation will oppose polarization and create power losses. Therefore, dielectric polarization and relaxation is a combined process. This complex dielectric properties can be seen in the dielectric spectroscopy spectrum.

Dielectric polarization can be classified into electronic polarization, ionic polarization, dipolar polarization and space charge polarization [22-25]. The different kinds of polarizations and their behaviour with frequency as shown in Figure 2.2.

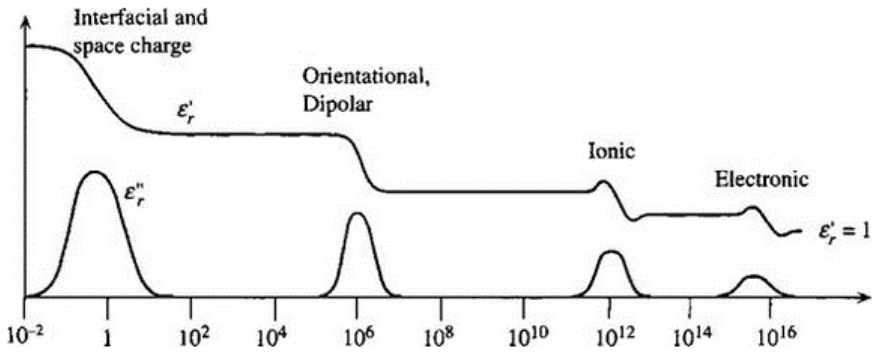

Figure 2.2. Real and imaginary part of permittivity varies with frequency [26].

Details are summarized as follows:

- **Electronic polarization**: In the atoms of the dielectric materials, the centre of electron cloud distorts from the nucleus when an external voltage is applied. This process is called electronic polarization. As electronic polarization can quickly

respond to the shift of an applied field, it just needs about 10^{-15} s to establish. On dielectric spectrum, electronic polarization occurs in the ultraviolet frequency range (around 10^{15} Hz [27]).

- **Ionic polarization**: This mechanism occurs in ionic crystals and occurs due to relative displacements of the positive and negative ions as a result of the applied field. The displacement of mobile ions creates a dipole moment and therefore a polarisation in the system. Ions exist in polymers but in normal conditions their concentration is low and their behaviour is more often associated with space charge polarisation. However, ionic polarisation is also used to describe the behaviour of functional polar groups within a molecule, where a dipole moment exists across a bond. Application of the applied electric field causes changes in the lengths of such bonds and leads to a net polarisation in the system. Ionic polarization needs about 10^{-13} s to establish. In a dielectric spectrum, ionic polarization occurs in the 10^{9} to 10^{13} Hz frequency range and is associated with infrared spectroscopy.
- **Orientation polarization**: Under external electric stress, at lower frequencies polar groups can rotate around the backbone of the molecule or change the molecular orientation. The polarization caused by diversion of molecular chains, side groups and dipole moments is called orientation polarization. As a polymer structure is complex and the motion of the dipoles can be impeded by adjacent polymer molecules, this polarization needs about 10^{-10}-10^{-2} s to establish. Orientation polarization occurs in the low frequency area (about 10^{3} to 10^{8} Hz).
- **Space charge polarization**: In non-uniform polymers, distribution of free electrons changes with external voltage so that space charge collects close to both electrodes [28]. In addition, the migration of any ions present, through hopping processes, can contribute to this process. This polarization needs a long time to establish. It occurs in the very low frequency range (about 10^{-3} to 10^{2} Hz).

In a certain frequency area, when relaxation occurs, the dielectric constant decreases as the frequency increases. It is also found that the dielectric loss increases. As the frequency increases, the polarization process cannot respond to the shift of the external electric field and hence, the degree of polarization and therefore ε' decreases. As the net change in polarization is decreasing the relaxation makes less contribution to energy loss. Therefore, energy dissipation reduces. The process can be demonstrated as a peak in loss spectrum. Dielectric spectroscopy in the range of (10^{-2}-10^{4} Hz) can provide information about changes in the number of dipolar groups present in the system from changes in the value of ε'. If loss peaks are present, information about changes in the molecular and crystalline structure can be obtained from shifts in the position of loss peaks.

2.3 Fourier Transform Infrared Spectroscopy - Attenuated Total Reflection (FTIR-ATR) Measurement

FTIR provides information about the chemical structure of a polymer and allows the identification of chemical bonds presents. Although it is not possible to directly find out the complete molecular structure of the polymer from FTIR, changes in the concentrations of groups attached to polymer molecules can be determined which provide insights to the chemical reactions occurring in a molecule.

An FTIR-ATR spectrum provides information from the surface of the sample rather than the bulk. As the degradation process is expected to be on the surface of the sample in this project, FTIR-ATR is a good tool to analyse changes in the chemical structures.

2.3.1 Fundamental

When preforming FTIR-ATR measurement, the sample is in close contact with the ATR crystal. This crystal should be of a relatively higher refractive index compared to the sample. When the IR beam is directed into the crystal, total internal reflection will take place as incident angle θ is larger than the critical angle θ_c, the reflection can be obtained. The critical angle is defined in equation 2.12 [29]:

$$\theta_c = \sin^{-1}\left(\frac{n_2}{n_1}\right) \tag{2.12}$$

Where, θc is the critical angle, n_1 is the refractive index of the crystal and n_2 is the refractive index of the sample.

The ATR phenomenon is shown graphically for a single reflection ATR in Figure 2.3.

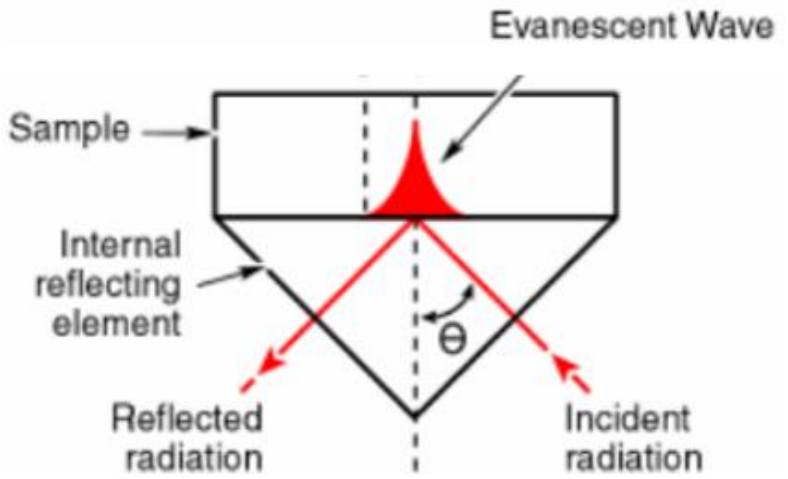

Figure 2.3. Graphical representation of a signal reflection ATR [30].

As shown in Figure 2.3, when reflection occurred inside the crystal, an evanescent wave is created and penetrated into sample to a certain depth. The evanescent wave occurs due to the constructive interference of the H fields associated with the incident and reflected E fields and must exist to insure continuity in the Maxwell equations at the boundary. The evanescent wave decays exponentially within the material due to the requirements of energy conservation. The depth of penetration is wavelength

dependent and normally is in the range of about 0.5 microns to about 5 microns, which will be much smaller than the whole depth of the sample. Part of the evanescent wave will be absorbed by the sample so that the reflected IR beam is attenuated. The attenuated IR beam passes back to the detector and the system will generate the IR spectrum. The depth of penetration (d_p) is given by equation (2.13) [31],

$$d_p = \frac{\lambda}{2\pi\sqrt{n_1^2 \sin^2\theta - n_2^2}} \tag{2.13}$$

Where, d_p is the penetration depth, α is the angle of incidence of the IR beam relative to a perpendicular from the surface of the crystal, λ is the wavelength of the light, n_1 is refractive index of the crystal and n_2 is the refractive index of the sample.

2.3.2 IR Spectrum

The infrared spectrum covers a wide wavelength range (0.78~1000 μm). It is common to use wavenumber rather than wavelength to describe the IR spectrum. Wavenumber v has a reciprocal relationship with wavelength λ, as shown in equation (2.14):

$$v=10000/\lambda \tag{2.14}$$

where, v unit in cm^{-1}, λ unit in μm.

The whole spectrum could be divided into three regions:

- near-infrared region (13000~4000 cm^{-1})
- mid-infrared region (4000~400 cm^{-1})
- far-infrared region (400~10 cm^{-1})

The IR region typically used for FTIR-ATR is the mid-infrared. The mid-infrared range can be divided into two regions: the 4000~1300 cm^{-1} region and the 1300~400 cm^{-1} region. Strong and sparse absorption peaks appear in the first region. The peaks are generated by stretching vibration in the molecular structure. The peaks in this region are helpful to identify molecular groups in materials. The second region is called fingerprint region as materials have a unique spectrum in this area. In this

region, although peaks are weak, intensive and hard to distinguish, they are good for determining small differences in molecular structures in different materials. Therefore, a spectrum is useful for distinguishing between similar compounds.

Details about wavenumber range and corresponding function groups are shown in Appendix B [32].

2.4 Phase Resolved Partial Discharge (PRPD) Measurement

2.4.1 Partial Discharge

Partial discharge (PD) was defined by IEC 60270 [33] as a "*localized electrical discharge that only partially bridges the insulation between conductors and which can or cannot occur adjacent to a conductor*".

2.4.1.1 Classifications of Partial Discharge

Partial discharge includes a wide group of discharge types [34-36]:

- corona discharge
- surface discharge
- internal discharge
- electrical trees

The different types of discharge are schematically presented in Figure 2.4.

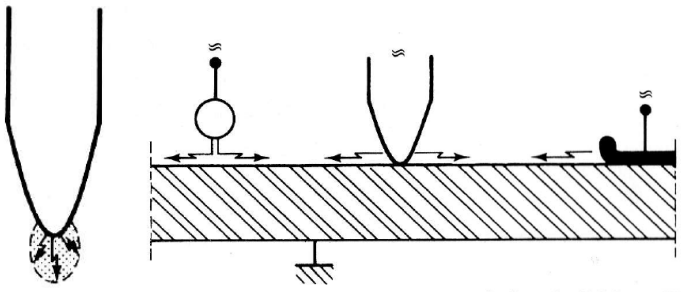

(a) Corona discharge (b) Surface discharge

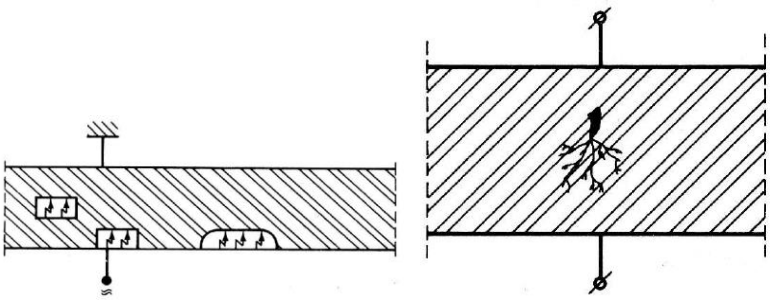

(c) Internal discharge (d) Electrical trees

Figure 2.4. Types of partial discharges [37].

1) Corona discharges [38-41]

In electrical equipment or systems, an electric field could be enhanced due to sharp points, rough surfaces or small radii of metal conductors. The local electric field near these defects may be 10 times higher than the average [42]. The higher local electric field can encourage transient gas ionization and cause streamer discharges that do not completely cross the gap to another conductor or terminate on a dielectric surface (Dielectric Barrier Discharge). This kind of discharge is called corona discharge Figure 2.4(a). Corona discharges appear in gaseous dielectrics.

2) Surface discharges

Surface discharge [43-46] occurs along the interfaces of two dielectrics, Figure 2.4(b), where the electric field component parallel with the interface is high. The interfaces could be the interface of a solid and a liquid or the interface of a solid and a gas. For polymer insulation, surface discharges may encourage chemical reactions and therefore lead to deterioration of the electrical and mechanical properties of the surface. Surface discharges can take place at cable terminations. Stages of PD induced damage at the insulator surface are shown in Figure 2.5.

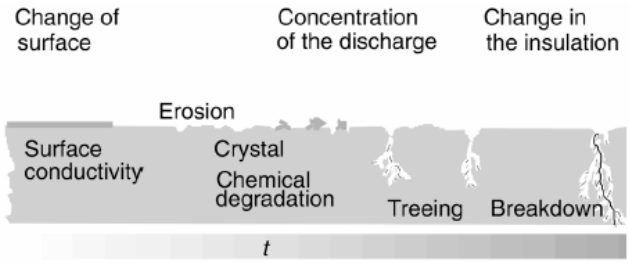

Figure 2.5. Stages of PD induced damage at the insulator surface [47].

3) Internal discharge [48]

For insulation materials, no matter how good the manufacturing process is, cavities or voids cannot be avoided within the insulation or at boundaries between solid dielectrics [49] (Figure 2.4(c)). The cavities or voids are commonly filled with mediums with lower electric strength (e.g. gas or liquid). Under high electrical field, discharges occur within these cavities due to a combination of dielectric mismatch enhancing the local field and reduced breakdown strength compared to the solid insulation and may initiate a breakdown eventually [50].

4) Electrical trees

Electrical treeing [51-52] could be regarded as a special kind of internal discharge. Electrical treeing originates from defects in a polymeric insulation or from high field regions on the conductor. The treeing process causes the development of channels within the insulation with a branching structure. The diameter of these channels are normally of the order of μm. PD activity occurs within the gas filled channels and will contribute to the further development of the channel. When a channel traverses the dielectric between the conductors, the dielectric strength is severely reduced and a breakdown will rapidly occur in the insulation system.

2.4.1.2 Effects of Partial Discharge

PD events can cause deterioration of insulation material, leading to a decline of insulation properties and result in electrical breakdown [53]. In HV cables and equipment, PD events damage the insulation and may cause a total breakdown in the electric facilities. PD activity is often accompanied by emission of sound, light, heat and causes chemical reactions. The energy realised by the PD results in [54-57]:

- The emission of electromagnetic radiation in the form of: radio waves, light (U.V. and visible) and heat.
- Acoustic emission in the audio and ultrasonic regions.
- The production of gases, such as ozone and nitrous oxides.

PD normally causes insulation damage in the following ways:

- High energy electron or ions
- Thermal effects
- Interactions with ozone and reactive gas species
- UV radiation from the discharges
- Mechanical effect

For each of the above, details are explained in the following:

- High energy electrons or ions: The charged particles can be the electrons injected from a conductor or the electrons and ions produced during the development of the PD. These charged particles are accelerated by the local field and thermal processes and obtain high energy. When high energy electrons or ions hit the surface of the material [58-59], the molecular chains may be broken and the molecular structure may be damaged.
- Thermal effect: When a PD occurs, it will lead to local heating and high temperatures [60]. These high temperature could cause thermal cracking or chemical decomposition of the polymer. High temperature not only causes thermal cracking, but also causes cracking caused by oxidation. The increase in

the temperature causes an increase of conductivity and energy loss of the polymer. These mechanism can cause polymer failure eventually.

- Ozone and reactive gas interactions [61]: PD could generate excited molecules or secondary active products (such as O, O_2^+ and O_2^-). These new products can react with the polymer surface and cause damage and erosion. The polymer may be affected by erosion more than high energy charged particles or thermal factors. The short lived, active oxygen species mainly react with surface of the polymer. Secondary products such as ozone (O_3) and nitric oxide (NO) could react with PE to create carbonyl compounds or nitro compounds. O_3 can react with air and moisture to produce compound such as nitric acid and nitrous acid, which not only erode polymer but can also erode the metal material.
- UV radiation from the discharges: PD could generate UV radiation. The bond strength for a C-C bond, typical for a polymer backbone is 3.59eV. UV photons with a frequency higher than 0.8 PHz have an energy greater than this. Therefore if a polymer molecule absorbs one of these photons this can result in a C-C bond breaking. This will affect the insulation properties.
- Mechanical effect: The PD leads to an increase in the temperature of the gas in its local region. This can lead to an increase in pressure or the generation of acoustic waves. These lead to an increased and changing mechanical stress on the polymer which can lead to fatigue cracking. The presence of these cracks can lead to new sites for the initiation of PD activity.

All of the mechanisms above can contribute to damage of the surface which may lead to, pits appearing on the surface. With time and repeated activity the depth of these pits increases, leading to eventual insulation breakdown [62] as a result of partial discharge activity at the surface of the sample.

The five main damage mechanisms may occur simultaneously but vary with material and with working conditions. Sometimes, one mechanism is the main factor. High

energy electrons or ions would be the main factor to degrade a polymer under high electric field and larger air gap conditions. Thermal effects would be the main factor for a polymer with higher dissipation loss, lower heat resistance or operating under higher temperature. Ozone interaction would be the main factor under contamination condition.

2.4.1.3 Mechanisms of Partial Discharge

PD mechanisms can be classified into three categories:

- Townsend discharge
- Streamer discharge
- Pitting

1) Townsend discharge

The Townsend discharge occurs within a short-gap and happens when the following condition is met:

- The product of the size of the cavity times the pressure in the cavity exceed the Paschen's curve for the gas within the cavity.

An example of a Paschen's curve for air is shown in Figure 2.6.

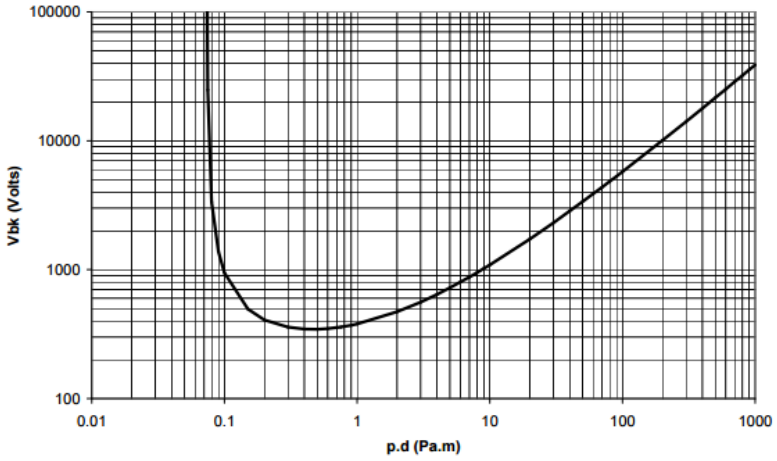

Figure 2.6. Paschen's curve [63].

The Townsend breakdown mechanism requires one or more free electrons [64] to appear in the gap between electrodes. The electron is accelerated by the external electrical field and collides with the air atoms. If the electron gains sufficient energy between collisions, new electrons and positive ions will be generated through the collision. These new electrons also get energy from the external electric field and collide to produce more charged particles. Through this way, the number of electrons grows exponentially creating an electron avalanche. As the mass of an electron is less than that of an ion, electrons move faster than ions in electrical field. In addition, the positive ions move in the opposite direction to the electrons when they reach the negative electrode, they can have sufficient energy to cause the release of more electrons from this electrode triggering further avalanches and causing the discharge to become self-sustaining. Negative ions may also be present in the system due to attachment. If attachment is occurring the electron population will be reduced and the rate of ionization will decrease.

The Townsend discharge includes the following forms: rapid and slow rise time spark-type pulses, true pulseless glows [65] or pseudo-glow discharges [66-67] which are all cathode emission sustained discharges. The rise time of these pulses can be as long as several tens of nanoseconds and their duration can last several hundreds of nanoseconds [58].

2) Streamer discharge

The streamer discharges occur in long gaps. They do not depend on secondary electron cathode emission, but depend on photoionization in the gas. If the avalanche triggered by the presence of a free electron grows sufficiently large (~10^8 electrons) significant charge separation occurs between the rapidly moving electrons and the much slower ions. This space charge field results in high electric fields in the region in front of the negative head of the avalanche and behind the slow moving ion trace. These high field regions can lead to the formation of new avalanches ahead of and behind the original avalanche. As fast moving electrons in the avalanches encounter

the positive ion traces recombination occurs, producing photons with sufficient energy to cause further free electrons in the gas. The streamer discharge therefore involves an ionization wave propagation in these high field regions. The presence of space charge fields have an important role in the corona and spark discharge in non-uniform field gaps. Streamer discharges are commonly of shorter duration than Townsend discharges; the streamer discharge pulse length can vary from 1 ns to 10 ns [68].

3) Pitting Produced by Discharges [68]

When partial discharges occur in a cavity, pitting of the wall may occur under AC voltage. During these discharges, chemical reactions occur and by-products are produced. After a long period of discharging, the concentration of these by-products is sufficiently large that they form a conductive layer of crystals at the cavity wall. When these crystals are formed they have sharp edges, resulting in field enhancement at the sharp edges of the crystals. At these edges, due to the field enhancement, discharges occur far earlier than in other locations in the material. The discharges take place in smaller space and have a low magnitude in combination with a relative high repetition rate. The literature suggests [69-70] that these discharges are occurring through a glow or a pseudo-glow discharge mechanism. Due to the low magnitude (0.2pC) and the high repetition rate discharges associated with pitting are much harder to measure.

2.4.2 PRPD Measurement

PD analysis has been widely used in electric equipment insulation diagnosis [71].
PD measurement can be dated to 1936, when Arman and Starr [72] applied resonance circuits with narrow-band amplifiers to detect PD in dielectric material. Tanaka and Okamote [73] recorded PD data by the first sophisticated computer based system. The PD data recorded by the digital systems were helpful in distinguishing different discharge sources. The measurement of PD in gas, liquid and solid showed that a few

parameters could be used to describe different discharges. The IR experience provided basic understanding for future investigations and diagnosis of PD in insulation [74-91].

2.4.2.1PD Characteristics (AC Stress)

As until recently, most of the cables in power systems operate under AC conditions, research about partial discharge are mainly under AC stress [33, 92-104]. The traditional PD detection method was according to Standard IEC60270.

The PD measurement system recommended by IEC 60270 is shown in Figure 2.7. In Figure 2.7, T_r is the HV test transformer, Z_n is the noise blocking filter, C_a is virtual test object capacitance, C_k is the coupling capacitor, Z_m is the measuring impedance as part of the coupling device and M_i is the PD measuring instrument. Z_n is to remove electromagnetic noise from the HV side of T_r. C_k is in series with Z_m.

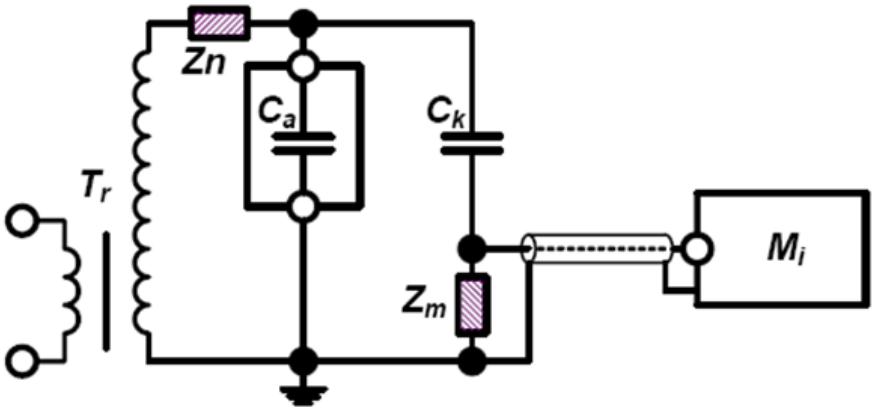

Figure 2.7. PD measurement circuit [33].

The PD measurement circuit in this project is shown in Section 3.2.5.

The phase-resolved distributions of three discharge types (Streamer-like. Townsend-like and Pitting) of cavity within a PE sample can be shown in Figure 2.8-2.10. In each figure, x-axis is the phase-angle ϕ (90°, 180°, 270° and 360° are mentioned), y-axis (from top to the bottom) are the maximum discharge magnitude H_{qmax}, the average discharge magnitude H_{qn} and the number of discharges per phase window H_n.

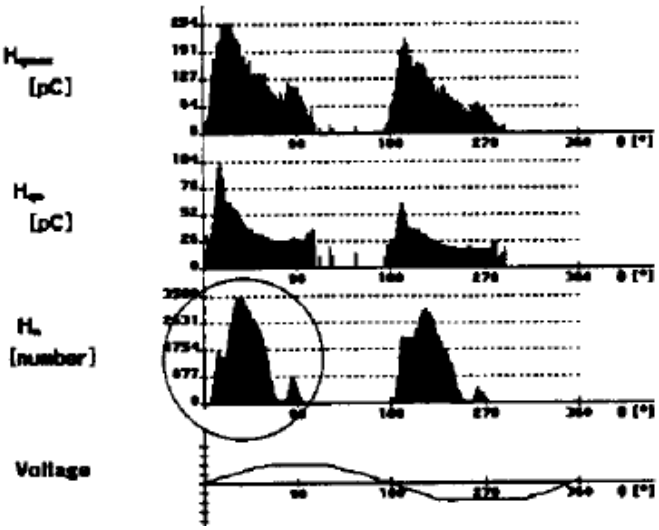

Figure 2.8. Phase-resolved distributions as observed by detection of Streamer-like discharges in a cavity in PE [92].

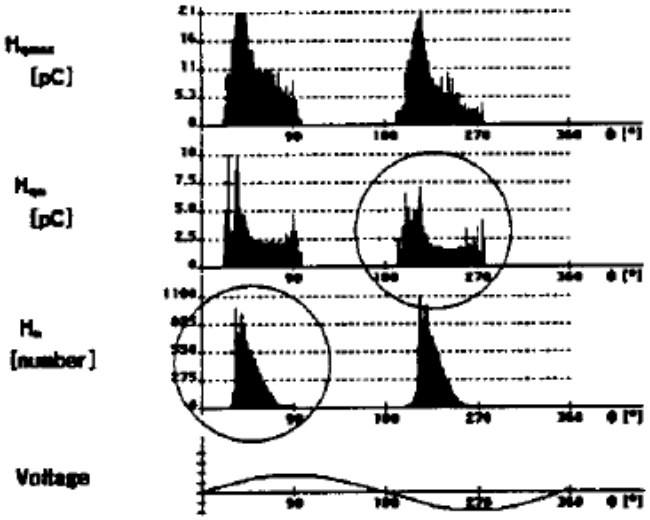

Figure 2.9. Phase-resolved distributions as observed by detection of Townsend-like discharges in a cavity in PE [92].

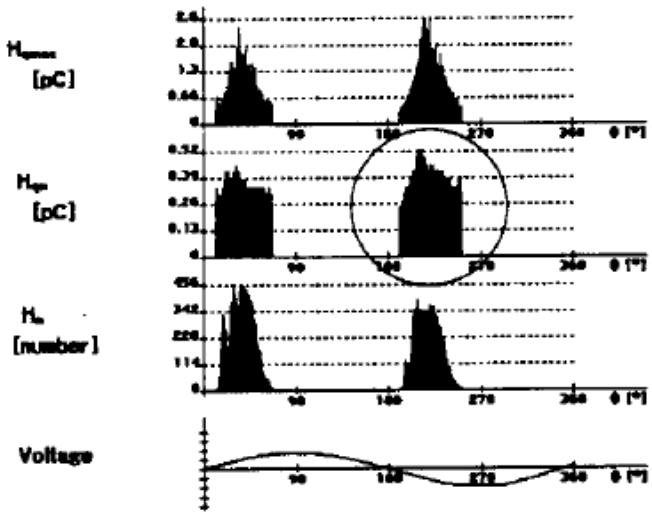

Figure 2.10. Phase-resolved distributions as observed by detection of Pitting discharges in a cavity in PE [92].

It can be seen that the shapes of the distributions of H_{qmax}, H_{qn} H_n with phase are significantly different for the Townsend, streamer and pitting discharges indicating the utility of this approach to identifying the causes of PD activity.

2.4.2.2Partial Discharges and Aging Modelling

1) AC Stress

G C. Montanari [93] proposed the insulation aging model of XLPE cable and the generator stator bar, which showed that insulation aging characteristics meeting a certain functional relation with tree discharge length or partial discharge frequency. R. Bozzo [94] applied Weibull model to investigate the electrical tree aging characteristics in insulation and to analyse the shape parameters and scale parameters of partial discharge activity in air gaps. The results demonstrated that there was a good correlation between Weibull distribution and electrical tree generation and development of the aging process in organic solid insulation under different voltages. Contin [95] analyzed PD characteristics of polyethylene (PE) and epoxy insulators under long-term voltage stress and reached a similar conclusion to Bozzo. He also showed the unreliability of applying maximum apparent discharge in insulation

diagnosis. M. Dilorenzo [96] carried out accelerated aging test according to CIGRE II protocol to examine the aging mechanisms of internal cavities in insulation and demonstrated there was a linear relationship between PD energy and the duration of aging under different temperatures. With continuous research, the previous method of determining insulation condition according to PD maximum apparent discharge was gradually replaced. For example, G. C. Stone [97] studied the statistical data of the PD characteristics of the solid insulation from generator windings which had been in service between 1 and 50 years and determined that the maximum discharge level of aged insulation was approximately equal to or even lower than that seen in new insulation.

D. Adhikari et al. [98] investigated the PD characteristics, analysed the degradation of PD and compared properties of poly(ether sulphone) (PES), poly(ethylene terephthalate) (PET), poly(propylene) (PP) and low-density poly(ethylene) (LDPE). The results show that LDPE and PP has a lower PD resistance than PET and PES. S. Rudd et al. [99] applied PRPD as an input and introduced a knowledge-based system (KBS) to help to classify defect types in either IEC 60270 and ultra-high frequency (UHF) sensor data. Through the KBS system, it is possible to identify the physical PD processes according to PD pattern. The knowledge can be applied on various equipment, including transformers and gas insulated substations (GIS), as PD performance is independent of the type of equipment. I.K. Kyere et al. [100] examined XLPE samples with artificial defects at different depths from the surface and the results shown that 3D PRPD was a good method to identify the defects through the combined information it provided on the distribution of the charge associated with the PD activity as a function of phase (ϕ, n, q).

In summary, the investigations of PD characteristics in insulation in power systems under AC stresses were developed and the methods increased. The methods used for AC stress could also be used for the analysis of PD characteristics under DC&AC combined stresses.

2) DC Stress

Although there are lots of studies about PD features arising from faults in insulations in AC power systems, there are fewer researches in PD characteristics in DC power systems. Among the DC-stress studies, most were for PD analysis in DC only stress and it is rare for the analysis of DC and AC combined stresses to be considered.

E. Takahashi et al. [105] studied PD features of oil-paper insulation faults under combined AC&DC voltages and under a polarity reversed voltage. They analyzed the DC electrical field distribution and verified the existence of space charge. They studied the method of calculating electric field distribution in complex voltages and the PD features under combined AC&DC voltages. R. Sarathi and G. Koperundevi [106-107] made special models and used UHF signals to analyze the PD phenomena from freely moving metallic particles in transformer oil under combined AC&DC voltages. Fewer scholars have studied the PD features under the combined stresses. Their objectives and emphasis were different from those in this work. In fact, the PD analysis was limited to DC voltage.

The concept of PD phenomena in HVDC systems was defined as more than one repeat discharge per minute but this was only applied in the military area at that time. Until 1950s, with the development of DC power transmission systems, when PD in DC equipment attracted more attention. At that time, due to the dominance of AC transmission systems in the 20^{th} century, research concentrated on PD under AC conditions. People used the AC PD detection method to measure DC PD signals. The main targets were cables. The parameters helped to evaluate the stage of insulation included number of discharge and quantity of discharge. American Sandia Lab [108] applied DC PD detection techniques to detect cable aging condition, results described the relation between cable storage time and number of discharge, quantity of discharge. The results demonstrated that PD was the main cause for cable degradation. Peter H. F. Morshuis, Johan J. Smit, U. Fromm et al. investigated the PD phenomenon under DC voltage [109-114]. They focused on determining the phenomena, revealing the mechanisms and finding the causes. Their achievements summarized below:

a) Established capacitance resistance equivalent circuit model for oil-paper

under DC voltage, analyzed incipient discharge voltage value and extinction voltage recovery time in air gaps.

b) Demonstrated that discharges with small pulse values satisfied the Townsend discharge mechanism. As the size of the air gap increased, the pulse width increased. Pulses with steep rising edges satisfied the streamer discharge criteria.

c) DC electric field distribution was determined by conductivity of insulation material. As conductivity is highly dependent on temperature, temperature would affect the DC electric field distribution and hence, the pulse frequency. A conductivity increase of two orders of magnitude could cause pulse frequency to increase by two orders of magnitude.

d) The repetition rate of DC PD was low. The discharge interval could be 30mins or even 60mins. With the increase of DC voltage, the value of discharge pulse was a constant but frequency increased exponentially.

e) When PD arose from a fault in an internal area, the following amplitude discharge pulse was not affected by the previous one. When PD cause from a fault in oil, the following discharge pulse amplitude had a positive correlation with the previous one. For creeping discharge, the following discharge pulse amplitude had a negative correlation with the previous one.

A. Caballini and G C. Montanari et al. [115-116] worked to distinguishing PD pattern which appeared on HVDC apparatus. The work showed that corona discharge was easy to distinguish, but it is hard to distinguish internal discharge and surface discharge. Investigation of the effect of moisture on surface discharge demonstrated that the frequency of PD depended on moisture but the amplitude did not. Internal discharge highly depended on temperature, but not moisture.

Erling Ildstad and Terje Haave [117] investigated partial discharge characteristics in HVDC cable, carried out modelling simulation and researched the influence of temperature and external voltage on partial discharge. They figured out that the pulse width increase could be due to the larger conductivity, the higher electric field or the

bigger air gap.

3) Combined AC and DC Stress

Fewer paper exist about PD under AC&DC stress. M. Azizian Fard et. al [118] applied rippled DC voltages on samples with artificial voids and investigated the PD characteristics with various harmonic orders and amplitudes. The results showed that compared to the sample aged by purely DC voltage, the samples aged by combined AC&DC voltage have a higher PD pulse repetition rate. The rate of PD pulses increases with increasing of harmonic orders and amplitudes.

2.5 Summary

In this chapter, the stresses which cause degradation in cable insulation have been summarized and the aging models have been introduced. Possible ageing stresses used in the literature have been discussed. It is clear that there is little research on the area of combined AC&DC stress indicating that the proposed research to investigate the effect of the combined voltages on the properties of polymer is timely. The fundamentals of the measurement techniques that will be used to monitor the stressing of and the changes in the polymer: PRPD measurement; FTIR-ATR measurement and DS measurement; have been introduced. PRPD measurements will be used to investigate the polymer during aging. After aging FTIR-ATR and DS will be used to investigate the changes in the chemical structure and the electrical properties of the insulation systems. The comparison of the results will help to build an understanding of relationship between the electrical energy dissipated in the PD activity and the changes of the polymers.

2.6 References

[1] M. T. Shaw and S. H. Shaw, “Water Treeing in Solid Dielectrics”, IEEE Transactions on Electrical Insulation, Vol. EI-19, Issue 5, pp.419 – 452, 1984.

[2] Faruk Aras, Vilayed Alekperov, Nursel Can and Hulya Kirkici, “Aging of 154 kV Underground Power Cable Insulation under Combined Thermal and Electrical Stresses”, IEEE Electrical Insulation Magazine, Vol.23, Issue 5, pp.25–33, 2007.

[3] Bella H. Chudnovsky, Electrical Power Transmission and Distribution: Aging and Life Extension Techniques, CRC Press, 2012.

[4] Yang Yang, Di Yin, Rui Xiong, Jing Shi, Fuqiang Tian, Xuan Wang and Qingquan Lei, “FTIR and Dielectric Studies of Electrical Aging in Polyimide under AC Voltage”, IEEE Transactions on Dielectrics and Electrical Insulation, Vol.19, Issue 2, pp.574–581, 2012.

[5] T. Tanaka, “Aging of Polymeric and Composite Insulating Materials: Aspects of Interfacial Performance in Aging”, IEEE Transactions on Dielectrics and Electrical Insulation, Vol. 9, Issue 5, pp.704-716, 2002.

[6] J. Kuffel and P. Kuffel, High Voltage Engineering Fundamentals. Newnes, 2000.

[7] J. C. Fothergill, G.C. Montanari, G. C. Stevens, C. Laurent, G. Teyssedre, L. A. Dissado, U. H. Nilsson and G. Platbrood, “Electrical, Microstructural, Physical and Chemical Characterization of HV XLPE Cable Peelings for an Electrical Aging Diagnostic Data Base”, IEEE Transactions on Dielectrics and Electrical Insulation, Vol.10, Issue 3, pp.514–527, 2003.

[8] J. C. Chan and S. M. Jaczek, “The Moisture Absoeption of XLPE Cable Insulation under Simulated Service Conditions”, IEEE Transactions on Electrical Insulation, Vol.EI-13, Issue 3, pp.194–197, 1978.

[9] Jan-Ove Bostrom and Eric Marsden, R. Nigel Hampton and Ulf Nilsson and Hakan Lennartsson, “Electrical stress enhancement of contaminants in XLPE insulation used for power cables”, IEEE Electrical Insulation Magazine, Vol.19, Issue 4, pp.6–12, 2003.

[10] Tadao Seguchi, Kiyotoshi Tamura, Takeshi Ohshima, Akihiko Shimada and Hisaaki Kudoh, “Degradation mechanisms of cable insulation materials during radiation–thermal ageing in radiation environment”, Radiation Physics and Chemistry, Vol.80, pp.268–273, 2011.

[11] John Densley, “Ageing mechanisms and diagnostics for power cables - an overview”, IEEE Electrical Insulation Magazine, Vol.17, Issue 1, pp.14–22, 2001.

[12] A.C. Gjerde, “Multifactor ageing models - origin and similarities”, IEEE Electrical Insulation Magazine, Vol.13, Issue 1, pp.6-13, 1997.

[13] Simoni L, “General equation of the decline in the electric strength for combined thermal and electrical stresses”, IEEE Transactions on Electrical Insulation, Vol.EI-19, Issue 1, pp.45-52, 1984.

[14] Kenneth N. Mathes, “Thermal Aging of Electrical Insulation - Technology and Standardization”, IEEE Electrical Insulation Magazine, Vol.1, Issue 1, pp.29-35, 1985.

[15] L. Simoni, “A General Approach to the Endurance of Electrical Insulation under Temperature and Voltage”, IEEE Transactions on Electrical Insulation, Vol.EI-16, Issue 4, pp.277-289, 1981.

[16] Thomas W. Dakin, “Electrical Insulation Deterioration Treated as a Chemical Rate Phenomenon”, Transactions of the American Institute of Electrical Engineers, Vol.67, Issue 1, pp.113-122, 1948.

[17] P. Cygan and J.R.Lahari, “Models for insulation aging under electrical and thermal multistress”, IEEE Transactions on Electrical Insulation, Vol.25, Issue 5, pp.923-934, 1990.

[18] Williams, J.A. Underground Transmission Systems. New York : Electrical Power Research Institute, Inc., c1992.

[19] Haddad, A. and Warne, D. Advances in High Voltage Engineering. London : MPG Books Limited, c2004.

[20] Maik Koch, Michael Krueger and Markus Puetter, “Advanced Insulation Diagnostic by Dielectric Spectroscopy”, TechCon Asia Pacific, Sydney, Australia, 2009.

[21] G. L. Johnson, Solid State Thesla Coil, www.eece.kce.edu/johnson, Chapter 3-1, 2001.

[22] Kwan-Chi. Kao, “Dielectric phenomena in solids: with emphasis on physical concepts of electronic processes”, Amsterdam ; Boston : Academic Press, 2004.

[23] B. K. P. Scaife, Principles of Dielectrics (Oxford Science Publications, Oxford, 1998).

[24] H. Frohlich, Theory of Dielectrics: Permittivity and Dielectric Loss (Oxford Science Publications, Oxford, 1958.

[25] C. J. F. Bottcher, Theory of Electric Polarization (Elsevier Publishing Company, Amsterdam, 1952.

[26] http://elektroarsenal.net/frequency-dependence-dielectric-constant-and-dielectric-loss.html, [Accessed: 18 March 2016].

[27] J. Lu, “High Dielectric Constant Polymer Nanocomposites for Embedded Capacitor Applications,” School of Material Science and Engineering, Georgia Institute of Technology, Georgia, 2008.

[28] R. Valenzuta, magnetic ceramics, Cambridge university press, New York (1994).

[29] Mirabella, F. M., Ed.; In Internal Reflection Spectroscopy: Theory and Applications; Marcel Dekker, Inc.; New York, 1993; vol.15.

[30] http://mmrc.caltech.edu/FTIR/Harrick/GATR/ATR.pdf, [Accessed: 18 March 2016].

[31] https://zh.scribd.com/document/249946151/ATR-FTIR-Spectroscopy-in-the-Undergraduate-Chemistry-Laboratory-Part-I-Fundamentals-and-Examples#, [Accessed: 18 March 2016].

[32] Siwatt Pongpiachan, “FTIR Spectra of Organic Functional Group Compositions in PM2.5 Collected at Chiang-Mai City, Thailand during the Haze Episode in March 2012”, Journal of Applied Sciences, Vol.14, Issue 22, pp.2967-2977, 2014.

[33] IEC 60270: 'IEC International Standard 60270. High Voltage Test Techniques - Partial Discharge Measurements, International Electrotechnical Commission (lEC), Geneva, Switzerland, 3rd edition, 2000.

[34] M. G. Danikas, “The definitions Used for Partial Discharge Phenomena”, IEEE Transactions on Electrical Insulation, Vol.28, Issue 6, pp.1075-1081, 1993.

[35] S. A. Boggs, “Partial Discharge: Overview and Signal Generation”, IEEE Electrical Insulation Magazine, Vol.6, Issue 4, pp.33-39, 1990.

[36] Steven A. Boggs, “Partial discharge: overview and signal generation”, IEEE Electrical Insulation Magazine, Vol.6, Issue 4, pp.33-39, 1990.

[37] F. H. Kreuger. Partial Discharge Detection in High-Voltage Equipment. Butterworths, London, 1989.

[38] Jen-Shih Chang, Phil A. Lawless and Toshiaki Yamamoto, “Corona discharge processes”, IEEE Transactions on Plasma Science, Vol.19, Issue 6, pp.1152-1166, 1991.

[39] José A. Giacometti and Osvaldo N. Oliveira Jr., “Corona charging of polymers”, IEEE Transactions on Electrical Insulation, Vol.27, Issue 5, pp.924-943, 1992.

[40] Trinh N. Giao and Jan B. Jordan, “Modes of Corona Discharges in Air”, IEEE Transactions on Power Apparatus and Systems, Vol.PAS-87, Issue 5, pp.1207 -1215, 1968.

[41] C. F. Gallo, “Corona-A Brief Status Report”, IEEE Transactions on Industry Applications, Vol.IA-13, Issue 6, pp.550-557, 1977.

[42] T. J. Gallagher and A. J. Pearmain, High Voltage: Measurement, Testing and Design, Eds. John Wiley & Sons, New York, 1983.

[43] Y. Murooka, T. Takada and K. Hiddaka, “Nanosecond surface discharge and charge density evaluation Part I: review and experiments”, IEEE Electrical Insulation Magazine, Vol.17, Issue 2, pp.6-16, 2001.

[44] R. Sarathi, I. P. Merin Sheema, J. Sundara Rajan and M. G. Danikas, “Influence of harmonic AC voltage on surface discharge formation in transformer insulation”,

IEEE Transactions on Dielectrics and Electrical Insulation, Vol.21, Issue 5, pp.2383-2393, 2014.

[45] Masahiro Sato, Akiko Kumada, Kunihiko Hidaka, Keisuke Yamashiro, Yuji Hayase and Tetsumi Takano, "Surface discharges in silicone gel on AlN substrate", IEEE Transactions on Dielectrics and Electrical Insulation, Vol.23, Issue 1, pp.494-500, 2016.

[46] Ricardo Fernandes da Silva and Vitoldo Swinka Filho, "Analysis of electrical tracking by energy absorption during surface discharge in polymeric materials", IEEE Transactions on Dielectrics and Electrical Insulation, Vol.23, Issue 1, pp.501-506, 2016.

[47] K. Temmen, "Evaluation of surface changes in flat cavities due to ageing by means of phase-angle resolved partial discharge measurement", Journal of Physics D: Applied Physics, Vol.33, No.6, pp.603-608, 2000.

[48] J. H. Mason, "The deterioration and breakdown of dielectrics resulting from internal discharges", Proceedings of the IEE - Part I: General, Vol.98, Issue 109, pp.44-59, 1951.

[49] Tony Byrne, "Humidity Effects in Substations", Petroleum and Chemical Industry Conference Europe, 3-5 June 2014.

[50] A. E. W. Austen and W. Hackett, "Internal discharges in dielectrics: their observation and analysis", Journal of the Institution of Electrical Engineers - Part I: General, Vol.91, Issue 44, pp.298-312, 1944.

[51] Michael G. Danikas and Toshikatsu Tanaka, "Nanocomposites-a review of electrical treeing and breakdown", IEEE Electrical Insulation Magazine, Vol.25, Issue 4, pp.19-25, 2009.

[52] A. Cavallini, M. Conti, G. C. Montanari, C. Arlotti and A. Contin, "PD Inference for the Early Detection of Electrical Treeing in Insulation Systems", IEEE Transactions on Dielectrics and Electrical Insulation, Vol.11, Issue 4, pp.724-735, 2004.

[53] T. Tanaka, "Internal partial discharge and material degradation", IEEE Transactions on Electrical Insulation, Vol.EI-21, Issue 6, pp.899-905, 1986.

[54] Tony Byrne, “Humidity Effects in Substations”, Petroleum and Chemical Industry Conference Europe, 3-5 June 2014.

[55] M. Muhr, T. Strehl, E. Gulski, K. Feser, E. Gockenbach, W. Hauschild, and E. Lemke, "Sensors and sensing used for non-conventional PD detection," 2006 CIGRE Paris Session, Paris, France, 2006.

[56] Y. Tian, P. L. Lewin and A. E. Davies, “Comparison of On-line Partial Discharge Detection Method For HV Cable Joints”, IEEE Transactions on Dielectrics and Electrical Insulation, Vol.9, Issue 4, pp.604-615, 2002.

[57] M. Goldman, A. Goldman and J. Gatellet, “Physical and chemical aspects of partial discharges and their effects on materials”, IEE Proceedings - Science, Measurement and Technology, Vol.142, Issue 1, pp.11-16, 1995.

[58] F. Kreuger, Industrial high voltage - v.1: Delft University Press, 1991.

[59] Peter H.F. Morshuis, “Degradation of Solid Dielectrics due to Internal Partial Discharge: Some thoughts on progress made and where to go now”, IEEE Transactions on Dielectrics and Electrical Insulation, Vol.12, No.5, pp.905-913, 2005.

[60] T. Tanaka, “Internal Partial Discharge and Material Degradation”, IEEE Transactions on Electrical Insulation, Vol.EI-21, No.6, pp.899-905, 1986.

[61] W. J. M. Samaranayake, Y. Miyahara, T. Namihira, S. Katsuki, R. Hackam and H. Akiyama, “Ozone Production Using Pulsed Dielectric Barrier Discharge in Oxygen”, IEEE Transactions on Dielectrics and Electrical Insulation, Vol.7, Issue 6, pp.849-854, 2000.

[62] Eka PW, T. Okazaki, Y. Murakami, N., Hozumi and M. Nagao, “Breakdown of LDPE Film under Heavy Water Absorption”, World Academy of Science, Engineering and Technology, Vol.26, pp.471-476, 2009.

[63] Lei Zhang, “Electrical tracking over solid insulating materials for aerospace applications” PhD thesis, University of Manchester, 2011.

[64] A. Cavallini, F. Ciani, G. Mazzanti and G. C. Montanari, “First electron availability and partial discharge generation in insulation cavities: effect of light irradiation”, Vol.12, Issue 2, pp.387-394, 2005.

[65] König, D.: Impulslose Teilentladungen in Hohlräumen von Epoxydharzformstoff-Isolierungen. ETZ-Archiv 90, (1969), 156-8

[66] R. Bartnikas, “Partial Discharges, Their Mechanism, Detection and Measurement”, IEEE Transaction on Dielectric and Electrical Insulation, Vol. 9, pp.763-808, 2002.

[67] Bartnikas, R.: Note on discharge in helium under ac conditions. J. Appl. Phys. D, 1, (1968), 659-661.

[68] L. W. van Veen, “Comparison of measurement methods for partial discharge measurement in power cables”, Delft University of Technology, 2014.

[69] R Bartnikas and J P Novak, “On the spark to Ppsuedoglow and glow transition mechanism and discharge detectability”, IEEE Transactions on Electrical Insulation, Vol.27, Issue 1, pp.3-14, 1992.

[70] T Tanaka, “Internal partial discharge and material degradation”, IEEE Transactions on Electrical Insulation, Vol.EI-21, pp.899-905, 1986.

[71] N. H. Aziz, V. M. Catterson, S. M. Rowland and S. Bahadoorsingh, “Analysis of Partial Discharge Features as Prognostic Indicators of Electrical Treeing”, IEEE Transactions on Dielectrics and Electrical Insulation, Vol.24, No.1, pp.129-136, 2017.

[72] N. Arman and A. T. Starr, “The measurement of discharges in dielectrics”, Journal of the Institution of Electrical Engineers, Vol.79, No.475, pp.67-81, 1936.

[73] T. Tanaka and T. Okamoto, “A minicomputer based partial discharge measurement system”, IEEE International Symposium on Electrical Insulation, pp.86-89, 1978.

[74] E. Gulski and F. H. Kreuger, “Digital computer system for measurements of PD in insulation structures”, Conduction and Breakdown in Solid Dielectrics Conference, pp.582-586, 1989.

[75] E. Gulski and F. H. Kreuger, “Computer-aided analysis of discharge patterns”, Journal of Physics D: Applied Physics, Vol.23, No.12, pp.1569- 1575, 1990.

[76] E. Gulski and F. H. Kreuger, “Computer-aided recognition of discharge sources,” IEEE International Workshop on PD Measurement and their Traceability, 1990.

[77] E. Gulski, P. H. F. Morshuis and F. H. Kreuger, “Automized recognition of PD in cavities,” Japanese Journal of Applied Physics, Vol.29, No.7, pp.1329-1335, 1990.

[78] S. A. Boggs, “Partial discharge: overview and signal generation,” IEEE Electrical Insulation Magazine, Vol.6, No.4, pp.33-39, 1990.

[79] M. Hikita, K. Yamada, A. Nakamura, T. Mizutani and A. Oohasi,“Measurements of PD by computer and analysis of PD distribution by the Monte Carlo method”, IEEE Transactions on Electrical Insulation, Vol.25, No.3, pp.453-468, 1990.

[80] J. Fuhr, M Haessig, B. Fruth and T. Kaiser, “PD fingerprints of some HV apparatus,” IEEE International Symposium on Electrical Insulation, pp.129-132, 1990.

[81] E. Gulski and F. H. Kreuger, “Recognition of discharge sources using statistical tools,” Properties and Applications of Dielectric Materials Conference, 1991.

[82] E. Gulski and F. H. Kreuger, “Computer-aided recognition of discharge patterns,” 7th International Symposium on HV Engineering, 1991.

[83] E. Gulski, “Computer-aided recognition of partial discharges using statistical tools,” PhD Thesis, Delft University, Netherlands, ISBN 90-6275-728-6, 1991.

[84] J. Fuhr, B. Fruth, L. Niemeyer, D. Koenigstein, M. Haessing and F. Gutfleisch, “Generic procedure for classification of aged insulating systems,” Dielectric Materials Conference, pp.35-38, 1991.

[85] E. Gulski and F. H. Kreuger, “Diagnosis of insulation systems using statistical tools”, IEEE International Symposium on Electrical Insulation, pp.393-397, 1992.

[86] Y. J. Kim and J. K. Nelson, “Assessment of deterioration in epoxy/mica machine insulation”, IEEE Transactions on Electrical Insulation, Vol.27, No.5, pp.1026-1039, 1992.

[87] E. Gulski, “Computer-aided measurement of PD in HV equipment”, IEEE Transactions on Electrical Insulation, Vol.28, No.6, pp.969-983, 1993.

[88] E. Gulski and P. Seitz, “Computer-aided registration and analysis of PD in HV equipment”, 8th International Symposium on HV Engineering, Vol.3, pp. 13, 1993.

[89] F. H. Kreuger, E. Gulski and A. Krivda, “Classification of partial discharges,” IEEE Transactions on Electrical Insulation, Vol.28, No.6, pp.917-931, 1993.

[90] M. Cacciari, A. Contin, G. Rabach and G. C. Montanari, “Diagnosis of practical insulation systems by PD measurements in the presence of multidischarge phenomena”, Electrical Insulation and Dielectric Properties Conference, pp.414-419, 1993.

[91] E. Gulski, “Digital analysis of partial discharges”, IEEE Transactions on Electrical Insulation, Vol.2, No.5, pp.822-837, 1995.

[92] E. Gulski, P.H.F. Morshuis and F.H. Kreuger, “Conventional and Time-Resolved Measurements of Partial Discharges as a Tool for Diagnosis of Insulation Materials”, Properties and Applications of Dielectric Materials Conference, pp.666-669, 1994.

[93] G. C. Montanari, “Aging and life models for insulation systems based on PD detection”, IEEE Transactions on Dielectrics and Electrical Insulation, Vol.2, Issue 4, pp.667-675, 1995.

[94] R. Bozzo, C. Gemme, F. Guastavino, M. Cacciari, A. Contin and G. C. Montanari, “Aging diagnosis of insulation systems by PD measurements-extraction of partial discharge features in electrical treeing”, IEEE Transactions on Dielectrics and Electrical Insulation, Vol.5, Issue 1, pp.118-124, 1998.

[95] A. Contin, E. Gulski, M. Cacciari and G. C. Montanari, “Inference of PD in electrical insulation by charge-height probability distribution-diagnosis of insulation system degradation”, IEEE Transactions on Dielectrics and Electrical Insulation, Vol.5, Issue 1, pp.110-117, 1998.

[96] M. Di Lorenzo del Casale, “On multistress aging of epoxy resins PD and temperature”, IEEE Transactions on Dielectrics and Electrical Insulation, Vol.8, Issue 2, pp.299-303, 2001.

[97] G. C. Stone and V. Warren, “Effect of manufacturer, winding age and insulation type on stator winding partial discharge levels”, IEEE Electrical Insulation Magazine, Vol.20, Issue 5, pp.13-17, 2004.

[98] D. Adhikari, D. M. Hepburn and B.G. Stewart, “Comparison of partial discharge characteristics and degradation in several polymeric insulators”, IET Science, Measurement & Technology, Vol.6, Issue 6, pp.474-484, 2012.

[99] S. Rudd, S. D. J. McArthur and M. D. Judd, “A Generic Knowledge-based Approach to the Analysis of Partial Discharge Data”, IEEE Transactions on Dielectrics and Electrical Insulation, Vol.17, Issue 1, pp.149-156, 2010.

[100] I.K. Kyere and J.J. Walker, “Partial Discharge Pattern Characterization of Different Defects Using 3D Phase Resolved Technique”, High Voltage Engineering and Application Conference, pp.1-4, 2014.

[101] R. Clemence Kiiza, M. Ghaffarian Niasar, R. Nikjoo, X. Wang, H. Edin and Z. Ahmed, “Comparison of Phase Resolved Partial Discharge Patterns in Small Test Samples, Bushing Specimen and Aged Transformer Bushing”, Annual Report Conference on Electrical Insulation and Dielectric Phenomena, pp.88-91, 2012.

[102] Riccardo Bodega, Peter H. F. Morshuis, Massimo Lazzaroni, and Frank J. Wester, “PD Recurrence in Cavities at Different Energizing Methods”, IEEE Transactions on Instrumentation and Measurement, Vol.53, Issue 2, pp.251-258, 2004.

[103] M. Florkowski and B. Florkowska, “Phase-resolved rise-time-based discrimination of partial discharges”, IET Generation, Transmission & Distribution, Vol.3, Issue 1, pp.115-124, 2009.

[104] G. C. Stone, “Relevance of Phase Resolved PD Analysis to Insulation Diagnosis in Industrial Equipment”, Solid Dielectrics Conference, pp.1-5, 2010.

[105] E. Takahashi, Y. Tsutsumi, K. Okuyama and F. Ogata, “Partial discharge characteristic of oil-immersed insulation system under DC, combined AC-DC and DC reversed polarity voltage”, IEEE Transactions on Power Apparatus and Systems, Vol.95, Issue 1, pp.411-420,1976.

[106] R. Sarathi and G. Koperundevi, “YHF technique for identification of partial discharge in a composite insulation under AC and DC voltages”, IEEE Transactions on Dielectrics and Electrical Insulation, Vol.15, Issue 6, pp.1724-1730, 2008.

[107] R. Sarathi, A. V. Giridhar, Abirami Mani and K. Sethupathi, “Investigation of partial discharge activity of conducting particles in liquid nitrogen under DC voltage using UHF technique”, IEEE Transactions on Dielectrics and Electrical Insulation, Vol.15, Issue 3, pp.655-662, 2008.

[108] J. B. Mathes, T. J. Whelan and C. J. Uhlrich, “DC partial discharge detection and analysis techniques”, Annual Report Conference on Electrical Insulation and Dielectric Phenomena, pp.736-739, 2002.

[109] Peter H. F. Morshuis and Johan J. Smit, “Partial Discharges at DC Voltage: Their Mechanism, Detection and Analysis”, IEEE Transactions on Dielectrics and Electrical Insulation, Vol.12, Issue 2, pp.328-340, 2005.

[110] Peter Morshuis and Jens Beyer, “Quality assessment of HVDC components by PD analysis”, IEEE annual report conference on electrical insulation and dielectric phenomena, pp. 542-545, 1997.

[111] G.Hoogenraad P. H. F. Morshuis and C.Petrarca, “Classification of partial Discharge for DC Equipment”, IEEE annual report conference on electrical insulation and dielectric, pp.111-113, 1996.

[112] U. Fromm and P. H. F. Morshuis, “Partial Discharge Classification at DC Voltage”, IEEE International Conference on Conduction and Breakdown in Solid Dieleetrics, pp.403-407, 1995.

[113] U. Fromm, “The Ageing Behaviour of Epoxy Resin at DC Voltage”, Conference on Electrical Insulation and Dielectric Phenomena, pp.235-238, 1995.

[114] U. Fromm, “Interpretation of partial Discharges at DC Voltages”, IEEE Transactions on Dielectrics and Electrical Insulation, Vol.2, Issue 5, pp.761-770, 1995.

[115] H. Q. Niu, A. Cavallini and G. C. Montanari, “Identification of partial Discharge Phenomena in HVDC Apparatus”, Conference Record of the 2008 IEEE International Symposium on Electrical Insulation, pp.373-376, 2008.

[116] Andrea Cavallini, Xiaolin Chen, Haiqing Niu and Gian Carlo Montanari, “Strategies for PD Source Identification in HVDC Systems”, International Conference on High Voltage Engineering and Application, pp.649-652, 2008.

[117] Erling Ildstad and Terje Haave, “Conduction and partial Discharge Activity in HVDC Cable Insulation of Lapped Polypropylene Films”, IEEE International Conference on Solid Dielectrics, pp.137-140, 2001.

[118] M. Azizian Fard, A. J. Reid and D. M. Hepburn, “Analysis of HVDC Superimposed Harmonic Voltage Effects on Partial Discharge Behavior in Solid Dielectric Media”, IEEE Transactions on Dielectrics and Electrical Insulation, Vol.24, Issue 1, pp.7-16, 2017.

3. Project Design

Before experiments are undertaken, target material should be chosen from many kinds of polymers. Information of the experiment circuit and equipment will also be introduced in this chapter.

Section 3.1 shows the criteria used to select high-density polyethylene (HDPE) and polypropylene (PP) as target materials in this project. The properties of the two materials are introduced.

Section 3.2 introduces the thermo-electrical aging circuit and the PD detection system. The information of each piece of equipment in the circuit is provided. The way to produce combined AC & DC voltages is described. Details of aging electrodes and the experimental arrangements are provided. In addition, it also provides information on decisions of aging temperatures, voltage ratios, superimposed frequencies and aging duration. The method used to collect PD data is described in detail.

Section 3.3 provides information on the FTIR-ATR measurement equipment.

Section 3.4 provides information on the DS measurement equipment and the way that these measurements were undertaken.

3.1 Material Selection

3.1.1 Selection Criteria

For cable insulation, thermal stress and electrical stress are the two main factors that cause insulation degradation. Therefore, people are normally concerned about: Whether the material can work without breakdown under the operating temperature and voltage? What the electric strength and dielectric properties of the materials will be? The electrical strength is important as it will control the maximum voltage that can be applied to the insulating system. The dielectric properties will be important as they will control the capacitance and conductance of the cable. High values of capacitance can introduce a significant current component associated with the charging and discharging of the cable. The conductance will contribute to losses in the cable and may lead to heating of the cable insulation.

Will it cost too much when this material is used? Therefore, before making a decision, people should take the cost, electric strength and dielectric properties of the material into consideration.

As XLPE is a popular insulation material nowadays, it was intended that the properties of XLPE would be used as a bench-mark. However it was difficult to get suitable XLPE film to test. Among thermoplastic materials, HDPE has the most similar properties to XLPE (Table 3.1).Therefore it was decided to use HDPE films to provide a bench mark assuming that their behaviour would be similar to XLPE results. PP was selected due to its low cost, good breakdown strength as well as good thermal and dielectric properties. Details is shown in Table 3.1.

Table 3.1. Polymer selection criteria.

	Density	Melting temperature (℃)	Breakdown voltage (kV/mm)	Dielectric constant	Dissipation factor
Test method	ASTM D792	--	ASTM D149	ASTM D150	ASTM D150
XLPE	0.907~0.976	130	20~47.2	2.30~3.70	3.0E-4~0.010
HDPE	0.947~0.977	127~136	19.7~30.3	2.24~2.60	2.0E-5~2.7E-4
PP	0.910~1.20	140.6~182.2	18.1~20.1	2.29~2.31	2.0E-4~3.1E-3

Further details of the structure and properties of HDPE and PP are given in Sections 3.1.2-3.1.3.

Thermoplastic materials can be divided into different categories [1]:

1) Crystalline thermoplastics: In a crystalline thermoplastic structure, the molecules are arranged in order, as shown in Figure 3.1. With increasing temperature, molecules will obtain higher energy to break the existing order and the crystalline structure will be turned into an amorphous structure. However, when it is cooled down, the molecular structure may not return to the original state. The percentage of crystalline region depends on temperature and how quickly the temperature changed. If it is cooled quickly, most of the molecules would have not enough time to respond to the change and the resulting crystalline regions would be small. If the temperature changes slowly, most of the crystalline region will be retained. Undoubtedly, a thicker sample will have relatively more crystalline region retained because of non-uniform temperature variation during cooling compared with that in a thinner sample. Crystalline thermoplastics have higher and more clearly defined melting temperatures.
2) Amorphous thermoplastic material: Properties of amorphous thermoplastic materials are quite different from those of crystalline thermoplastic materials. Molecules in amorphous thermoplastic material structures are not arranged in order as shown in random structure of amorphous region in Figure 3.1.

3) Semi-crystalline thermoplastics: Semi-crystalline polymers have the status between crystalline material and amorphous material. Therefore, their properties lie between those of crystalline materials and that of amorphous materials.

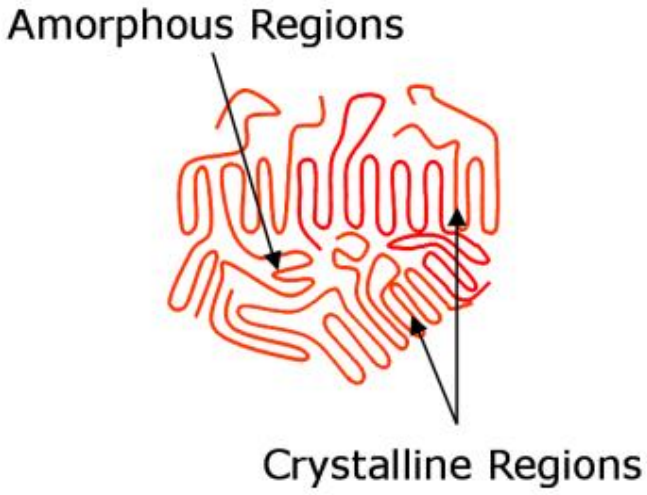

Figure 3.1. Amorphous region and crystalline region in polymer [2].

3.1.2 High-density Polyethylene (HDPE)

Polyethylene (PE) is a kind of thermoplastic resin formed through polymerization of ethylene. With its simple chemical structure, PE has became one of the most popular resins. PE was widely used due to its low cost, easy manufacture, higher chemical resistance and higher environmental resistance.

The physical and chemical properties of more complex PE materials are different due to their different manufacture processes. The properties mainly depend on density, crystallinity, molecular weight, molecular weight distribution, degree of branching of the chain and crystallization. PE is a typical semi-crystalline polymer, i.e. a material with crystalline regions and amorphous regions. In crystalline regions, the molecules are arranged regularly and the intermolecular forces are higher than in amorphous regions. There is no certain melting temperature in amorphous regions changes being

defined by the glass transition temperature T_g. This reflects the change in state of the amorphous regions from one were the polymer chains a relatively immobile and are locked in position (the glassy state) to one where polymer chains can move past each other leading to a state that is effectively an extremely viscous liquid. T_g is of the order of $-125℃$ for polyethylene so the amorphous regions will not be in a glassy state. The mechanical properties of amorphous regions are lower than those of crystalline regions. The degree of crystallization has linear relation with density. The existence of side branches in PE molecules impede the formation of the well organised crystalline structures. Therefore, a reduction of number and size of side branches should in carefully controlled increase the degree of crystallization and therefore density. In general, with increased crystallisation and density, the properties of PE such as tensile strength, stiffness, hardness and heat resistance increase.

Two main types of PE are low density polyethylene (LDPE) and high density polyethylene (HDPE), as shown in Figure 3.2.

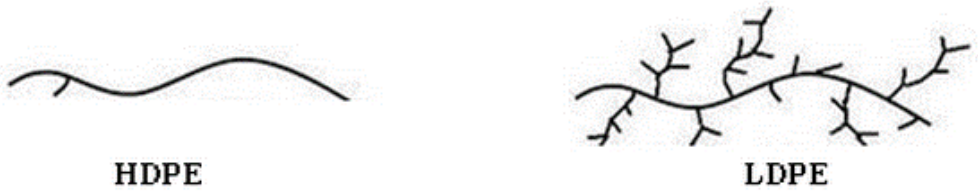

Figure 3.2. Molecular structure of LDPE and HDPE [3].

LDPE and HDPE have different molecular weight, molecular weight distribution and branched structure. In Figure 3.2, LDPE has more side branches both long and short. HDPE has a linear molecular chain with fewer small branches compared to LDPE but no long branches, as shown in Figure 3.2. HDPE is a semi-crystalline polymer with a high degree of crystallization. Therefore, the mechanical properties of HDPE are better than those of LDPE. The specific gravity of HDPE is in range of 0.941~0.965 g/cm^3 [4]. The melting temperature of HDPE is 130°C.

In addition, HDPE has good chemical stability, can operate at low temperatures and has good insulation properties, which make it widely used in electric wires, cable

insulation, tubes, commodities, industrial packing film, constructional materials, mechanical elements, coating and other industries. HDPE has good heat resistance, good cold resistance, good chemical stability, higher stiffness and toughness, higher mechanical strength, excellent insulation properties and higher environmental stress cracking resistance. With such advantages, HDPE can be used in food, automotive and chemical industries. HDPE is suitable for various manufacture processes, such as hollow blow moulding, injection moulding and extrusion, to make products which are applied in cable coating, tubes and sheets and so on. HDPE has a wide range of applications in various fields due to its lower costs and good machinability. However, HDPE is difficult to bond and can expand at high temperature. It still need to be developed.

3.1.3 Polypropylene (PP)

Polypropylene (PP) has been in industrial use since 1957. In general, PP is the popular and fast-growing material.

Advantages of PP are summarized as below:

- Lower specific gravity: the specific gravity is normally between 0.89~0.91. It has one of the lower values among general polymers in use.
- Excellent dielectric properties.
- Good thermal properties: the melting temperature of polypropylene is 160°C, which is the best thermostablity among general polymers in use.
- Good physical and mechanical properties: polypropylene has high surface hardness, good elasticity and good abrasion resistance.
- Good chemical stability: no reaction when in contact with most chemicals. High resistance to chemical corrosion.
- Good properties for manufacturing: polypropylene is easy to manufacture. Extrusion, injection moulding and blow moulding are the common methods to

make polypropylene products.

Disadvantages of PP are:

- Crack development when PP material is being bended
- Expansion at high (close to melting) temperatures

According to various positions of methyl (CH_3) groups in the long chain, polypropylene can be classified into isotactic polypropylene (iPP), syndiotactic polypropylene (sPP) and atactic polypropylene (aPP), as shown in Figure 3.3.

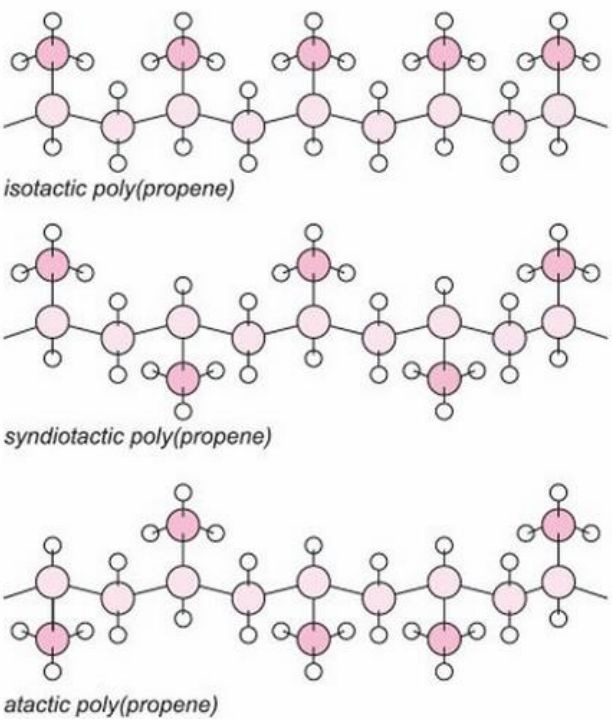

Figure 3.3. Different kinds of polypropylene (PP): isotactic (iPP); syndiotactic (sPP) and atactic (aPP) [5].

The structure of the three form of PP shown in Figure 3.3, are summarized as follows:

a) Isotactic polypropylene (iPP): all methyl groups are positioned at the same side with respect to the backbone of the chain plane.
b) Syndiotactic polypropylene: the methyl groups are positioned at alternate sides of the backbone of the chain plane.

c) Atactic Polypropylene: the methyl groups are positioned randomly.

3.2 Thermo-electrical Aging Experiment with PD Detection Set- up

3.2.1 Thermo-electrical Aging Experiment Set-up

The circuit of the thermo-electrical aging experiment with PD detection is shown in Figure 3.4. The thermo-electrical system is shown in the dashed box area.

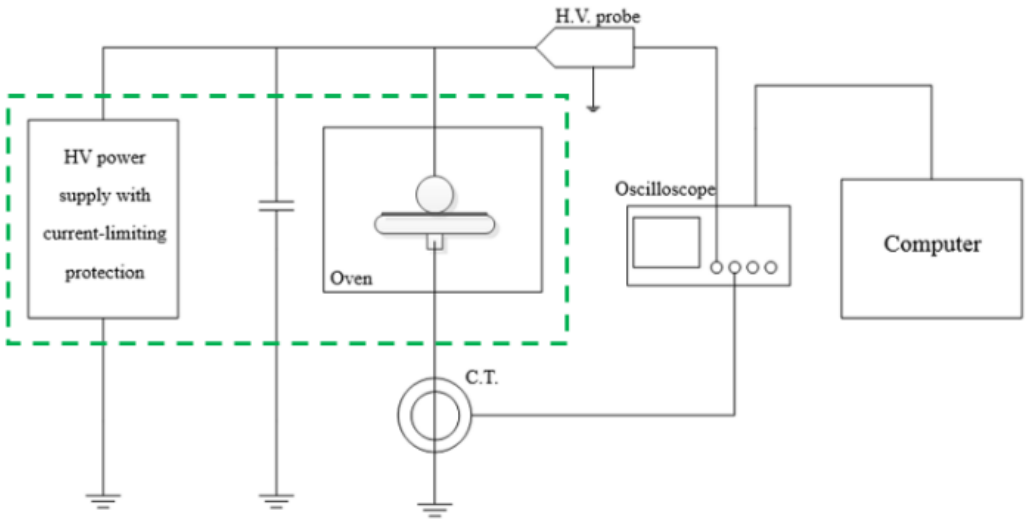

Figure 3.4. Thermo-electrical aging system.

Types of each piece of equipment in the thermo-electrical system are shown in Table 3.2, with details of each.

Table 3.2. Name and types of experimental set-up.

	Name	Types
HV power supply with current-limiting protection	Signal generator	Agilent 33500B Series Waveform Generator
	Power amplifier	Model 50/12 produced by TRek Inc. with a gain of 5000. Details are given in the following paragraph.
Temperature controlled oven		Maximum temperature 200 °C
Electrodes		Stainless steel
Oscilloscope		YOKOGAWA DL6154 10GS/s 1.5GHz

The H.V. power supply was a combination of a signal generator and power amplifier (mentioned in Table 3.2). The signal generator produced a signal of several volts with the combined voltages at high frequency and was used as an input to the power amplifier with a gain of 5000 to achieve the high voltage output. The power amplifier could produce any waveform as long as the output voltage range for DC or peak AC lies between +/- 50 kV. The output current range for DC or peak AC lies between +/- 12 mA. The oven was used to provide a high ambient temperature to accelerate the aging of the samples. The oven could operate at temperatures up to 200°C.

The test sample and the stainless steel electrodes (shown in Figure 3.4) were placed in the oven to control the ambient temperature the test sample was exposed to. Sphere-plane electrodes are used in this project (see Figure 3.5) as it produces a slightly non-uniform electric field which is appropriate for modelling discharges in a coaxial cable geometry. This is explained in more detail in Section 3.2.2. Each polymer sample was 60×60 mm in size and was cut from sheets of 50 µm thickness. Individual 50 µm samples suffered from bulk breakdown at voltages below that required to initiate PD activity. Therefore a 100 µm thickness of insulation was formed by placing two sample films between the sphere-plane electrodes. The total thickness of the sample was therefore 100. As the ageing occurs on the upper surface of the upper film, the upper film is used for DS measurement and its upper surface is used for FTIR-ATR measurement. The upper sphere electrode with a 20 mm diameter was connected to the high voltage power supply, while the lower electrode was connected to ground. The samples were exposed to air at atmospheric pressure during aging.

3.2.2 Electrode Geometry

The geometry of the electrodes is shown in Figure 3.5.

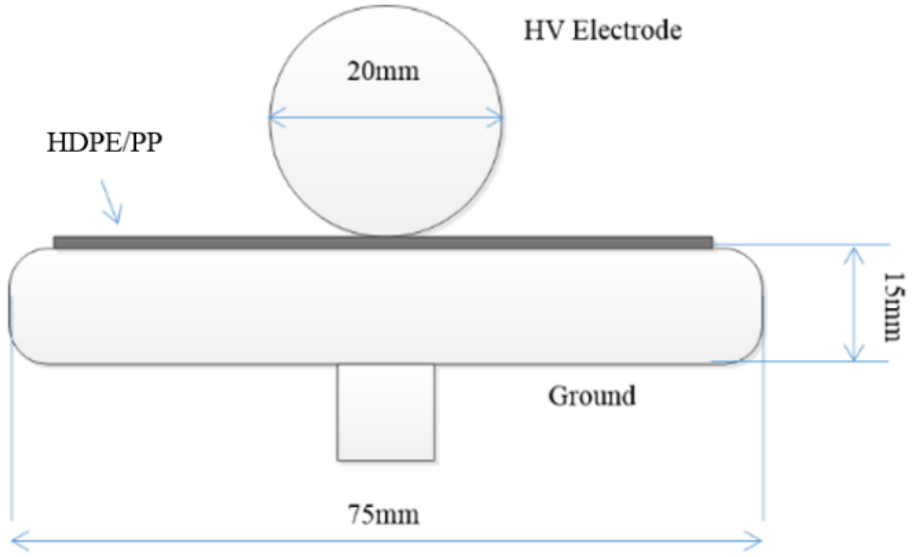

Figure 3.5. Thermo-electrical aging electrodes.

The degree of uniformity of an electric field η, is defined as [6]:

$$\eta = \frac{\hat{E}_{mean}}{\hat{E}_{\max}} \tag{3.1}$$

Where, $\hat{E}_{mean}$ and $\hat{E}_{\max}$ are the peak value of the mean and the maximum field intensities in a dielectric respectively. The value of η lies between $0 \le \eta \le 1$. η can also be represented by p (the geometrical characteristic factor for electrode configurations).

$$p = \frac{r + d}{r} \tag{3.2}$$

Where, r is the radius of the upper electrode, d is the shortest gap distance between the two electrodes, $1 \le p < \infty$.

$$\eta = f(p) \tag{3.3}$$

where , $f(p)$ represents the " degree of non-uniformity" of an electric field. The degree of uniformity η as a function of geometrical characteristic p in different electrode configurations is shown in Figure 3.6.

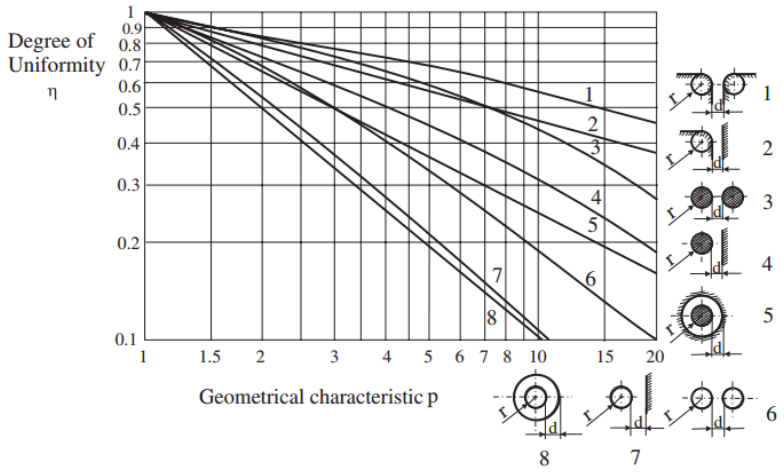

Figure 3.6. Schwaiger curves for fields with spherical, cylindrical and curved electrode configurations [6].

According to equation 3.2, p of the sphere-plane electrode system used in this project is:

$$p = \frac{10mm + 50\mu m \times 2}{10mm} = \frac{10mm + 0.1mm}{10mm} = 1.01 \qquad 3.4$$

According to Figure 3.6, η of sphere-plane electrode system is close to 1 (which is a slightly non-uniform electric field).

Needle-plate electrodes produce an extremely non-uniform electric field. Parallel plate electrodes produce a uniform electric field. These two kinds of electrodes cannot model the electric field in cable systems. As defects in cable insulation suffer a slightly non-uniform electric field, the sphere-plane electrodes are used in this project.

3.2.3 Voltages Applied to the Samples

It was decided that a positive DC stress with a superimposed AC waveform would be applied to the samples. The resultant AC & DC combined voltage waveform is shown in Figure 3.7.

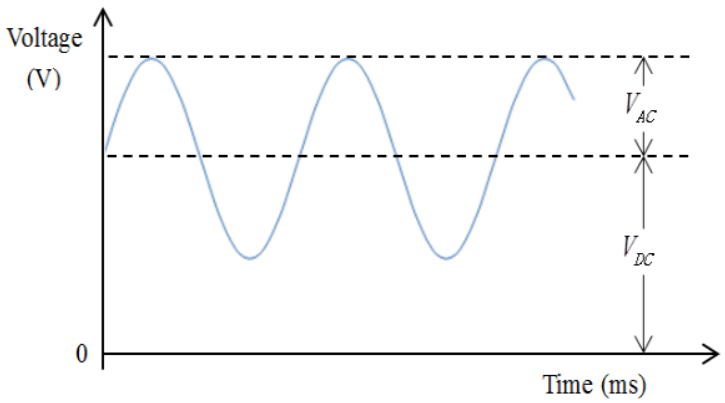

Figure 3.7. AC&DC combined voltage waveform.

The voltage ratio (*AC%*) was used to describe the combined voltage stress, as shown in equation 3.5:

$$AC\% = \frac{V_{AC}}{V_{DC}} \times 100\% \qquad 3.5$$

where, V_{DC} is the DC voltage, V_{AC} is the peak value of the AC voltage. In this project, the voltage ratios were chosen as 10%, 30% and 50%. This was because in service conditions, the voltage ratio could reach 10% at the output side of converter [7]. To accelerate the aging of the samples and to see how polymer properties vary with AC/DC voltage ratios and superimposed frequencies, higher AC/DC voltage ratios (30% and 50%) were also selected. To assess the degree of aging of the polymer chemical properties, dissipation factor (*tanδ*) and dielectric constant (*ε'*) were investigated.

In this project, the DC voltage was chosen as 6 kV. This was because when higher DC voltages were applied, breakdown was happening within 10 mins at the 50% voltage ratio. When the DC voltage was much lower than 6 kV, it took several hours to see property changes as a result of aging. Therefore, 6 kV was a suitable choice. The DC electric field across the polymer was 6×10^4 kV/m. To achieve the 10%, 30% and 50% voltage ratios the AC peak values were chosen as 0.6 kV, 1.8 kV and 3 kV.

As the superimposed frequency of the resulting waveform in HVDC cable systems could be in the kHz frequency (as mentioned in Section 1.1.1), the aging frequencies were chosen as 1 kHz, 1.5 kHz, 2 kHz and 2.5 kHz.

3.2.4 Thermal Properties of the Polymers and Thermal Ageing Conditions

The thermal properties of HDPE and PP in terms of their melting behaviour are shown in the Differential Scanning Calorimetry (DSC) thermograms in Figure 3.8 and Figure 3.9 respectively.

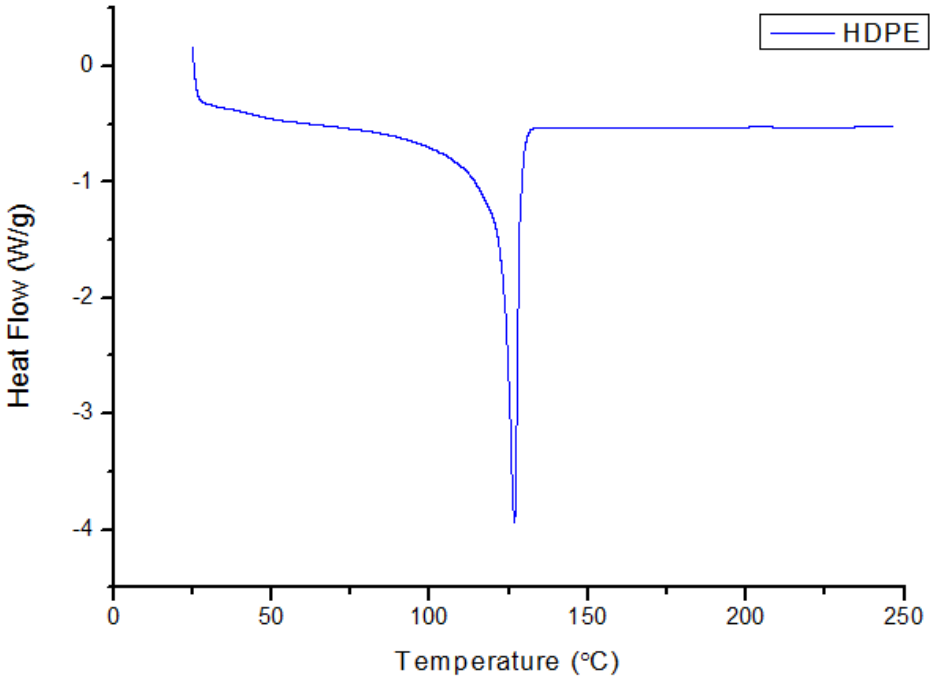

Figure 3.8. DSC result of HDPE.

From Figure 3.8, the melting temperature (T_m) of HDPE was 128°C. The aging temperature should be below the melting temperature of the material. As cable operating temperatures can reach 90°C [8], in this project, the aging temperature for HDPE was set as 90°C.

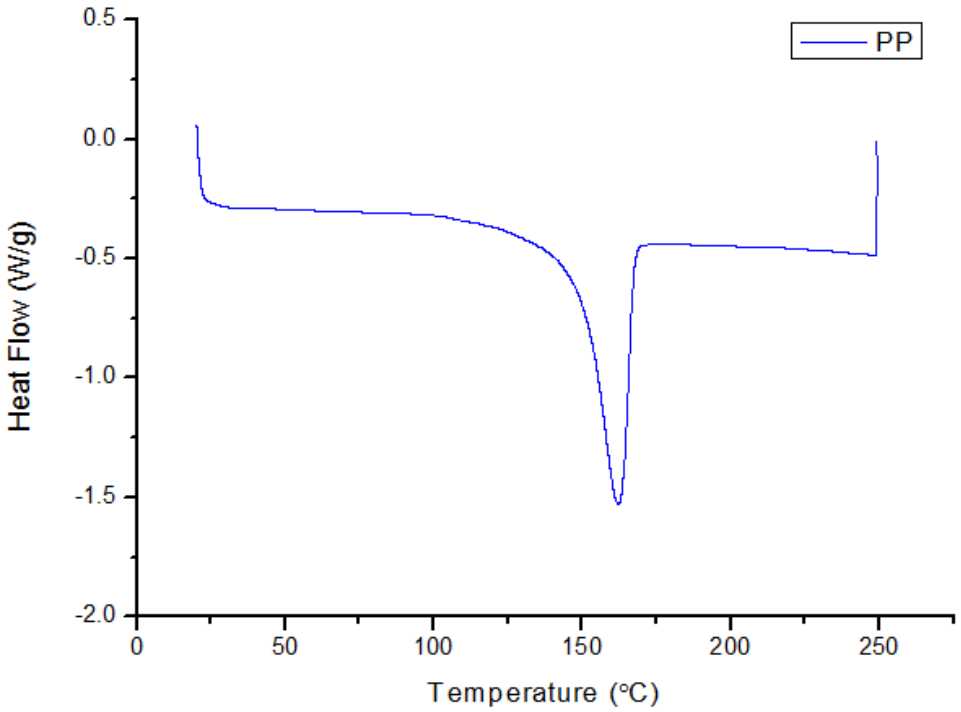

Figure 3.9. DSC result of PP.

From Figure 3.9, the melting temperature (T_m) of PP was 161°C. To allow comparison with the results of HDPE, PP was aged under 90°C as well. As PP has a higher melting temperature (compared with HDPE), PP cables may be operated at a higher temperature. To investigate the behaviour of PP at such higher temperatures, 110°C was chosen as a second aging temperature for PP.

From initial trials it was found that changes in the properties between the aged sample and the reference sample could be detected by DS and FTIR-ATR measurements without breakdown, with an aging duration of 1h. The 1h ageing duration was as a result of operational limitations in the amplifier used to generate the applied voltages.

The aging conditions of HDPE and PP are summarized in Table 3.3 and Table 3.4, respectively.

Table 3.3. Aging conditions of HDPE.

Conditions		Values
Temperature		90 °C
Voltage	DC	6 kV
	Ratio of AC ripple over DC voltage (*AC%*)	10%, 30% and 50%
Frequency		1 kHz, 1.5 kHz, 2 kHz and 2.5 kHz
Duration		1h

Table 3.4. Aging conditions of PP.

Conditions		Values
Temperature		90 °C and 110 °C
Voltage	DC	6 kV
	Ratio of AC ripple over DC voltage (*AC%*)	10%, 30% and 50%
Frequency		1 kHz, 1.5 kHz, 2 kHz and 2.5 kHz
Duration		1h

3.2.5 PD Detection System

As shown in Figure 3.4, the PD detection system consisted of a current transformer (CT), coaxial cables, an oscilloscope and a computer. The CT was a high frequency current transformer (HFCT, type KH-100M) with 2k-120MHz bandwidth and a sensitivity of 1mA-0.2mV. The computer was connected with the oscilloscope through a USB cable. The PD data was collected by LabVIEW virtual instrument.

As it was not possible to calibrate the experimental system in terms of charge, the recorded PD pulses are expressed in Volts in this study because the output of the HFCT is in Volts. However, this deficiency is not a problem because the author was looking at the relative behaviour of polymers after aging. During the one hour aging period, the system captured the resolved PD signals over 2 cycles of the AC component of the applied waveform every 2.4 seconds. When analyze the data, the first cycle of the 2 cycles is chosen. Therefore, 1500 packets of data was collected

during the 1h aging time.

The output signal of the CT includes substantial noise. The noise includes Gaussian white noise, random noise and the leakage current signal. To increase the accuracy of partial discharge signals analysis, it was necessary to carry out de-noising processing. As wavelet domain de-noising technology could decompose the PD signals in different frequency range, it is possible to set the threshold value in each frequency range to filter the corresponding Gaussian white noise. As PD signals also have a concussion index attenuation characteristic, the sym8 wavelet is much more suitable for PD signal analysis [9]. The wavelet analysis based on the sym8 package in Matlab is shown in Figure 3.10. The original and de-noised signal are shown in Figure 3.11 and Figure 3.12 respectively.

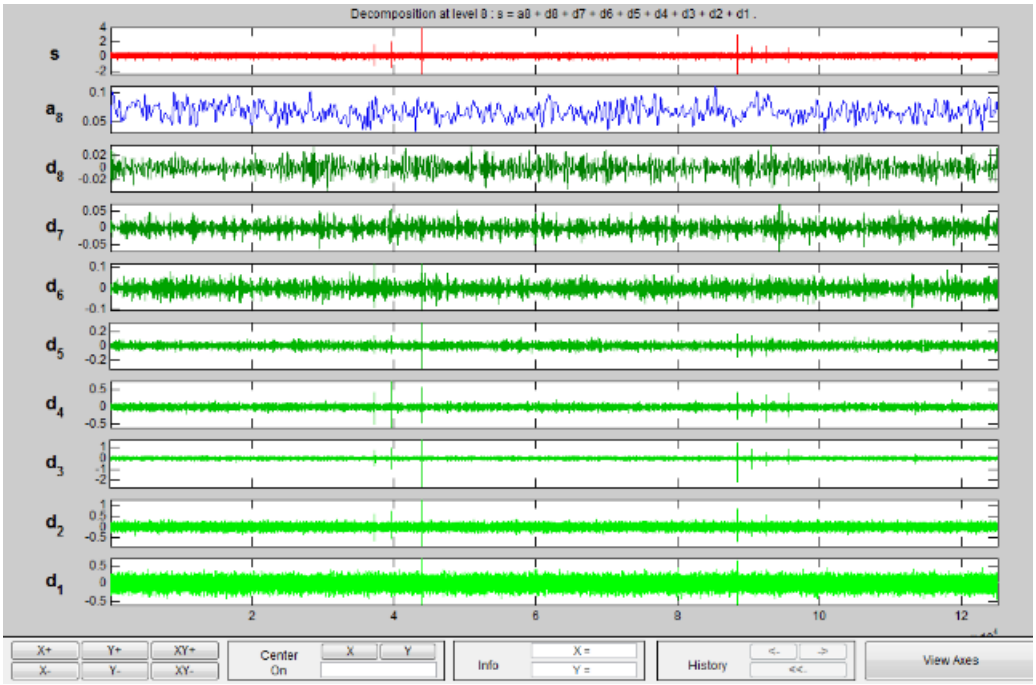

Figure 3.10. Wavelet analysis based on sym8.

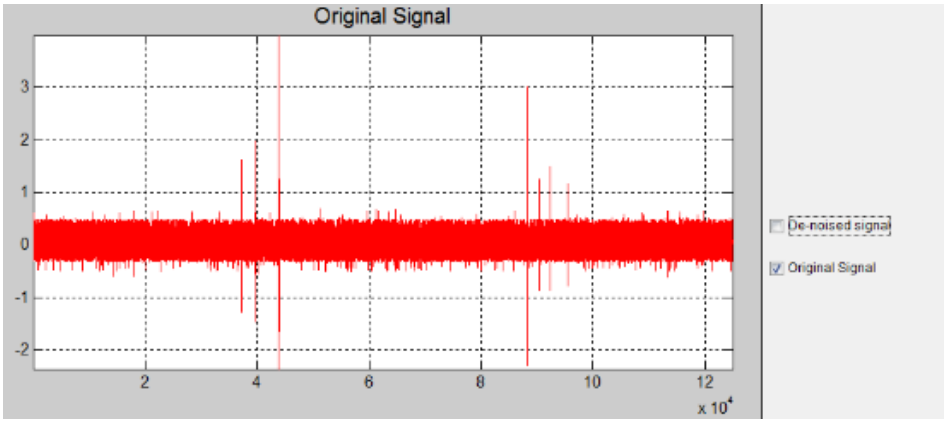

Figure 3.11. Original signal.

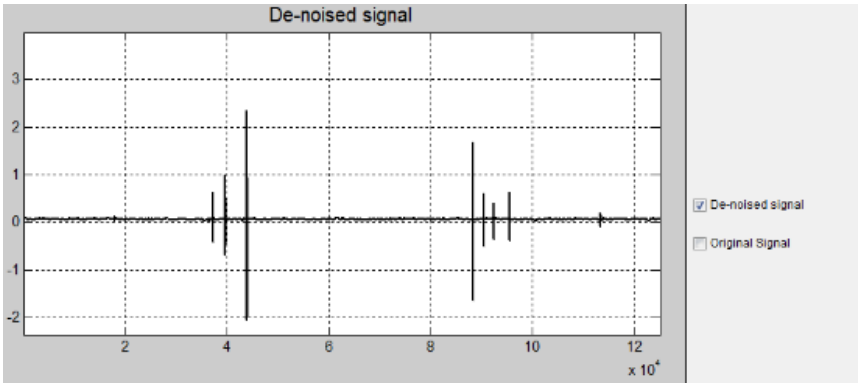

Figure 3.12. De-noised signal.

As the time for each PRPD measurement was 1 hour, there were 1500 packets of data collected in total. After MatLab processing, an Excel spreadsheet was generated. In the spreadsheet, each PD amplitude (v) and the corresponding AC source phase (ϕ) were recorded. According to the data from the spreadsheet, the equivalent PRPD plots (equivalent because charge in Coulombs was not used) could be generated. PD activity is related to the phase of the applied AC voltage. PD voltage amplitude was used to represent the PD charge. In this study, the PD mean amplitude, the number of discharges and the PD cumulative apparent energy E_{CA} and the apparent energy per second $\dot{E_{CA}}$ were used to describe the PD activities. The derivation of E_{CA} and $\dot{E_{CA}}$ is shown below.

For each PD pulse, real PD energy should be calculated by equation 3.6.

$$E = \frac{R_D}{g}\int_0^T V_{Meas}{}^2(t)dt \qquad 3.6$$

Where, E is real PD energy, R_D is the resistance of the discharge channel, g is trans-resistance gain of the current transformer, t is time, T is the pulse duration which is assumed to be constant. $v_{Meas}(t)$ is the measured voltage amplitude which changes with duration for each pulse,

$$V_{Meas}(t) = gI_D(t) \qquad 3.7$$

Where, I_D is the transient current flowing through the current transformer.

The total PD energy during aging will be the sum of the energy of each PD pulse as shown in equation 3.8, assuming that discharge channel resistance R_D was also constant.

$$\sum_{k=1}^{n} E_k = \sum_{k=1}^{n} \frac{R_D}{g}\int_0^T V_{Meas}{}^2(t)dt = \frac{R_D}{g}\sum_{k=1}^{n}\int_0^T V_{Meas}{}^2(t)dt \qquad 3.8$$

Where, E_k is real PD energy for each pulse, k is an index, n is the number of PD pulses. Assuming T is a constant, equation 3.8 could be changed to equation 3.9.

$$\sum_{k=1}^{n} E_k = \sum_{k=1}^{n} V_k{}^2 T \propto \sum_{k=1}^{n} V_k{}^2 \qquad 3.9$$

As the total PD energy calculated according to equation 3.9 is not real energy but should be proportional to the real energy, it was called the apparent cumulative energy E_{CA} in this study.

$$E_{CA} = \sum_{k=1}^{n} V_k{}^2 \qquad 3.10$$

The value of E_{CA} in equation 3.10 has been calculated over a fixed number of cycles of the applied voltage N. As different frequencies are being considered in the AC component of the sample electrical stress direct comparisons of E_{CA} may not be informative. Therefore a second parameter $\dot{E_{CA}}$, the apparent cumulative energy per second was calculated.

$$\dot{E_{CA}} = \frac{f}{N}E_{CA} \qquad 3.11$$

The parameter $\dot{E_{CA}}$ allows direct comparison between the experiments were different values of frequency for the superimposed AC waveform where used. It is equivalent to the average apparent power delivered by the PD activity.

PD results were gathered and processed for 7 samples for each test condition.

3.3 FTIR-ATR Measurement

The FTIR-ATR measurements were carried out by model Nicolet iS 16 produced by Thermo Fisher Company, which could measure the absorbance of the sample from 350 cm^{-1} to 4000 cm^{-1}. Three samples aged under the same sets of test conditions were used for the measurements. An aged sample is shown in Figure 3.13. The diameter of the region of discoloration, assumed to correspond to the area of aging, increases with the increase of superimposed frequency or increase of voltage ratio. The radius of the aging area reached a maximum of 6 mm for a voltage ratio of 50% and an AC frequency of 2.5 kHz. Initial measurements showed that more significant changes in the ATR spectra were observed at positions close to the center of the aged area as compared to measurements taken at the edge of the aged area. It was therefore decided to base the ATR measurements for each sample on six separate points in the aged area at a distance of 1mm from the centre of the aged area.

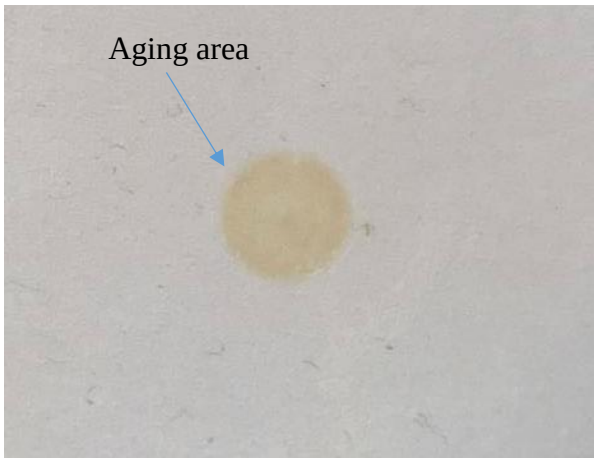

Figure 3.13. Aging area in HDPE.

3.4 Dielectric Spectroscopy Measurement

The broadband dielectric spectroscopy measurement was carried out by using a model Concept82, which was produced by NOVOCONTROL Company. The equipment could measure the dielectric response of the sample from 3 μHz to 3 GHz. Before doing the DS measurement, each sample should be placed in a gold plating machine to deposit a layer of gold through sputtering. The layer of gold was 20 *mm* in diameter on both faces and ensured good electrical contact with the electrodes. No Guard ring was used in the DS measurement. For each sample, the area directly below the electrode was the aging area (Figure 3.13). The DS results will provide information on dielectric properties of aging area for each condition. 3 samples were tested for each test condition.

The dielectric spectroscopy measurement provides information about the real part and the imaginary part of the complex permittivity as well as the dissipation factor. The data is stored in computer and displayed using WinDETA software. The structure of the test system is shown in Figure 3.14.

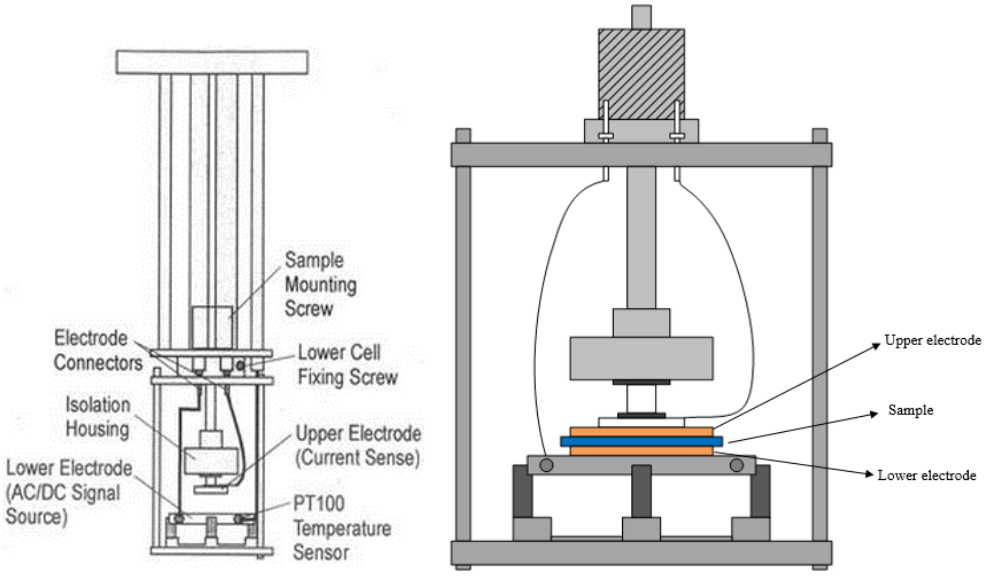

(a) (b)

Figure 3.14. Sample holder for dielectric spectroscopy [10].

3.5 References

[1] S. Amin and M. Amin, “Thermoplastic elastomeric (tpe) materials and their use in outdoor electrical insulation”, Reviews on advanced materials science, Vol. 29, pp.15-30, 2011.

[2] http://www.materials.unsw.edu.au/tutorials/online-tutorials/5-crystalline-or-amorphous [Accessed: 16 March 2016].

[3] http://www.differencebetween.com/difference-between-hdpe-and-vs-ldpe/ [Accessed: 16 March 2016].

[4] http://www.parsethylene-kish.com/UserFiles/Uploads/HDPE%20Corrugated [Accessed: 16 March 2016].

[5] http://www.essentialchemicalindustry.org/polymers/polypropene.html [Accessed: 16 March 2016].

[6] Ravindra Arora and Wolfgang Mosch, “High Voltage and Electrical Insulation Engineering”, Wiley-IEEE Press, Chapter 2, pp.11-68, 2011.

[7] P. K. Olsen, F. Mauseth and E. Iidstad, “The effect of DC superimposed AC Voltage on Partial Discharges in Dielectric Bounded Cavities”, International Conference on High Voltage Engineering and Application (ICHVE), pp.1-4, 2014.

[8] V. Buchholz, M. Colwell, H. E. Orton and J. Y. Wong, “Elevated temperature operation of XLPE distribution cable systems”, IEEE Transactions on Power Delivery, Vol.8, Issue 3, pp.743-749, 1993.

[9] NGO Xuan Thuy, “Analysis, Classification Partial Discharge with wavelet transform and artificial neural network”, http://eprints2.insa-strasbourg.fr/1016/1/GE5S-2011-NGO_Xuan_Thuy-Rapport_de_PFE.pdf, [Accessed: 1 April 2016].

[10] http://www.csr.res.in/dielectric_spectroscopy.html [Accessed: 16 March 2016].

4. HDPE Results

HDPE samples are aged at 90°C with a 6 kV DC voltage at 3 different AC/DC voltage ratios (10%, 30% and 50%) and four frequencies (1 kHz, 1.5 kHz, 2 kHz and 2.5 kHz). After ageing PRPD, FTIR-ATR and DS measurements were carried out for analysis. In this chapter, the data obtained is reported and summarized.

Section 4.1 presents the PRPD results. The mean $\overline{V_{PD}}$and standard deviation σ_{PD} of PD voltage, number of discharges n_{PD}, the apparent cumulative PD energy E_{CA} and the apparent cumulative energy per second $\dot{E}_{CA}$ are the indexes used to describe the PRPD results. How these indexes change with superimposed frequency and voltage ratio are shown. The standard deviation for PRPD results is within ±10% range.

Section 4.2 discusses a possible mechanism for the observed behaviour of the PRPD results.

Section 4.3 presents the FTIR-ATR results. The method used to calculate the Carbonyl Index (CI) as a way of assessing the degree of aging is introduced. The way that the CI of HDPE samples change with superimposed frequencies and voltage ratios is summarized. The standard deviation for FTIR-ATR results is within ±3% range.

Section 4.4 presents the DS results. The method of calculating the low frequency conductivity σ and a susceptibility index χI from the values of ε' and ε'' as a way of assessing the degree of aging is introduced. The behaviours of σ and χI with different superimposed frequencies and voltage ratios are summarized. The standard deviation for DS results is within ±2% range.

Section 4.5 examines the relationship of $\dot{E}_{CA}$, CI, σ and χI across the various experimental conditions.

Section 4.6 presents some general conclusions on the behaviour of the HDPE samples

under combined DC and AC electrical stress.

4.1 PRPD Results

When the voltage ratio is 10%, there was no detected PD signals at any of the AC frequencies considered. When *AC%* was increased to 30%, PD signals could be detected. The equivalent PRPD plots of samples aged by 30% AC/DC voltage ratio at frequencies of 1 *kHz* is shown in Figure 4.1.

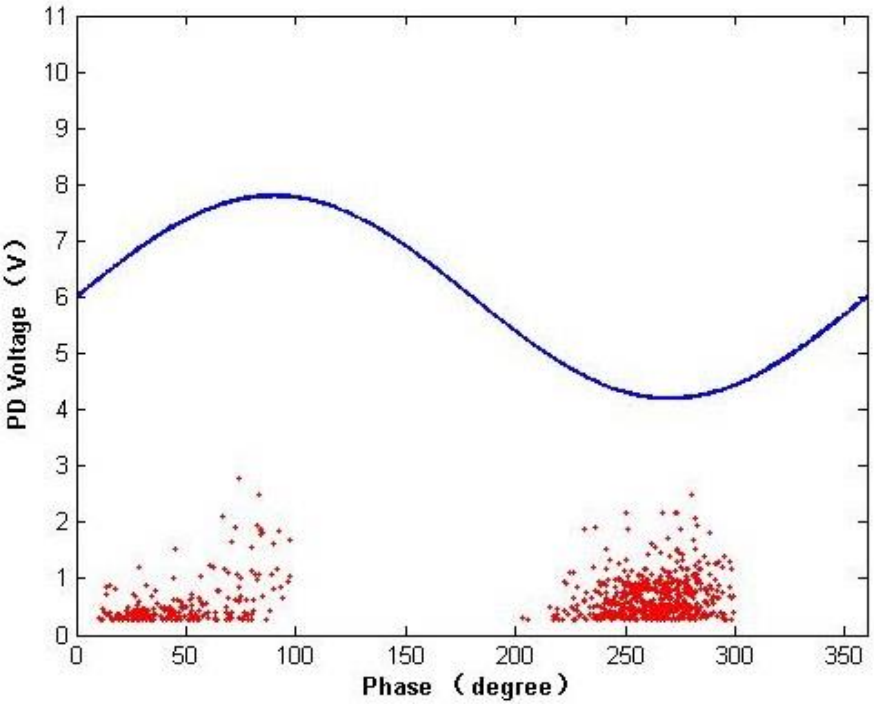

Figure 4.1. PRPD of HDPE aged with 1 *kHz*, 30% voltage ratio.

In Figure 4.1, the y-axis describes the measured discharge amplitudes in unit of volts. In the first half cycle, PD generally occurs in the rising 1st quadrant of the applied voltage. In the second half cycle, PD generally appears in the falling 3rd quadrant.

The equivalent PRPD plots of samples aged by 50% AC/DC voltage ratio at frequencies of 1 *kHz* is shown in Figure 4.2. Compared with Figure 4.1, the amplitudes of PD in Figure 4.2 have doubled in both the 1st quadrant and the 3rd quadrant. In Figure 4.2, the phase dependence of PD in the 1st quadrant is similar with

that in Figure 4.1, while the phase of PD in 3rd quadrant shifts about 20 degree to about 180 degrees. A possible explanation of this behaviour is discussed in Section 4.2.

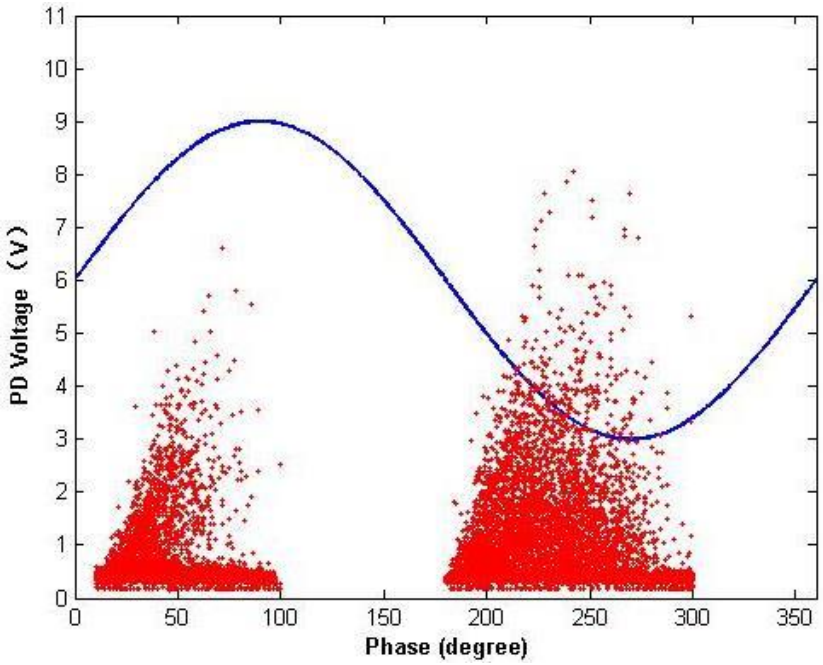

Figure 4.2. PRPD of HDPE aged with 1 *kHz*, 50% voltage ratio.

The equivalent PRPD plots of samples aged by 50% voltage ratio at frequencies of 1.5, 2 and 2.5 *kHz* are shown in figures 4.3-4.5.

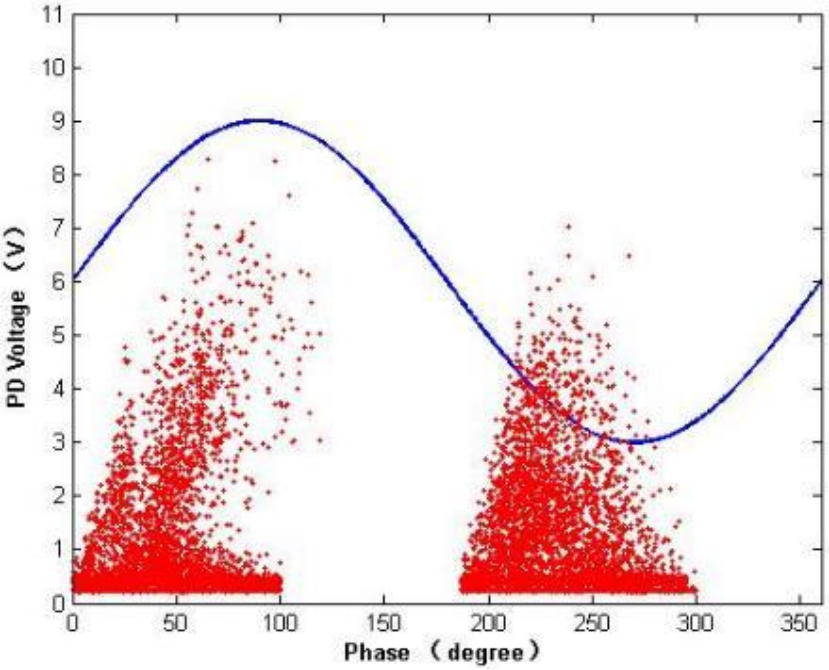

Figure 4.3. PRPD of HDPE aged with 1.5 *kHz*, 50% voltage ratio.

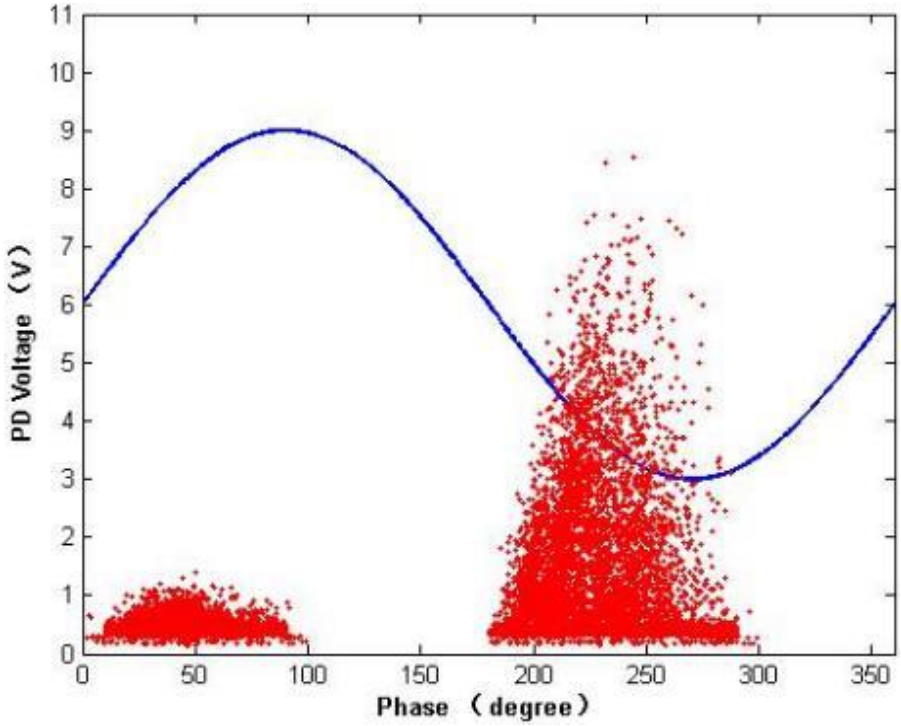

Figure 4.4. PRPD of HDPE aged with 2 *kHz*, 50% voltage ratio.

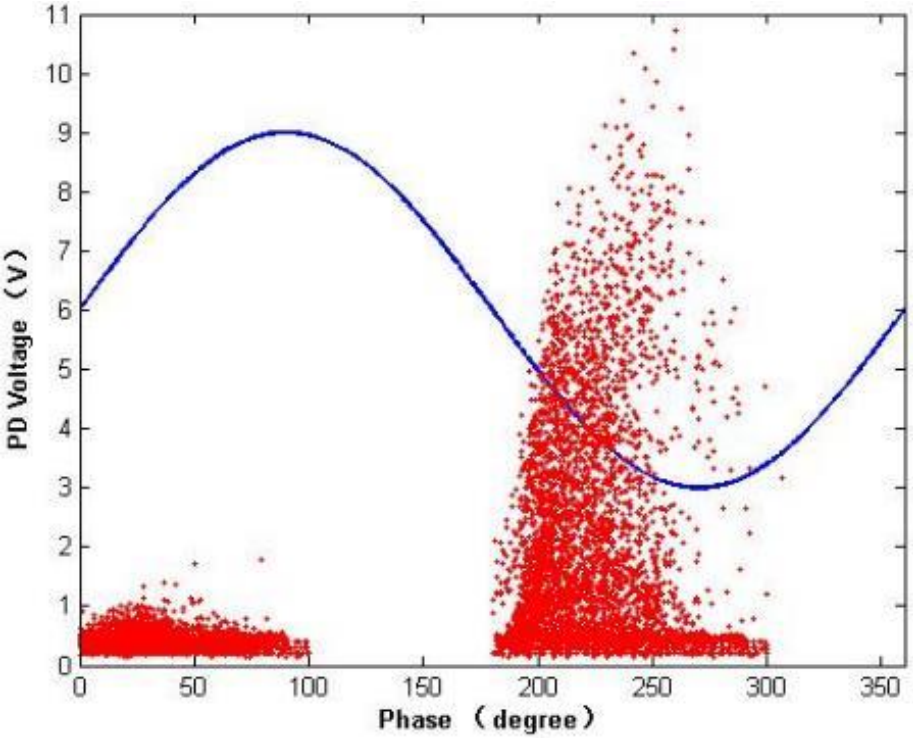

Figure 4.5. PRPD of HDPE aged with 2.5 *kHz*, 50% voltage ratio.

Figure 4.2-4.5 shows that with the superimposed frequency increasing, the discharge amplitudes decreases in the 1st quadrant. In the third quadrant there is a significant increase in discharge amplitudes at 2.5 *kHz* and a suggestion of an increase of amplitude with frequency at lower frequencies. Similar changes are observed in the data for the 30% voltage ratio in HDPE but the changes in the first and third quadrant are smaller. The number of PD pulses per cycle decreases with increasing frequency. As the AC frequency increases the period of the waveform decreases and, given that the recording time is fixed by the number of cycles recorded and so will decrease, therefore the number of PD events recorded would be expected to decrease.

To help to analyse the PD activity over all the cycles during the aging period, four initial parameters were calculated: the number of discharges n_{PD}, the mean PD voltage $\overline{V_{PD}}$, the standard deviation of the PD voltages σ_{PD} and E_{CA} the apparent cumulative energy, see Section 3.2.5. The data is summarized in Figure 4.6 – Figure 4.8, Table 4.1 - Table 4.5.

As PD only appears at 30% and 50% voltage ratio, the mean PD voltage with standard

deviation of HDPE is shown in Table 4.1.

Table 4.1. Mean PD voltage with standard deviation of HDPE at 30% and 50% voltage ratios.

Frequency (kHz)	PD voltage (V) at 30% voltage ratio		PD voltage (V) at 50% voltage ratio	
	$\overline{V_{PD}}$	σ_{PD}	$\overline{V_{PD}}$	σ_{PD}
1	0.237	0.022	0.72	0.065
1.5	0.241	0.027	0.76	0.073
2	0.247	0.03	0.81	0.076
2.5	0.251	0.036	1.08	0.113

Figure 4.6 can be drawn according to the data in Table 4.1.

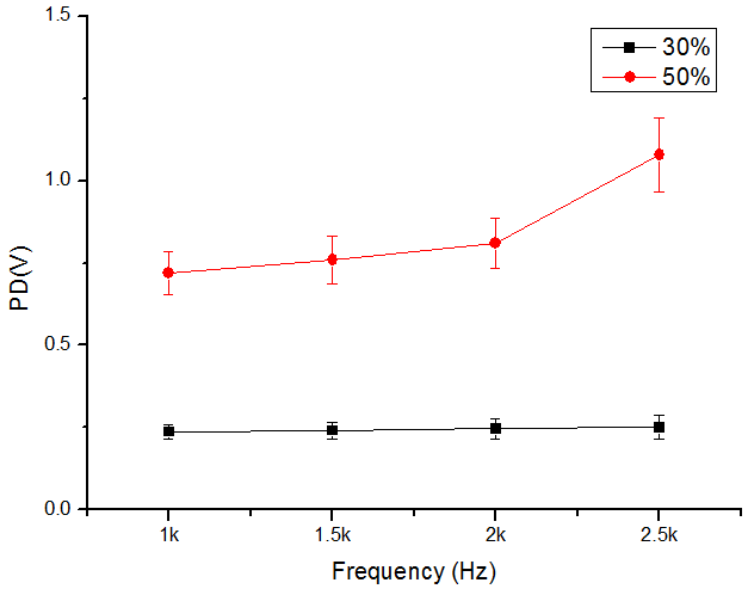

Figure 4.6. Mean with standard deviation of PD voltage.

In Figure 4.6, for the HDPE samples aged at 30% voltage ratio, $\overline{V_{PD}}$ is around 0.25 V. The value does not change too much with change of superimposed frequency. For the HDPE samples aged at 50% voltage ratio, $\overline{V_{PD}}$ is more than three times the value at 30% voltage ratio. In addition when the superimposed frequency is below 2 *kHz*, the mean PD voltage increases slowly with superimposed frequency and it is around 0.8 *V* at 2 *kHz*. The value increases rapidly to about 1.1 *V* when the superimposed frequency increases to 2.5 kHz. Possible reasons for this difference in the behaviour of $\overline{V_{PD}}$ as a

function of voltage ratio and frequency are discussed in Section 4.2.

Data on the number of discharges recorded n_{PD} and the total measurement time $T_{Meas} = 1500/f$ is shown in Table 4.2 and Table 4.3 for 30% and 50% voltage ratio, respectively. From n_{PD} and T_{Meas} the mean discharge rate $\dot{n}_{PD} = n_{PD}/T_{Meas}$ can be calculated.

Table 4.2. Number of discharges of HDPE at 30% voltage ratio.

Frequency (kHz)	n_{PD}	T_{Meas}(s)	$\dot{n}_{PD}(s^{-1})$
1	6619	1.5	4413
1.5	6612	1	6612
2	6571	0.75	8761
2.5	6513	0.6	10855

In Table 4.2, there is little change in the n_{PD} as the frequency is changed. However when the difference in period of the AC stress component is taken into account it can be seen that the mean discharge rate $\dot{n}_{PD}$ was increasing.

Table 4.3. Number of discharges at 50% voltage ratio.

Frequency (kHz)	n_{PD}	T_{Meas}(s)	$\dot{n}_{PD}(s^{-1})$
1	19030	1.5	12687
1.5	17534	1	17534
2	16337	0.75	21783
2.5	13289	0.6	22148

Superimposed frequency vs. $\dot{n}_{PD}$ is shown in Figure 4.7, the data is according to that in Table 4.2 and Table 4.3.

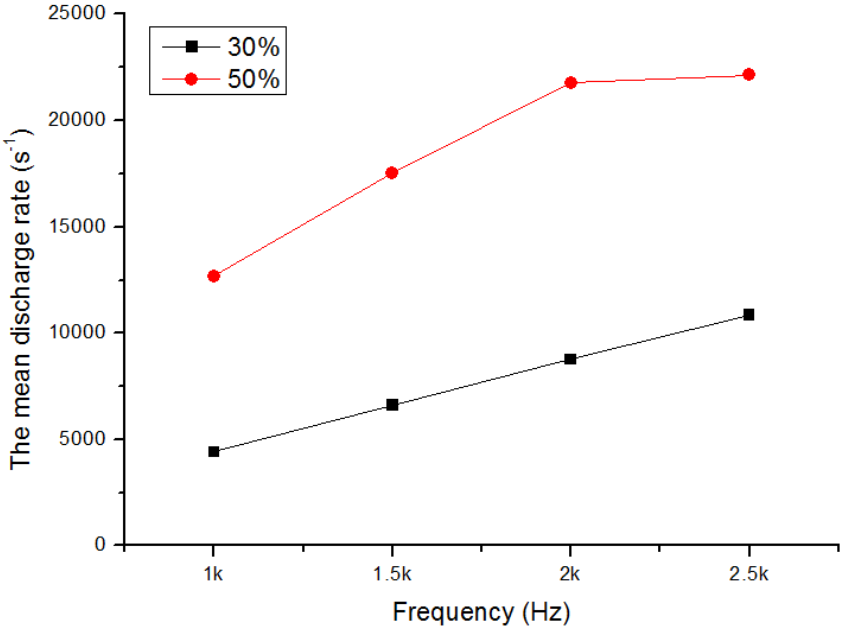

Figure 4.7. $\dot{n}_{PD}(s^{-1})$ of HDPE at 30% and 50% voltage ratio.

In Figure 4.7, $\dot{n}_{PD}(s^{-1})$ increases with the increase in the superimposed frequency in each curve. For HDPE aged at 30% voltage ratio, $\dot{n}_{PD}(s^{-1})$ increases with the superimposed frequency in 5000-10000 range. For HDPE aged at 50% voltage ratio, the value is at least 2 times that of 30% voltage ratio at each frequency.

Data of apparent cumulative energy E_{CA} and the apparent cumulative energy per second $\dot{E}_{CA}$ at 30% and 50% voltage ratio is shown in Table 4.4 and Table 4.5, respectively.

Table 4.4. Apparent cumulative energy per second of HDPE at 30% voltage ratio.

Frequency (kHz)	E_{CA}	T_{Meas}(s)	$\dot{E}_{CA}$
1	1569	1.5	1046
1.5	1593	1	1593
2	1623	0.75	2164
2.5	1635	0.6	2725

Table 4.5. Apparent cumulative energy per second of HDPE at 50% voltage ratio.

Frequency (kHz)	E_{CA}	T_{Meas}(s)	$\dot{E}_{CA}$
1	13702	1.5	9135
1.5	13326	1	13326
2	13233	0.75	17644
2.5	14352	0.6	23920

Figure 4.8 is drawn according to the data from Table 4.4 and Table 4.5.

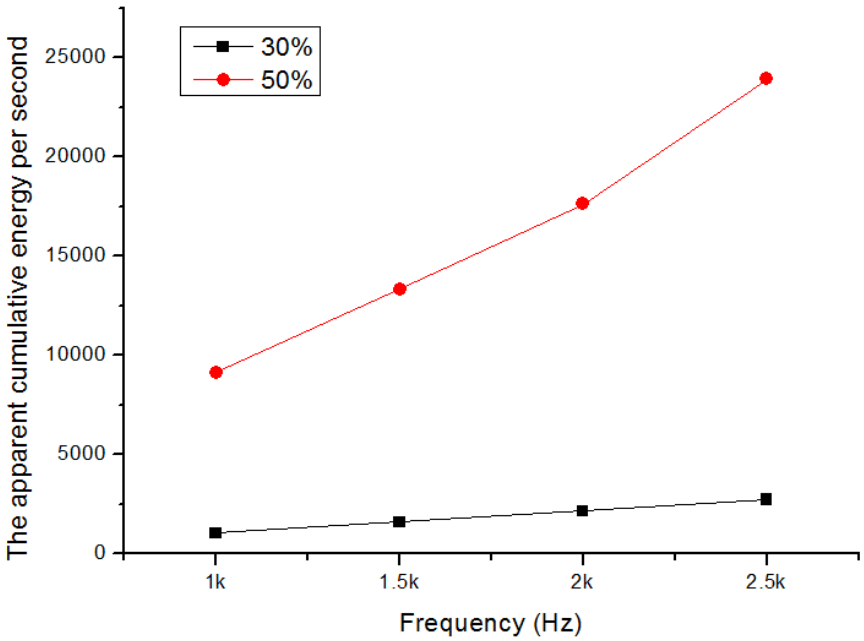

Figure 4.8. $\dot{E}_{CA}$ of HDPE at 30% and 50% voltage ratio.

In Figure 4.8, $\dot{E}_{CA}$ of each voltage ratio increases with the increase in the superimposed frequency. At 30% voltage ratio, the value increases steadily in the range from 1000 to 3000. At 50% voltage ratio, the values are significantly higher than the corresponding values at the 30% voltage ratio at each frequency. The value is about 9000 at 1 *kHz* and as the superimposed frequency increases, the value rapidly increases to about 24000 at 2.5 *kHz*.

4.2 Proposed Mechanism of Partial Discharge

The discharge patterns observed are broadly similar to those reported in [1] and are typical of surface discharges occurring in the system. The authors in [1] attributed the small number of discharges in the first quadrant to the low probability of initiating electrons being produced from the dielectric surface. The higher number of discharges in the third quadrant was associated with the greater number of initiating electrons

that would be produced from the metallic electrode when it is at a more negative potential than the polymer surface. However in their work a simple AC field was being applied across the system. The situation in this experimental work is more complex. If simple capacitive division is considered under combined AC and DC stress the voltage difference between the electrode and the surface does not become negative when the phase angle is greater than 180° due to the presence of the DC component of the voltage at the surface of the polymer. The voltage difference is greater during the first half cycle than the second half cycle. From results presented for a void under combined AC and DC stressing [2] the majority of discharges were observed in the first quadrant which would be expected as the electrons would always be emitted by a polymer surface in a void so no change in the number of electrons initiating avalanches would be expected with different gap polarities. To explain the discharge pattern observed charge transfer due to PD activity must be taking place to increase the DC potential of the surface to a level that causes field reversal in the third cycle allowing the higher electron emissivity of the metal electrode to come into play.

This process can be explained as Figure 4.9. Assume external voltage is V_E and the resulting potential distribution on the surface as a function of radial position on the surface is $V_S(r)$.

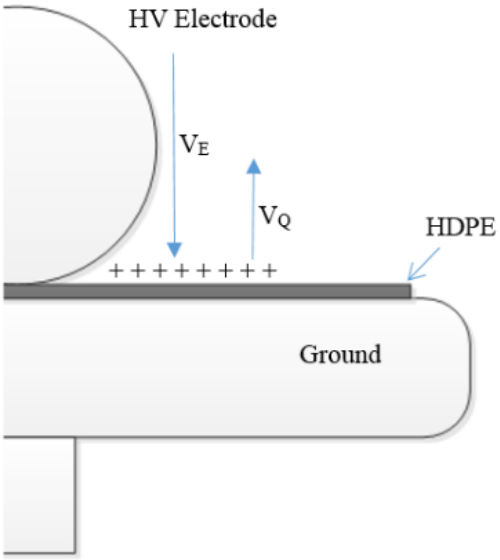

Figure 4.9. Mechanism of PD during aging.

The voltage across the gap will be given by:

$$V_I(r) = V_E - V_S(r) = \big(1 - \alpha(r)\big)V_E \qquad 4.1$$

Where $\alpha(r)$ is a function depending on the system geometry in the range of $0 \leq \alpha(r) \leq 1$. At the limits of r, $\alpha(0) = 1$ and $\alpha(\infty) = 1$. At any point on the surface the potential across the gap due to the combined stress will be positive and have a maximum value when the AC voltage is at its +ve peak and at its minimum when the AC voltage is at its –ve peak.

Therefore in the first quarter cycle, when $V_I(r)$ exceeds the partial discharge inception voltage (PDIV), PDs will occur in the air gap in the triple junction (the area between the sphere electrode and upper surface of the sample) and also possibly across the surface of the sample. The direction of the field which is from the electrode to the surface will cause electrons to move to the electrode and positive ions created during the discharge to move to the surface of the HDPE. The positive charges establish an additional potential on the surface $V_Q(r)$. The resulting voltage $V_I(r)$ across the triple junction is:

$$V_I(r) = \big(1 - \alpha(r)\big)V_E - V_Q(r) \qquad 4.2$$

This reduction in the voltage across the region of discharge activity means that to reach the PDIV, V_E needs to increase which will occur in the first quarter cycle. In the second quarter cycle, as V_E and V_S decrease, $V_Q(r)$ will tend to surpress partial discharge activity. If the charge is still present on the surface during the next positive half cycle then $V_Q(r)$ will tend to surpress the PD activity in this half cycle.

During the negative half cycle if sufficient charge has been deposited on the surface $V_Q(r)$ may become sufficiently large that although the value of V_E and therefore $V_S(r)$ will always be positive with $V_E > V_S(r)$ the value of $V_I(r)$ can become negative. This occurs in the regions where

$$V_Q(r) > \big(1 - \alpha(r)\big)V_E$$

This field reversal allows the greater electron emissivity of the metal electrode to come into play leading to a large number of discharges occurring.

As the magnitude of the superimposed AC voltage increases, $V_Q(r)$ increases and the decrease in V_E in the second half cycle results in larger negative values of $V_I(r)$ and therefore greater discharge activity in the third quadrant.

The value of $V_Q(r)$ will tend to decrease with time due to charge mobility across the surface. It is known, the charge dissipation rate has a positive relation with the charge mobility. More transfer of charge per cycle, across the surface away from the triple junction, will occur at lower frequencies due to the longer period. Therefore the value of $V_Q(r)$ is likely to be smaller at lower frequencies leading to less discharge activity in the third quadrant. This approach provides an explanation for the observed discharge pattern. However it does not include the effects of the charge transfer in the third quadrant on the value of V_Q. This requires further investigation to look at the competing processes of higher electron emission and reduced voltage across the gap and surface.

4.3 FTIR-ATR Result

In this section, the FTIR-ATR results and analysis of the Carbonyl Index will be demonstrated. The Carbonyl Index provides a way to estimate the degree of aging that has occurred in the sample.

Details of the main peaks of reference for HDPE are shown in Table 4.6.

Table 4.6. Wavenumber and vibration of main peaks in HDPE [3].

Wavenumber (cm^{-1})	Vibration
2914	CH_2 asymmetric stretching
2847	CH_2 symmetric stretching
1472 and 1461	Bending deformation
1378	CH_3 symmetric deformation
1367 and 1353	Wagging deformation
1302	Twisting deformation
718 and 730	Rocking deformation

In Table 4.6, the reference for HDPE mainly consists of methylene groups. Methylene groups can be described with four peaks, 2914 cm^{-1}, 2847 cm^{-1}, 1472 cm^{-1} and 718 cm^{-1}. Among them, 1472 cm^{-1} and 718 cm^{-1} can be divided into 1472 cm^{-1} and 1461 cm^{-1}, 730 cm^{-1} and 718 cm^{-1}, respectively.

When the HDPE samples are aged, hydroxyl groups (O-H) and carbonyl groups (C=O) can occur [4]. The O-H group appears between 3500 cm^{-1} to 3000 cm^{-1}. The C=O group appears between 1750 cm^{-1} and 1600 cm^{-1}. The C-O group which may also occur during ageing, appears at 1200 cm^{-1}. The likely aging mechanism will involve chain scission with subsequent reactions causing the formation of O-H and C=O groups in the sample. If this process is occurring, it would be expected that the methylene peaks in the spectra would be reduced while the peaks associated with carbonyl groups would increase. Carbonyl Index (CI), an index of aging, is defined as the ratio of the absorbance of the carbonyl group A_{1720} to that of the absorbance at 1463 cm^{-1} [5-7]. For HDPE, CI is shown in equation 4.3 [8]:

$$CI = \frac{A_{1720}}{A_{1463}} \tag{4.3}$$

The FTIR-ATR results of HDPE, which change with superimposed AC power frequency and with three voltage ratios, are shown in Figure 4.10-4.21.

4.3.1 10% Voltage Ratio

Full-scale and detailed sectional views of FTIR-ATR spectra at 10% voltage ratio are shown in Figure 4.10-4.13. When a HDPE sample is subjected to DC stress at 90°C, the intensity of peaks at 2914 cm^{-1} and 2847 cm^{-1} are lower than in the reference see Figure 4.11. Any increase in the peaks associated with the carbonyl group is hard to see Figure 4.13. This suggests that aging is occurring at a relatively low rate under DC conditions. When HDPE samples are aged under combined AC and DC stresses, the changes in the peaks at 2914 cm^{-1} and 2847 cm^{-1} show a further slight decrease in intensity. This suggests that aging is occurring at a higher but still relatively low rate under combined AC and DC stress at 10% voltage ratio.

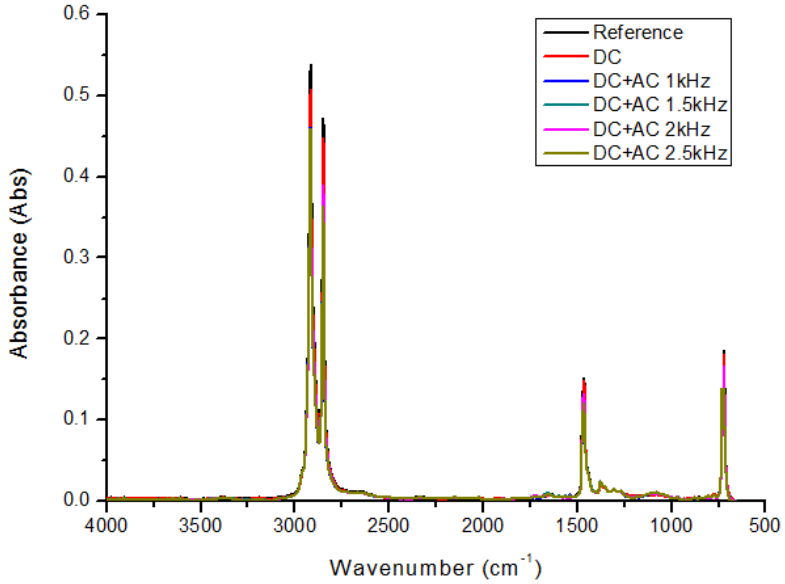

Figure 4.10. FTIR-ATR results of HDPE (aged under 10% voltage ratio at various frequencies).

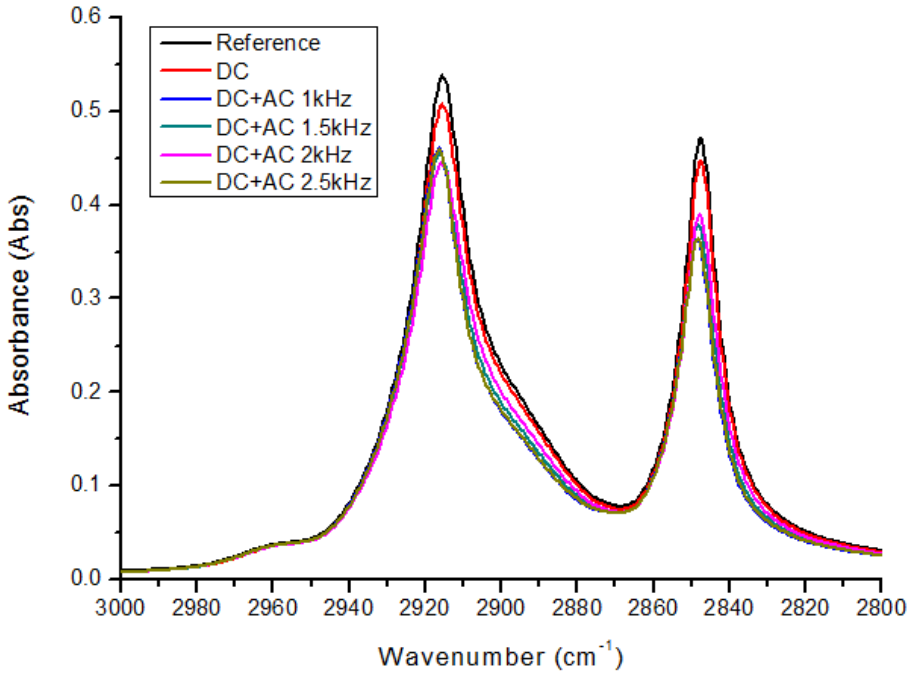

Figure 4.11. FTIR-ATR results for HDPE detailed view of C-H-groups (aged under 10% voltage ratio at various frequencies).

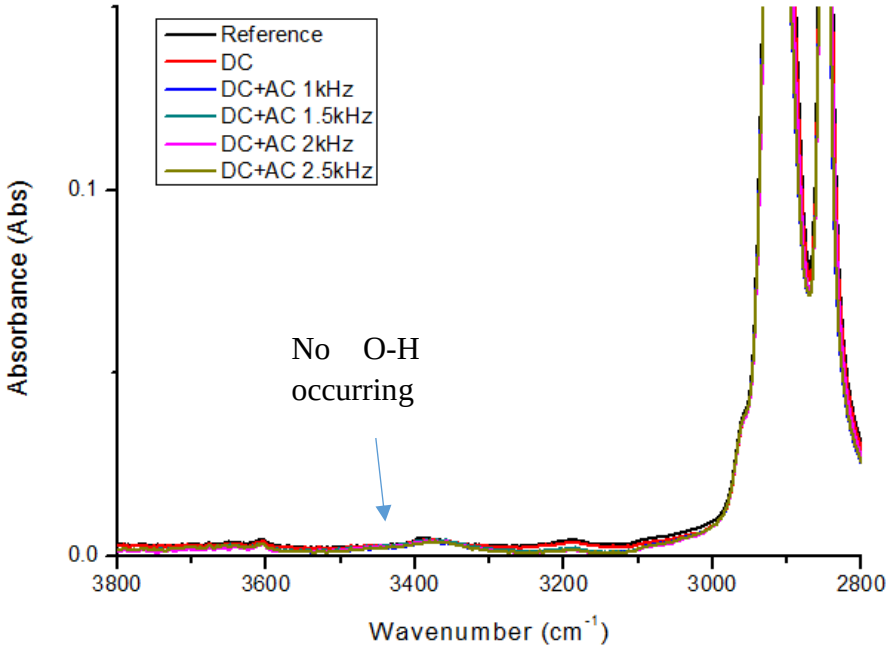

Figure 4.12. FTIR-ATR results for HDPE detailed view of OH-group (aged under 10% voltage ratio at various frequencies).

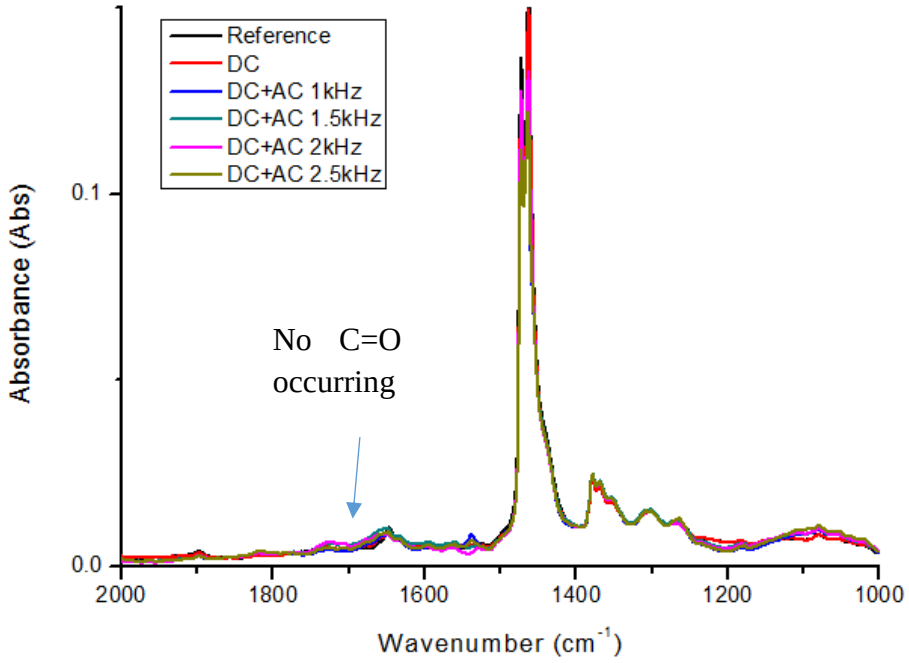

Figure 4.13. FTIR-ATR results for HDPE detailed view of carbonyl group and C-O group (aged under 10% voltage ratio at various frequencies).

4.3.2 30% Voltage Ratio

Full-scale and detailed views of FTIR-ATR spectra at 30% voltage ratio are shown in Figure 4.14-4.17. The spectra for unaged samples and for samples subjected to a purely DC stress are included for reference. Figure 4.15 shows the methylene group absorption bands at 2914 cm^{-1} and 2847 cm^{-1} in HDPE. The absorption of the methylene groups for all aged samples are less than the reference unaged sample. The effect on the absorption of the methylene groups for the HDPE aged by combined voltages is more significant than for the sample aged only with DC. The change in absorption also depends on the superimposed frequency. Looking at the intensity due to the carbonyl groups in Figure 4.17 show there is no change between the reference unaged sample and the DC sample. When samples are subject to combined AC and DC voltages, the change in absorption indicates that C=O groups are being created. The absorption of C=O groups is dependent on the superimposed frequency. These changes indicated that an oxidative aging process is occurring and that it is enhanced by the combination of AC and DC voltages.

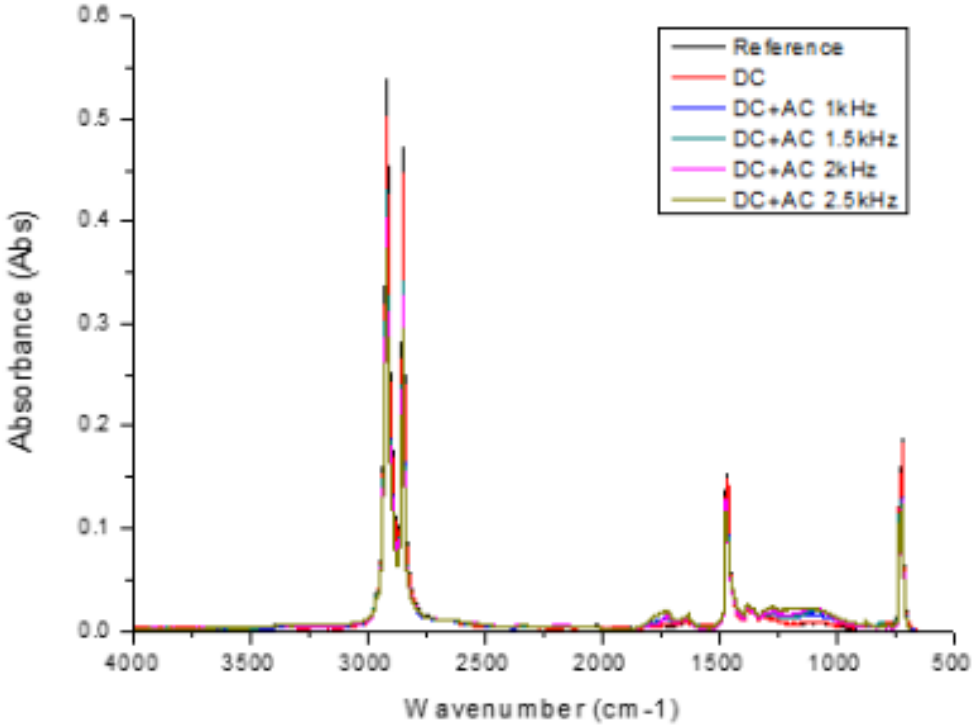

Figure 4.14. FTIR-ATR results of HDPE (aged under 30% voltage ratio at various frequencies).

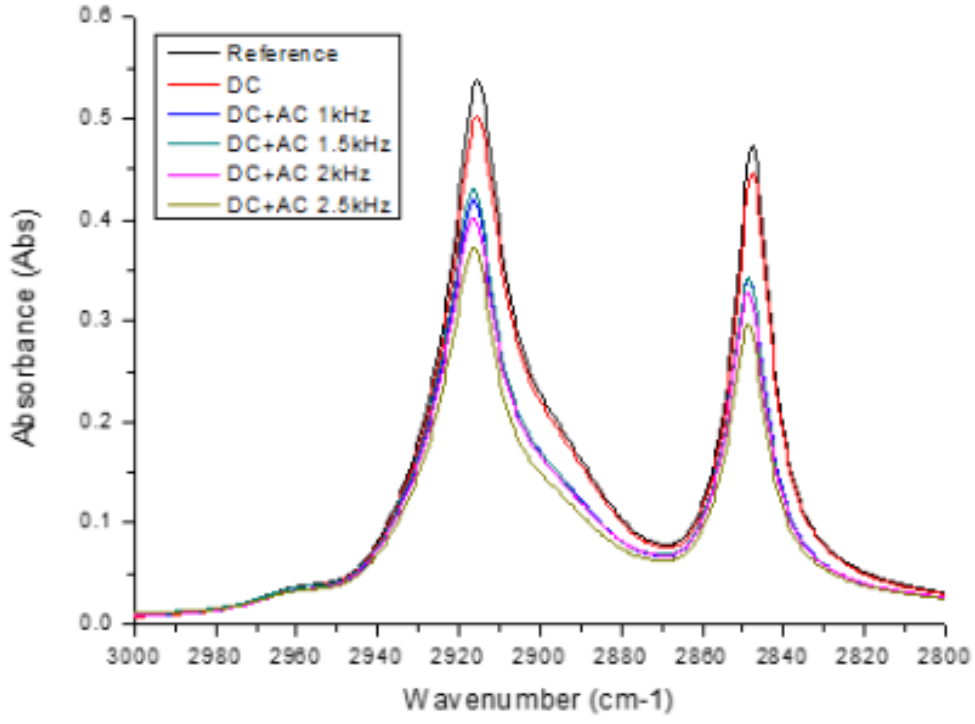

Figure 4.15. FTIR-ATR results for HDPE detailed view of C-H-groups (aged under 30% voltage ratio at various frequencies).

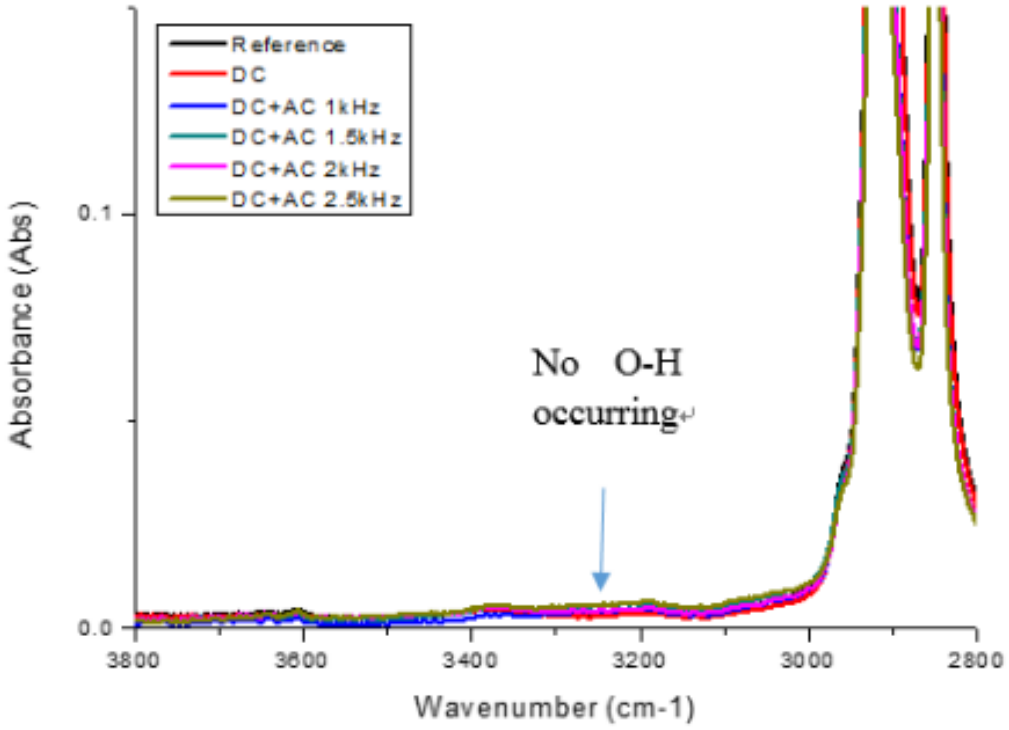

Figure 4.16. FTIR-ATR results for HDPE detailed view of OH-group (aged under 30% voltage ratio at various frequencies).

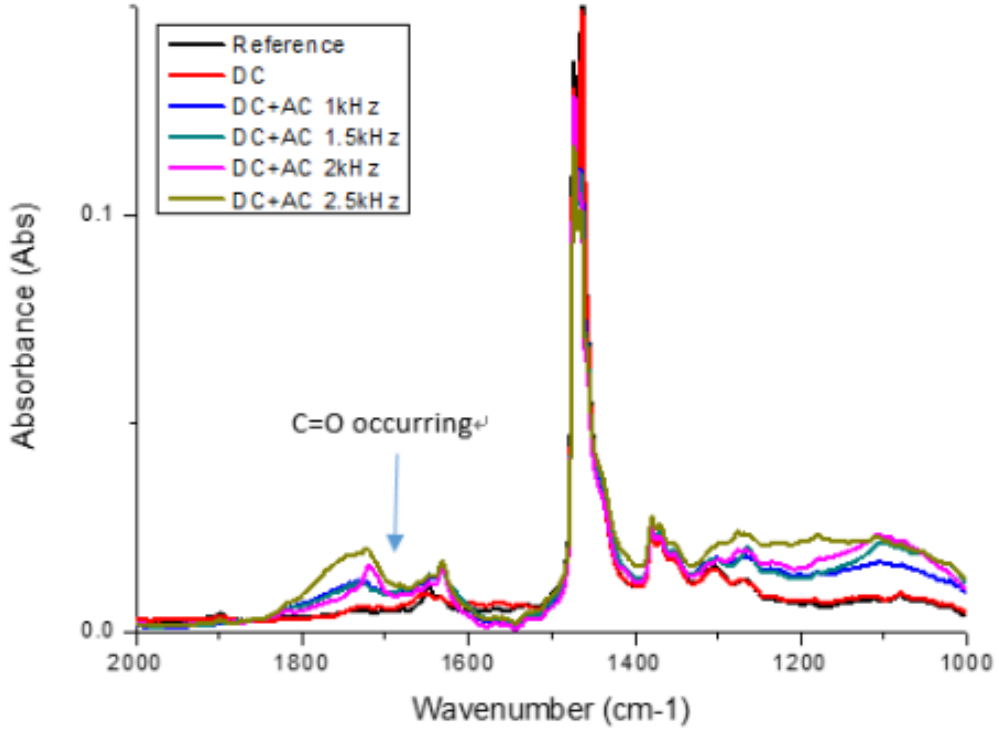

Figure 4.17. FTIR-ATR results for HDPE detailed view of carbonyl group and C-O group (aged under 30% voltage ratio at various frequencies).

4.3.3 50% Voltage Ratio

Full-scale and detailed views of FTIR-ATR spectra at 50% voltage ratio are shown in Figure 4.18-4.21. The behaviour is similar to that observed at 30% voltage ratio with the decrease in methylene absorption being dependent on the superimposed frequency and carbonyl absorption observed in samples aged by AC and DC superimposed voltages. However, at 50% voltage ratio, there is evidence of the formation of O-H groups and C-O groups which is not observed at 30% voltage ratio. The absorption of O-H and C-O groups is enhanced by increasing of superimposed frequency.

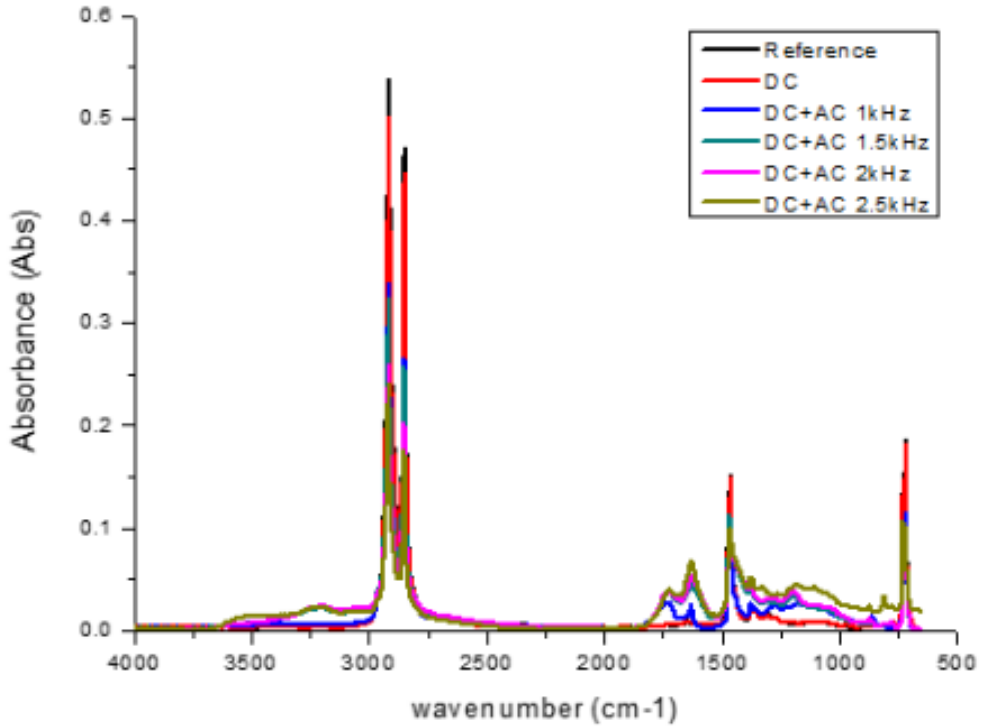

Figure 4.18. FTIR-ATR results of HDPE (aged under 50% voltage ratio at various frequencies).

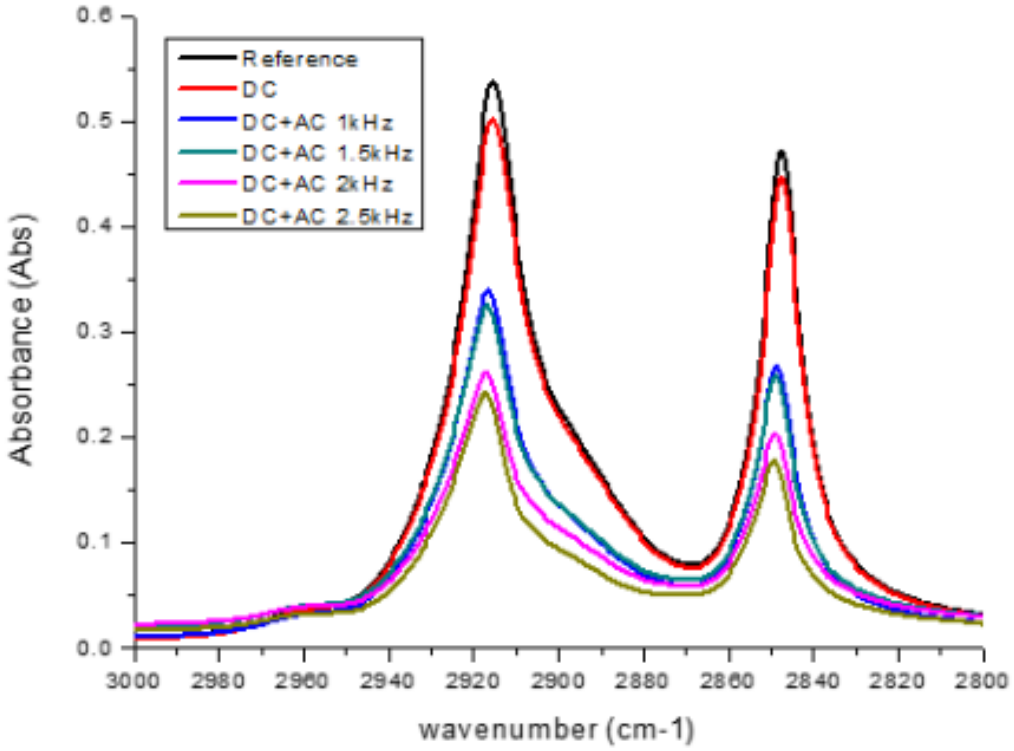

Figure 4.19. FTIR-ATR results for HDPE detailed view of C-H-groups (aged under 50% voltage ratio at various frequencies).

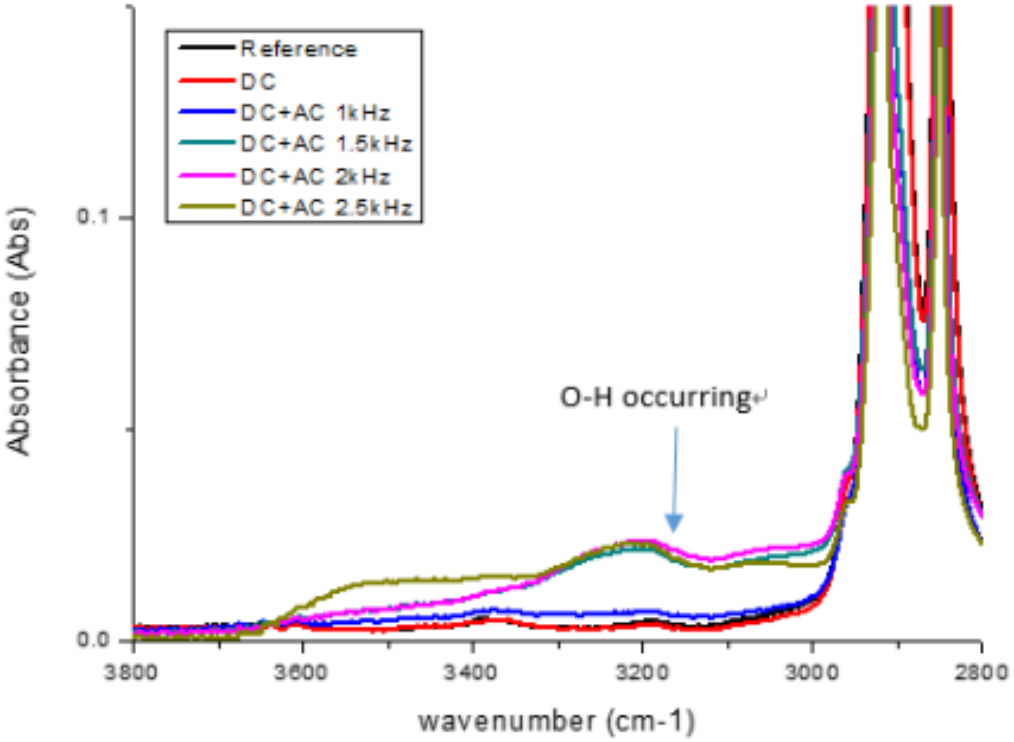

Figure 4.20. FTIR-ATR results for HDPE detailed view of OH-group (aged under 50% voltage ratio at various frequencies).

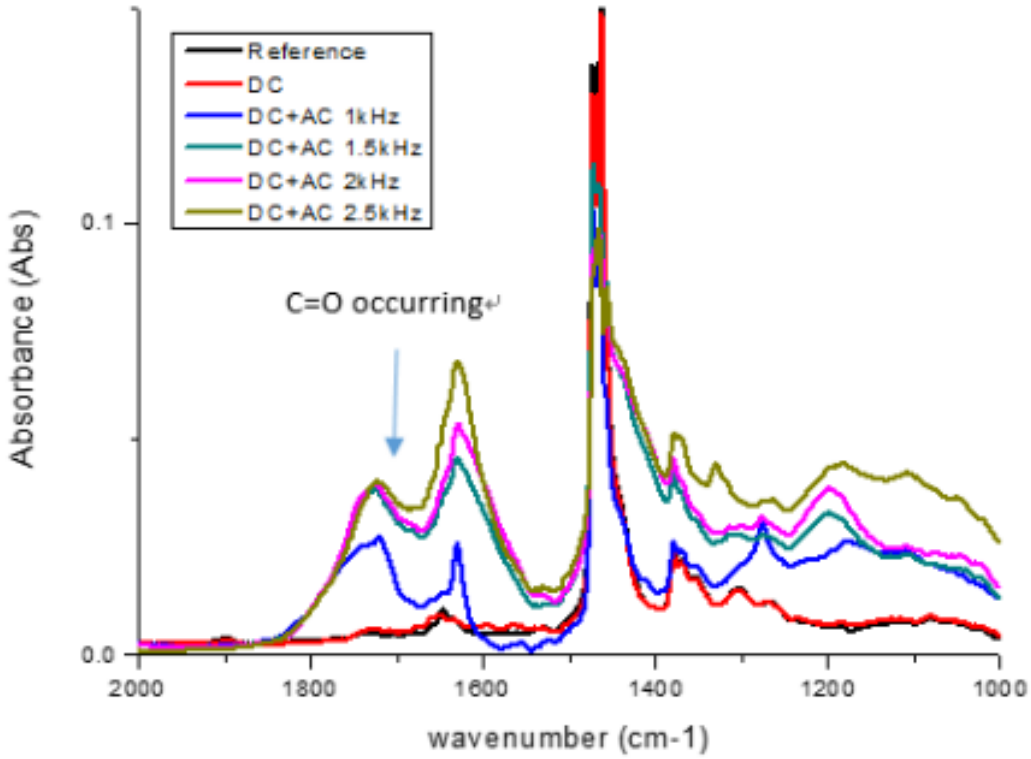

Figure 4.21. FTIR-ATR results for HDPE detailed view of carbonyl group and C-O group (aged under 50% voltage ratio at various frequencies).

4.3.4 Carbonyl Index Comparison

According to Figure 4.10-4.21 and Carbonyl Index (CI) equation (4.3), the CI of HDPE aged at 30% and 50% voltage ratio can be summarized in Table 4.7 and Table 4.8, respectively. As there was no absorption observed at 1720 cm^{-1} the CI for 10% voltage ratio HDPE will be zero.

Table 4.7. Carbonyl Index of HDPE aged at 30% voltage ratio.

Frequency (kHz)	A_{1720}	A_{1463}	CI
1	0.0109	0.1187	0.0921
1.5	0.0117	0.1183	0.0986
2	0.0154	0.1153	0.1336
2.5	0.0198	0.1151	0.1719

Table 4.8. Carbonyl Index of HDPE aged at 50% voltage ratio.

Frequency (kHz)	A_{1720}	A_{1463}	CI
1	0.0274	0.1088	0.2523
1.5	0.0378	0.1024	0.3689
2	0.0390	0.0898	0.4339
2.5	0.0402	0.0851	0.4728

Based on the data in Table 4.7 and Table 4.8, CI of HDPE aged at 30% and 50% voltage ratio is summarized in Figure 4.22.

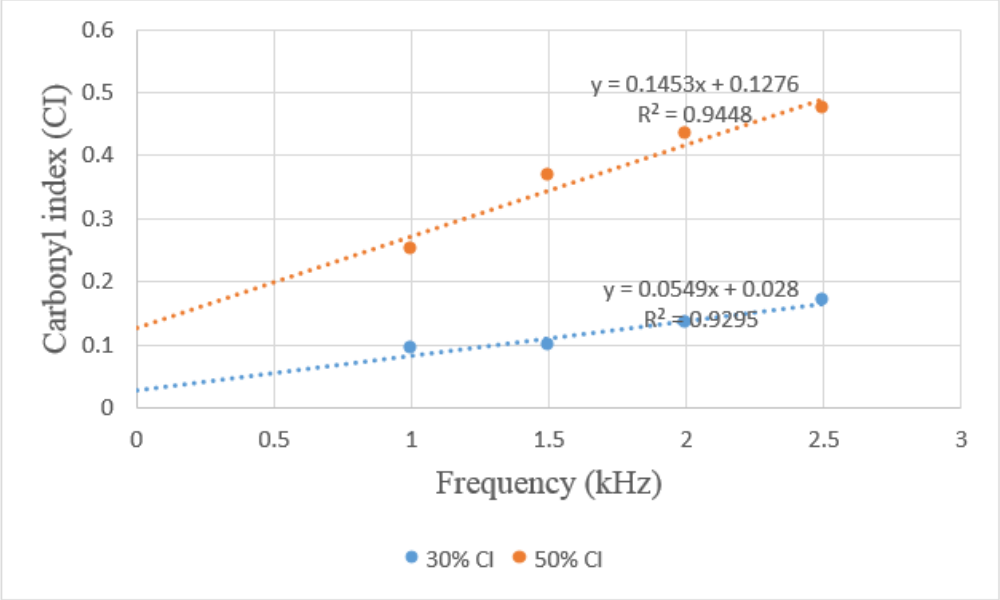

Figure 4.22. Carbonyl Index of HDPE aged at 30% and 50% voltage ratio.

In Figure 4.22, for the 30% voltage ratio, CI increases as the superimposed frequency increases within a range of 0.09 to 0.17. The gradient is 0.0549 (Hz^{-1}). At 50% voltage ratio, the CI value increases significantly, it is about 2.7 times that of the 30% voltage ratio. The gradient increases to 0.1453 (Hz^{-1}). This is because the apparent cumulative energy per second increases significantly in 50% voltage ratio (as mentioned in Section 4.1). The changes in the CI value can be correlated with changes of susceptibility index and conductivity of HDPE samples, see Section 4.5.

4.4 Dielectric Spectroscopy Results

This section contains the measurement of dielectric constant ε' and dissipation factor $tan\delta$ of HDPE (shown in Figure 4.23-4.28). The samples were aged with the same three voltage ratios and four superimposed frequencies. The investigated frequency for the DS measurements is in range of 10^{-2} to 10^{4} Hz.

4.4.1 10% Voltage Ratio

The dielectric constant and dissipation factor of HDPE aged at 10% voltage ratio are shown in Figure 4.23-4.24.

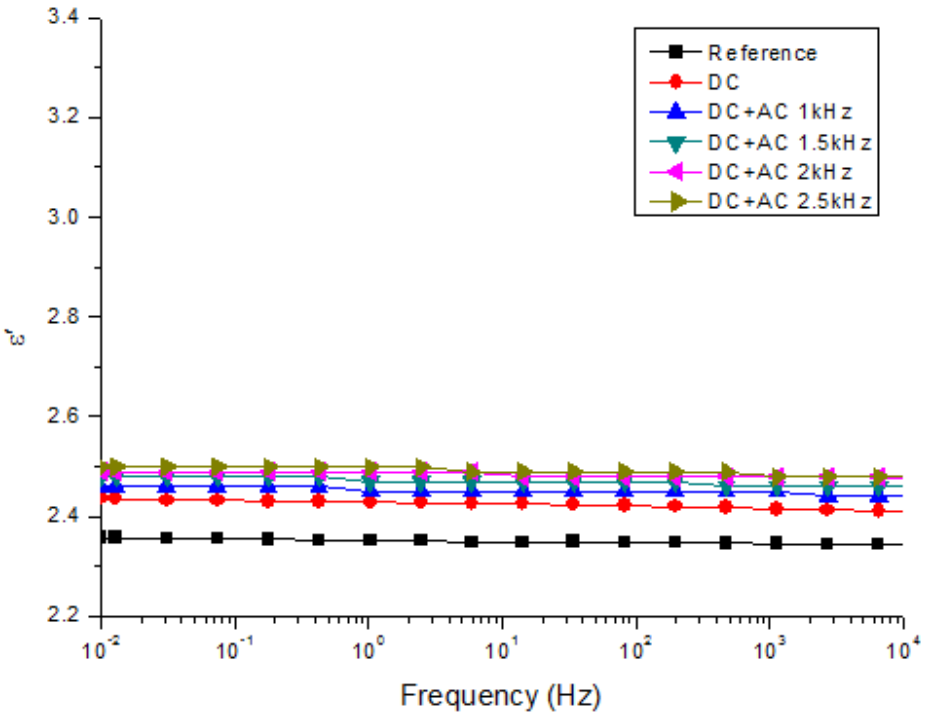

Figure 4.23. Dielectric constant of HDPE aged under 10% voltage ratio at various frequencies.

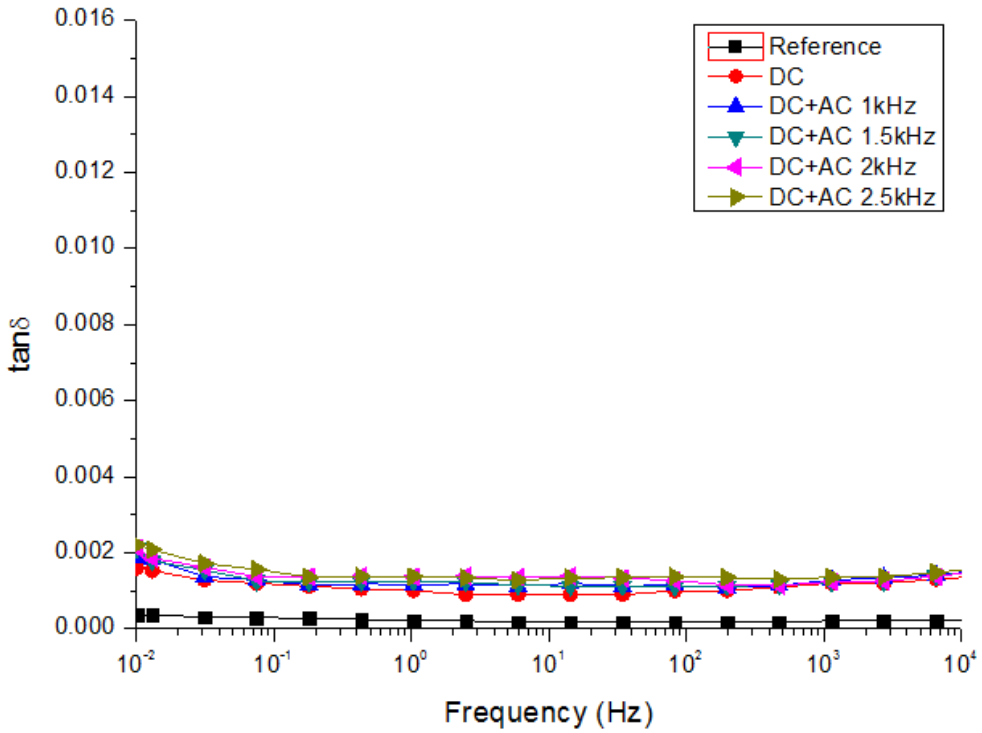

Figure 4.24. Dissipation factor of HDPE aged under 10% voltage ratio at various frequencies.

In Figure 4.23, ε' of each sample is nearly constant in the frequency range from 10^{-2} to 10^4 Hz. Across all aging conditions the values are within the range of 2.35 to 2.5.The value of ε' of samples subjected to DC stress is higher than that of the unaged reference sample. All samples aged by combined AC and DC voltages are slightly higher than the DC value.

In Figure 4.24, *tanδ* of all aged samples are higher than the reference value in the frequency range from 10^{-2} to 10^4 Hz. The *tanδ* of samples subject to DC with AC superimposed frequency overlap with the sample aged by pure DC. The small differences, if any, between the DC aged and DC/AC aged samples may be explained by the lack of evidence for significant differences in the formation of polar molecular groups produced in 10% voltage ratio stressed material (see Section 4.3.1).

4.4.2 30% Voltage Ratio

The dielectric constant and dissipation factor of HDPE at 30% voltage ratio are shown

in Figure 4.25-4.26.

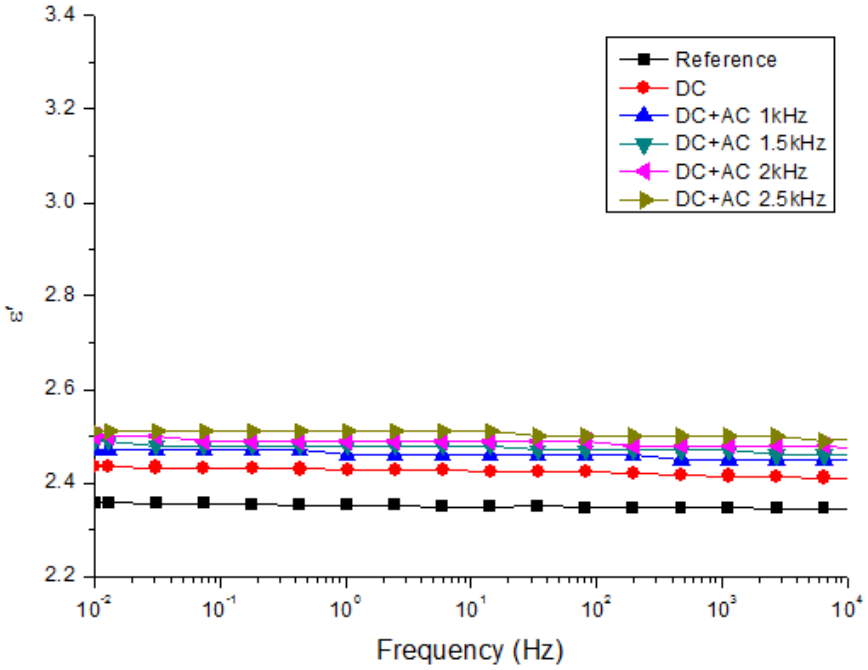

Figure 4.25. Dielectric constant of HDPE aged under 30% voltage ratio at various frequencies.

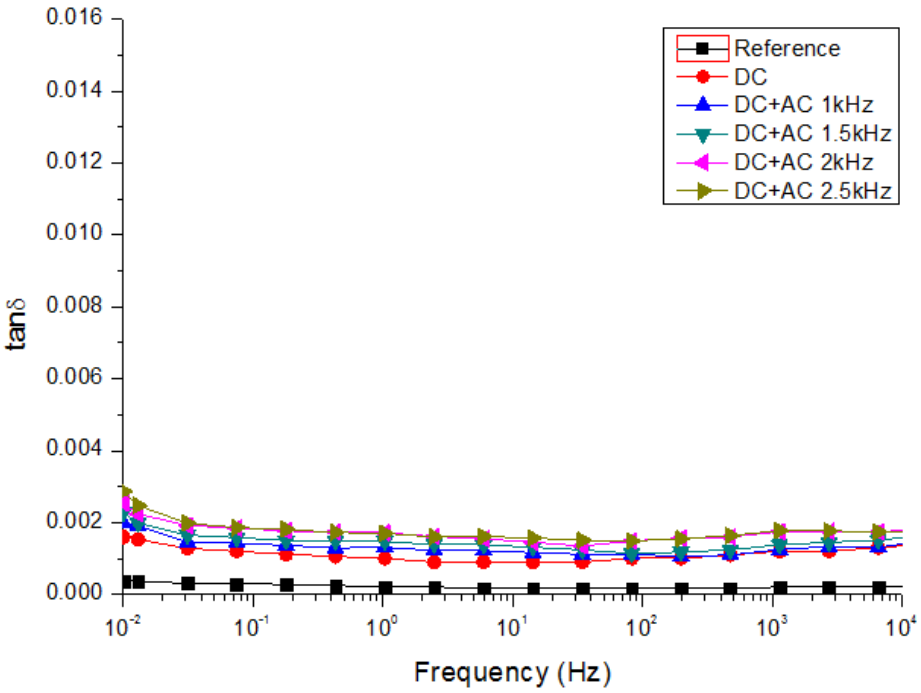

Figure 4.26. Dissipation factor of HDPE aged under 30% voltage ratio at various frequencies.

In Figure 4.25, ε' of the unaged reference sample and the sample subjected to a purely DC stress are included for reference. ε' of samples subjected to combined AC and DC voltages increase slightly above this level. Across all aging conditions the values lie in the region around 2.45 to 2.52.

In Figure 4.26, *tanδ* of samples subjected to combined AC and DC voltages no longer overlap with the DC value and appear to be increasing with the applied AC frequency. There is also evidence of an increase in *tanδ* at low frequencies. These changes may be occurring due to the formation of polar groups as shown in the FTIR-ATR results in 4.3.2.

4.4.3 50% Voltage Ratio

The dielectric constant and dissipation factor of HDPE at 50% voltage ratio are shown in Figure 4.27-4.28.

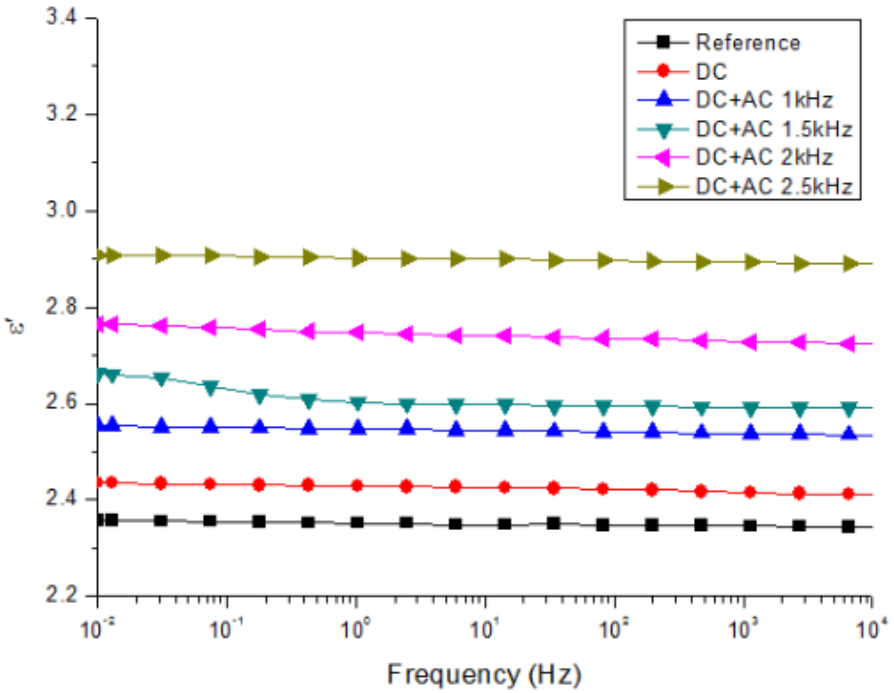

Figure 4.27. Dielectric constant of HDPE aged under 50% voltage ratio at various frequencies.

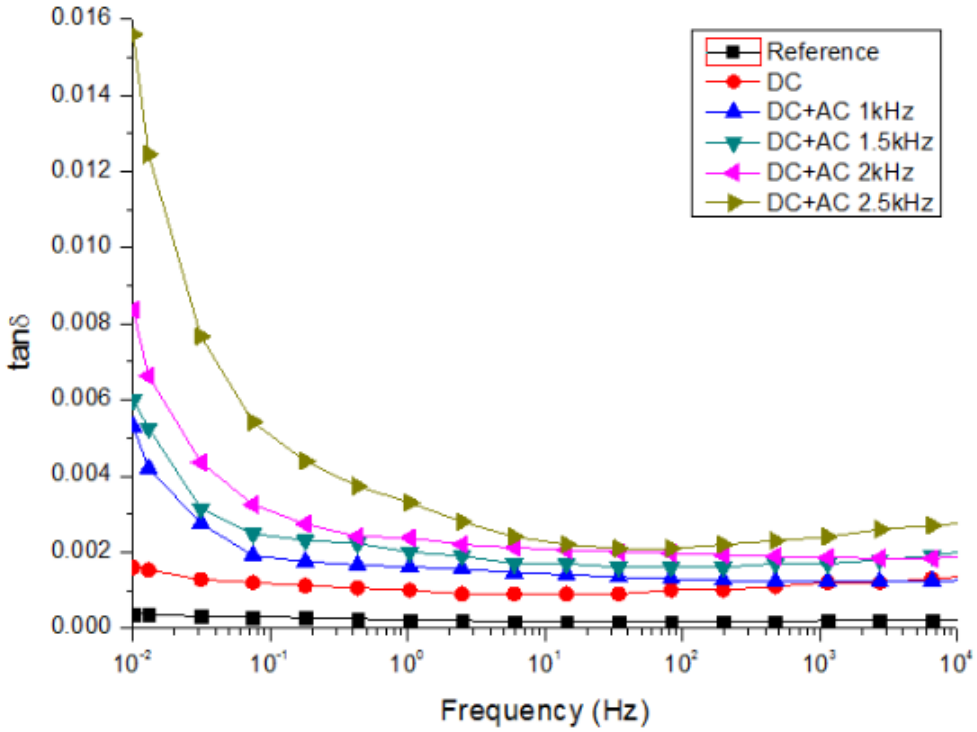

Figure 4.28. Dissipation factor of HDPE aged under 50% voltage ratio at various frequencies.

In Figure 4.27, ε' of samples subjected to combined AC and DC stress are much higher than the DC and reference values and higher than the corresponding values for the 30% voltage ratio. The values across the aging conditions lie in the region from 2.55 to 2.9. It is clear to see ε' increases with the increase of the superimposed frequency. This is because many more polar molecular groups are generated at 50% voltage ratio, such as O-H, C=O, C-O as mentioned in Section 4.3.3. As superimposed frequency increases, the amount and kinds of polar molecular groups increases which make ε' increase.

In Figure 4.28, *tanδ* of all samples subjected to combined AC and DC voltages are higher than the DC value. For each curve, *tanδ* increases for measurement frequencies below 1 Hz. For samples aged by combined voltages, overall *tanδ* increases with increases in the superimposed AC frequency. This is because more polar groups are formed at the higher frequency values as discussed in Section 4.3.3. The peak

observed at low measurement frequencies is associated with DC conduction processes which will be discussed in section 4.4.4.1.

4.4.4 Discussion

4.4.4.1 Conductivity

In the low frequency range, an observed increase in imaginary permittivity ε'' coupled with a relatively constant value of ε' is associated with DC conduction [9]. The relation is shown in equation 4.4:

$$\varepsilon_0 \varepsilon'' = \frac{\sigma}{\omega} \qquad 4.4$$

Where, σ is the conductivity, ω is the angular frequency.

If the conductivity at low frequencies is constant, a plot of ε'' against $1/\omega$ should produce a straight line. The gradient of the line gives σ/ε_0 of HDPE samples. This analysis was performed and the results are shown in Figures 4.29 to 4.31. The data used to make these plots is shown in Tables C.1 to C.3 in Appendix C.

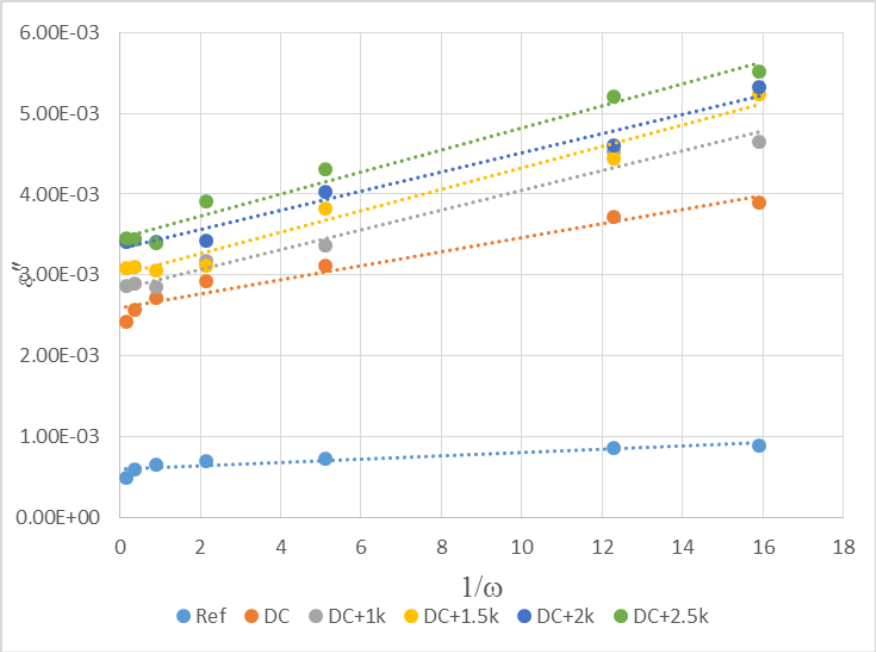

Figure 4.29. ε'' vs. 1/ω of HDPE aged by 10% voltage ratio.

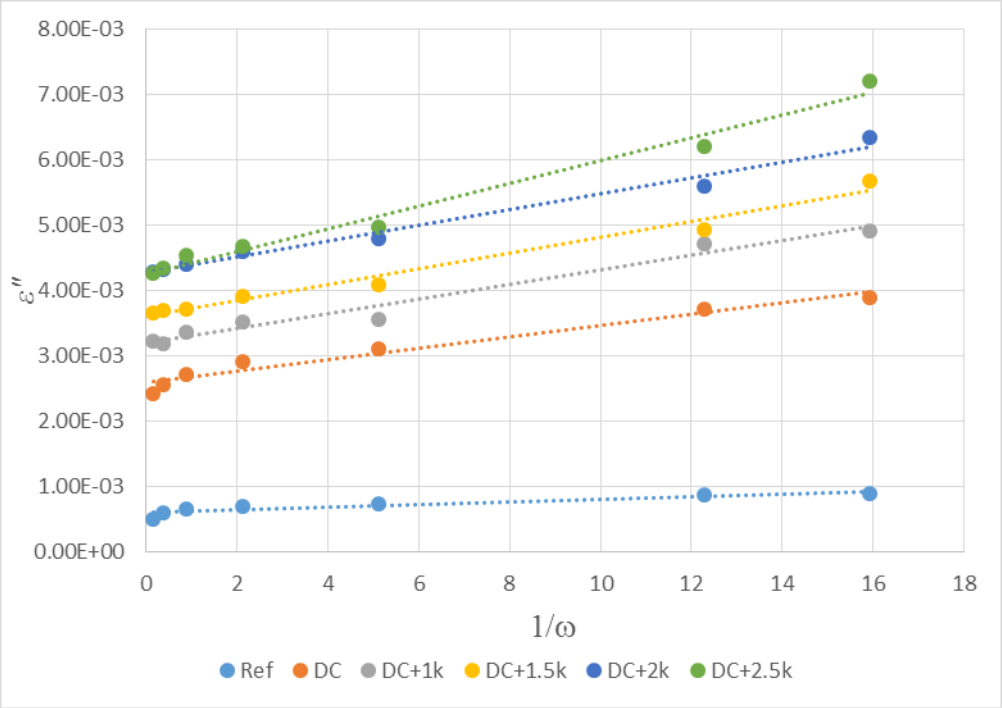

Figure 4.30. ε'' vs. 1/ω of HDPE aged by 30% voltage ratio.

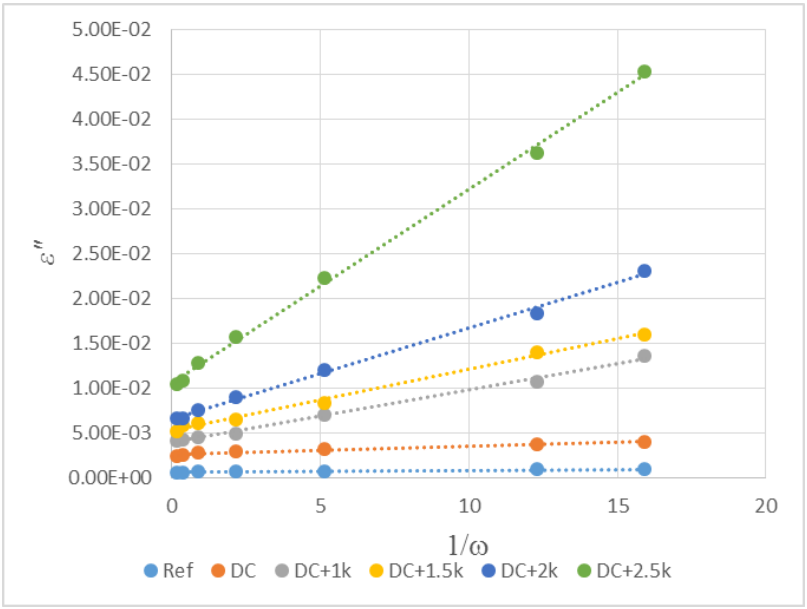

Figure 4.31. ε'' vs. 1/ω of HDPE aged by 50% voltage ratio.

Based on the gradients obtained from Figure 4.29-4.31, the calculated conductivity of HDPE can be summarized in Table 4.9 and Figure 4.32.

Table 4.9. Conductivity of HDPE.

Waveform	Conductivity (*fS/m*)		
	10% Voltage Ratio	30% Voltage Ratio	50% Voltage Ratio
Reference	0.1832	0.1832	0.1832
DC	0.7735	0.7735	0.7735
DC+1kHz	1.0797	0.9912	5.1950
DC+1.5kHz	1.1771	1.0709	6.0446
DC+2kHz	1.0443	1.0797	9.0270
DC+2.5kHz	1.2125	1.5311	19.1160

The data from Table 4.9 is plotted in Figure 4.32 below.

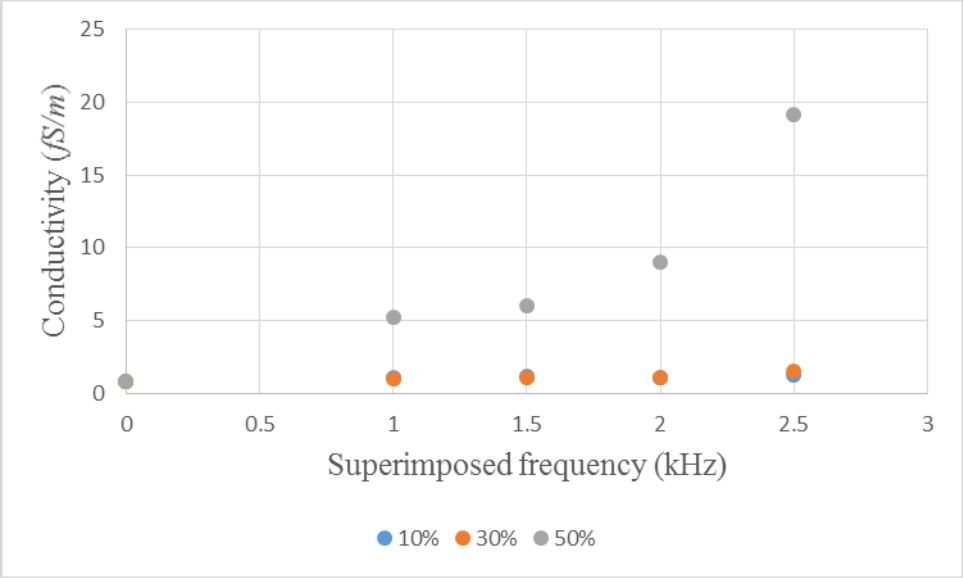

Figure 4.32. Conductivity of HDPE.

From this table and figure it can be seen that the conductivity under DC stressing is greater than that for the unaged sample. The conductivity is also higher under combined stress as compared to DC stressing. The conductivity is significantly higher for the 50% voltage ratio aging and there is a clear increase in the conductivity with AC component frequency. This increase in conductivity may be occurring for the 10% and 30% voltage waveforms but the trend is much less clear.

4.4.4.2Dielectric Susceptibility Index (χI)

χ' is the real part of dielectric susceptibility of a material, which is defined as:

$$\chi' = \varepsilon' - 1 \quad 4.5$$

To have a way of quantifying the change in the permittivity a dielectric susceptibility index (χI) was defined as:

$$\chi I = \frac{\chi'_A - \chi'_{REF}}{\chi'_{REF}} \quad 4.6$$

Where, χ'_A is the dielectric susceptibility of an aged sample and χ'_{REF} is the dielectric susceptibility of the reference sample. The index reflects the change in the susceptibility normalised by the susceptibility of the unaged sample and reflects the normalised changes in the polarisation density in the material at constant field.

The values calculated are shown Table 4.10 and their behaviour as a function of AC frequency are shown in Figure 4.33. As by definition the values of χI of reference unaged samples will be zero, they are not included in this table.

Table 4.10. Dielectric susceptibility index χI of HDPE.

Waveform	Susceptability Index χI		
	10% Voltage Ratio	30% Voltage Ratio	50% Voltage Ratio
DC	0.0571	0.0571	0.0571
DC+1kHz	0.0749	0.0822	0.1444
DC+1.5kHz	0.0896	0.0970	0.2243
DC+2kHz	0.0970	0.1043	0.2985
DC+2.5kHz	0.1043	0.1117	0.4058

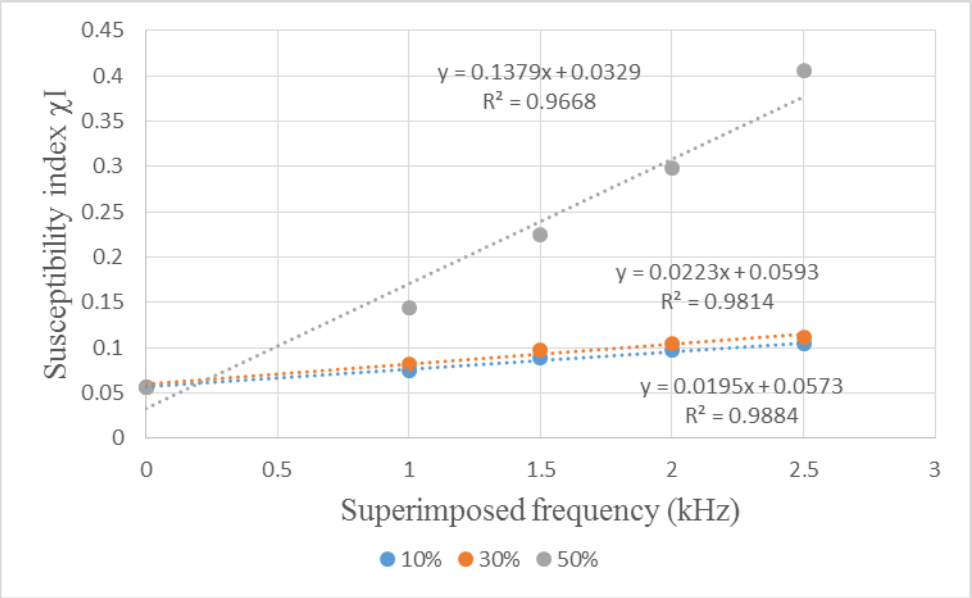

Figure 4.33. Dielectric susceptibility index χI of HDPE.

From Figure 4.33 it can be seen that the susceptibility index, as defined above by the authors, increases with the frequency of the AC component of stressing for all voltage conditions. There appears to be a slight difference in the values for 10% and 30% voltage ratio with the results at 30% being higher.

4.5 Discussion

It is useful to explore the relationships between the apparent cumulative energy per second $\dot{E}_{CA}$ and the indices derived from the FTIR-ATR and DS results which are expected to relate to the degree of aging. The relationship between Carbonyl Index (CI) and apparent cumulative energy per second $\dot{E}_{CA}$ is shown in Table 4.11 and Figure 4.34.

Table 4.11. Apparent cumulative energy per second vs. Carbonyl Index.

Frequency (kHz)	30% Voltage Ratio		50% Voltage Ratio	
	$\dot{E}_{CA}$	CI	$\dot{E}_{CA}$	CI
1	1046	0.0921	9135	0.2523
1.5	1593	0.0986	13326	0.3689
2	2164	0.1336	17644	0.4339
2.5	2725	0.1719	23920	0.4728

In Figure 4.34, it can be seen that as the value of $\dot{E}_{CA}$ increases the value of CI is increasing. It also appears that the CI value may be saturating at large values of $\dot{E}_{CA}$.

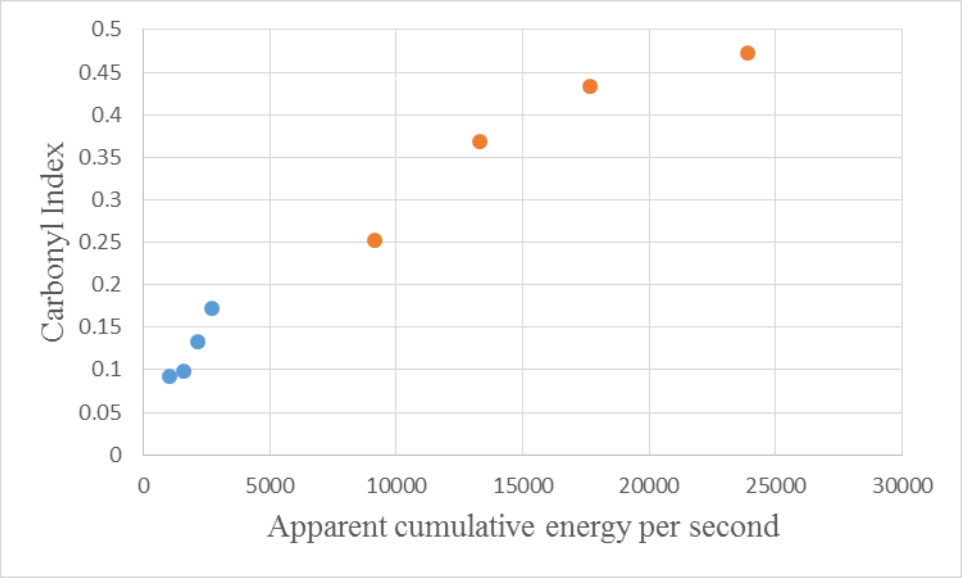

Figure 4.34. Apparent cumulative energy per second vs. Carbonyl Index.

The relationship of $\dot{E}_{CA}$ and σ is shown in Table 4.12 and Figure 4.35.

Table 4.12. Apparent cumulative energy per second vs. conductivity.

Frequency (kHz)	30% Voltage Ratio		50% Voltage Ratio	
	$\dot{E}_{CA}$	σ (*fS/m*)	$\dot{E}_{CA}$	σ (*fS/m*)
1	1046	0.9912	9135	5.1950
1.5	1593	1.0709	13326	6.0446
2	2164	1.0797	17644	9.0270
2.5	2725	1.5311	23920	19.1160

In Figure 4.35, the conductivity is increasing as the value of $\dot{E}_{CA}$ increases. Unlike the behaviour of CI there is no evidence of any saturation. This may be due to the fact that the CI derived from the FTIR-ATR measurements only reflects the changes in the surface layer of the polymer while conductivity reflects a bulk change in the system.

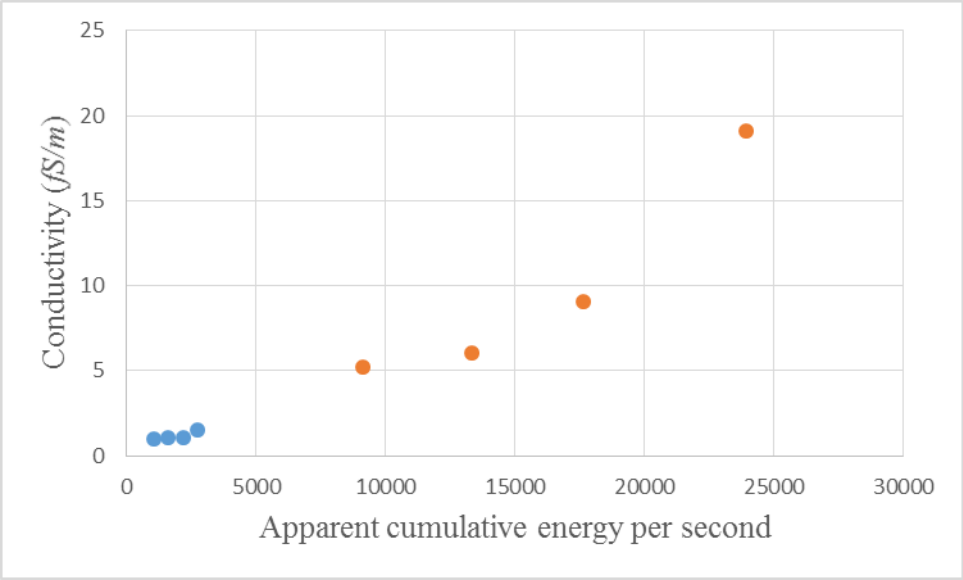

Figure 4.35. Apparent cumulative energy per second vs. conductivity.

The relationship of $\dot{E}_{CA}$ and χI is shown in Table 4.13 and Figure 4.36.

Table 4.13. Apparent cumulative energy per second vs. χI.

Frequency (kHz)	30% Voltage Ratio		50% Voltage Ratio	
	$\dot{E}_{CA}$	χI	$\dot{E}_{CA}$	χI
1	1046	0.0822	9135	0.1444
1.5	1593	0.0970	13326	0.2243
2	2164	0.1043	17644	0.2985
2.5	2725	0.1117	23920	0.4058

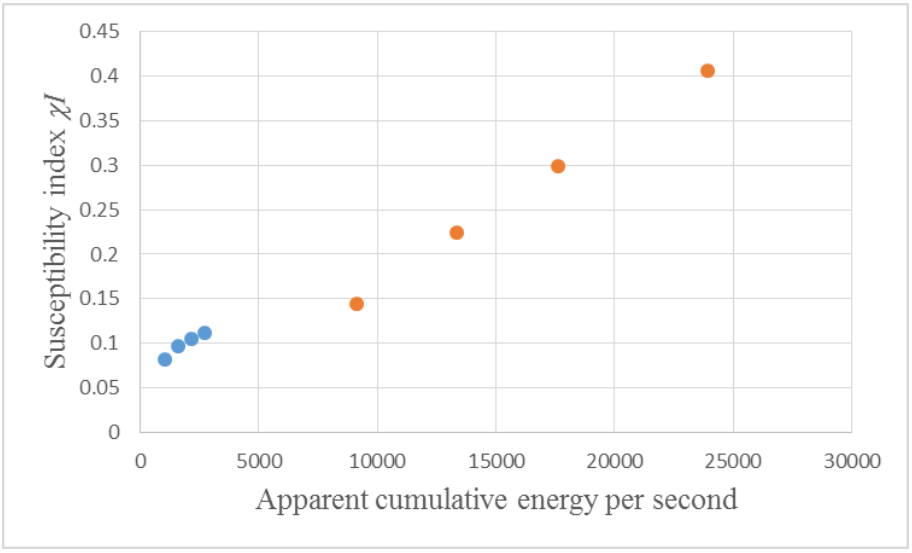

Figure 4.36. Apparent cumulative energy per second vs. Susceptibility Index.

As with the CI and conductivity the susceptibility index χI increases as $\dot{E}_{CA}$ increases. Unlike CI and in a similar manner to the conductivity there is no evidence of saturation in the behaviour of χI and at large values of $\dot{E}_{CA}$ the rate of change seems to be increasing. This again may occur as χI reflects the behaviour of the bulk of the material.

The relationship of CI and conductivity (σ) is shown in Figure 4.37.

In Figure 4.37, as would be expected from Figure 4.34 and Figure 4.35 as the value of CI increases the value of conductivity increases. At lower values of CI there is a broadly linear relationship between CI and conductivity. At high values of CI the value of conductivity increases more rapidly due to the observed saturation in the Carbonyl Index.

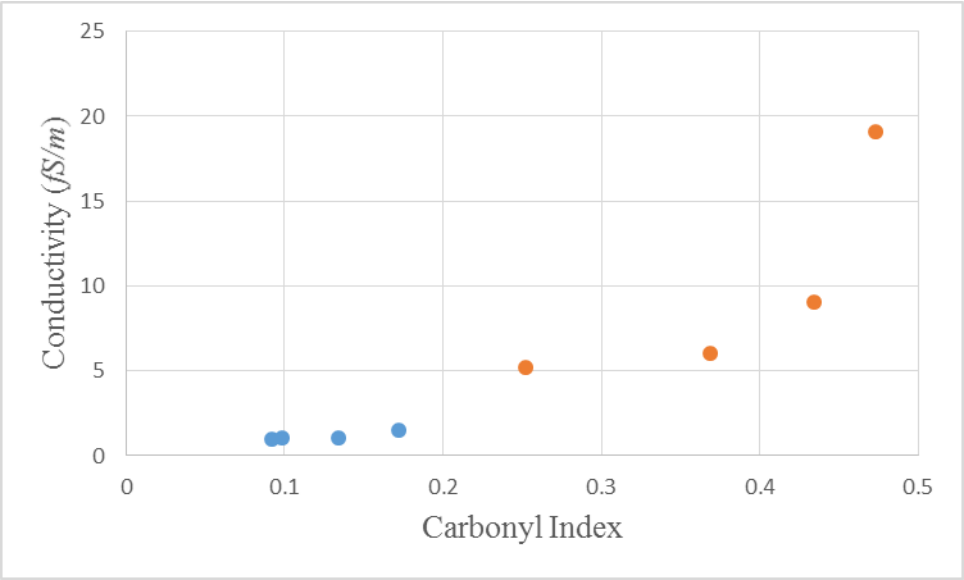

Figure 4.37. Carbonyl Index vs. conductivity.

The relationship of CI and χI is shown in Figure 4.38.

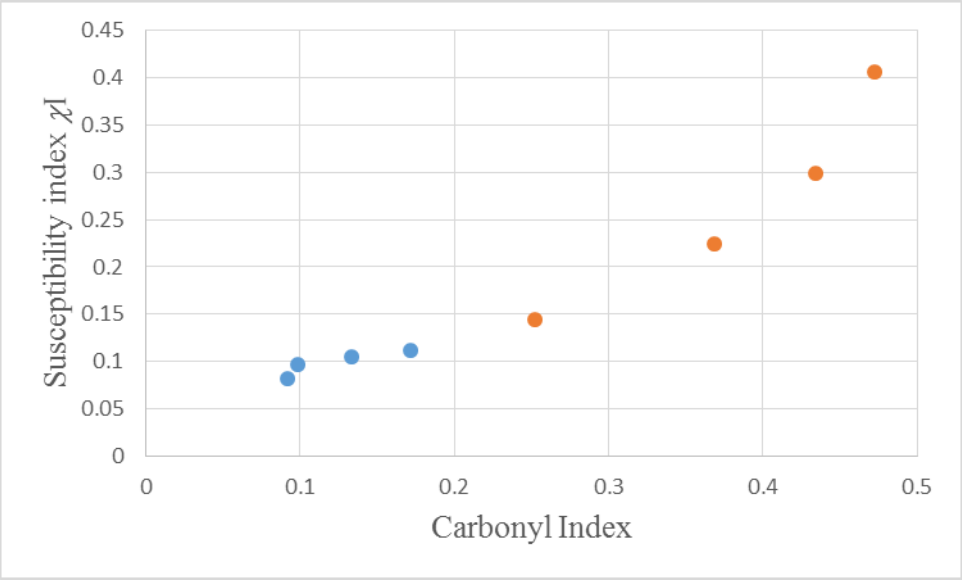

Figure 4.38. Carbonyl Index vs. χI.

As would be expected from Figure 4.34 and Figure 4.36 as the value of CI increases the value of χI increases. At lower values of CI there is a broadly linear relationship between CI and χI. Again at higher values of CI the value of χI increases more rapidly due to the observed saturation in the Carbonyl Index. This appears to occur at a lower value of the Carbonyl Index.

4.6 Conclusions

From the PD data it can clearly be seen that the AC frequency has an effect on both the phase distribution of the partial discharge activity and the magnitude of the partial discharge activity. The behaviour observed is similar to that observed for surface discharges under purely AC conditions. However the situation with combined AC and DC stress is more complicated and for this behaviour to be observed the potential of the surface must increase to a value above the minimum potential caused by the applied stress. The mechanism by which this occurs is not clear at this point.

The apparent cumulative energy per second has been calculated and this index increases as the voltage ratio increases and as the frequency of the AC component is

increased.

From the FTIR-ATR values for the Carbonyl Index which reflects the chemical changes on the surface have been calculated. The changes in the Carbonyl Index with frequency and voltage ratio correlate with the apparent cumulative energy per cycle.

From the dielectric spectroscopy data values for the conductivity and an index reflecting the change in susceptibility have been calculated. These indeces also correlate with the apparent cumulative energy per cycle.

4.7 References

[1] Hazlee Illias, Teo Soon Yuan, Ab Halim Abu Bakar, Hazlie Mokhlis, George Chen and Paul L. Lewin, "Partial Discharge Patterns in High Voltage Insulation", 2012 IEEE International Conference on Power and Energy (PECon), pp.750-755, 2012.

[2] Zhiman He, Jian Li, Tianyan Jiang, Lianwei Bao and Changkui Cheng, "Partial Discharge Characteristics Influenced by Different Temperatures under Pulsating DC Voltages", 2013 IEEE International Conference on Solid Dielectrics (ICSD), pp. 1001-1004, 2013.

[3] J.V. Gulmine, P.R. Janissek, H.M. Heise and L. Akcelrud, "Polyethylene characterization by FTIR", Polymer Testing, Vol.21, pp. 557–563, 2002.

[4] Tidjani, A, "Comparison of formation of oxidation products during photo-oxidation of linear low density polyethylene under different natural and accelerated weathering conditions", Polym. Degrad. Stabil. 2000, 68, 465–469.

[5] E. Chiellini, A. Corti, S. D'Antone and R. Baciu, "Oxo-biodegradable carbon backbone polymers-Oxidative degradation of polyethylene under accelerated test conditions", Polymer Degradation and Stability, Vol.91, pp. 2739-2747, 2006.

[6] Chiellini, E.; Corti, A.; Swift, G. Biodegradation of thermally-oxidized, fragmented low-density polyethylenes. Polym. Degrad. Stabil. 2003, 81, 341–351

[7] Koutny, M.; Sancelme, M.; Dabin, C.; Pichon, N.; Delort, A.-M.; Lemaire, J. Acquired biodegradability of polyethylene containing pro-oxidant additives. Polym. Degrad. Stabil. 2006, 9, 1495–1503.

[8] Emma Strömberg, Sigbritt Karlsson, "The Design of a Test Protocol to Model the Degradation of Polyolefins During Recycling and Service Life", Journal of applied polymer science, Vol.112, Issue 3, pp.1835-1844, 2009.

[9] A. K. Jonscher, "A new understanding of the dielectric relaxation of solids", Journal of Materials Science, Vol.16, pp.2037-2060, 1981.

5. Results of Polypropylene Aged by 90°C

PP samples were aged at 90°C with 3 voltage ratios (10%, 30% and 50%) and four frequencies (1 kHz, 1.5 kHz, 2 kHz and 2.5 kHz) using the same approach as for HDPE. Again the PRPD, FTIR-ATR and DS measurements were carried out to analyse the changes due to aging. In this chapter, the data is demonstrated and summarized.

Section 5.1 describes the PRPD results. The mean and standard deviation of PD voltages, the number of discharges, the PD apparent cumulative energy and the apparent cumulative energy per second are the indeces used to describe the PRPD data. How these indeces change with superimposed frequency and voltage ratio are reported. The standard deviation for PRPD results is within ±10% range.

Section 5.2 describes the FTIR-ATR results. The behaviour of the Carbonyl Index of samples changes with various superimposed frequencies and voltage ratios is summarized. The standard deviation for FTIR-ATR results is within ±3% range.

Section 5.3 describes the DS results. The variation of the conductivity and dielectric susceptibility index with superimposed frequencies and voltage ratios are summarized. The standard deviation for DS results is within ±2% range.

Section 5.4 shows the relationship of PD apparent cumulative energy per second, Carbonyl Index, conductivity and dielectric susceptibility index.

Section 5.5 is the conclusions.

5.1 PRPD Results

When the voltage ratio is 10%, there is no detected PD signal at any of the AC frequencies considered. PD signals could be detected at 30% and 50% voltage ratio. The PRPD patterns of PP (Appendix F) and their behaviour for different frequencies and voltage ratios aged at 90°C is similar to that of HDPE.

The data of mean PD voltage with standard deviation, number of discharges and PD apparent cumulative energy per second is shown in Table 5.1-5.5 and Figure 5.1-5.3.

As PD appears at 30% and 50% voltage ratio, data of the mean PD voltage with standard deviation is shown in Table 5.1.

Table 5.1. Mean PD voltage with standard deviation for PP aged at 90°C and 30% and 50% voltage ratios.

Frequency (kHz)	PD voltage (V) at 30% voltage ratio		PD voltage (V) at 50% voltage ratio	
	$\overline{V_{PD}}$	σ_{PD}	$\overline{V_{PD}}$	σ_{PD}
1	0.215	0.0203	0.55	0.05
1.5	0.214	0.0205	0.61	0.056
2	0.216	0.0205	0.68	0.062
2.5	0.223	0.021	0.76	0.069

Figure 5.1 is drawn according to the data in Table 5.1.

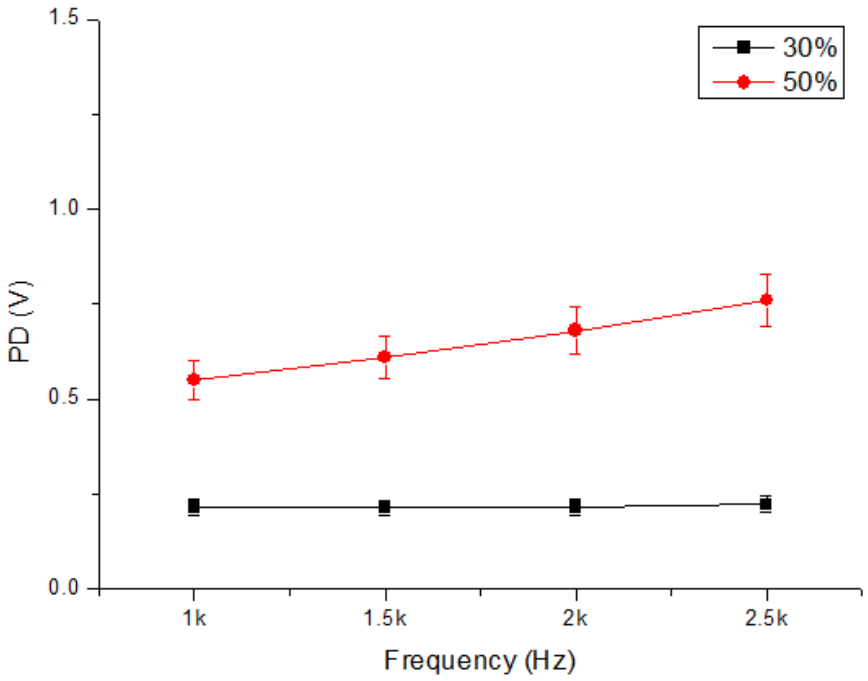

Figure 5.1. Mean with standard deviation of PD voltage.

In Figure 5.1, for PP samples aged at 30% voltage ratio, $\overline{V_{PD}}$ is around 0.2 V at any of the AC frequencies considered. The value does not change significantly with change of superimposed frequency. This may be because at this voltage ratio, the combined voltage is not high enough to cause sufficient charging on the surface to develop a large number of discharges in the 3rd quadrant. When the voltage ratio increases to 50%, $\overline{V_{PD}}$ is at least 0.3 V higher than the value of 30% voltage ratio at each frequency. The mean PD voltage increases along with the increase of superimposed frequency. It is 0.55 V at 1 kHz and increases to 0.76 V at 2.5 kHz. Again, the discharge behaviour is depressed in the first quadrant and increases significantly in the third quadrant. Depending on the mechanism of partial discharge (mentioned in Section 4.2).

Data of number of discharge n_{PD} and the mean discharge rate $\dot{n}_{PD}(s^{-1})$ is shown in Table 5.2 and Table 5.3 for 30% and 50% voltage ratio, respectively.

Table 5.2. Number of discharges of PP aged by 90°C at 30% voltage ratio.

Frequency (kHz)	n_{PD}	T_{Meas}(s)	$\dot{n}_{PD}(s^{-1})$
1	5880	1.5	3920
1.5	5819	1	5819
2	5771	0.75	7695
2.5	5637	0.6	9395

Table 5.3. Number of discharges of PP aged by 90°C at 50% voltage ratio.

Frequency (kHz)	n_{PD}	T_{Meas}(s)	$\dot{n}_{PD}(s^{-1})$
1	17400	1.5	11600
1.5	16810	1	16810
2	15713	0.75	20951
2.5	13133	0.6	21888

$\dot{n}_{PD}(s^{-1})$ vs. superimposed frequency is shown in Figure 5.2.

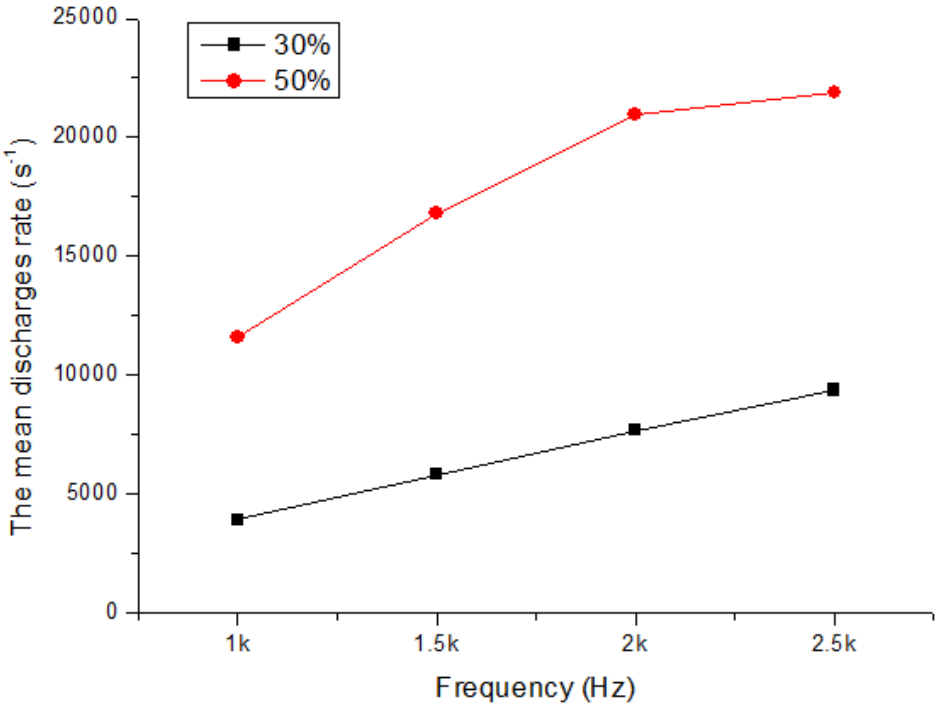

Figure 5.2. $\dot{n}_{PD}(s^{-1})$ of PP aged by 90°C at 30% and 50% voltage ratio.

In Figure 5.2, $\dot{n}_{PD}(s^{-1})$ increases with the increase in the superimposed frequency for both voltage ratios. When aged at 30% voltage ratio, $\dot{n}_{PD}(s^{-1})$ increases with the superimposed frequency from 4000 at 1 kHz to 9000 at 2.5 kHz. For PP samples aged

at 50% voltage ratio, $\dot{n}_{PD}(s^{-1})$ increases from 11600 to 21888 discharges per second over the same frequency range. At each frequency the value at 50% voltage ratio is at least 2 times that of 30% voltage ratio.

Data of apparent cumulative energy E_{CA} and the apparent cumulative energy per second $\dot{E}_{CA}$ at 30% and 50% voltage ratio is shown in Table 5.4 and Table 5.5, respectively.

Table 5.4. Apparent cumulative energy per second of PP aged by 90°C at 30% voltage ratio.

Frequency (kHz)	E_{CA}	T_{Meas}(s)	$\dot{E}_{CA}$
1	1264	1.5	842
1.5	1245	1	1245
2	1247	0.75	1663
2.5	1257	0.6	2095

Table 5.5. Apparent cumulative energy per second of PP aged by 90°C at 50% voltage ratio.

Frequency (kHz)	E_{CA}	T_{Meas}(s)	$\dot{E}_{CA}$
1	9570	1.5	6380
1.5	10370	1	10370
2	10880	0.75	14507
2.5	11400	0.6	19000

Figure 5.3 shows the behaviour of the data from Table 5.4-5.5.

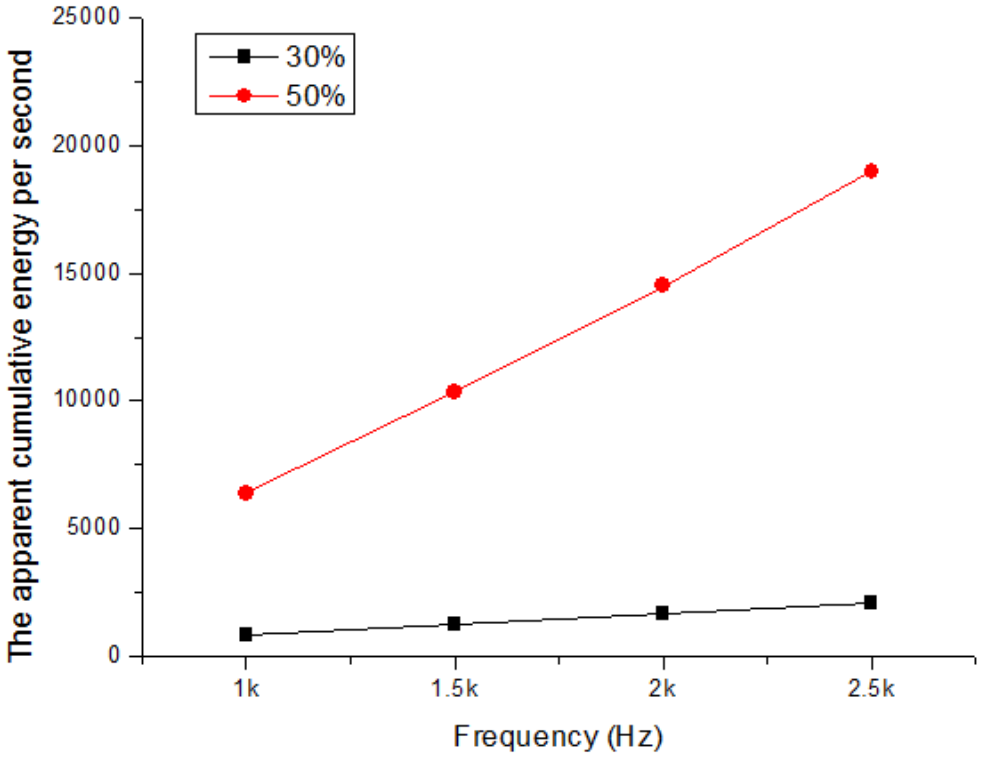

Figure 5.3. $\dot{E}_{CA}$ of PP aged by 90°C at 30% and 50% voltage ratio.

In Figure 5.3, $\dot{E}_{CA}$ of each voltage ratio increases with the increase of the superimposed frequency. At 30% voltage ratio, the value increases steadily from 842 to 2095. At 50% voltage ratio, the values significantly increase to at least 8 times that of the value at 30% voltage ratio at each frequency with the value increasing from 6380 at 1 kHz to 19000 at 2.5 kHz.

As the behaviour of the PD activity is similar to that for HDPE it is assumed that the mechanism of PD discussed in Section 4.2 also applies to the PP behaviour.

5.2 FTIR-ATR Result

In this section, the FTIR-ATR results and analysis of Carbonyl Index will be reported and discussed.

Details of main peaks of reference for PP are shown in Table 5.6.

Table 5.6. Peaks of reference PP [1].

Wavenumber (cm^{-1})	Vibration
2955	CH_3 asymmetric stretching vibrations
2922	Main chain CH_2 asymmetric stretching vibration
2873	CH_3 symmetric stretching vibrations
2843	Main chain CH_2 symmetric stretching vibration
1460	CH_3 asymmetric deformation vibrations or CH_2 scissor vibrations
1378	CH_3 symmetric deformation vibrations
1167	C-C asymmetric stretching, CH_3 asymmetric rocking and C-H wagging vibrations
998	CH_3 asymmetric rocking vibrations
974	CH_3 asymmetric rocking and C–C asymmetric stretching vibrations
901	CH_3 asymmetric rocking and C–C asymmetric and symmetric stretching vibrations
844	CH_2 rocking vibrations
810	CH_2 rocking vibrations

Details of new peaks which appear in aged PP are shown in Table 5.7.

Table 5.7. New peaks in aged PP [1].

Wavenumber (cm^{-1})	Shape	Vibration
3650-3300	Broad	OH stretching vibrations
1738	Broad	The presence of carbonyl (C=O) groups in ketones, aldehydes and carboxylic acids
1647		The formation of hydrogen bonds between hydrogen atoms of aldehydes, carboxylic acids and alcohols at the surface. Hydrogen bonding tends to decrease the double-bond character of the C=O group, which results in a shift of the C=O absorption band to a lower frequency. C=C stretching vibrations

It is believed that the broad O-H peak belongs to the O-H groups of alcohols and carboxylic acids, while the C=O peak confirms the presence of aldehydes, ketones and carboxylic acids on the surface. The Carbonyl Index (CI) can be used to define the degree of aging that has occurred based on FTIR-ATR measurements. For PP, CI [2] is shown in equation 5.1:

$$CI = \frac{A_{1738}}{A_{1460}} \quad 5.1$$

Where, A_{1738} is the absorbance of carbonyl group (-CO-); A_{1460} is the absorbance of methylene group (-CH_2-), symmetric stretching vibration.

The changes in the FTIR-ATR results of PP aged by 90°C with different superimposed frequency and in three voltage ratios are shown in Figure 5.4-5.15.

5.2.1 10% Voltage Ratio

Full-scale and detailed sectional views of FTIR-ATR spectra of PP aged at 90°C with the 10% voltage ratio are shown in Figure 5.4-5.7. When PP samples are subjected to DC stress at 90°C, the intensity of peaks between 3000 cm^{-1}-2800 cm^{-1} are slightly lower than in the unaged reference (Figure 5.5). Any increase in the peaks associated with the carbonyl group is hard to see in Figure 5.7. This suggests that aging is occurring at a relatively low rate under DC conditions. When PP samples are aged under combined AC and DC stresses, the changes in the peaks in range of 3000 cm^{-1}-2800 cm^{-1} decrease further slightly. This suggests that aging is, similar to that in HDPE, occurring at a relatively low rate under combined AC and DC stress at 10% voltage ratio.

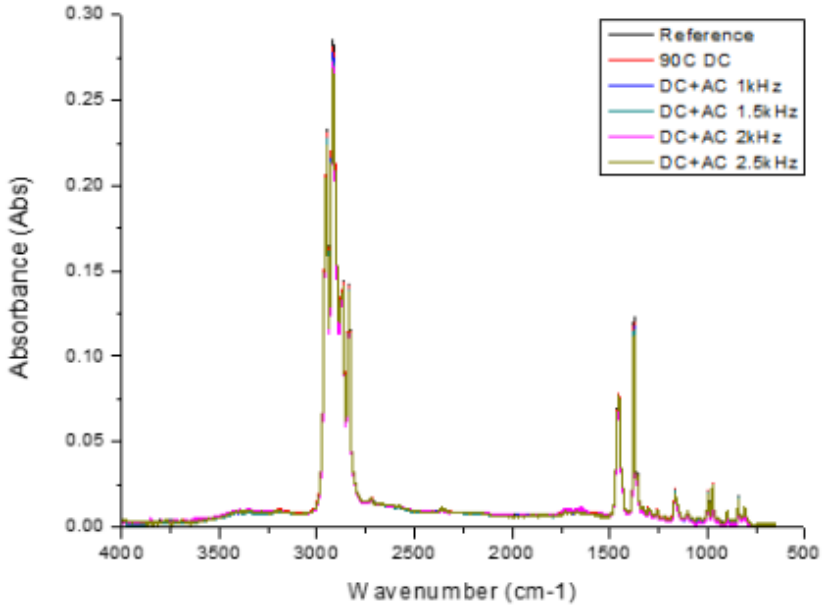

Figure 5.4. FTIR-ATR results of PP (aged under 10% voltage ratio at various frequencies).

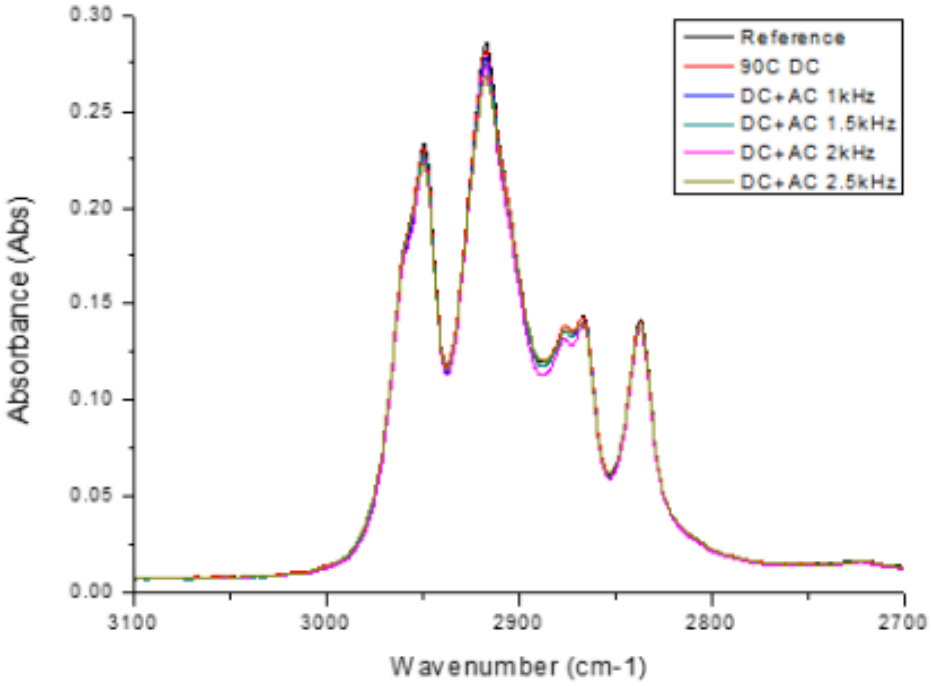

Figure 5.5. FTIR-ATR results for PP detailed view of C-H-groups (aged under 10% voltage ratio at various frequencies).

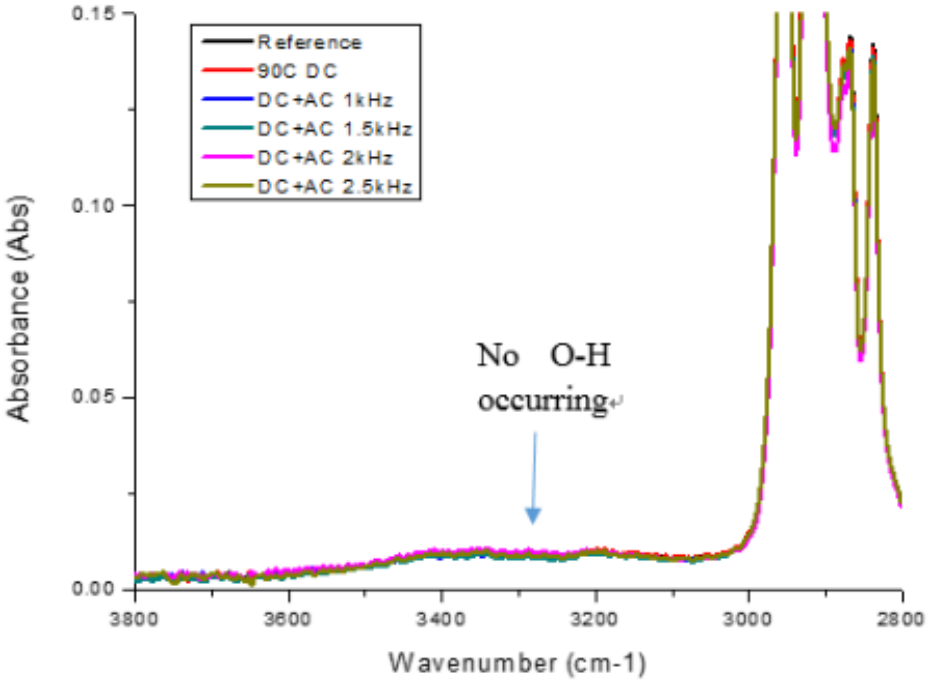

Figure 5.6. FTIR-ATR results for PP detailed view of OH-group (aged under 10% voltage ratio at various frequencies).

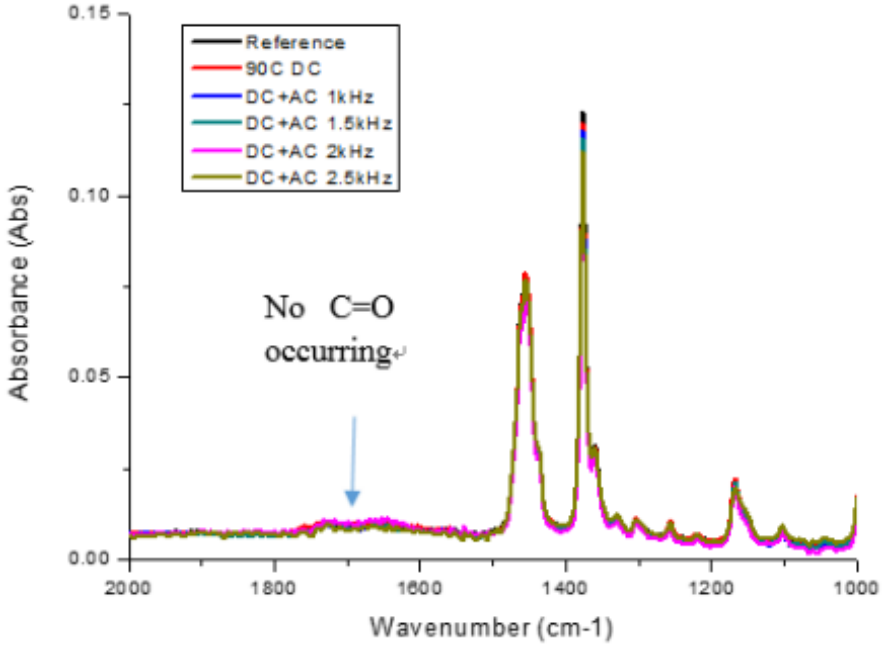

Figure 5.7. FTIR-ATR results for PP detailed view of carbonyl group (aged under 10% voltage ratio at various frequencies).

5.2.2 30% Voltage Ratio

Full-scale and detailed sectional views of FTIR-ATR spectra of PP aged at 90°C in 30% are shown in Figure 5.8-5.11. The spectra for unaged samples and for samples subjected to a purely DC stress are included for reference. Figure 5.9 shows the absorption peaks 3000 cm^{-1}-2800 cm^{-1} for all aged samples are less than the unaged reference sample. The effect on the absorption of the peaks at 3000 cm^{-1}-2800 cm^{-1} for the PP aged by combined voltages is more significant than for the sample aged only with DC. The change in absorption also depends on the superimposed frequency. Figure 5.11 shows evidence of carbonyl groups appearing. There is no change between the reference unaged sample and the DC sample. When samples are aged by combined AC and DC voltages, the carbonyl group absorption peak starts to appear. The intensity of the carbonyl group peak increases with the superimposed frequency. These changes indicated that an oxidative aging process is occurring and that it is enhanced by the combined AC and DC stress.

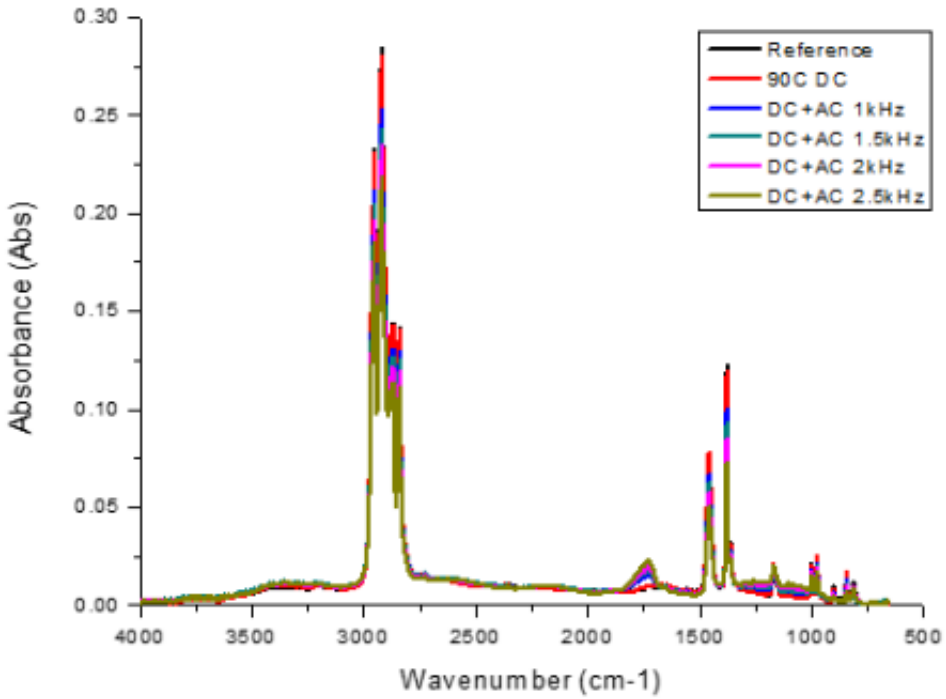

Figure 5.8. FTIR-ATR results of PP (aged under 30% voltage ratio at various frequencies).

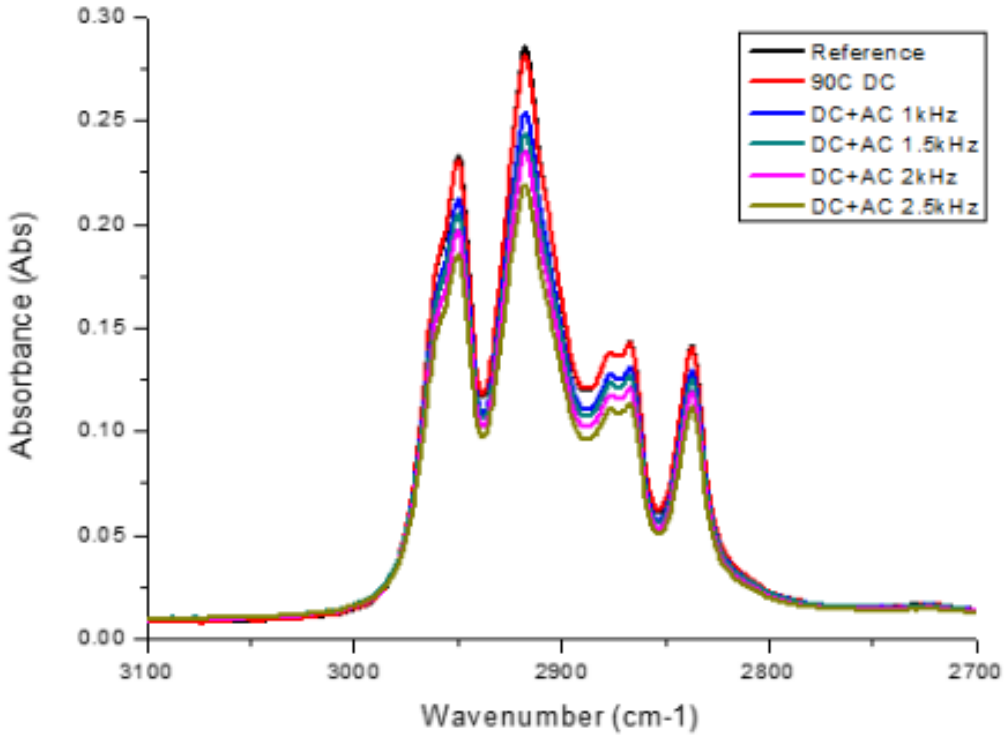

Figure 5.9. FTIR-ATR results for PP detailed view of C-H-groups (aged at 30% voltage ratio with various frequencies).

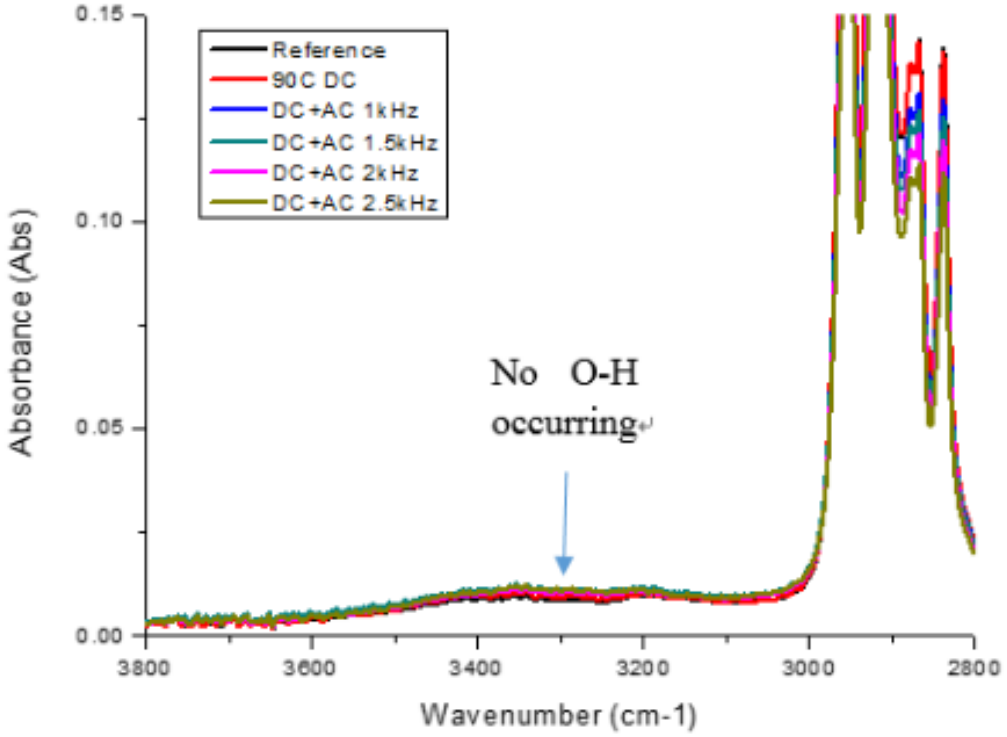

Figure 5.10. FTIR-ATR results for PP detailed view of OH-group (aged at 30% voltage ratio with various frequencies).

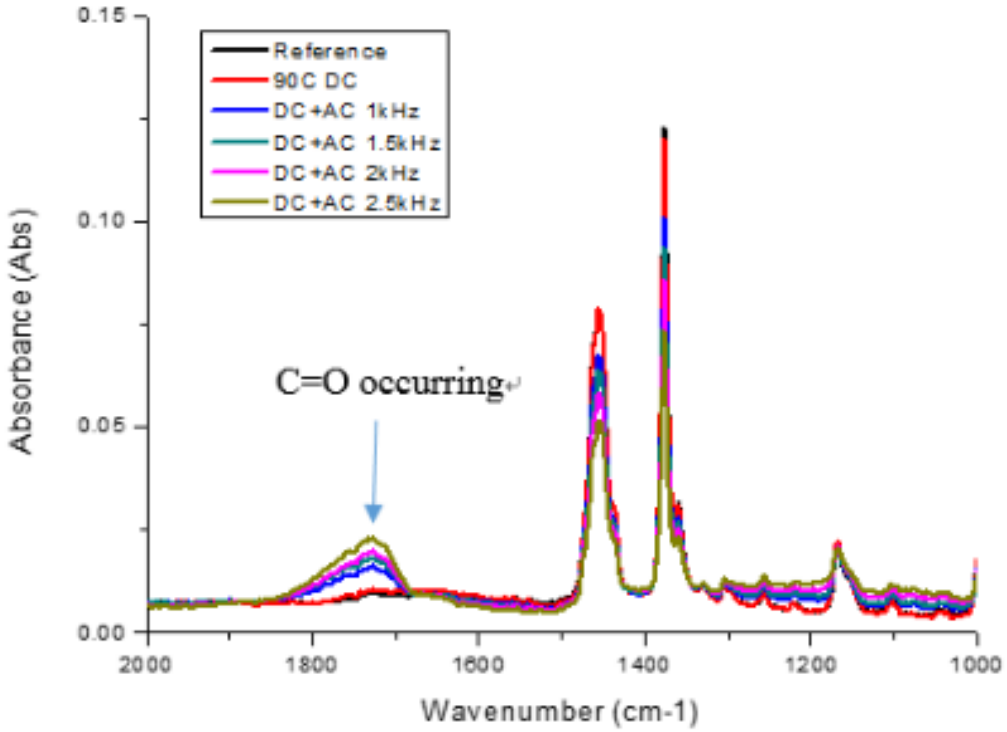

Figure 5.11. FTIR-ATR results for PP detailed view of carbonyl group (aged under 30% voltage ratio at various frequencies).

5.2.3 50% Voltage Ratio

Full-scale and detailed sectional views of FTIR-ATR spectra of PP aged at 90°C in 50% are shown in Figure 5.12-5.15. The behaviour is similar to that observed at 30% voltage ratio with a decrease in the 3000 cm^{-1}-2800 cm^{-1} absorption band (Figure 5.13) being dependent on the superimposed frequency and carbonyl absorption (Figure 5.15) observed in samples aged by AC and DC superimposed voltages. However, at 50% voltage ratio, there is evidence of the formation of O-H groups which is not observed at 30% voltage ratio (Figure 5.14). The absorption of O-H groups is enhanced by the increase of the superimposed frequency.

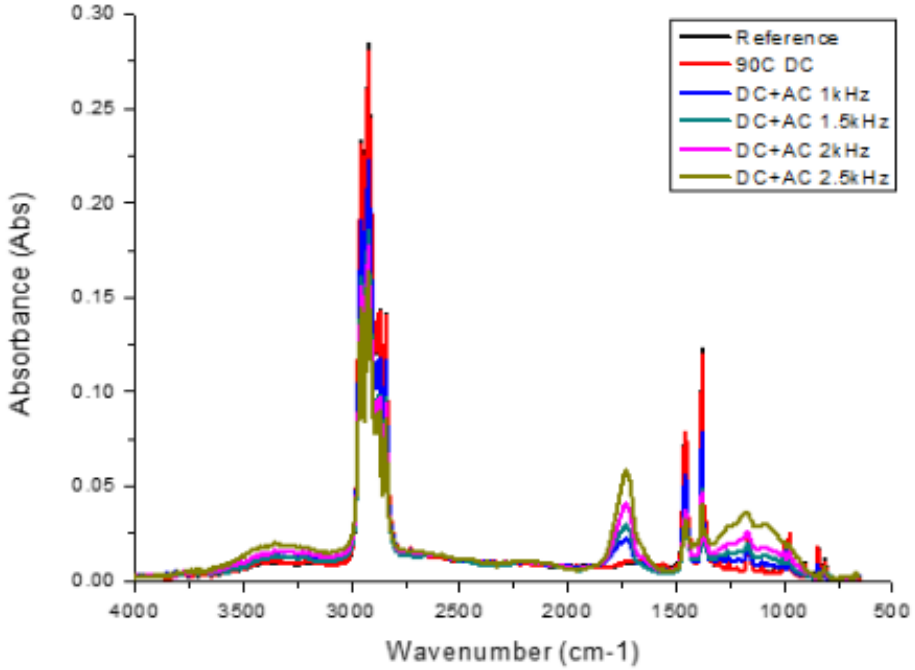

Figure 5.12. FTIR-ATR results of PP (aged under 50% voltage ratio at various frequencies).

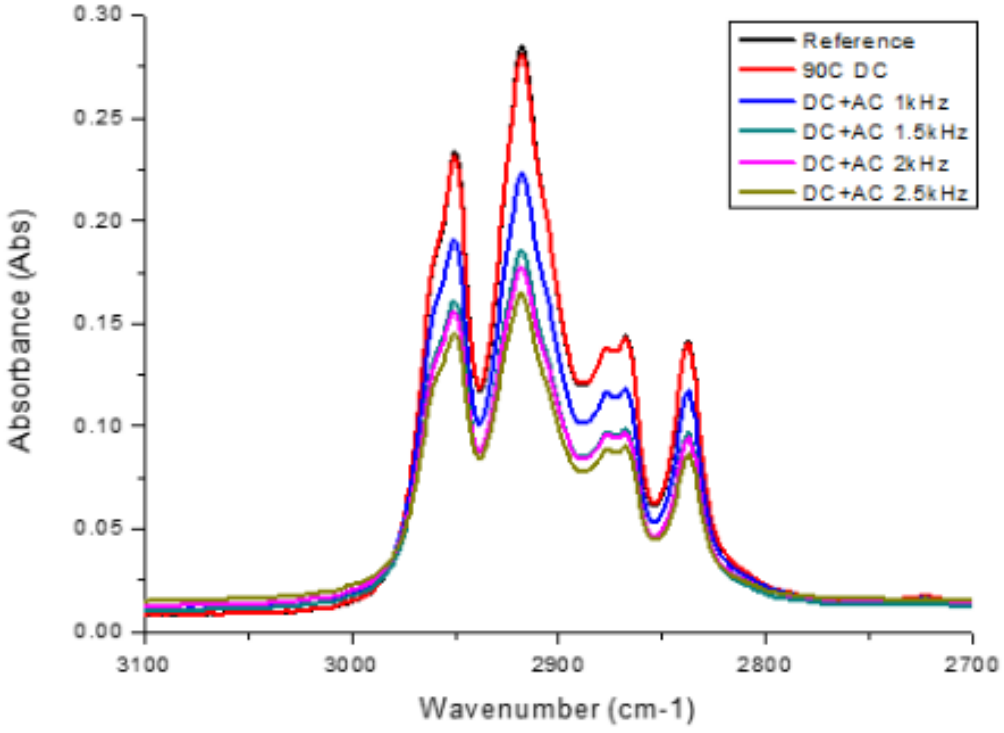

Figure 5.13. FTIR-ATR results for PP detailed view of C-H-groups (aged at 50% voltage ratio with various frequencies).

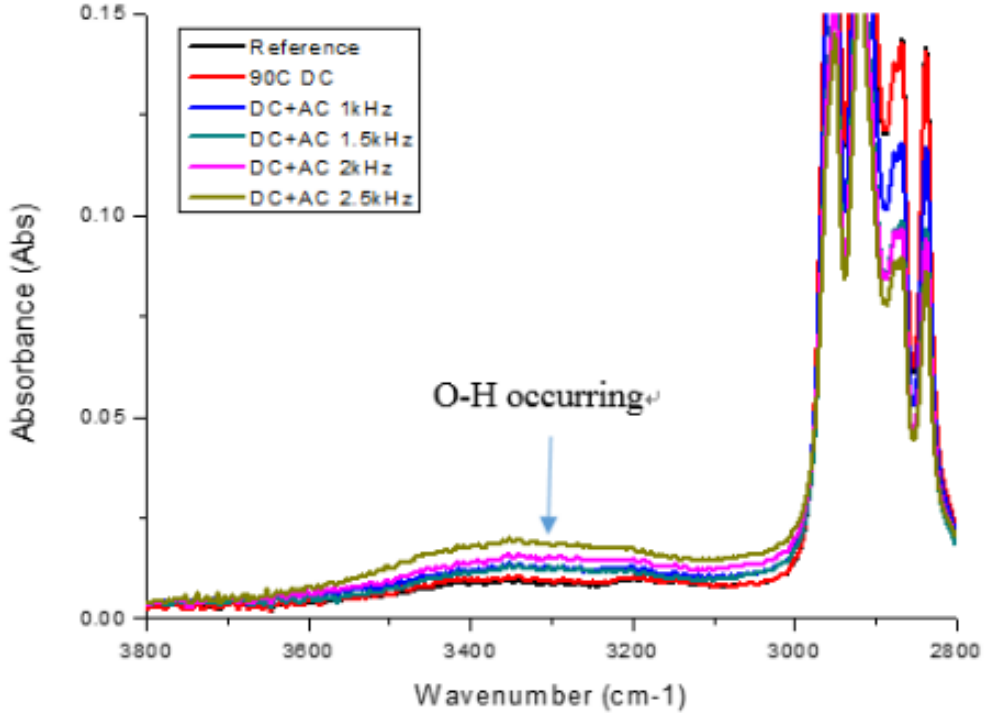

Figure 5.14. FTIR-ATR results for PP detailed view of OH-group (aged at 50% voltage ratio with various frequencies).

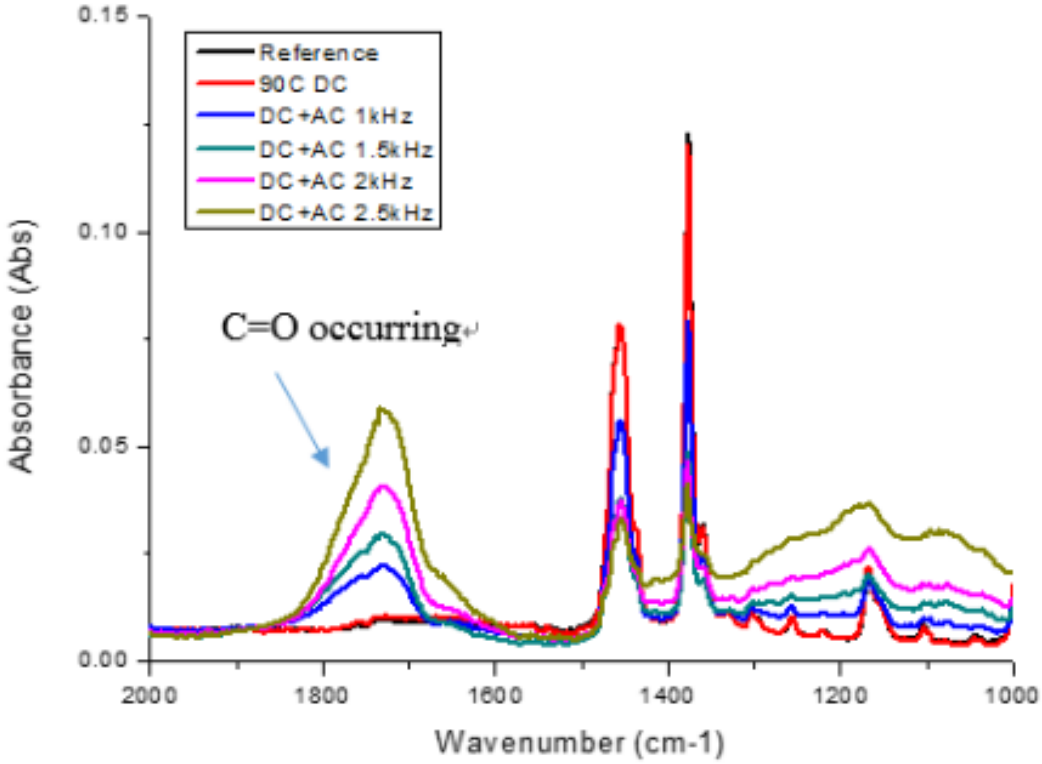

Figure 5.15. FTIR-ATR results for PP detailed view of carbonyl group (aged under 50% voltage ratio at various frequencies).

5.2.4 Carbonyl Index Comparison

From the data in Figure 5.8-5.15 and Carbonyl Index (CI) equation (5.1), the CI of PP aged at 90°C and at 30% and 50% voltage ratio can be calculated and is shown in Table 5.8 and Table 5.9, respectively. As there was no absorption observed at 1738 cm^{-1} the CI of PP for the 10% voltage ratio will be zero.

Table 5.8. Carbonyl Index of PP aged at 90°C at 30% voltage ratio.

Frequency (kHz)	A_{1738}	A_{1460}	CI
1	0.0158	0.0673	0.2350
1.5	0.0179	0.0636	0.2815
2	0.0194	0.0582	0.3341
2.5	0.0221	0.0562	0.3932

Table 5.9. Carbonyl Index of PP aged at 90°C at 50% voltage ratio.

Frequency (kHz)	A_{1738}	A_{1460}	CI
1	0.0227	0.0514	0.4419
1.5	0.0293	0.0379	0.7729
2	0.0404	0.0371	1.0887
2.5	0.0582	0.0330	1.7636

Figure 5.16 is based on the data in Table 5.8 and Table 5.9 for the CI of PP aged at 90°C with the 30% and 50% voltage ratios.

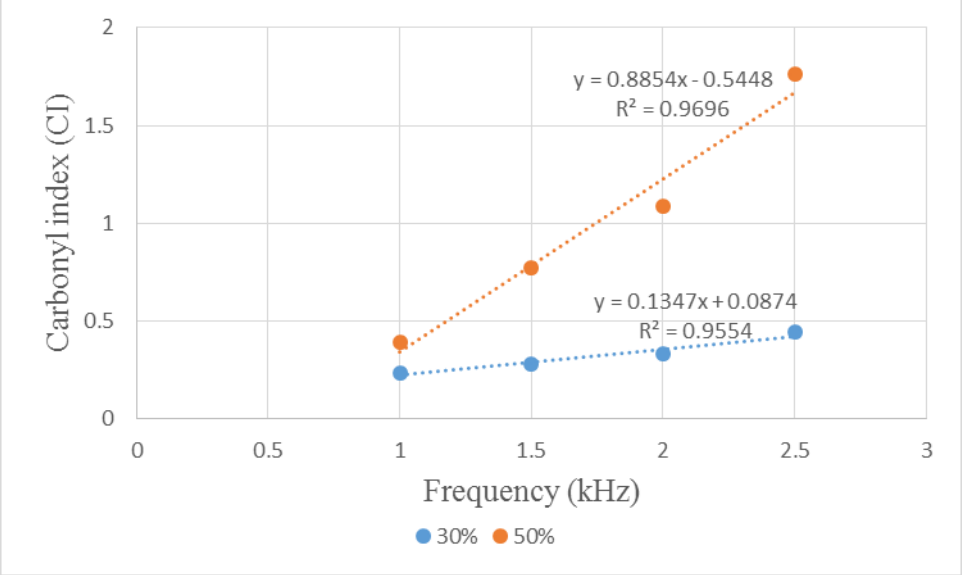

Figure 5.16. Carbonyl Index of PP aged by 90 °C at 30% and 50% voltage ratio.

In Figure 5.16, at 30% voltage ratio, CI increases from 0.23 to 0.39 with an increase of the superimposed frequency. The gradient is 0.1347 (Hz^{-1}). At 50% voltage ratio, CI value increases significantly. The gradient increases to 0.8854 (Hz^{-1}). This is because the apparent cumulative energy per second increases significantly more in the 50% voltage ratio than in 30% voltage ratio tests (as mentioned in Section 5.1). The changes in the CI value can be correlated with changes of susceptibility index and conductivity of PP samples, this will be demonstrated in Section 5.4.

5.3 Dielectric Spectroscopy Results

In this section, ε' and $tan\delta$ of PP aged under 90°C are shown in Figure 5.17-5.22. The samples were aged with the same three voltage ratios and four superimposed frequencies. In all figures, the investigated frequency for the DS measurements is in the range of 10^{-2} to 10^{4} Hz.

5.3.1 10% Voltage Ratio

The dielectric constant and dissipation factor of PP aged at 90°C at 10% voltage ratio are shown in Figure 5.17-5.18.

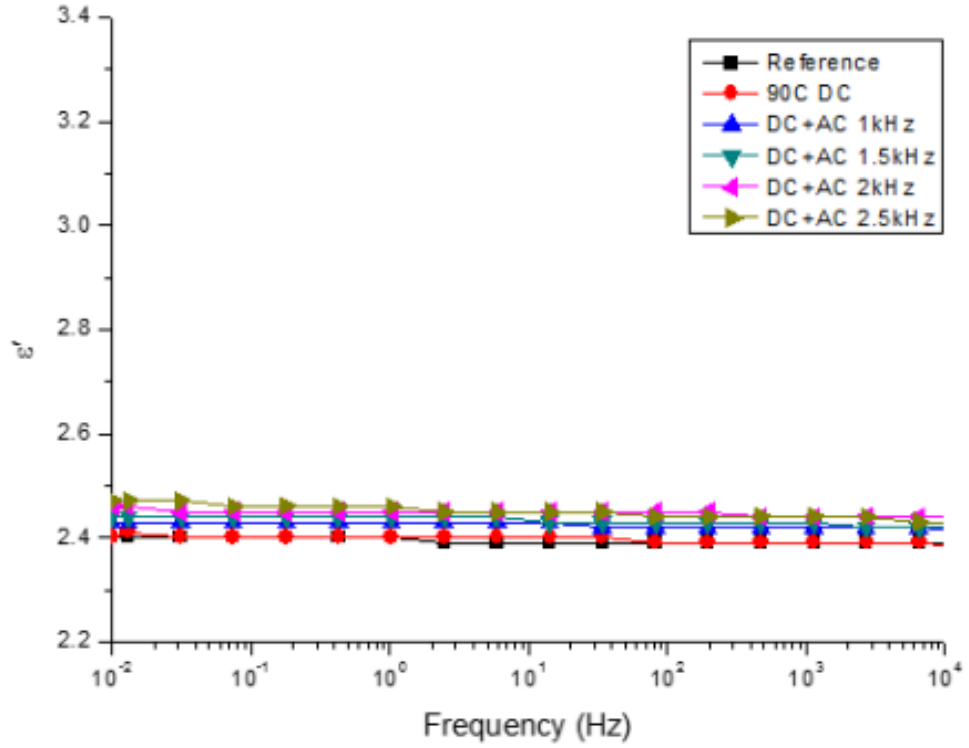

Figure 5.17. Dielectric constant of PP aged under 10% voltage ratio with various frequencies.

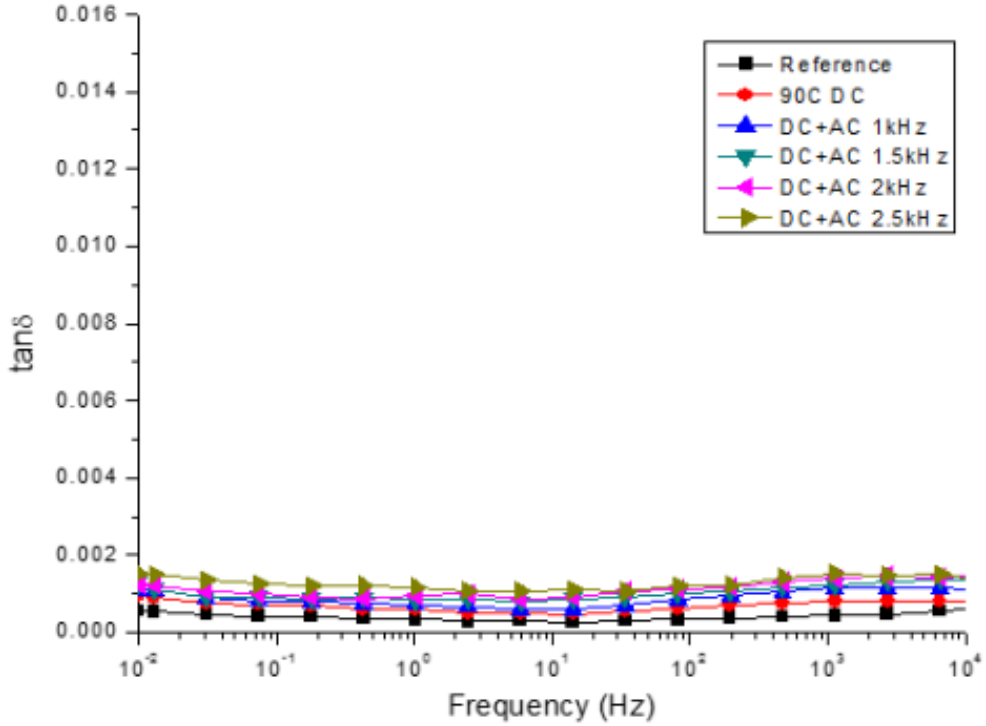

Figure 5.18. Dissipation factor of PP aged under 10% voltage ratio with various frequencies.

In Figure 5.17, ε' of each sample is almost constant in the measurement frequency range of 10^{-2}-10^{4} Hz. All values are within the range from 2.4 to 2.5. The ε' of the sample subjected to purely DC stress overlaps with ε' of the unaged reference sample. ε' of all samples aged by combined AC and DC voltages are slightly higher than the DC value.

In Figure 5.18, *tanδ* of all aged samples are higher than the reference value in the frequency range from 10^{-2} to 10^{4} Hz. The *tanδ* of samples subject to combined AC and DC voltages cannot be separated from the sample aged by pure DC stress. The small differences, if any, between the DC aged and DC/AC aged samples may be explained by the lack of evidence for the formation of polar molecular groups produced in 10% voltage ratio (see Section 5.2.1).

5.3.2 30% Voltage Ratio

The dielectric constant and dissipation factor of PP aged at 90°C at 30% voltage ratio are shown in Figure 5.19-5.20.

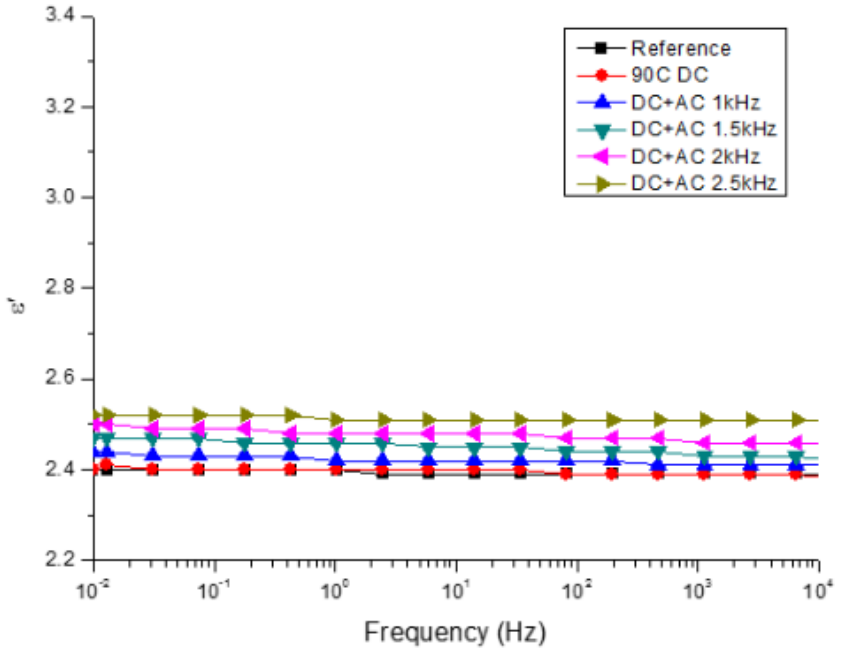

Figure 5.19. Dielectric constant of PP aged under 30% voltage ratio at various frequencies.

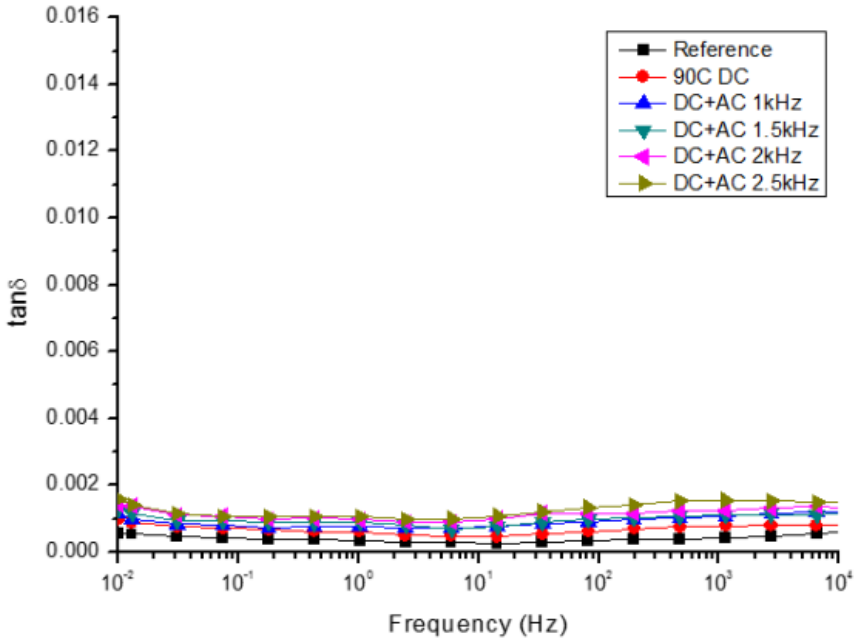

Figure 5.20. Dissipation factor of PP aged under 30% voltage ratio at various frequencies.

In Figure 5.19, ε' of the reference sample and the sample subjected to a purely DC stress are included for reference. The ε' of samples subjected to combined AC and DC voltages appear to be slightly larger. The values of ε' lie between 2.4 to 2.55.

In Figure 5.20, the *tanδ* of samples subjected to combined AC and DC voltages are slightly higher than the DC value and appear to be increasing with applied AC frequency. There is also evidence of an increase in *tanδ* at low frequencies.

5.3.3 50% Voltage Ratio

The dielectric constant and dissipation factor of PP aged at 90°C and at 50% voltage ratio are shown in Figure 5.21-5.22.

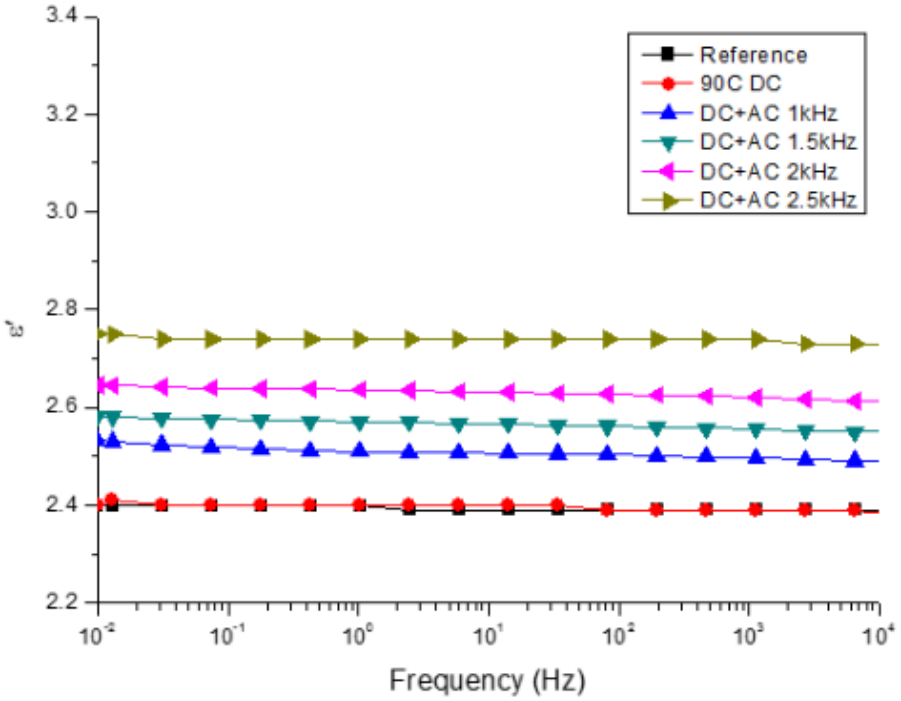

Figure 5.21. Dielectric constant of PP aged under 50% voltage ratio at various frequencies.

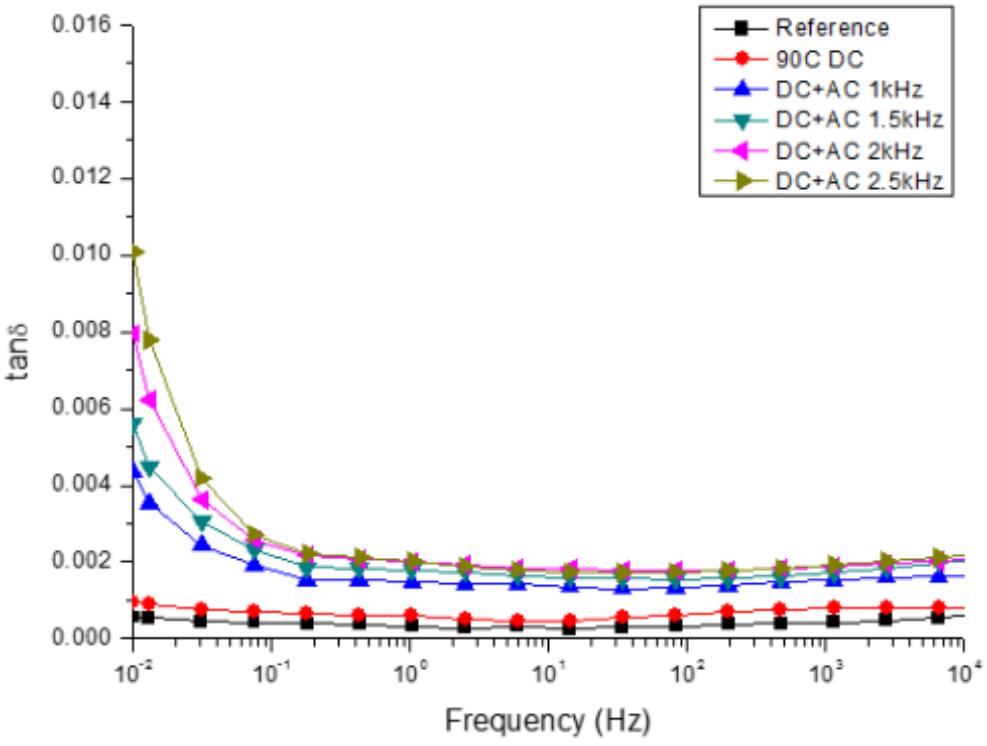

Figure 5.22. Dissipation factor of PP aged under 50% voltage ratio at various frequencies.

In Figure 5.21, ε' of samples subjected to combined AC and DC at 50% ratio stress are much higher than the DC value. The values lie in the region from 2.5 to 2.75. It is clear to see that ε' increases with increasing of superimposed frequency. This is because there were more polar molecular groups, such as O-H, C=O, generated at 50% voltage ratio, as shown in Section 5.2.3. As the superimposed frequency increases, the amount and kinds of polar molecular groups (O-H and C=O) increase which leads to ε' increasing.

In Figure 5.22, *tanδ* of all samples subjected to combined AC and DC voltages are higher than the DC value. For each curve, *tanδ* increases with the measurement frequency below 1 Hz. For samples aged by combined voltages, overall *tanδ* increases with increase of the superimposed AC frequency. Similar to the results for HDPE, the peak observed at low measurement frequencies is associated with DC conduction processes which will be discussed in section 5.3.4.1.

5.3.4 Discussion

5.3.4.1 Conductivity

Plots of ε'' vs. $1/\omega$ were made in a similar manner to 4.4.4.1 and were found to be linear. Values of σ/ε_0 were extracted from the gradients of these plots. The derived behaviour for the low frequency conductivity for PP aged at 90°C and at 10%, 30% and 50% voltage ratio are summarized in Appendix D: Table D.1-D.3 and Figure 5.23-5.25.

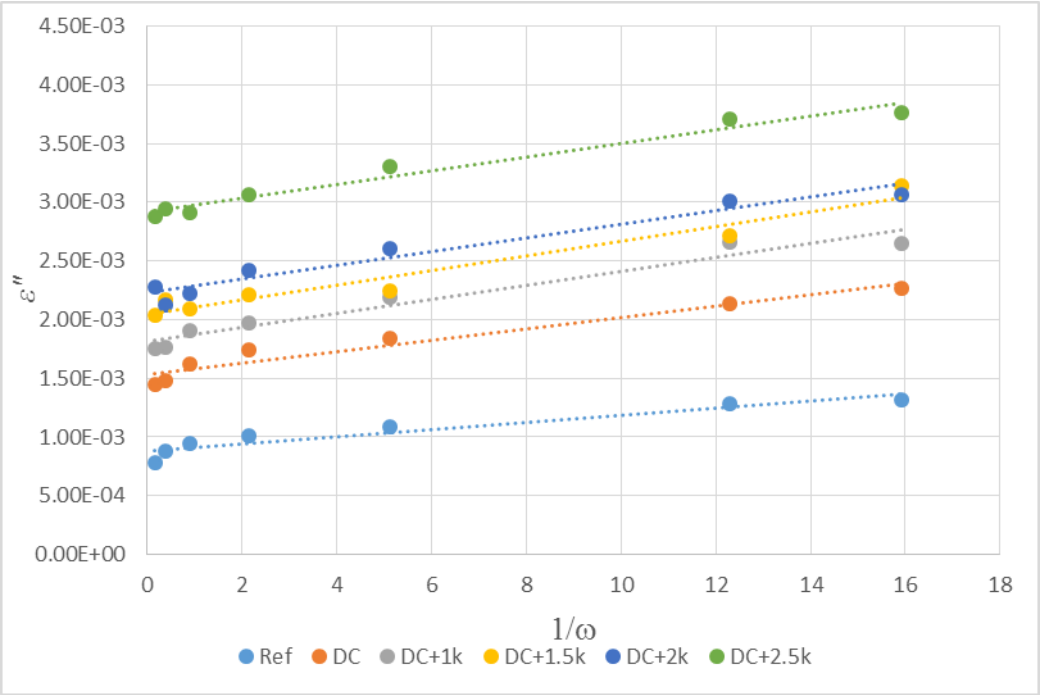

Figure 5.23. ε'' vs. 1/ω of PP aged at 90°C and at 10% voltage ratio.

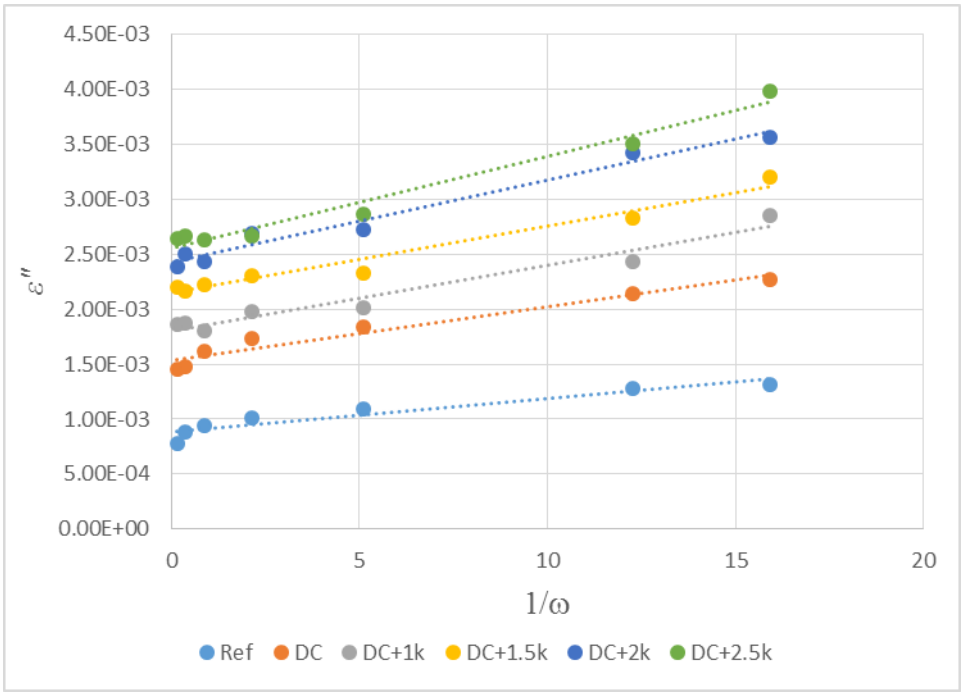

Figure 5.24. ε'' vs. 1/ω of PP aged at 90°C and at 30% voltage ratio.

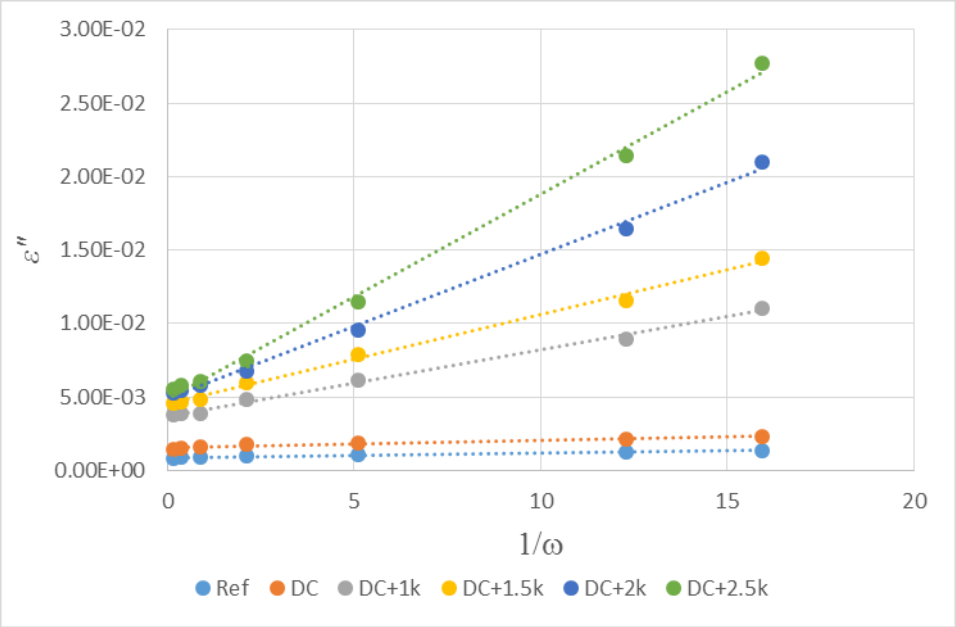

Figure 5.25. ε″ vs. 1/ω of PP aged at 90°C and at 50% voltage ratio.

Based on Figure 5.23-5.25, conductivity of PP aged by 90°C can be summarized in Table 5.10 and Figure 5.26.

Table 5.10. Conductivity of PP aged by 90°C.

Waveform	Conductivity (*fS/m*)		
	10% Voltage Ratio	30% Voltage Ratio	50% Voltage Ratio
Reference	0.2673	0.2673	0.2673
DC	0.4292	0.4292	0.4292
DC+1k	0.5275	0.5275	4.0091
DC+1.5k	0.5487	0.5390	5.4074
DC+2k	0.5142	0.6646	8.6907
DC+2.5k	0.5168	0.7372	12.3900

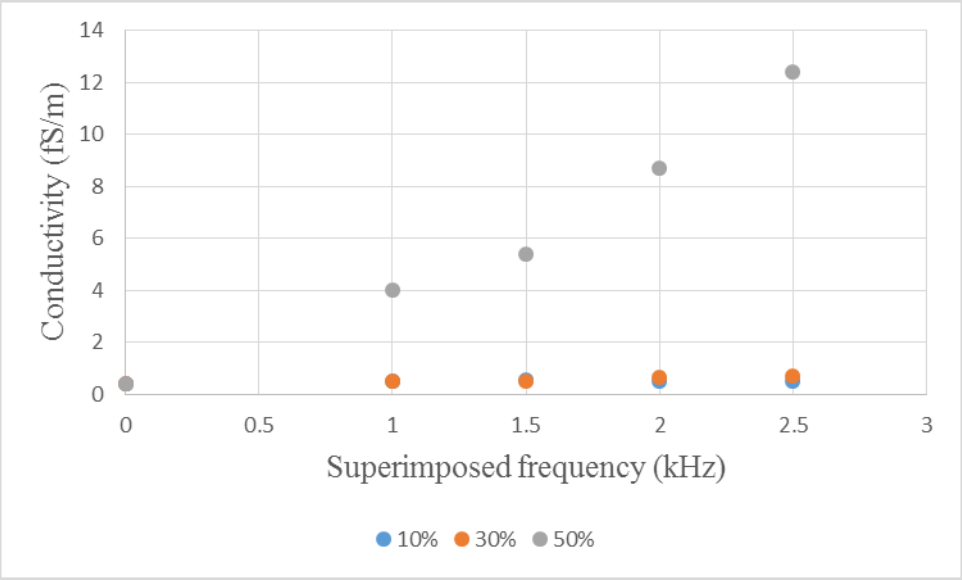

Figure 5.26. Conductivity of PP aged by 90°C.

According to the data in Table 5.10 and Figure 5.26, for PP aged at 90°C under purely DC voltage, the conductivity is higher than that seen for the unaged sample. For samples aged by combined AC and DC voltages, the conductivity is even higher. For the samples aged at 10% and 30% voltage ratios, the conductivity of all samples are below 1 *fS/m*. At 10% voltage ratio, no significant dependence on frequency of the AC voltage component is observed, at 30% voltage ratio the conductivity appears to increase for the higher frequencies of the AC voltage component. For the samples aged at 50% voltage ratio, the value of conductivity increases significantly and it is clear that the conductivity increases with increasing AC frequency.

5.3.4.2Dielectric Susceptibility Index (χI)

The calculated values of χI of PP aged at 90°C are shown in Table 5.11 and their behaviour as a function of AC frequency are shown in Figure 5.27.

Table 5.11. Dielectric susceptibility index χI of PP aged by 90°C.

Waveform	Susceptibility Index χI		
	10%	30%	50%
DC	0	0	0
DC+1k	0.0214	0.0286	0.0949
DC+1.5k	0.0286	0.0500	0.1296
DC+2k	0.0429	0.0643	0.1755
DC+2.5k	0.0500	0.0714	0.2500

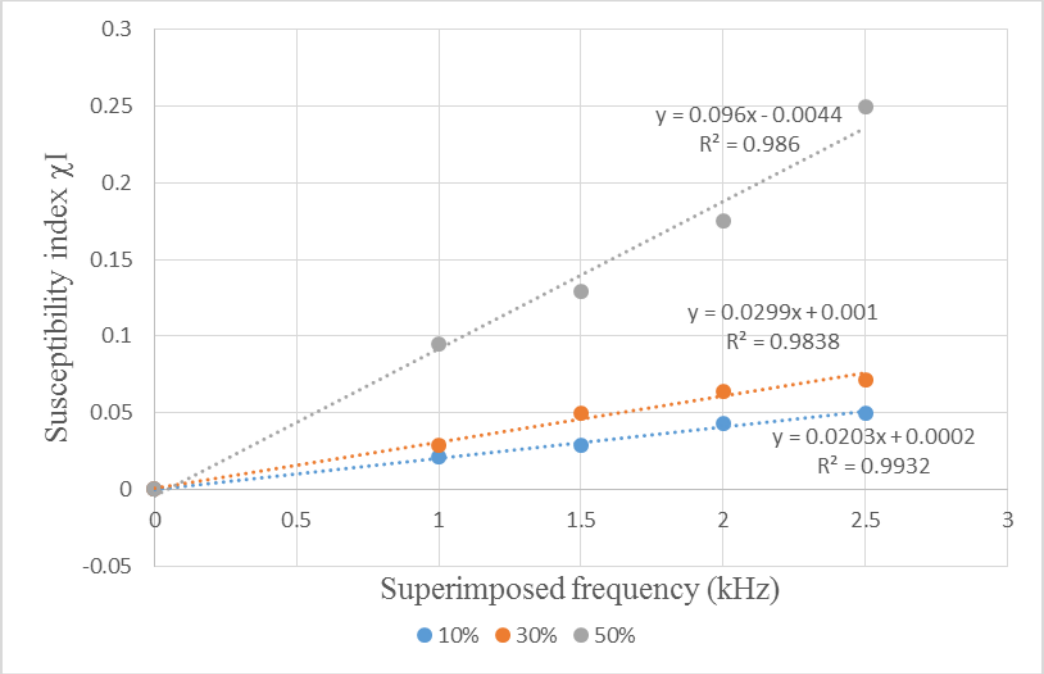

Figure 5.27. Dielectric susceptibility index χI of PP aged at 90°C.

From Figure 5.27 it can be seen that for all three voltage ratios χI increases with increasing frequency of the AC component of stress. At any given frequency the value of χI increases with the voltage ratio. The gradients of the lines of best fit also increase with increasing voltage ratio.

5.4 Discussion

The relationship between Carbonyl Index (CI) and apparent cumulative energy per second ($\dot{E}_{CA}$) is shown in Table 5.12 and Figure 5.28.

Table 5.12. Apparent cumulative energy per second vs. Carbonyl Index.

Frequency (kHz)	30% Voltage Ratio		50% Voltage Ratio	
	$\dot{E}_{CA}$	CI	$\dot{E}_{CA}$	CI
1	842	0.2350	6380	0.4419
1.5	1245	0.2815	10370	0.7729
2	1663	0.3341	14507	1.0887
2.5	2095	0.3932	19000	1.7636

In Figure 5.28, it can be seen that as the value of $\dot{E}_{CA}$ increases, the value of CI is increasing and that the behaviour appears to be linear.

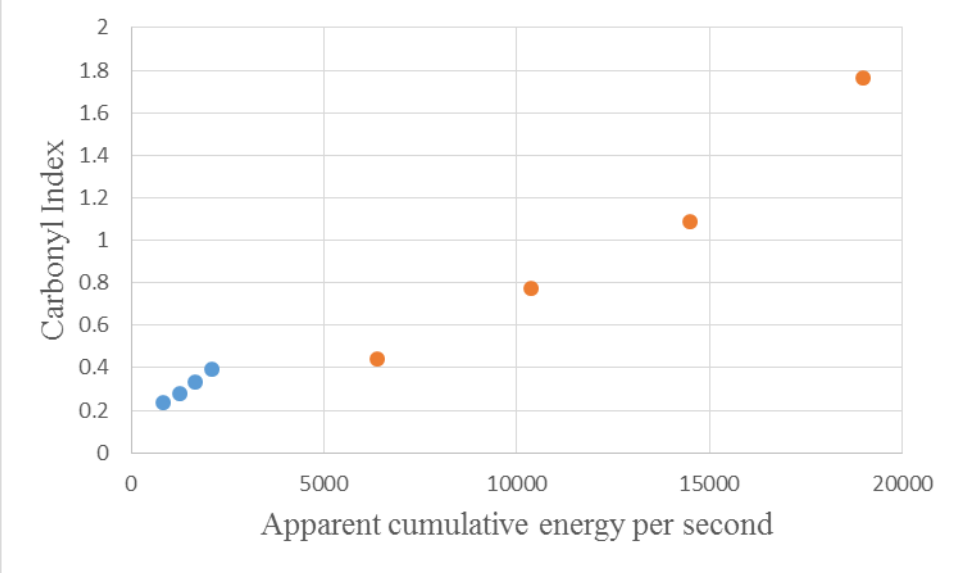

Figure 5.28. Apparent cumulative energy per second vs. Carbonyl Index.

The relationship of $\dot{E}_{CA}$ and σ is shown in Table 5.13 and Figure 5.29.

Table 5.13. Apparent cumulative energy per second vs. conductivity.

Frequency (kHz)	30% Voltage Ratio		50% Voltage Ratio	
	$\dot{E}_{CA}$	σ (*fS/m*)	$\dot{E}_{CA}$	σ (*fS/m*)
1	842	0.5275	6380	4.0091
1.5	1245	0.5390	10370	5.4074
2	1663	0.6646	14507	8.6907
2.5	2095	0.7372	19000	12.3900

In Figure 5.29, the conductivity is increasing as the value of $\dot{E}_{CA}$ increases, as with the Carbonyl Index there is a strong linear correlation between the conductivity and the apparent cumulative energy per second $\dot{E}_{CA}$.

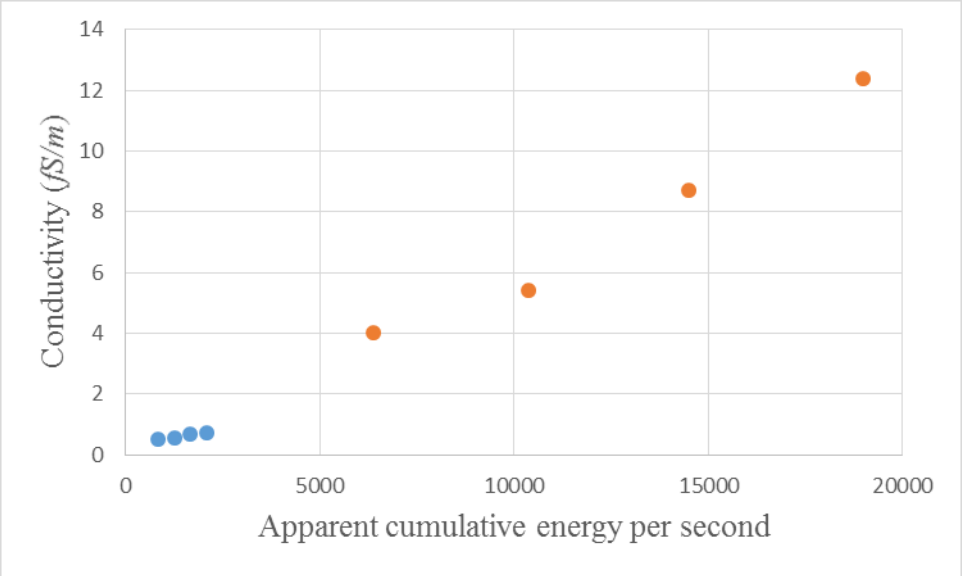

Figure 5.29. Apparent cumulative energy per second vs. conductivity.

The relationship of $\dot{E}_{CA}$ and χI is shown in Table 5.14 and Figure 5.30.

Table 5.14. Apparent cumulative energy per second vs. χI.

Frequency (kHz)	30% Voltage Ratio		50% Voltage Ratio	
	$\dot{E}_{CA}$	χI	$\dot{E}_{CA}$	χI
1	842	0.0286	6380	0.0949
1.5	1245	0.0500	10370	0.1296
2	1663	0.0643	14507	0.1755
2.5	2095	0.0714	19000	0.2500

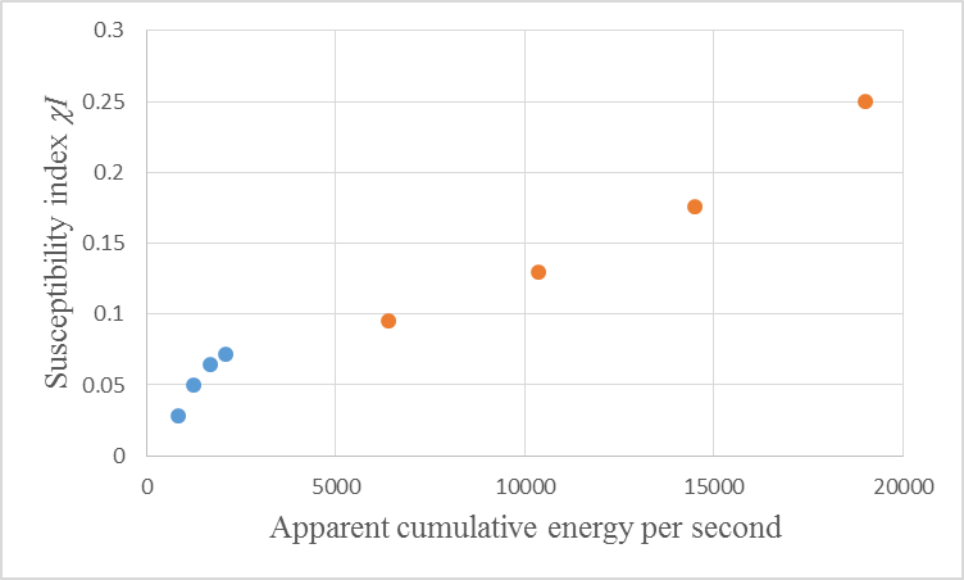

Figure 5.30. Apparent cumulative energy per second vs. χI.

As with the CI and conductivity the Susceptibility index χI increases as $\dot{E}_{CA}$ increases. The relationship is clearly linear at higher values of $\dot{E}_{CA}$ associated with the 50% voltage ratio. At lower values of $\dot{E}_{CA}$ there may be a different relationship between χI and the apparent cumulative energy per second.

In Figure 5.31, as would be expected from Figure 5.28 and Figure 5.29 as the value of CI increases the value of conductivity increases. There is a broadly linear relationship between CI and conductivity.

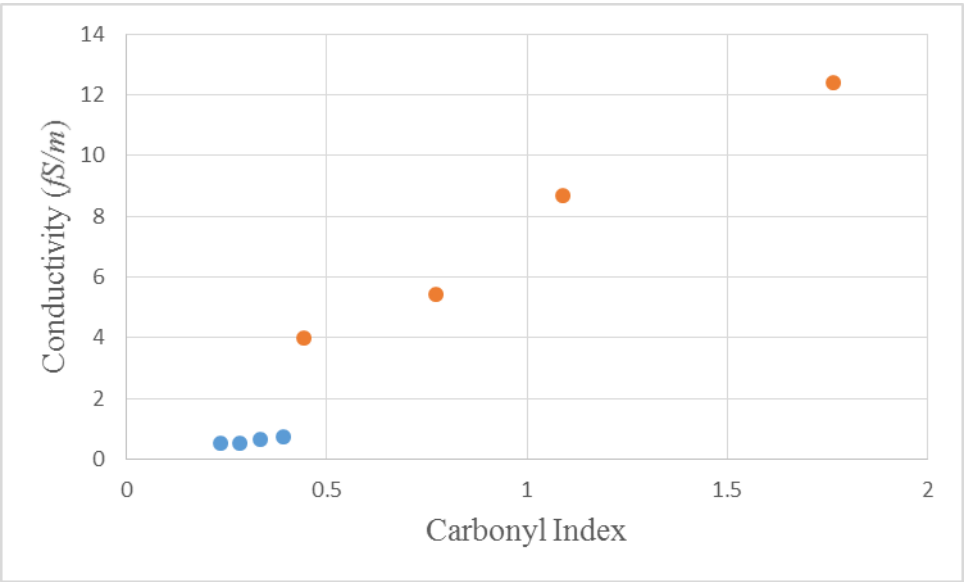

Figure 5.31. Carbonyl Index vs. conductivity.

As would be expected from Figure 5.28 and Figure 5.30 as the value of CI increases as the value of χI increases. There is a broadly linear relationship between CI and χI. Though they may be differences in behaviour at low values of CI associated with stressing at the 30% voltage ratio.

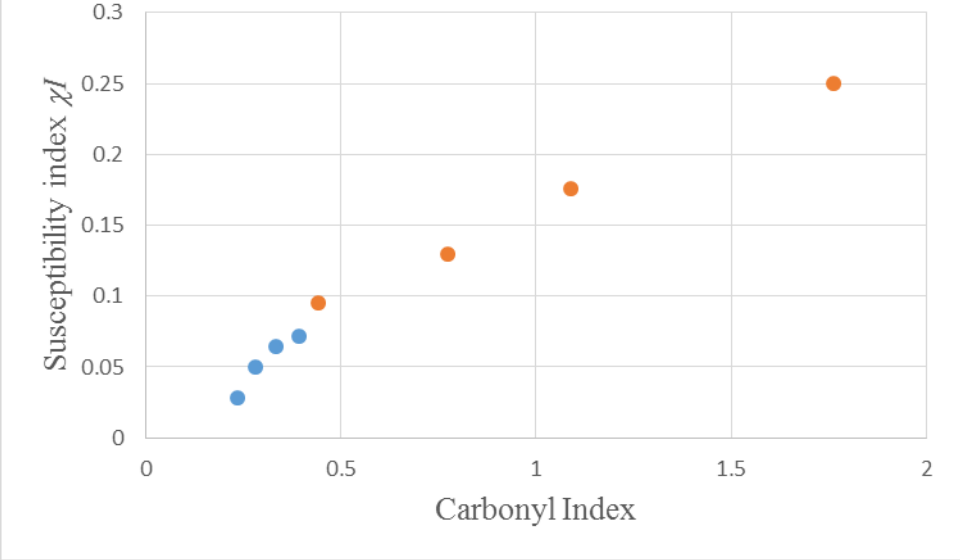

Figure 5.32. Carbonyl Index vs. χI.

5.5 Conclusions

The PD mechanism of PP aged at 90°C is similar to that of HDPE.

The apparent cumulative energy per second ($\dot{E}_{CA}$) has been calculated and this index increases as the voltage ratio increases and as the frequency of the AC component is increased. The value is 842 at 1 kHz at 30% voltage ratio and 19000 at 2.5 kHz at 50% voltage ratio.

From the FTIR-ATR values for the Carbonyl Index which reflects the chemical changes on the surface have been calculated. The changes in the Carbonyl Index with frequency and voltage ratio correlate with the apparent cumulative energy per cycle. The value is 0.2350 at 1 kHz at 30% voltage ratio and 1.7636 at 2.5 kHz at 50% voltage ratio.

From the dielectric spectroscopy data values for the conductivity (σ) and an index reflecting the change in susceptibility (χI) have been calculated. These indeces also correlate with the apparent cumulative energy per cycle. The value of σ is 0.5275 *fS/m* at 1 kHz at 30% voltage ratio and 12.3900 at 2.5 kHz at 50% voltage ratio. The value of χI is 0.0286 at 1 kHz at 30% voltage ratio and 0.2500 at 2.5 kHz at 50% voltage ratio.

5.6 References

[1] R. Morent, N. De Geyter, C. Leys, L. Gengembre and E. Payen, "Comparison between XPS- and FTIR-analysis of plasma-treated polypropylene film surfaces", Surf. Interface Anal, Vol. 40, pp. 597–600, 2008.

[2] Emma Strömberg, Sigbritt Karlsson, "The Design of a Test Protocol to Model the Degradation of Polyolefins During Recycling and Service Life", Journal of applied polymer science, Vol.112, Issue 3, pp.1835-1844, 2009.

6. Polypropylene aged at 110°C

PP samples are aged at 110°C with the same 3 voltage ratios (10%, 30% and 50%) and four frequencies (1 kHz, 1.5 kHz, 2 kHz and 2.5 kHz) as used in chapters 4 and 5. The PRPD, FTIR-ATR and DS measurements were carried out for analysis. In this chapter, the data is demonstrated and summarized.

Section 6.1 describes the PRPD results. The mean and standard deviation of PD voltages, the number of discharges, the PD apparent cumulative energy and the apparent cumulative energy per second are the indeces used to describe the PRPD data. How these indeces change with superimposed frequency and voltage ratio are reported. The standard deviation for PRPD results is within ±10% range.

Section 6.2 describes the FTIR-ATR results. The behaviour of the Carbonyl Index of samples changes with various superimposed frequencies and voltage ratios is summarized. The standard deviation for FTIR-ATR results is within ±3% range.

Section 5.3 describes the DS results. The variation of the conductivity and dielectric susceptibility index with superimposed frequencies and voltage ratios are summarized. The standard deviation for DS results is within ±2% range.

Section 6.4 shows the relationship of PD apparent cumulative energy per second, Carbonyl Index, conductivity and dielectric susceptibility index.

Section 6.5 is the conclusions.

6.1 PRPD Results

As with HDPE and PP aged at 90°C, when the voltage ratio was 10%, no PD signals were detected at any of the AC frequencies considered. PD signals could be detected at 30% and 50% voltage ratio. The PRPD patterns of PP aged at 110°C (Appendix G) behave in a similar manner to those of HDPE and PP aged at 90°C when the voltage ratios and frequencies are varied.

As before, statistical data of the mean PD voltage with standard deviation, the number of discharges was extracted and the PD apparent cumulative energy and apparent cumulative energy per second were calculated. This is shown in Table 6.1-6.5 and Figure 6.1-6.3.

Table 6.1. Mean PD voltage with standard deviation of PP aged by 110°C at 30% and 50% voltage ratios.

Frequency (kHz)	PD voltage (V) at 30% voltage ratio		PD voltage (V) at 50% voltage ratio	
	$\overline{V_{PD}}$	σ_{PD}	$\overline{V_{PD}}$	σ_{PD}
1	0.233	0.022	0.72	0.066
1.5	0.24	0.025	0.82	0.072
2	0.244	0.027	0.88	0.08
2.5	0.315	0.031	1.22	0.117

Figure 6.1 is drawn according to the data in Table 6.1.

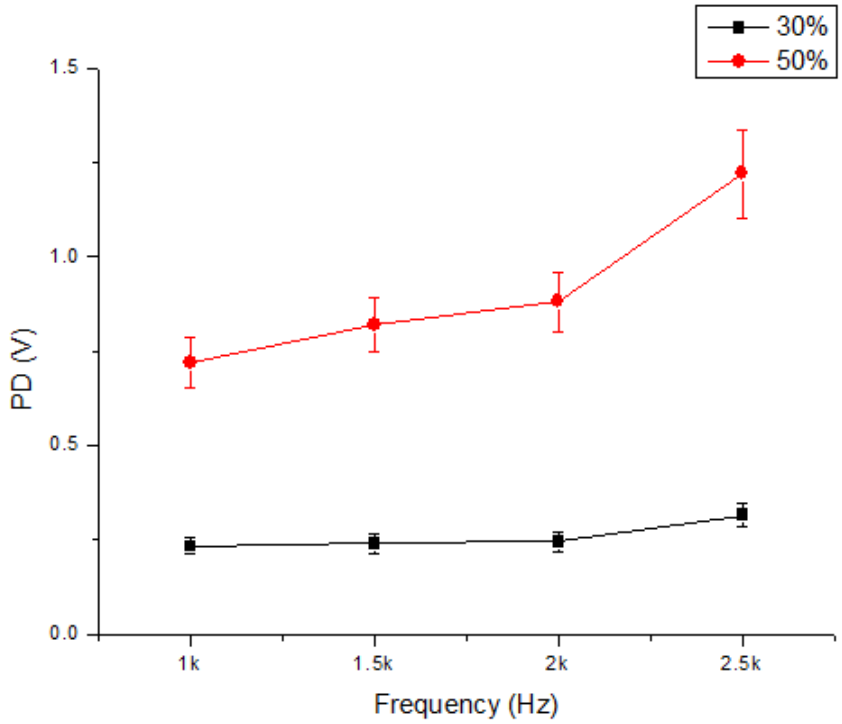

Figure 6.1. Mean with standard deviation of PD voltage.

In Figure 6.1, for PP samples aged at 30% voltage ratio, $\overline{V_{PD}}$ is in the range from 0.2-0.3 V. The value is reasonably constant ≈0.24 V in the range of 1-2 kHz but slightly increased to 0.315 V at 2.5 kHz. For the 50% voltage ratio, the mean PD voltage was at least 3 times that of the value of 30% voltage ratio at each frequency. $\overline{V_{PD}}$ increases along with the increase of superimposed frequency. The value is below 0.9 V at 1-2 kHz but rapidly increases to 1.22 V at 2.5 kHz.

Data of number of discharge n_{PD} and the mean discharge rate $\dot{n}_{PD}(s^{-1})$ is shown in Table 6.2 and Table 6.3 for 30% and 50% voltage ratio, respectively.

Table 6.2. Number of discharges of PP aged at 110°C and at 30% voltage ratio.

Frequency (kHz)	n_{PD}	T_{Meas}(s)	$\dot{n}_{PD}(s^{-1})$
1	7789	1.5	5193
1.5	7755	1	7755
2	7739	0.75	10319
2.5	7183	0.6	11971

Table 6.3. Number of discharges of PP aged at 110°C and at 50% voltage ratio.

Frequency (kHz)	n_{PD}	T_{Meas}(s)	$\dot{n}_{PD}(s^{-1})$
1	19951	1.5	13301
1.5	18880	1	18880
2	17150	0.75	22867
2.5	14005	0.6	23342

$\dot{n}_{PD}(s^{-1})$ vs. superimposed frequency is shown in Figure 6.2, from the data in Tables 6.2 and 6.3.

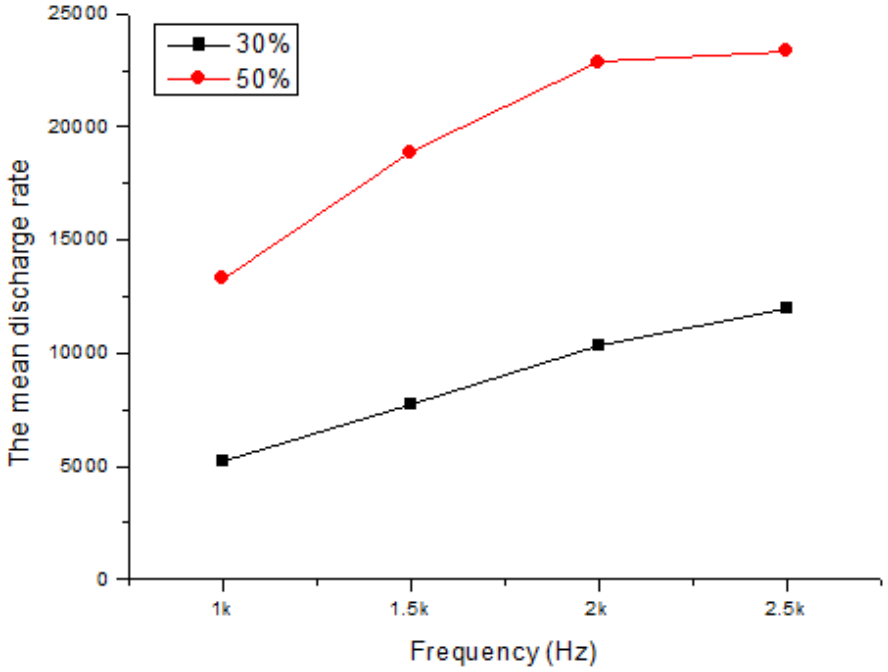

Figure 6.2. $\dot{n}_{PD}(s^{-1})$ of PP aged by 110°C at 30% and 50% voltage ratio.

Although the data in Table 6.2 and 6.3 again suggests that the partial discharge activity is falling with increasing frequency, once the changes in record time are taken into account $\dot{n}_{PD}(s^{-1})$ is increasing with frequency. As was observed before in PP at 90°C and for HDPE. The discharge activity is significantly larger for the 50% voltage ratio.

Data of apparent cumulative energy E_{CA} and the apparent cumulative energy per second $\dot{E}_{CA}$ at 30% and 50% voltage ratio is shown in Table 6.4 and Table 6.5, respectively.

Table 6.4. Apparent cumulative energy per second of PP aged at 110°C and at 30% voltage ratio.

Frequency (kHz)	E_{CA}	T_{Meas}(s)	$\dot{E}_{CA}$
1	1815	1.5	1210
1.5	1861	1	1861
2	1888	0.75	2517
2.5	2263	0.6	3772

Table 6.5. Apparent cumulative energy per second of PP aged at 110°C and at 50% voltage ratio.

Frequency (kHz)	E_{CA}	T_{Meas}(s)	$\dot{E}_{CA}$
1	14365	1.5	9577
1.5	15482	1	15482
2	15620	0.75	20827
2.5	16964	0.6	28273

Figure 6.3 is drawn according to the data from Table 6.4-6.5.

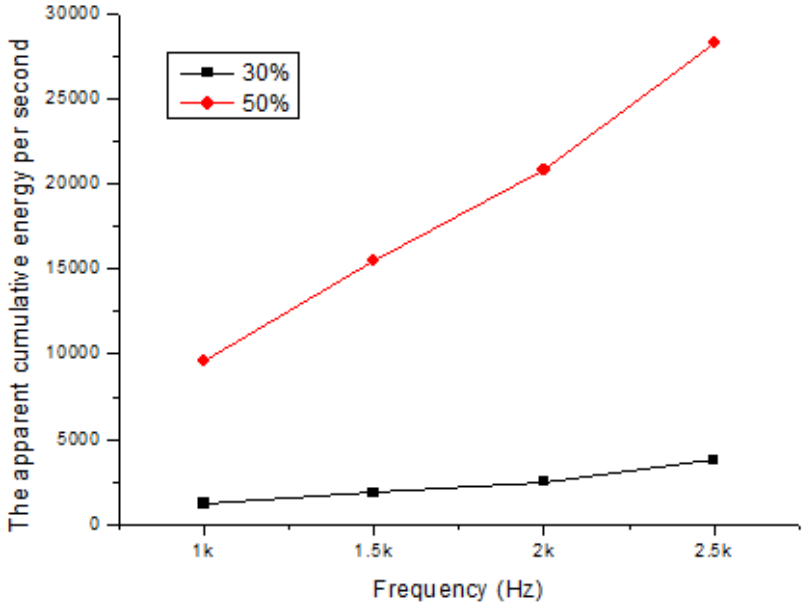

Figure 6.3. $\dot{E}_{CA}$ of PP aged at 110°C and at 30% and 50% voltage ratio.

In Figure 6.3, each curve increases with increasing superimposed frequency. At 30% voltage ratio, the value increases steadily from 1210 to 3772. At 50% voltage ratio, the values significantly increase to about 8 times of the value at 30% voltage ratio at each frequency and with increase in superimposed frequency increases, the value

rapid increases to 28273 at 2.5 kHz.

The possible mechanisms to explain the observed PD behaviour were discussed in Section 4.2.

6.2 FTIR-ATR Results

The FTIR-ATR results of PP aged at 110°C show that the behaviour is similar to that observed of PP aged by 90°C: absorption of C-H groups of all aged PP samples are lower than the reference unaged PP sample. It is hard to see any increase in the peaks associated with the carbonyl group in the reference unaged sample, the sample exposed to only DC and the samples aged by AC and DC combined voltages at 10% voltage ratio. Carbonyl groups appear at 30% and 50% voltage ratio. O-H groups appear in samples aged at 30% and 50% voltage ratio. The intensity of carbonyl group and O-H group increases with the superimposed frequency. These changes indicate that an oxidation aging process was occurring and it was enhanced by the combined AC and DC voltages. As the aging temperature was 20°C higher than in Chapter 5 any chemical reactions initiated by the partial discharges may progress more rapidly and have a different final equilibrium condition. This is supported by the behaviour of the absorption (of C-H group decreasing but the absorption of C=O group and O-H group is increasing). Details are shown in Section 6.2.1-6.2.3.

6.2.1 10% Voltage Ratio

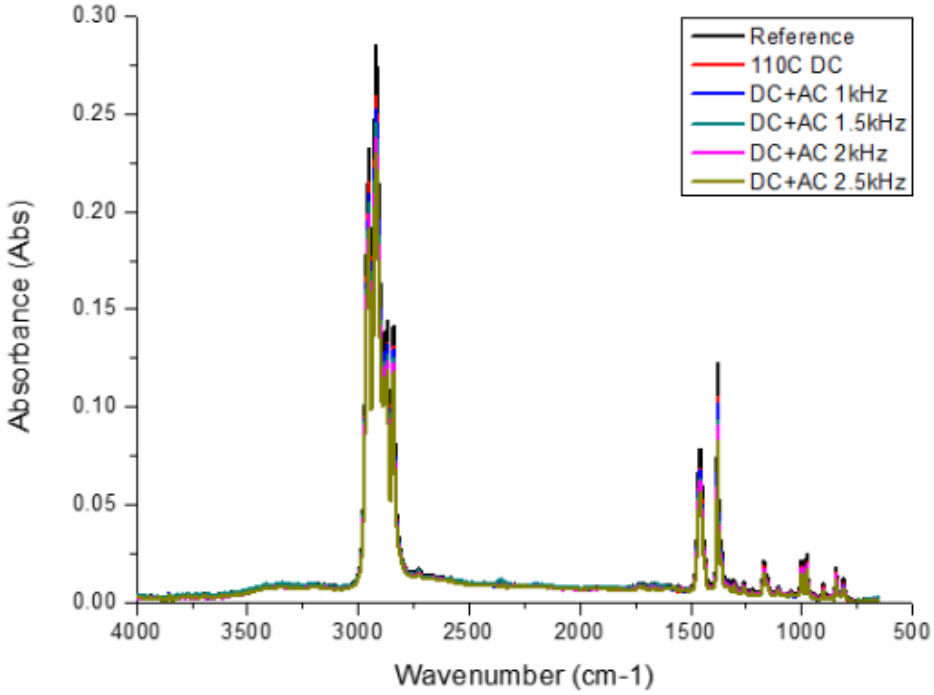

Figure 6.4. FTIR-ATR results of PP (aged under 10% voltage ratio at various frequencies).

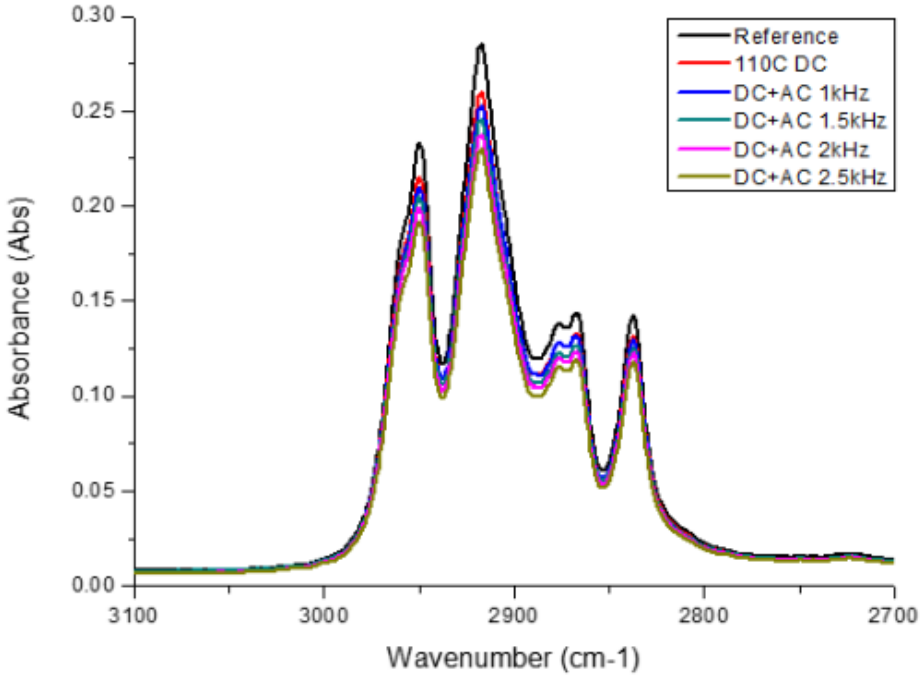

Figure 6.5. FTIR-ATR results for PP detailed view of C-H-groups (aged under 10% voltage ratio at various frequencies).

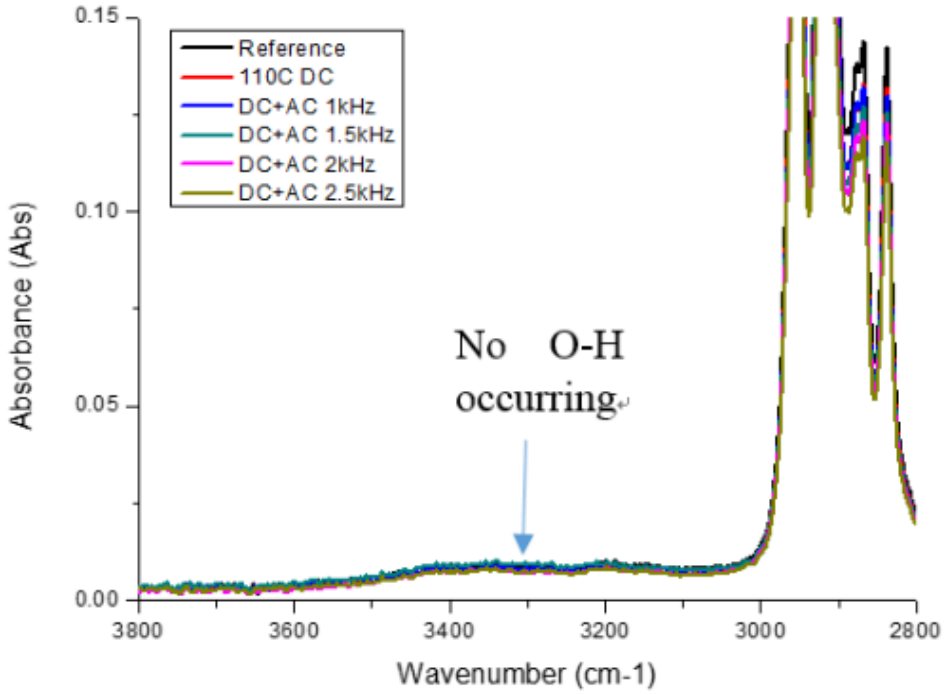

Figure 6.6. FTIR-ATR results for PP detailed view of OH-group (aged under 10% voltage ratio at various frequencies).

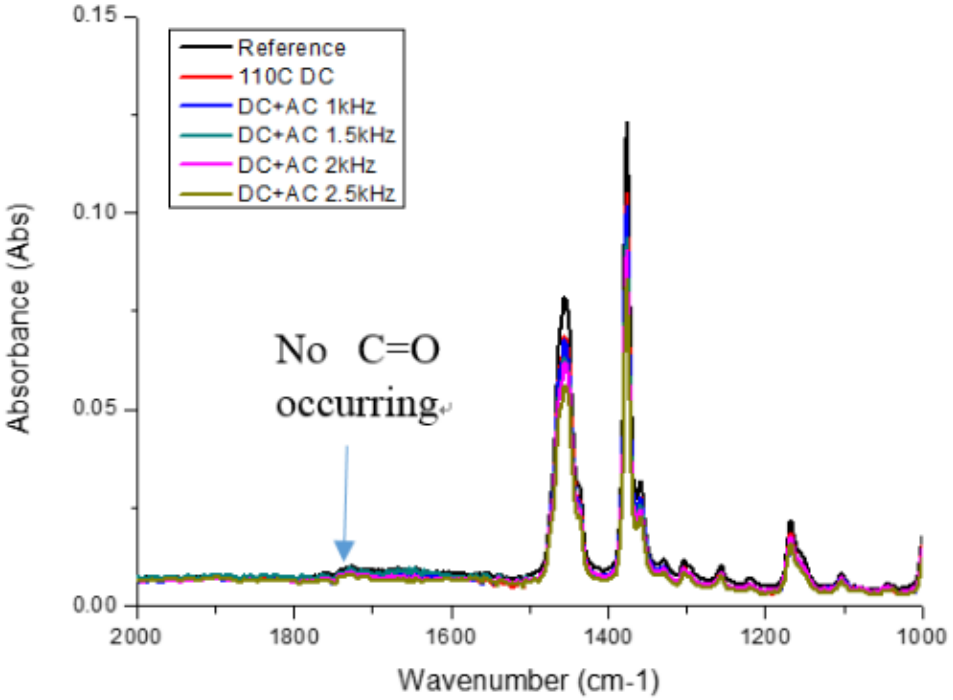

Figure 6.7. FTIR-ATR results for PP detailed view of carbonyl group (aged under 10% voltage ratio at various frequencies).

6.2.2 30% Voltage Ratio

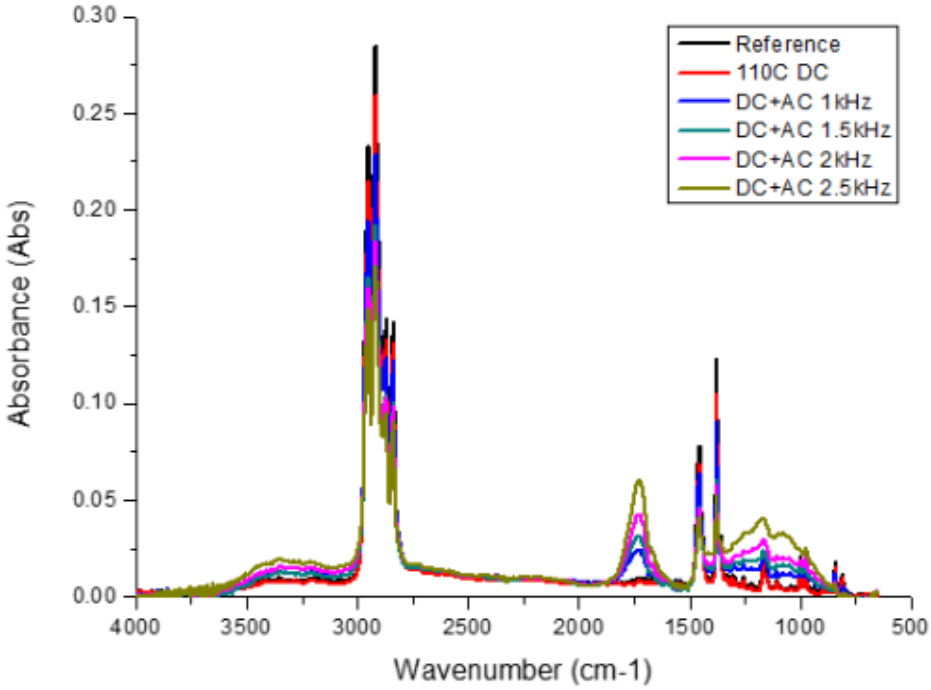

Figure 6.8. FTIR-ATR results of PP (aged under 30% voltage ratio at various frequencies).

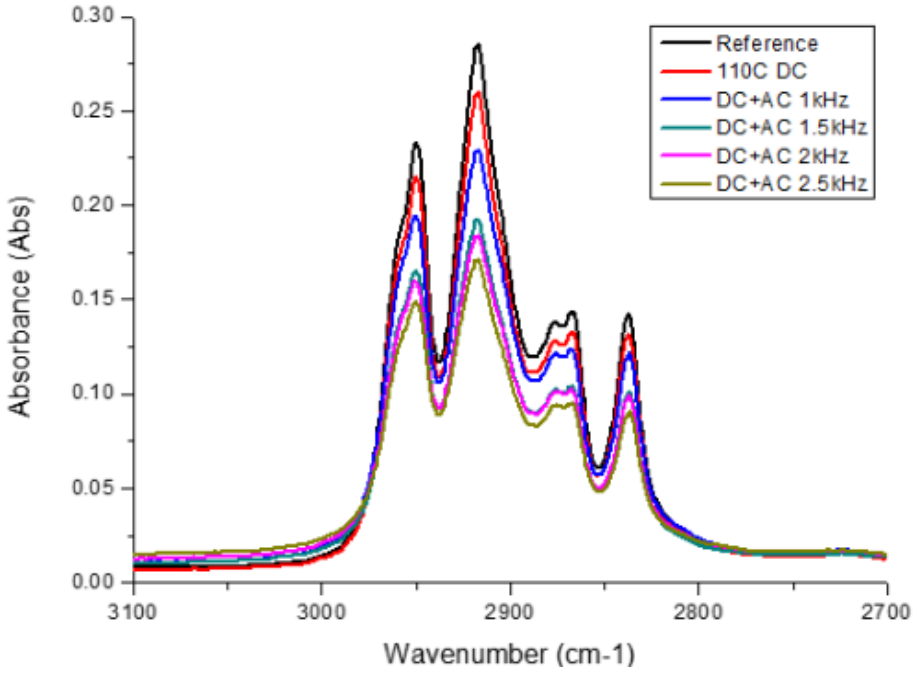

Figure 6.9. FTIR-ATR results for PP detailed view of C-H-groups (aged under 30% voltage ratio at various frequencies).

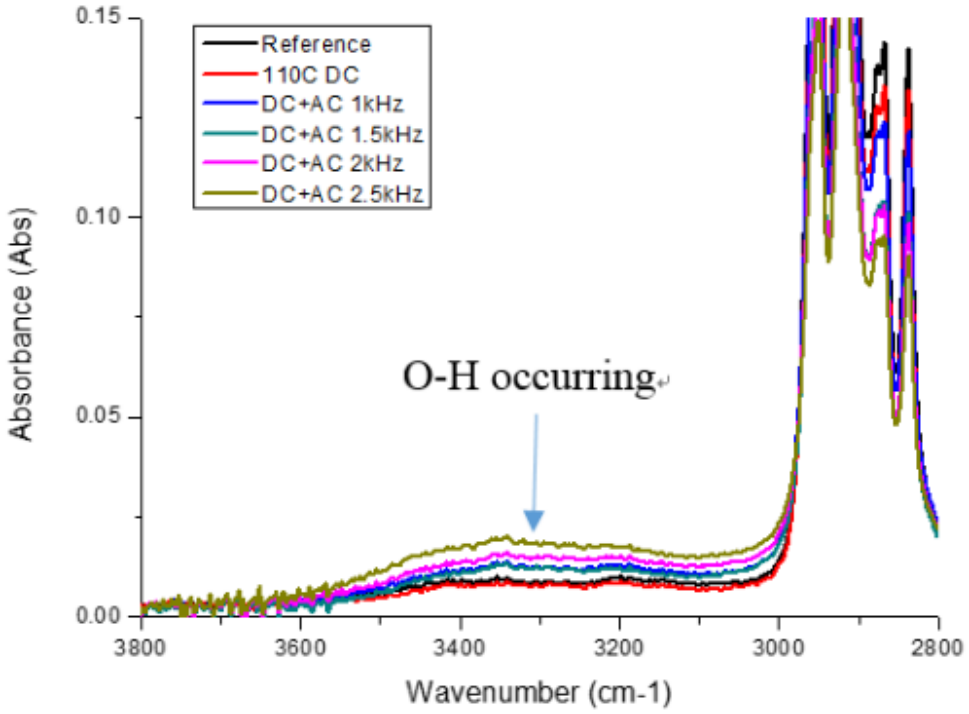

Figure 6.10. FTIR-ATR results for PP detailed view of OH-group (aged under 30% voltage ratio at various frequencies).

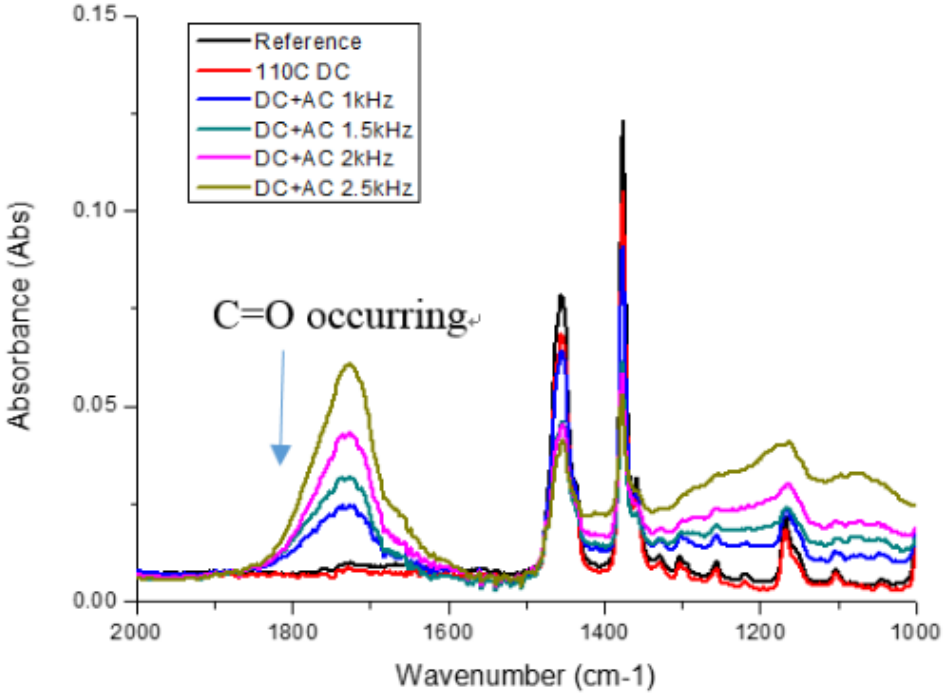

Figure 6.11. FTIR-ATR results for PP detailed view of carbonyl group (aged under 30% voltage ratio at various frequencies).

6.2.3 50% Voltage Ratio

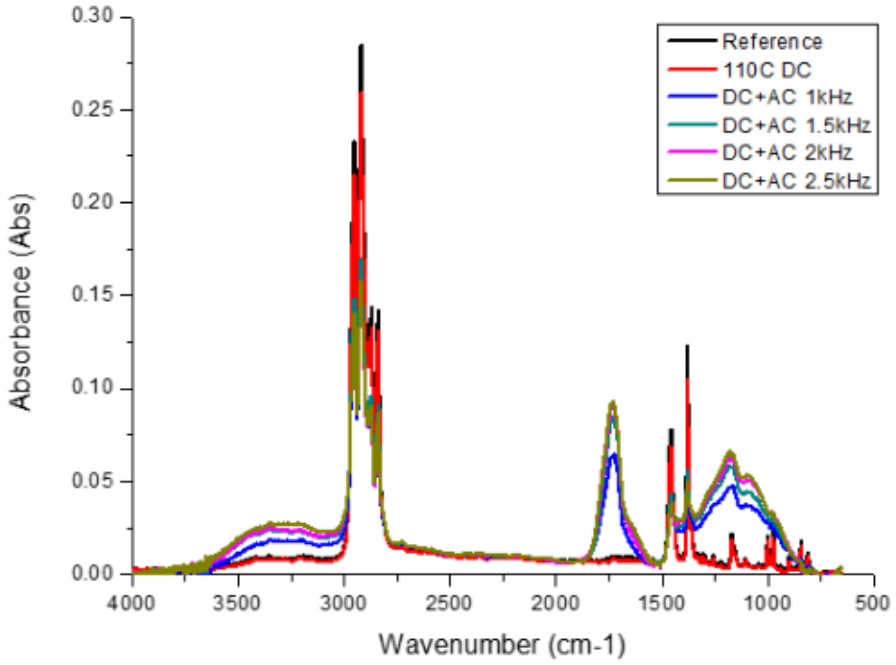

Figure 6.12. FTIR-ATR results of PP (aged under 50% voltage ratio at various frequencies).

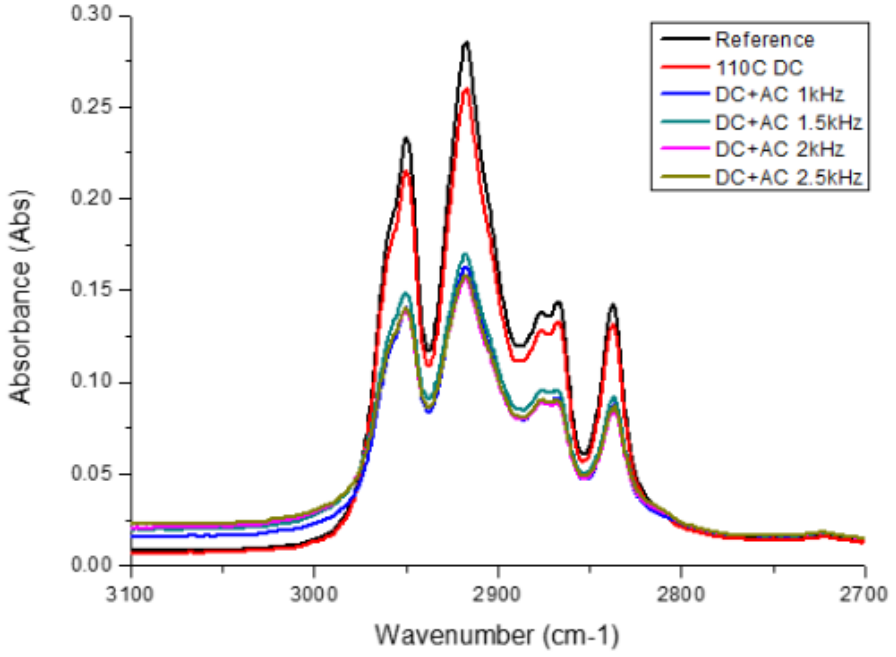

Figure 6.13. FTIR-ATR results for PP detailed view of C-H-groups (aged under 50% voltage ratio at various frequencies).

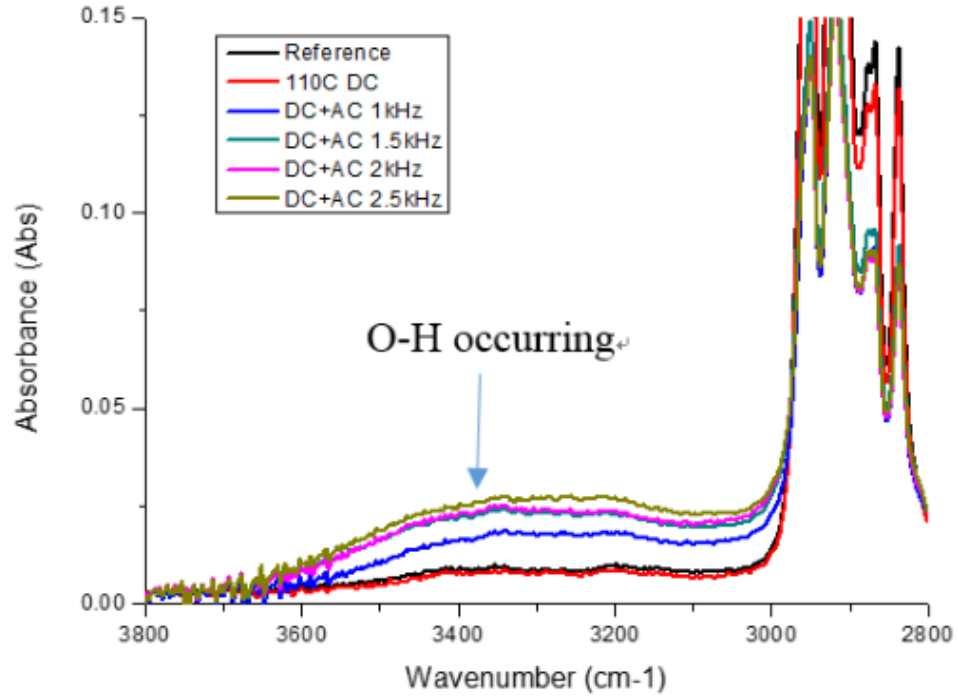

Figure 6.14. FTIR-ATR results for PP detailed view of OH-group (aged under 50% voltage ratio at various frequencies).

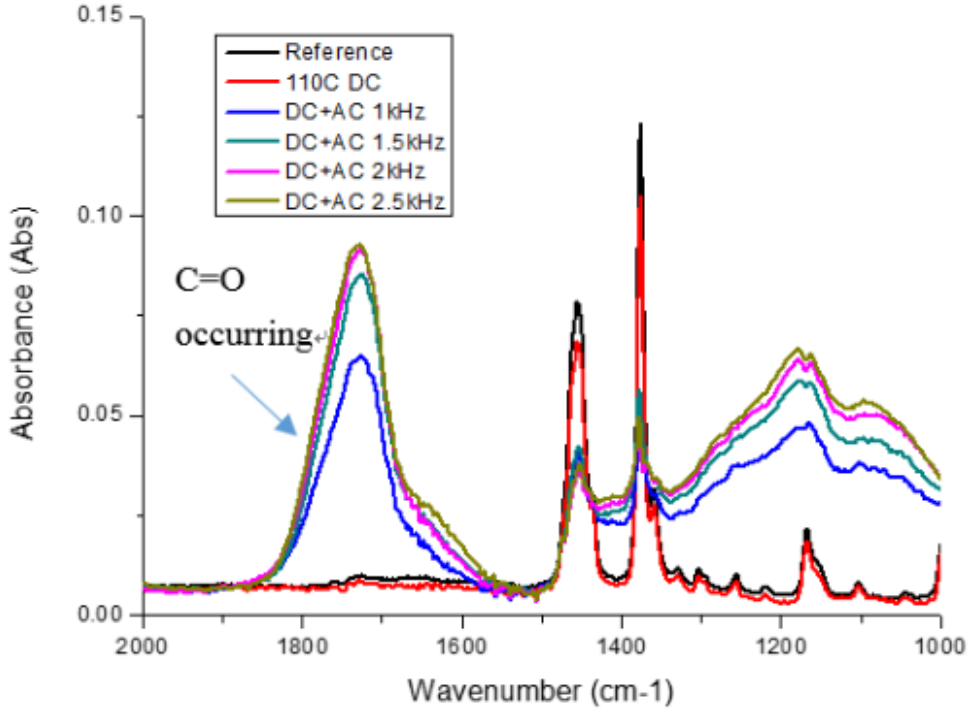

Figure 6.15. FTIR-ATR results for PP detailed view of carbonyl group (aged under 50% voltage ratio at various frequencies).

6.2.4 Carbonyl Index Comparison

The CI of PP aged at 110°C at 30% and 50% voltage ratios can be summarized in Table 6.6 and Table 6.7, respectively. As there is no absorption observed at 1738 cm^{-1} for the 10% voltage ratio, the CI of PP will be zero.

Table 6.6. Carbonyl Index of PP aged at 110°C and at 30% voltage ratio.

Frequency (kHz)	A_{1738}	A_{1460}	CI
1	0.0242	0.0639	0.3787
1.5	0.0314	0.0456	0.6886
2	0.0425	0.0448	0.9487
2.5	0.0603	0.0407	1.4816

Table 6.7. Carbonyl Index of PP aged at 110°C and at 50% voltage ratio.

Frequency (kHz)	A_{1738}	A_{1460}	CI
1	0.0642	0.0418	1.5359
1.5	0.0843	0.0396	2.1288
2	0.0907	0.0368	2.4647
2.5	0.0924	0.0355	2.6028

Based on the data in Table 6.6 and Table 6.7, the CI of PP aged at 110°C and at 30% and 50% voltage ratio is summarized in Figure 6.16.

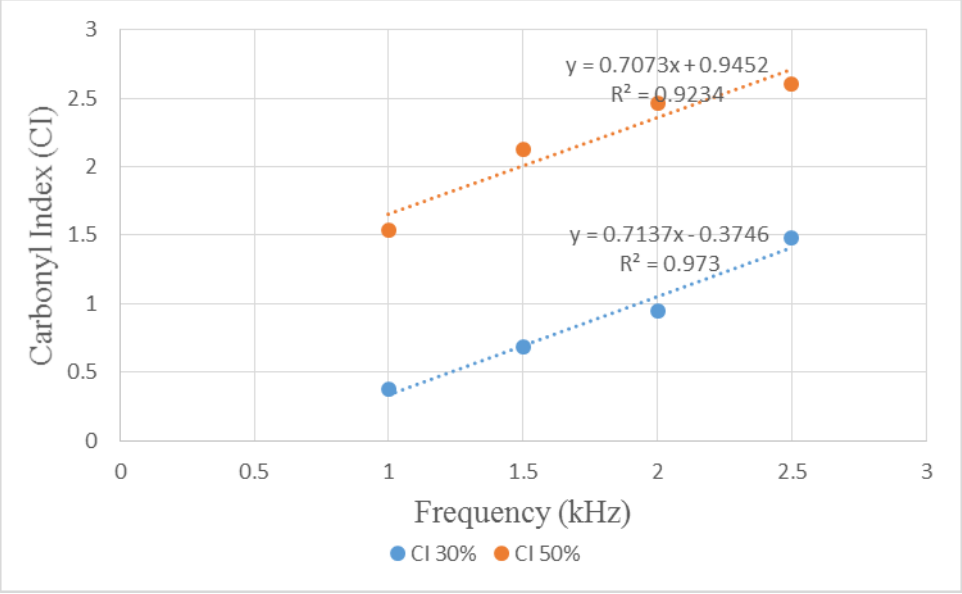

Figure 6.16. Carbonyl Index of PP aged at 110 °C and at 30% and 50% voltage ratio.

In Figure 6.16, at 30% voltage ratio, CI increases with increase of the superimposed frequency within 0.4 to 1.5. The gradient is 0.7137 (Hz^{-1}). At 50% voltage ratio, CI value increases significantly. The gradient increases to 0.7073 (Hz^{-1}). This is because the apparent cumulative energy per second increases significantly in 50% voltage ratio (as mentioned in Section 6.1). The changes in the CI value can be correlated with changes of susceptibility index and conductivity of PP samples as shown in Section 6.4.

6.3 Dielectric Spectroscopy Results

The change in dielectric constant and dissipation factor of PP with superimposed frequencies and in three voltage ratios are shown in Figure 6.17-6.22. The investigation frequency range is 10^{-2} to 10^{4} Hz.

6.3.1 10% Voltage Ratio

The dielectric constant and dissipation factor of PP aged at 110°C and at 10% voltage ratio are shown in Figure 6.17-6.18.

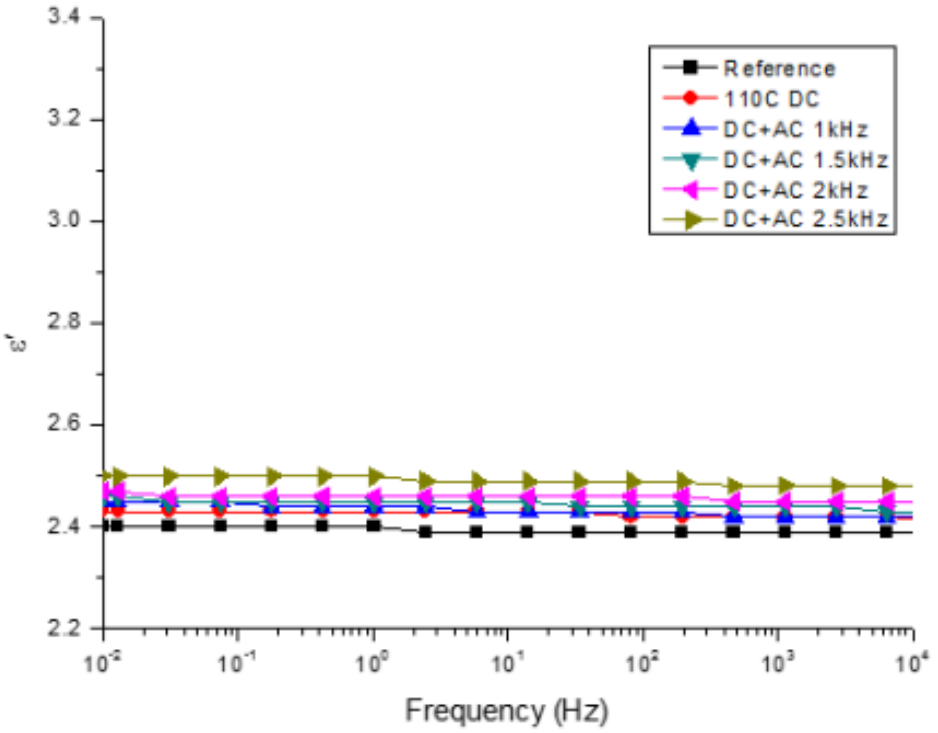

Figure 6.17. Dielectric constant of PP aged under 10% voltage ratio at various frequencies.

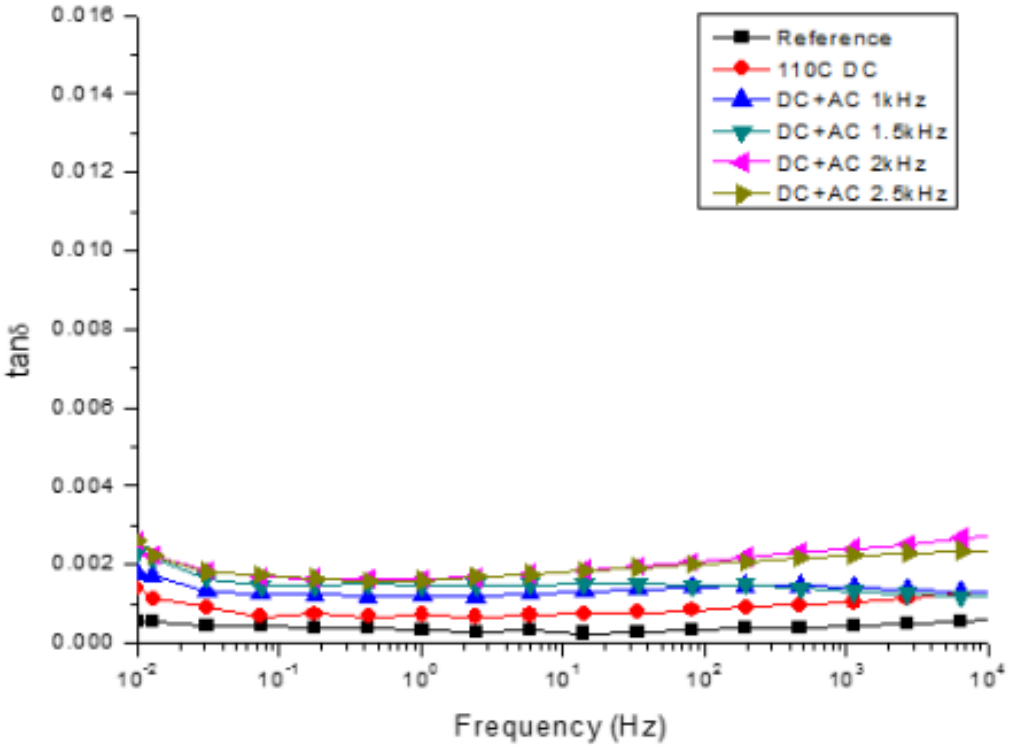

Figure 6.18. Dissipation factor of PP aged under 10% voltage ratio at various frequencies.

In Figure 6.17, ε' of each sample remain almost constant in the measurement frequency range of 10^{-2}-10^{4} Hz. All values are within the range from 2.4 to 2.5. ε' of the sample subjected to purely DC stress is slightly higher than ε' of unaged reference sample. All samples aged by combined AC and DC voltages are slightly higher than ε' of sample aged by purely DC voltage. The samples also appear to have an increasing values of ε' as the frequency increases. This was not observed so clearly in the PP sample aged at 90°C.

In Figure 6.18, *tanδ* of all aged samples are higher than the reference value in the frequency range from 10^{-2} to 10^{4} Hz. *tanδ* of samples subject to DC and AC superimposed frequency are slightly higher than the DC value and appear to be increasing with applied AC frequency. The formation of the low frequency peak associated with conductivity appears to be stronger in the results obtained at 110°C. These changes suggest that the rates associated with the chemical reactions leading to dipole formation and conductivity have been enhanced, as expected by the increase in temperature.

6.3.2 30% Voltage Ratio

The dielectric constant and dissipation factor of PP aged at 110°C using a 30% voltage ratio are shown in Figure 6.19-6.20.

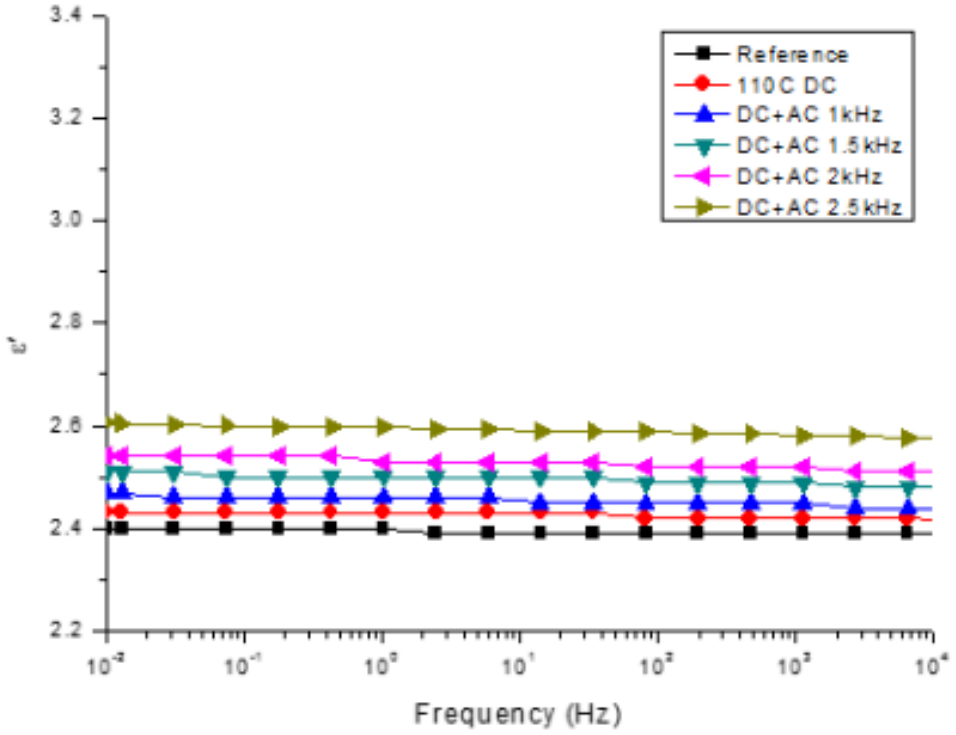

Figure 6.19. Dielectric constant of PP aged under 30% voltage ratio at various frequencies.

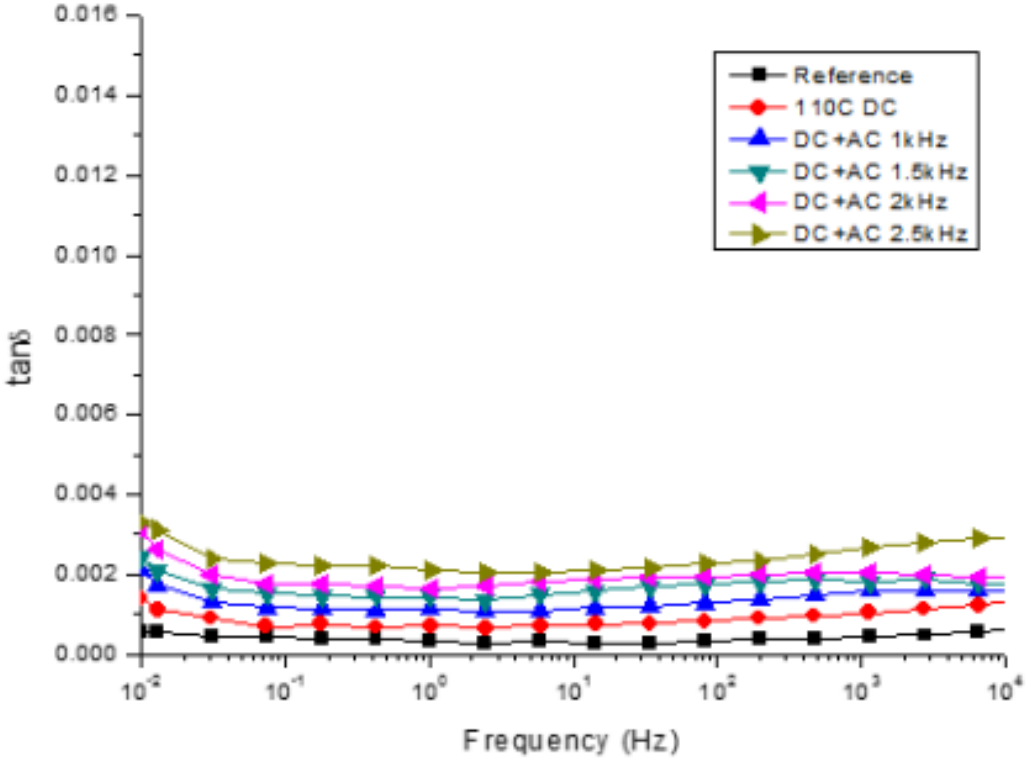

Figure 6.20. Dissipation factor of PP aged under 30% voltage ratio at various frequencies.

In Figure 6.19, ε' of an unaged sample and for a sample subjected to a purely DC stress are included for reference. ε' of samples subjected to combined AC and DC voltages are larger than those for the reference sample and the sample exposed to DC stress only. The values fall in the range between 2.45 and 2.6. Across the range of measuring frequencies employed for the DS measurements, the value of ε' appears to increase with the increase in frequency of the AC component of the ageing stress.

In Figure 6.20, *tanδ* of samples subjected to combined AC and DC voltages increase slightly and again seem to have a dependence on the applied frequency of the aging stress. These changes may be occurring due to the formation of polar groups as shown in the FTIR-ATR results in Section 6.2.2. There is also evidence of an increase in tanδ at low frequencies. This suggests that additional charge carriers or trapping sites have been created during aging.

6.3.3 50% Voltage Ratio

The dielectric constant and dissipation factor of PP aged at 110°C and at 50% voltage ratio are shown in Figure 6.21-6.22.

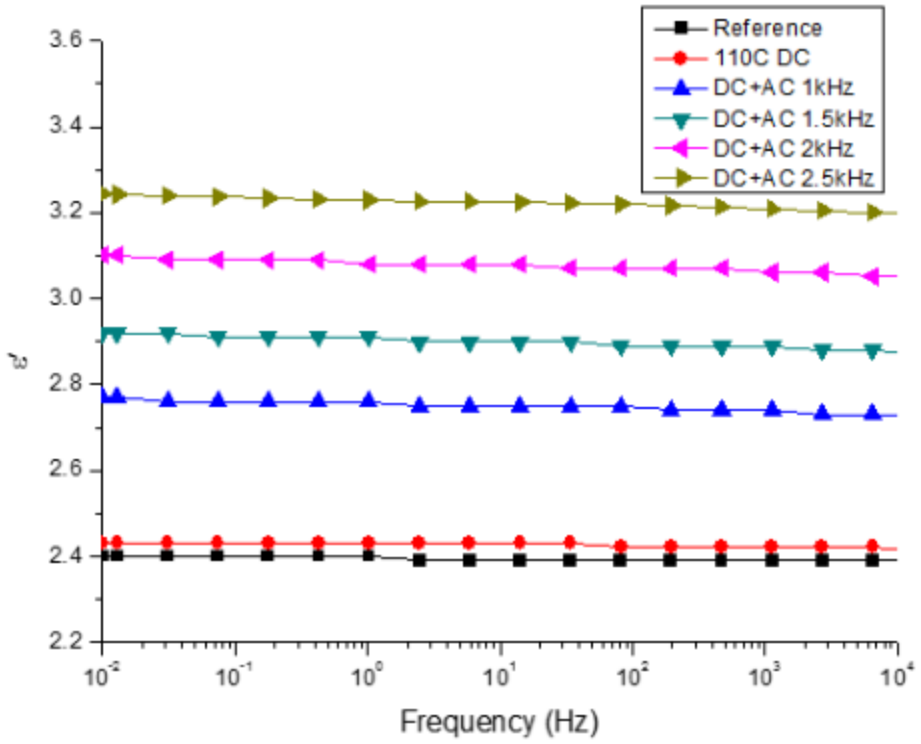

Figure 6.21. Dielectric constant of PP aged under 50% voltage ratio at various frequencies.

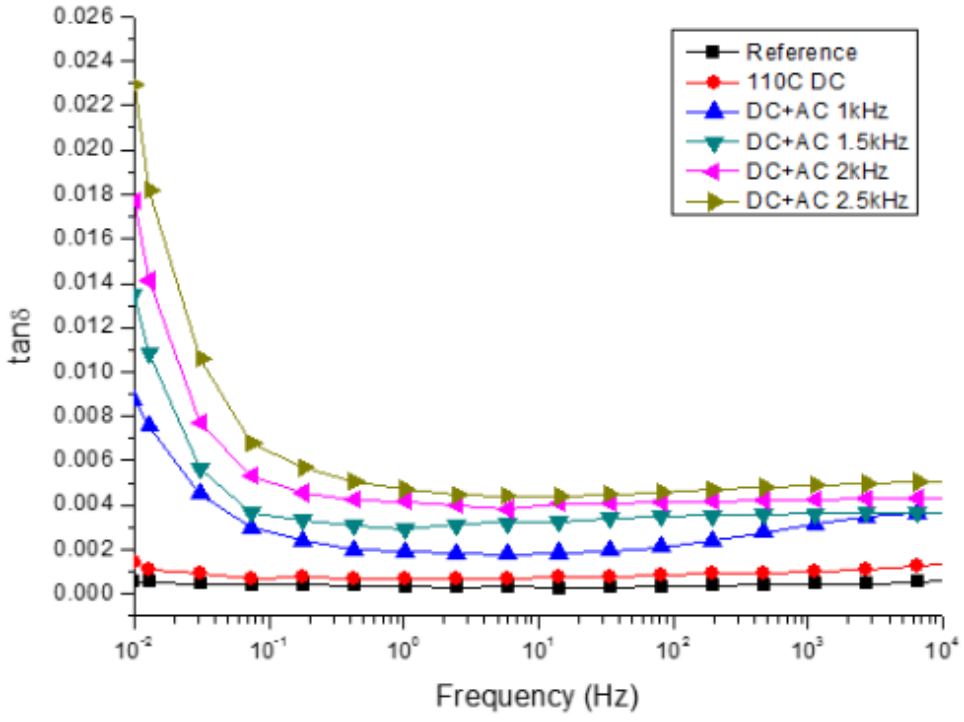

Figure 6.22. Dissipation factor of PP aged under 50% voltage ratio at various frequencies.

In Figure 6.21, the ε' of samples subjected to combined AC and DC stress are much

higher than the DC value and are significantly higher than those obtained under the same conditions with a 30% voltage ratio. The values lie in the region from 2.8 to 3.25. It is clear to see that ε' increases with the increase of superimposed frequency. This is because more polar molecular groups are generated at 50% voltage ratio (such as O-H, C=O as mentioned in Section 6.2.3). As superimposed frequency increases, the amount and kinds of polar molecular groups increase which make ε' increase higher.

In Figure 6.22, *tanδ* of all samples subjected to combined AC and DC voltages are higher than the DC value. For each curve, *tanδ* increases with the measurement frequency below 1 Hz. For samples aged by combined voltages, overall *tanδ* increases with the increase of the superimposed AC frequency. This is because more polar groups are formed at the higher frequency values. The peak observed at low measurement frequencies is associated with DC conduction processes which will be discussed in Section 6.3.4.1.

6.3.4 Discussion

6.3.4.1 Conductivity

Plots of ε'' vs $1/\omega$ for PP aged at 110°C using the 10%, 30% and 50% voltage ratio derived from are shown in Appendix E: Table E.1-E.3 and Figure 6.23-6.25.

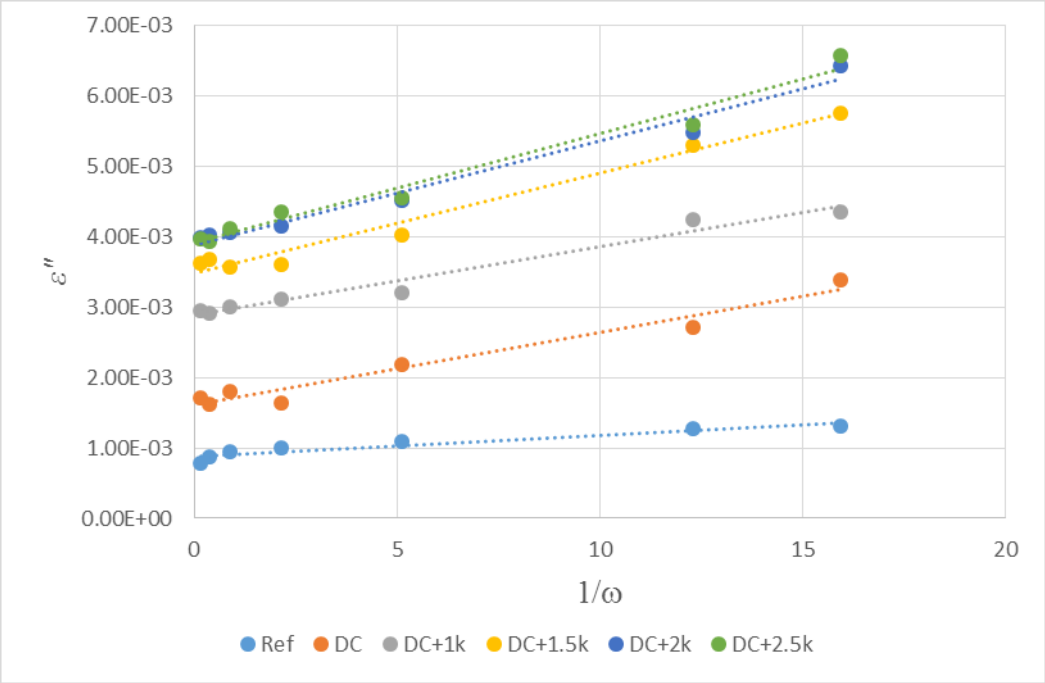

Figure 6.23. ε'' vs. 1/ω of PP aged at 110°C at 10% voltage ratio.

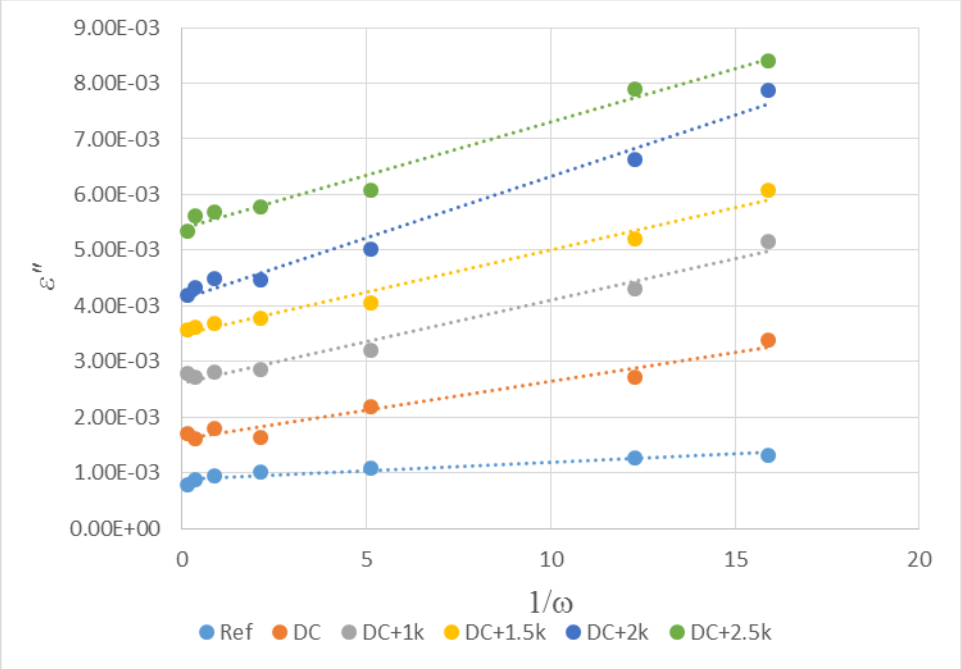

Figure 6.24. ε'' vs. 1/ω of PP aged at 110°C at 30% voltage ratio.

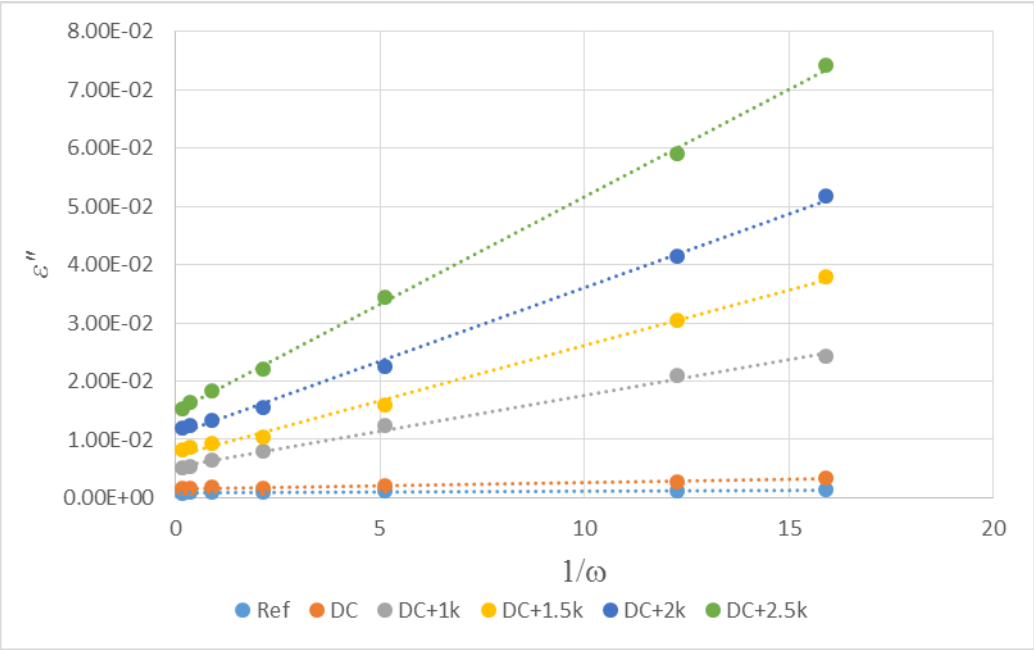

Figure 6.25. ε'' vs. 1/ω of PP aged at 110°C at 50% voltage ratio.

Based on Figure 6.23-6.25, the low frequency conductivity of PP aged at 110°C can be calculated and the results are summarized in Table 6.8 and Figure 6.26.

Table 6.8. Conductivity of PP aged at 110°C.

Waveform	Conductivity (*fS/m*)		
	10% Voltage Ratio	30% Voltage Ratio	50% Voltage Ratio
Reference	0.2699	0.2699	0.2699
DC	0.9116	0.9116	0.9116
DC+1k	0.8602	1.3187	10.7970
DC+1.5k	1.2567	1.3541	16.8150
DC+2k	1.3010	1.9470	22.3020
DC+2.5k	1.3718	1.6904	32.6565

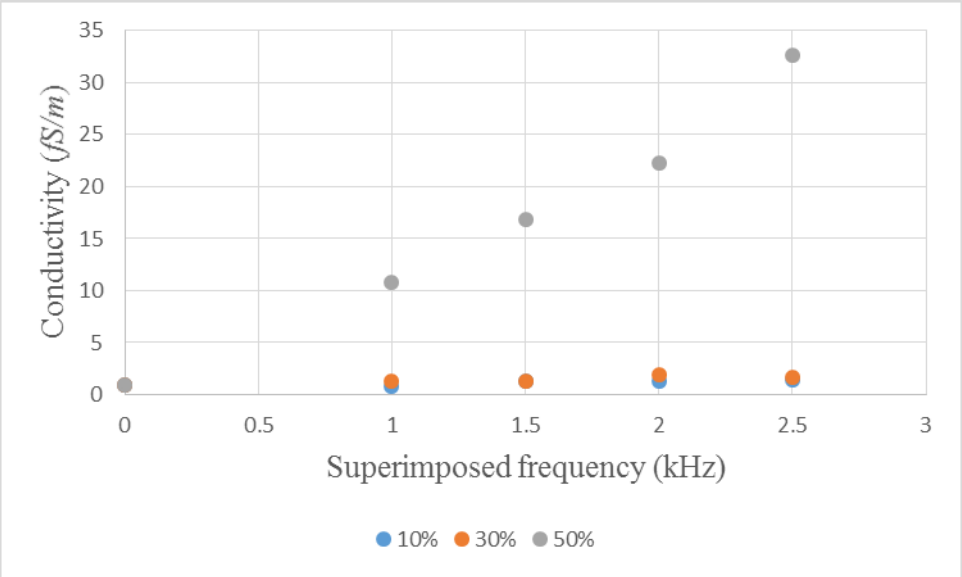

Figure 6.26. Conductivity of PP aged at 110°C.

According to the data in Table 6.8 and Figure 6.26, for PP aged at 110°C under purely DC voltage, the conductivity is about three times higher than that derived for the unaged sample. For samples aged by combined AC and DC voltages, the conductivity is even higher. For the samples aged at 10% and 30% voltage ratios, the conductivity is in general higher than the DC value and may be showing an upward trend with the frequency of the AC stressing component. However the conductivity of all the samples aged by 10% and 30% voltage ratios are below 2 *fS/m* and the increase in the conductivity is therefore not very clear. For the samples aged at 50% voltage ratio, the value of conductivity increases significantly and it is clear that the conductivity increases with increasing AC frequency.

6.3.4.2Dielectric Susceptibility Index χI

The calculated values of χI, as described in Section 4.4.4.2, of PP aged at 110°C are shown in Table 6.9 and their behaviour as a function of AC frequency is shown in Figure 6.27.

Table 6.9. Dielectric susceptibility index χI of PP aged at 110°C.

Waveform	Susceptibility Index χI		
	10%	30%	50%
DC	0.0214	0.0214	0.0214
DC+1k	0.0357	0.0500	0.2643
DC+1.5k	0.0429	0.0786	0.3000
DC+2k	0.0500	0.0857	0.3786
DC+2.5k	0.0714	0.1042	0.6033

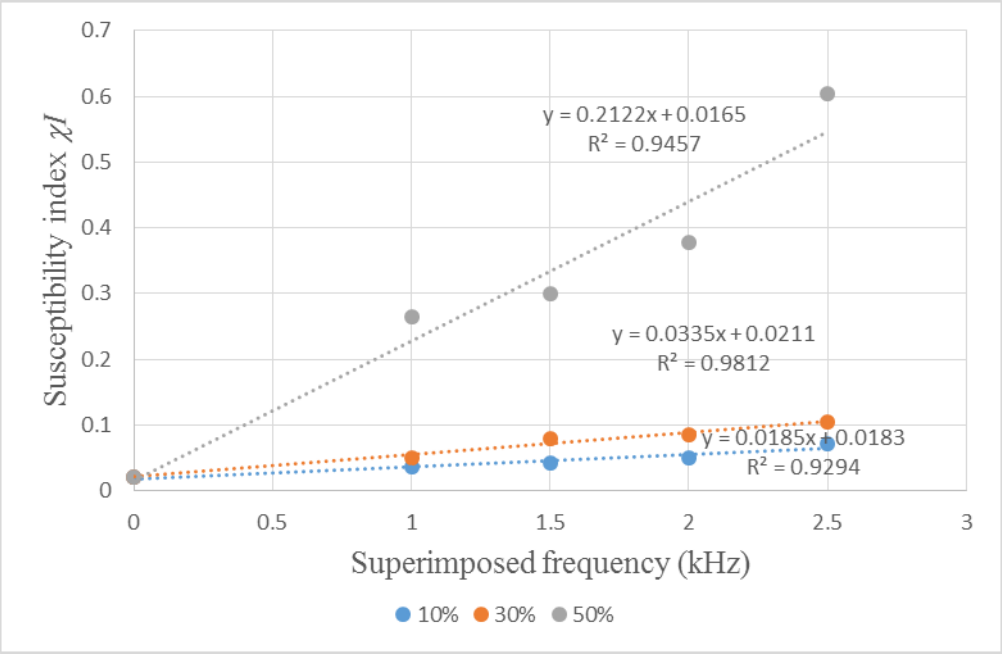

Figure 6.27. Dielectric susceptibility index χI of PP aged at 110°C.

It is clear that for all three voltage ratios that χI is increasing with the frequency of the AC stress component. It is also clear that the behaviour of χI is dependent on the voltage ratio of the stressing conditions.

6.4 Discussion

The relationship between Carbonyl Index (CI) and apparent cumulative energy per second ($\dot{E}_{CA}$) is shown in Table 6.10 and Figure 6.28.

Table 6.10. Apparent cumulative energy per second vs. Carbonyl Index.

Frequency (kHz)	30% Voltage Ratio		50% Voltage Ratio	
	$\dot{E}_{CA}$	CI	$\dot{E}_{CA}$	CI
1	1210	0.3787	9577	1.5359
1.5	1861	0.6886	15482	2.1288
2	2517	0.9487	20827	2.4647
2.5	3772	1.4816	28273	2.6028

In Figure 6.28, it can be seen that as the value of $\dot{E}_{CA}$ increases the value of CI is increasing. It also appears that the CI value may be saturating at large values of $\dot{E}_{CA}$. The change in the behaviour of the Carbonyl Index however is also associated with a change of the aging conditions from the 30% to the 50% voltage ratio.

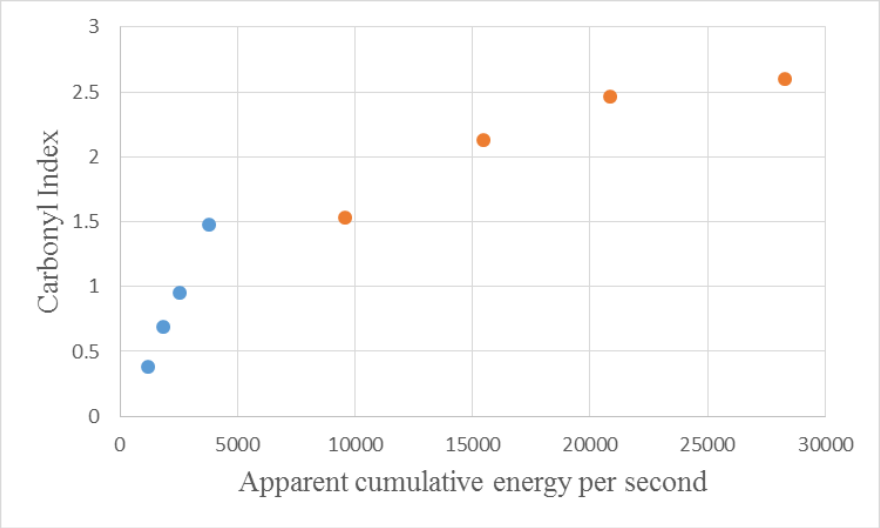

Figure 6.28. Apparent cumulative energy per second vs. Carbonyl Index.

The relationship of $\dot{E}_{CA}$ and σ is shown in Table 6.11 and Figure 6.29.

Table 6.11. Apparent cumulative energy per second vs. conductivity.

Frequency (kHz)	30% Voltage Ratio		50% Voltage Ratio	
	$\dot{E}_{CA}$	σ (fS/m)	$\dot{E}_{CA}$	σ (fS/m)
1	1210	1.3187	9577	10.7970
1.5	1861	1.3541	15482	16.8150
2	2517	1.9470	20827	22.3020
2.5	3772	1.6904	28273	32.6565

In Figure 6.29, the conductivity is increasing as the value of $\dot{E}_{CA}$ increases. Unlike the behaviour of CI there is no evidence of saturation. This may be due to the fact that the CI derived from the FTIR-ATR measurements only reflects the changes in the surface layer of the polymer while conductivity reflects a bulk change in the system.

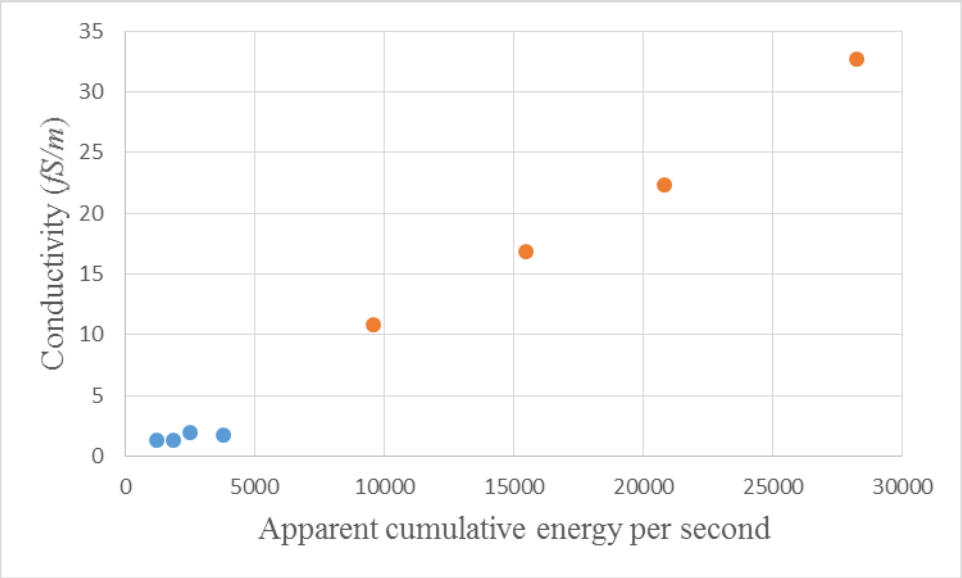

Figure 6.29. Apparent cumulative energy per second vs. conductivity.

The relationship between $\dot{E}_{CA}$ and χI is shown in Table 6.12 and Figure 6.30.

Table 6.12. Apparent cumulative energy per second vs. χI.

Frequency (kHz)	30% Voltage Ratio		50% Voltage Ratio	
	$\dot{E}_{CA}$	χI	$\dot{E}_{CA}$	χI
1	1210	0.0500	9577	0.2643
1.5	1861	0.0786	15482	0.3000
2	2517	0.0857	20827	0.3786
2.5	3772	0.1042	28273	0.6033

As shown in Figure 6.30, as with the CI and conductivity, the susceptibility index χI increases as $\dot{E}_{CA}$ increases. Unlike CI but in a similar manner to the conductivity, the data falls close to a straight line and there is no evidence of saturation in the behaviour of χI. At large values of $\dot{E}_{CA}$ the rate of change seems to be increasing. This again may occur as χI reflects the behaviour of the bulk of the material.

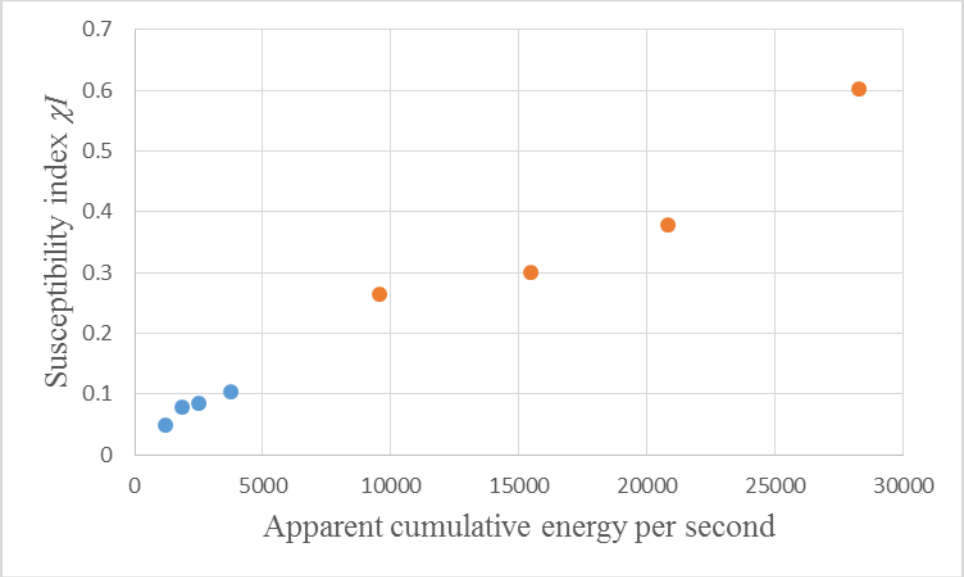

Figure 6.30. Apparent cumulative energy per second vs. χI.

In Figure 6.31, as would be expected from Figure 6.28 and Figure 6.29 as the value of CI increases the value of conductivity increases. There is some suggestion however of their being differences between the behaviour of the results with low values of CI associated with ageing at a 30% voltage ratio and the higher values associated with the 50% voltage ratio.

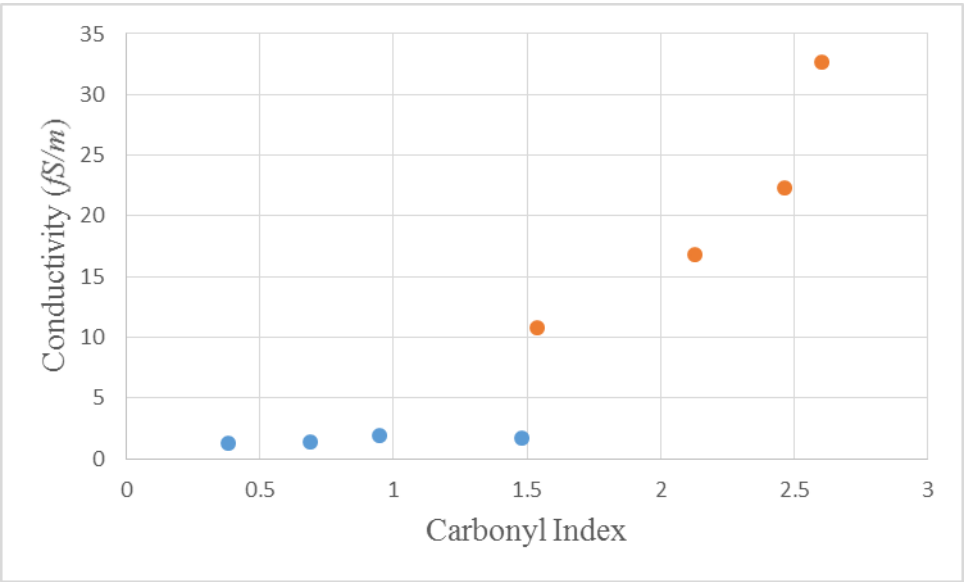

Figure 6.31. Carbonyl Index vs. conductivity.

In Figure 6.32, as would be expected from Figures 6.28 and Figure 6.30 as the value of CI increases the value of χI increases. At lower values of CI there is a broadly linear relationship between CI and χI. At higher values of CI, the value of χI increases more rapidly due to the observed saturation in the Carbonyl Index. This appears to occur at a lower value of the Carbonyl Index. Again there is some suggestion however of their being differences between the behaviour of the results with low values of CI associated with aging at a 30% voltage ratio and the higher values associated with the 50% voltage ratio.

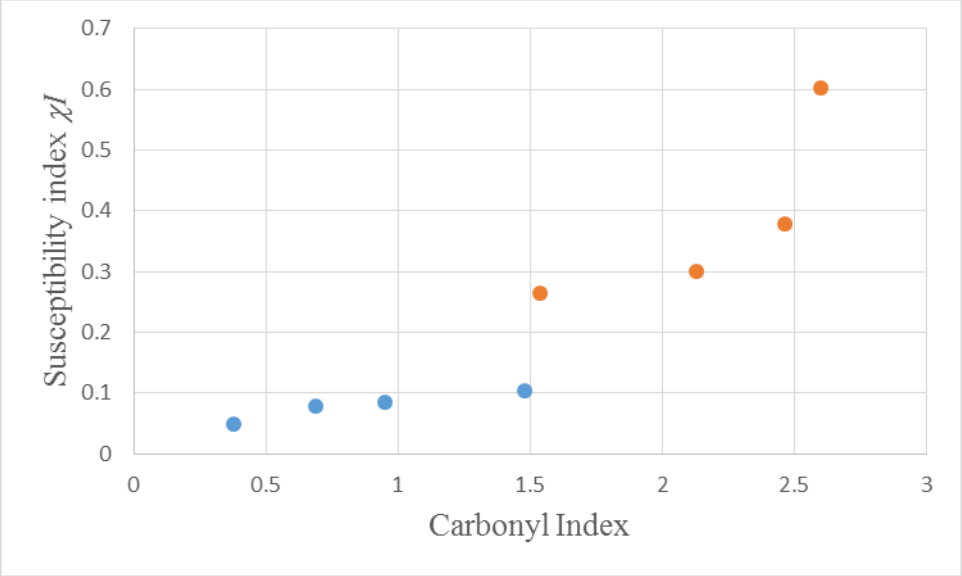

Figure 6.32. Carbonyl Index vs. χI.

6.5 Conclusions

The PD mechanism of PP aged at 110°C is similar to that of PP aged at 90°C.

The apparent cumulative energy per second ($\dot{E}_{CA}$) has been calculated and this index increases as the voltage ratio increases and as the frequency of the AC component is increased. The values however are higher than those observed for stressing at 90°C. The value is 1210 at 1 kHz at 30% voltage ratio and 28273 at 2.5 kHz at 50% voltage

ratio.

From the FTIR-ATR values for the Carbonyl Index which reflects the chemical changes on the surface have been calculated. The changes in the Carbonyl Index with frequency and voltage ratio correlate with the apparent cumulative energy per second. The value is 0.3787 at 1 kHz at 30% voltage ratio and 2.6028 at 2.5 kHz at 50% voltage ratio.

From the dielectric spectroscopy data, values for the conductivity (σ) and an index reflecting the change in susceptibility (χI) have been calculated. These indeces also correlate with the apparent cumulative energy per second. The value of σ is 1.3187 *fS/m* at 1 kHz at 30% voltage ratio and 32.6565 *fS/m* at 2.5 kHz at 50% voltage ratio. The value of χI is 0.0500 at 1 kHz at 30% voltage ratio and 0.6033 at 2.5 kHz at 50% voltage ratio.

7. Discussion

In this chapter, results from chapter 4-6 are summarized and discussed. The discussion will give some insights into the mechanism of material aging.

Section 7.1 discusses changes in the apparent cumulative energy per second ($\dot{E}_{CA}$) with different material and temperature.

Section 7.2 discusses the changes in conductivity (σ) with different materials and temperature.

Section 7.3 discusses changes in dielectric susceptibility index (χI) with different materials and different aging condition. Number of carbonyl group ($N_{1(C=O)}$) in each material and at both temperatures is calculated.

Section 7.4 discusses changes in Carbonyl Index (CI) with different materials and different aging condition. The relationship of CI and $N_{1(C=O)}$ is discussed.

Section 7.5 compares changes in measured indices with apparent cumulative energy per second of each material according to the data in Section 7.1-7.4.

Section 7.6 is a conclusion part.

7.1 Apparent Cumulative Energy Per Second

The $\dot{E}_{CA}$ of HDPE aged at 90°C, PP aged at 90°C and 110°C at the 30% and 50% voltage ratios are shown in Table 7.1-7.2 and Figure 7.1-7.2, respectively.

Table 7.1. Apparent cumulative energy per second at 30% voltage ratio.

Frequency (kHz)	HDPE	PP 90°C	PP 110°C
1	1046	842	1210
1.5	1593	1245	1861
2	2164	1663	2517
2.5	2725	2095	3772

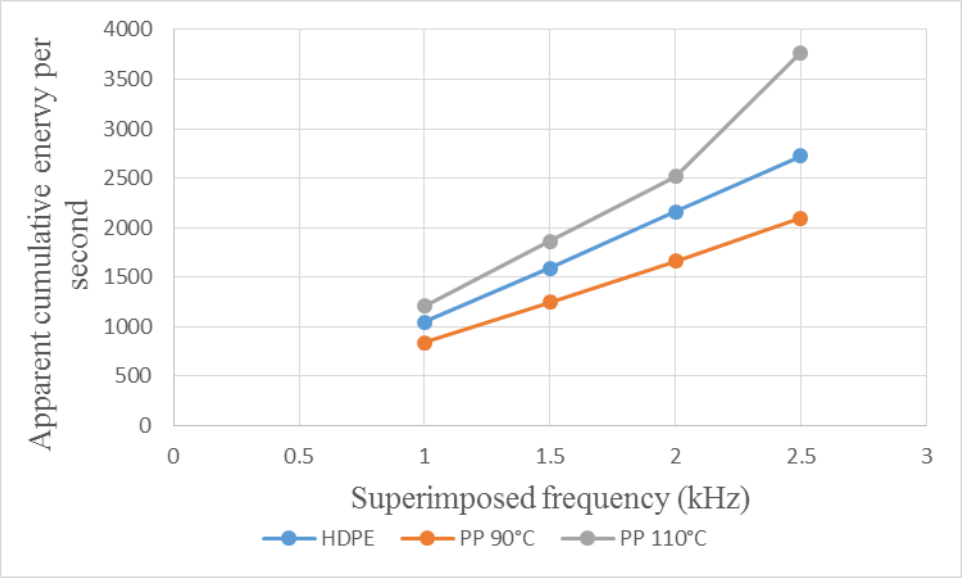

Figure 7.1. Apparent cumulative energy per second at 30% voltage ratio.

Table 7.2. Apparent cumulative energy per second at 50% voltage ratio.

Frequency (kHz)	HDPE	PP 90°C	PP 110°C
1	9135	6380	9577
1.5	13326	10370	15482
2	17644	14507	20827
2.5	23920	19000	28273

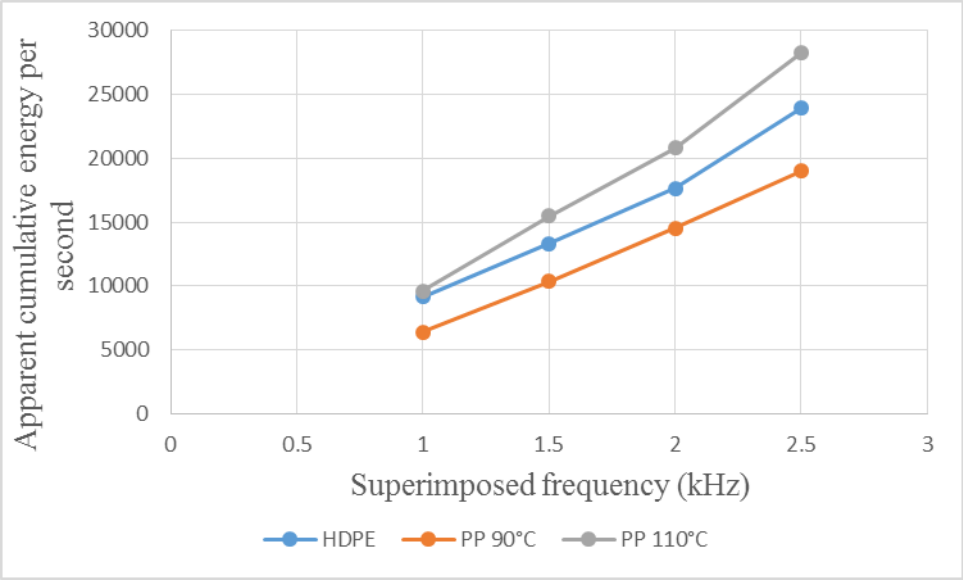

Figure 7.2. Apparent cumulative energy per second at 50% voltage ratio.

Figure 7.1 and Figure 7.2 show that in the measured frequency range, $\dot{E}_{CA}$ follows the order: (PP aged at 110°C)>(HDPE aged by 90°C)>(PP aged by 90°C), at both voltage ratios. A similar ranking can be observed in the behavior of the mean discharge energy (see Table 4.1, Table 5.1 and Table 6.1) and the number of discharges (see Table 4.2-4.3, Table 5.2-5.3 and Table 6.2-6.3).

For PP aged at 90°C and 110°C, the data shows a temperature effect in all measurements across the frequency range. This may be because of changes in the mobility of charge carriers which may affect the distribution of the surface potential $V_Q(r)$. This redistribution of charge would modify the voltage in the gap and may increase the size of the active area on the surface of the material. High temperature may also effect the morphology of the surface of the polymer which could lead to changes in the behaviour of the breakdowns. The increase in temperature would also lead, following the behaviours predicted by the aging models in Section 2.1, to an increase in the aging of the surface that would again modify the behaviour of the partial discharges in the gap. The increase in temperature would be expected to cause an increase in the emission of electrons from the electrode but the difference in electron emission associated with a change of temperature from 363K to 383K is

likely to be small.

7.2 Conductivity (σ)

Data of σ is shown in Table 7.3-7.4 and Figure 7.3-7.4.

Table 7.3. Conductivity (*fS/m*) at 30% voltage ratio.

Frequency (kHz)	HDPE	PP 90°C	PP 110°C
1	0.9912	0.5275	1.3187
1.5	1.0709	0.5390	1.3541
2	1.0797	0.6646	1.9470
2.5	1.5311	0.7372	1.6904

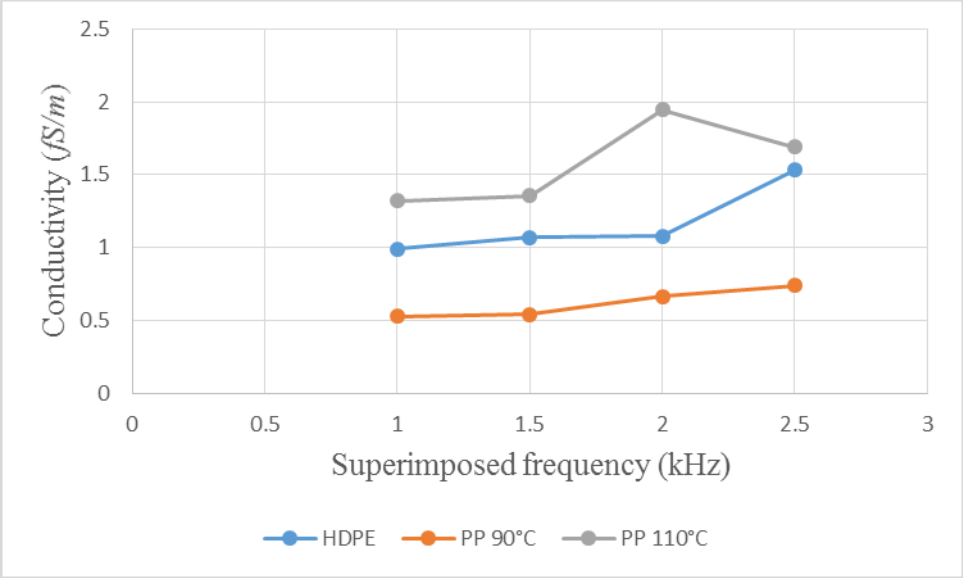

Figure 7.3. Conductivity (*fS/m*) at 30% voltage ratio.

Table 7.4. Conductivity (*fS/m*) at 50% voltage ratio.

Frequency (kHz)	HDPE	PP 90°C	PP 110°C
1	5.1950	4.0091	10.7970
1.5	6.0446	5.4074	16.8150
2	9.0270	8.6907	22.3020
2.5	19.1160	12.3900	32.6565

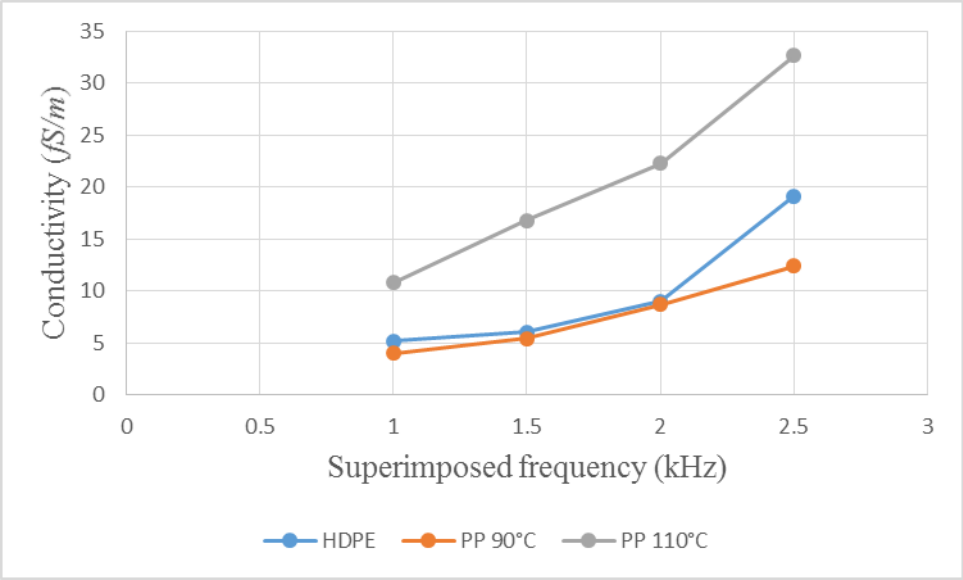

Figure 7.4. Conductivity (*fS/m*) at 50% voltage ratio.

Conductivity has the same trend as $\dot{E}_{CA}$: PP aged at 110°C>HDPE aged at 90°C>PP aged at 90°C.

As the measurement of the dielectric spectra were performed at the same temperature (23°C) and field conditions, the changes in conductivity observed in the PP samples cannot be attributed to a change in the effective mobility as a function of temperature. So the changes observed in the values of σ must be as a result of changes within the polymers as a result of the electrothermal aging rather than as a direct result of measurements being made at the different aging temperatures.

Some insights as to the possible changes in the system resulting in the observed change in conductivity can be made by assuming that the mobility arises from charge carriers hopping between trapping sites in the polymer. For mobility, the current flux J would take the form:

$$J=N\mu E \tag{7.1}$$

Where N is the number density of charge carriers, μ is the mobility and $\boldsymbol{E}$ is the applied field.

An expression for the expected mobility for a hopping conduction process following Mott and Gurney [1] is:

$$\mu = \frac{2va}{E} exp\left(-\frac{G}{kT}\right) sinh\left(\frac{qEa}{2kT}\right) \quad 7.2$$

Where *v* is the frequency associated with detrapping, *a* is the separation between adjacent trapping sites. *G* is an activation energy associated with the potential barrier between trapping sites, *E* is the applied field, *k* is Boltzmanns constant and *T* is the absolute temperature. At low values of *qEa/2kT* the sinh term approximates to *qEa/2kT* and the equation above takes the form:

$$\mu = \frac{qva^2}{kT} exp\left(-\frac{G}{kT}\right) \quad 7.3$$

Therefore the expected mobility flux can be written as:

$$J = N\frac{\alpha}{kT} exp\left(-\frac{G}{kT}\right) E \quad 7.4$$

Where $\alpha = qva^2$.

Expressing the flux in terms of a conductivity $j = \sigma E$ implies that the conductivity will take the form:

$$\sigma = N\frac{\alpha}{kT} exp\left(-\frac{G}{kT}\right) \quad 7.5$$

Therefore, if the temperature at which the conductivity is measured is fixed, changes can only occur due to changes in the value of *N*, α or *G*.

A decrease in the value of the activation energy could occur as a result of modifications to the polymer structure, e.g. either modifying the existing trapping site or by introducing additional trapping sites in the polymer with a lower potential barrier. The addition of new sites in the polymer would have an impact on the parameter $\alpha = qva^2$ as the separation of traps *a* would change. Finally increasing the number of charge carriers available in the system would cause an increase in the

conductivity. It is not possible from the data currently available in this project to determine the relative changes in N, α and G responsible for the observed increase in conductivity in the samples. Possible approaches to analyse this problem are given in the final chapter.

7.3 Dielectric susceptibility index (χI)

Data of χI is shown in Table 7.5-7.6 and Figure 7.5-7.6.

Table 7.5. χI at 30% voltage ratio.

Frequency (kHz)	HDPE	PP 90°C	PP 110°C
1	0.0822	0.0286	0.0500
1.5	0.0970	0.0500	0.0786
2	0.1043	0.0643	0.0857
2.5	0.1117	0.0714	0.1042

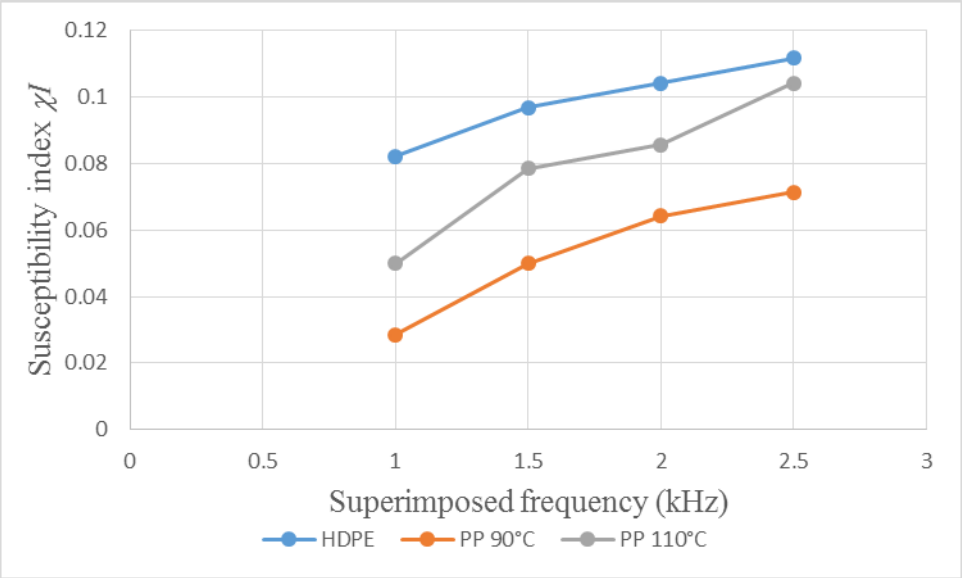

Figure 7.5. χI at 30% voltage ratio.

Table 7.6. χI at 50% voltage ratio.

Frequency (kHz)	HDPE	PP 90°C	PP 110°C
1	0.1444	0.0949	0.2643
1.5	0.2243	0.1296	0.3000
2	0.2985	0.1755	0.3786
2.5	0.4058	0.2500	0.6033

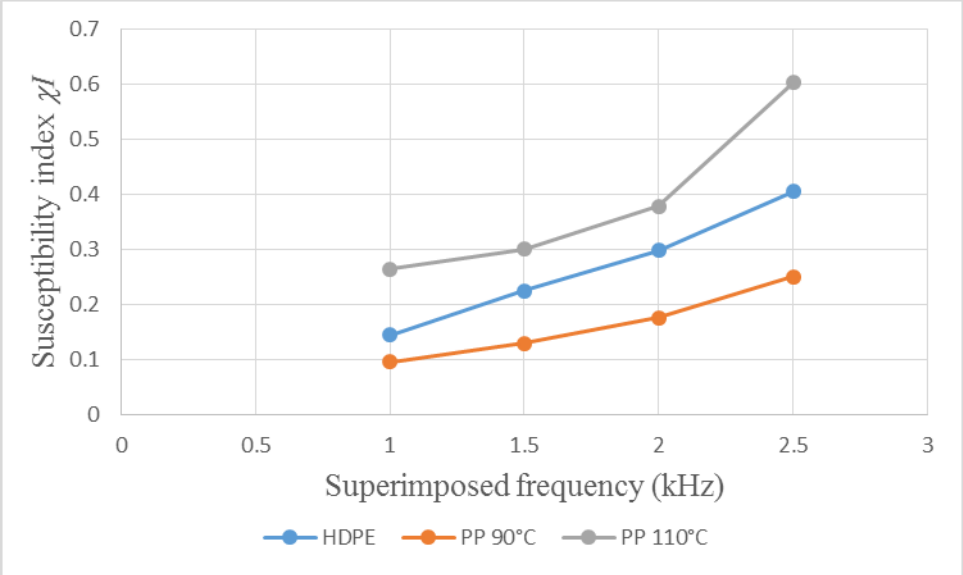

Figure 7.6. χI at 50% voltage ratio.

The measurements of ε' were all carried out at a common temperature so the changes observed in the values of ε' must again be as a result of changes within the polymers as a result of the electrothermal aging rather than as a direct result of measurements being made at the different temperatures. Therefore the increase in the polarization is probably due to changes in the structure of the polymer or to an increases in the number of dipoles in the system. As the dielectric spectra is relatively flat at higher frequencies, this means that there is unlikely to be a high frequency peak which would shift to lower frequencies as a result of structural modifications occurring in the polymers due to aging. Therefore the increase in the polarization of the system is likely to be due to an increase in the number of dipoles present in the system. An increase in the number of carbonyl groups, which have a significant dipole moment

has been observed in the FTIR-ATR results.

There is an expression relating polarization vector *P* to dipole moments and their number densities when the system has reached equilibrium.

$$P = \frac{N{p_0}^2}{3kT} E \tag{7.6}$$

Where *N* is number density of dipoles, p_0 is dipole moment, T is absolute Temperature. This *1/T* relationship is known as Curie's law. This is assuming no significant interactions between the dipoles [2].

If it is assumed that the dipoles in the system are behaving independently, an expression for the polarization in the system can be written as:

$$P = \left(\frac{N_0{p_0}^2}{3kT} + \frac{N_{C=O}{p_{C=O}}^2}{3kT}\right) E \tag{7.7}$$

Where N_0 represents the effective number density and p_0 is the dipole moment of all dipoles other than those associated with C=O groups and $N_{C=O}$ and $p_{C=O}$ represents the polarization component associated with the carbonyl groups. $N_{C=O}$ is known to change from the FTIR-ATR results.

The initial dielectric susceptibility χ_0 can be expressed as:

$$\chi_0 = \left(\frac{N_0{p_0}^2}{3kT} + \frac{N_{0(C=O)}{p_{C=O}}^2}{3kT}\right) \tag{7.8}$$

If it is assumed that N_0 has not significantly changed and the change in χ is purely due to a change in the number of carbonyl groups, the dielectric susceptibility after aging χ_1 can be expressed as:

$$\chi_1 = \left(\frac{N_0{p_0}^2}{3kT} + \frac{N_{1(C=O)}{p_{C=O}}^2}{3kT}\right) \tag{7.9}$$

The difference between χ_0 and χ_1 is:

$$\chi_1 - \chi_0 = \left(\frac{N_{1(C=O)} - N_{0(C=O)}}{T}\right)\frac{p_{C=O}{}^2}{3k} \quad 7.10$$

And

$$\chi_1 - \chi_0 = \left(\frac{\Delta N_{(C=O)}}{T}\right)\frac{p_{C=O}{}^2}{3k} \quad 7.11$$

Therefore, changes in the susceptibility should be directly related to changes in the concentration of carbonyl groups within the polymer.

In the analysis above we have assumed that the dipole moment $p_{C=O}$ of each material stays constant before and after aging which allowed its elimination from the change in susceptibility. However direct comparisons between the changes in susceptibility and the concentration of carbonyl groups between different polymers may not be possible as $p_{C=O}$ of HDPE may not have the same value as $p_{C=O}$ of PP.

For each material, equation 7.8 can be written as:

$$\Delta\chi \propto \frac{N_{1(C=O)} - N_{0(C=O)}}{T} \quad 7.12$$

As carbonyl absorption peaks were not detected in the FTIR-ATR spectra in the unaged reference sample, therefore it can be assumed that $N_{0(C=O)}$ is zero, equation 7.9 can be expressed as

$$\Delta\chi \propto \frac{N_{1(C=O)}}{T} \quad 7.13$$

Therefore, $N_{1(C=O)}$ of materials aged at 30% and 50% voltage ratio are summarized in Table 7.7-7.8 and Figure 7.7-7.8.

Table 7.7. $N_{1(C=O)}$ at 30% Voltage Ratio.

Frequency (kHz)	HDPE	PP 90°C	PP 110°C
1	57.4235	20.3159	35.5380
1.5	67.7591	35.5380	55.8539
2	72.8529	45.6960	60.9181
2.5	78.0059	50.7601	74.0375

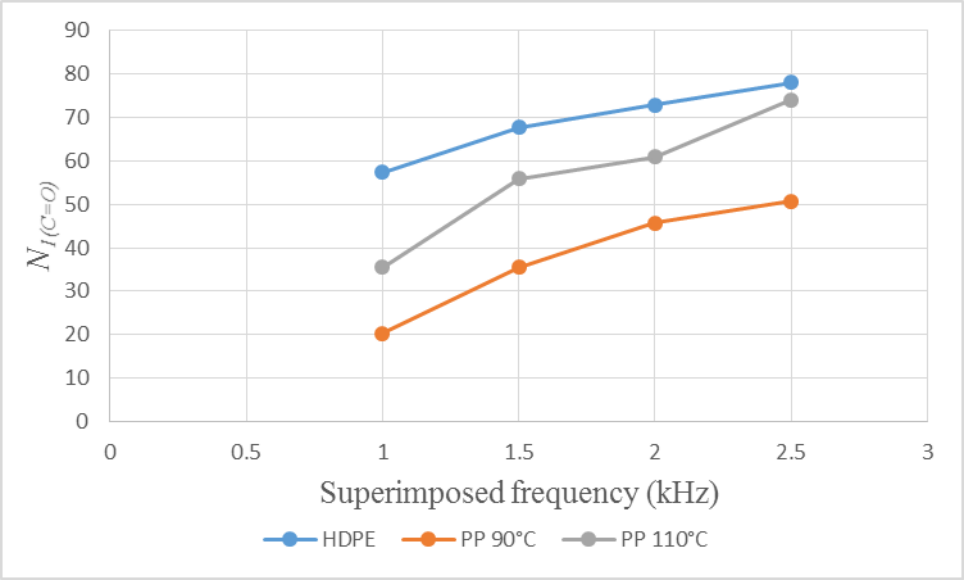

Figure 7.7. $N_{1(C=O)}$ at 30% Voltage Ratio.

Table 7.8. $N_{1(C=O)}$ at 50% Voltage Ratio.

Frequency (kHz)	HDPE	PP 90°C	PP 110°C
1	100.8391	67.4630	187.8479
1.5	156.6634	92.1027	213.2280
2	208.4896	124.7384	269.0819
2.5	283.4156	177.6900	428.7956

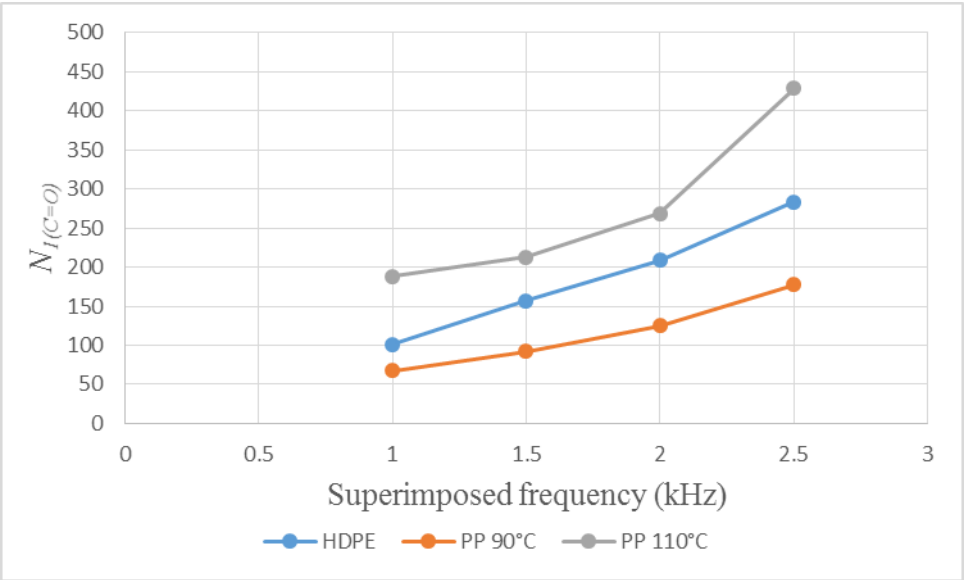

Figure 7.8. $N_{1(C=O)}$ at 50% Voltage Ratio.

In Figure 7.7-7.8, $N_{1(C=O)}$ of HDPE increases with increase of the superimposed frequency and increase of the voltage ratio. $N_{1(C=O)}$ of PP shows a dependence on the aging temperature. At the same aging condition, higher temperatures causes higher values of $N_{1(C=O)}$. The change of $N_{1(C=O)}$ may be correlated with the change of CI.

7.4 Carbonyl Index (CI)

The Carbonyl Index (CI) of HDPE and PP aged at different voltage ratios are shown in Table 7.9-7.10 and Figure 7.9-7.10.

Table 7.9. CI at 30% voltage ratio.

Frequency (kHz)	HDPE	PP 90°C	PP 110°C
1	0.0921	0.2350	0.3787
1.5	0.0986	0.2815	0.6886
2	0.1336	0.3341	0.9487
2.5	0.1719	0.3932	1.4816

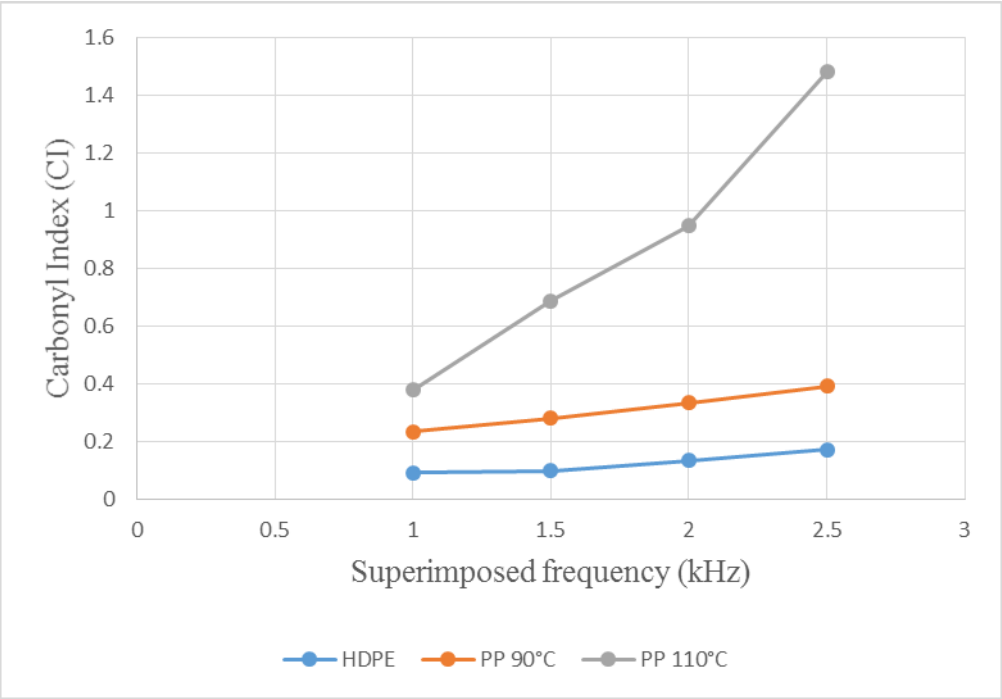

Figure 7.9. CI at 30% voltage ratio.

Table 7.10. CI at 50% voltage ratio.

Frequency (kHz)	HDPE	PP 90°C	PP 110°C
1	0.2523	0.4419	1.5359
1.5	0.3689	0.7729	2.1288
2	0.4339	1.0887	2.4647
2.5	0.4728	1.7636	2.6028

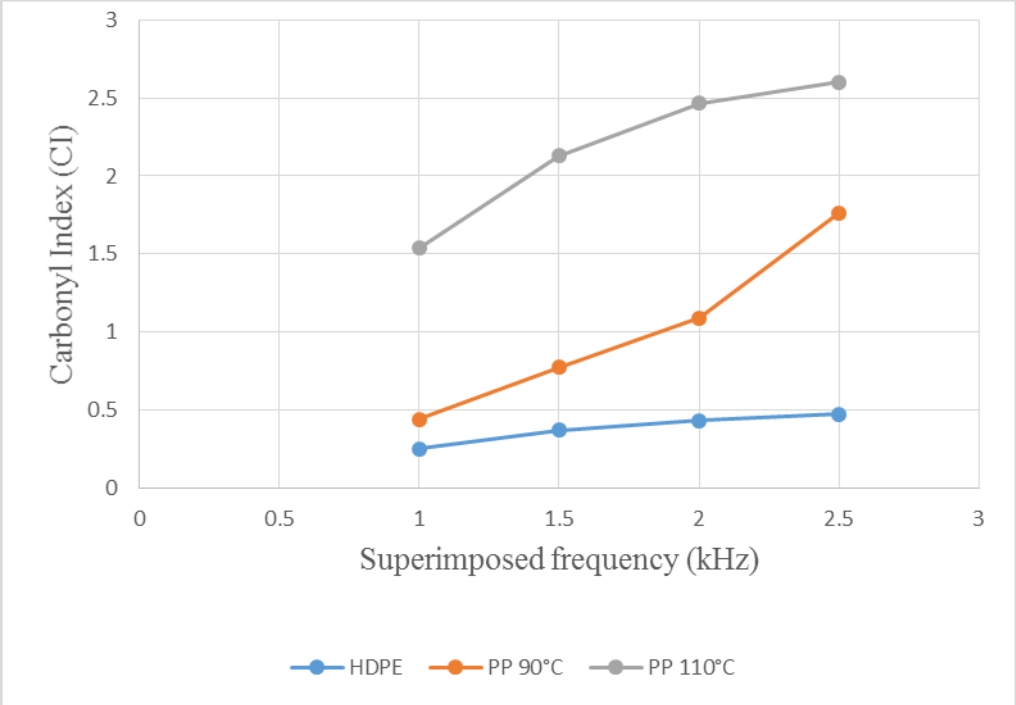

Figure 7.10. CI at 50% voltage ratio.

As shown in Figure 7.9 and Figure 7.10, the Carbonyl Index of PP follows the order: PP aged at 110°C> PP aged at 90°C. This is probably because higher temperature encourages the oxidation process. Therefore, the number of polar groups increases with increasing temperature.

$N_{1(C=O)}$ vs. CI of HDPE and PP are shown in Table 7.11-7.13.

Table 7.11. $N_{1(C=O)}$ vs. CI for HDPE.

Frequency (kHz)	30% Voltage Ratio		50% Voltage Ratio	
	$N_{1(C=O)}$	CI	$N_{1(C=O)}$	CI
1	57.4235	0.0921	100.8391	0.2523
1.5	67.7591	0.0986	156.6634	0.3689
2	72.8529	0.1336	208.4896	0.4339
2.5	78.0059	0.1719	283.4156	0.4728

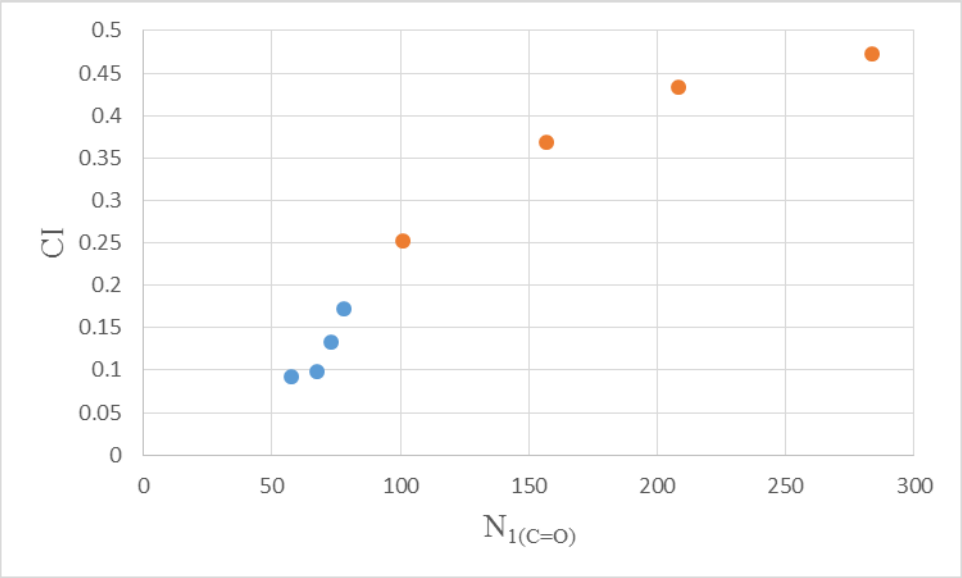

Figure 7.11. $N_{1(C=O)}$ vs. CI for HDPE.

In Figure 7.11, it can be seen that as the value of $N_{1(C=O)}$ of HDPE increases the value of CI is increasing. It also appears that the CI value may be saturating at large values of $N_{1(C=O)}$. This may be due to the fact that the CI derived from the FTIR-ATR measurements only reflects the changes in the surface layer of the polymer while $N_{1(C=O)}$ reflects a bulk change in the system.

Table 7.12. $N_{1(C=O)}$ vs. CI for PP aged at 90°C.

Frequency (kHz)	30% Voltage Ratio		50% Voltage Ratio	
	$N_{1(C=O)}$	CI	$N_{1(C=O)}$	CI
1	20.3159	0.2350	67.4630	0.4419
1.5	35.5380	0.2815	92.1027	0.7729
2	45.6960	0.3341	124.7384	1.0887
2.5	50.7601	0.3932	177.6900	1.7636

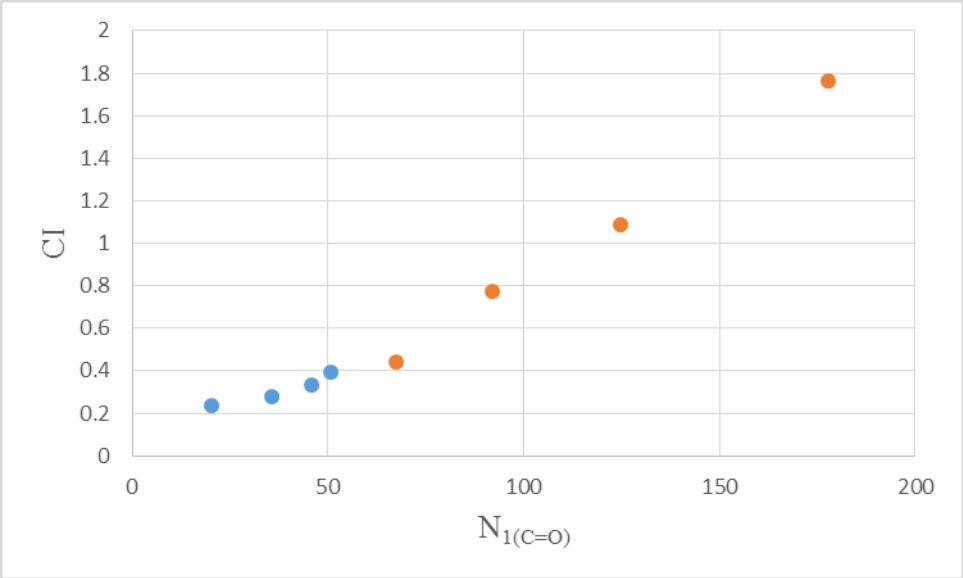

Figure 7.12. $N_{1(C=O)}$ vs. CI for PP aged at 90°C.

Figure 7.12 shows that as the value of $N_{1(C=O)}$ of PP aged at 90°C increases the value of CI is increasing. Unlike the trend in Figure 7.11, there is no saturation of CI in Figure 7.12. This is probably because the aging rate of PP aged at 90°C is not high enough, the changes in surface layer are similar to the changes in the bulk.

Table 7.13. $N_{1(C=O)}$ vs. CI for PP aged at 110°C.

Frequency (kHz)	30% Voltage Ratio		50% Voltage Ratio	
	$N_{1(C=O)}$	CI	$N_{1(C=O)}$	CI
1	35.5380	0.3787	187.8479	1.5359
1.5	55.8539	0.6886	213.2280	2.1288
2	60.9181	0.9487	269.0819	2.4647
2.5	74.0375	1.4816	428.7956	2.6028

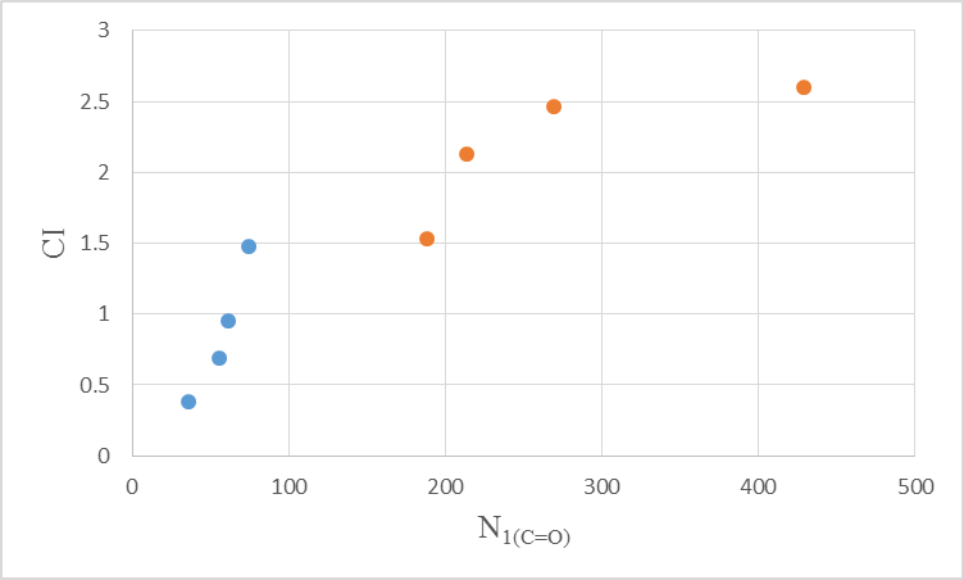

Figure 7.13. $N_{1(C=O)}$ vs. CI for PP aged at 110°C.

Figure 7.12 shows that as the value of $N_{1(C=O)}$ of PP aged at 110°C increases the value of CI is increasing. Again, the CI value may be saturating at large values of $N_{1(C=O)}$. This may be due to the higher aging conditions causing aging in the bulk as well as at the surface, these would not be detected by the FTIR-ATR. Therefore, the changes in the surface layer is no longer similar to changes in the bulk.

7.5 Comparison between Energy in Discharges and Measured Indices

According to the data from Section 7.1-7.4, changes in σ, $N_{1(C=O)}$ and CI with $\dot{E}_{CA}$ are shown in Figure 7.14-7.16.

In Figure 7.14, $N_{1(C=O)}$ in each condition increases with increasing $\dot{E}_{CA}$. The gradient (from low to high) is: PP aged at 90°C (0.0075), HDPE aged at 90 °C (0.0093) and PP aged at 110°C (0.0133). Higher gradient means the cumulative apparent energy $\dot{E}_{CA}$ impact more on $N_{1(C=O)}$ of the sample. The results show that for samples aged at 90°C, the conductivity of PP increases less than HDPE; when PP is aged at 110 °C, the

conductivity increases larger than that of HDPE.

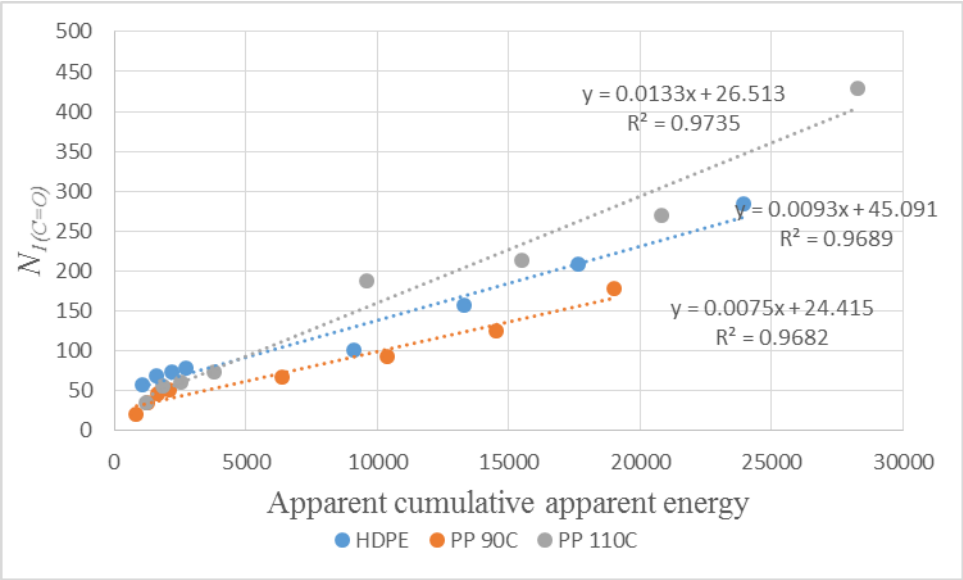

Figure 7.14. $N_{1(C=O)}$ vs. $\dot{E}_{CA}$.

A change in CI results from a change in $N_{1(C=O)}$. In Figure 7.15, CI in each condition increases with increase in $\dot{E}_{CA}$. As the CI of HDPE cannot be compared with the CI of PP, it is useful to get the information through the shape of curves. Unlike the situation in Figure 7.14, saturation can be seen in HDPE samples aged at 90 °C and PP samples aged at 110 °C. This is because samples are aged at higher aging levels. $N_{1(C=O)}$ of aged samples at these two conditions reach the threshold values, that is, even $N_{1(C=O)}$ increases the CI performs as a constant as CI can just show part of the changes (in the surface layer). However, saturation is not shown in PP aged at 90 °C, this is probably because $N_{1(C=O)}$ does not reach the threshold value at this condition and samples are at lower ageing level.

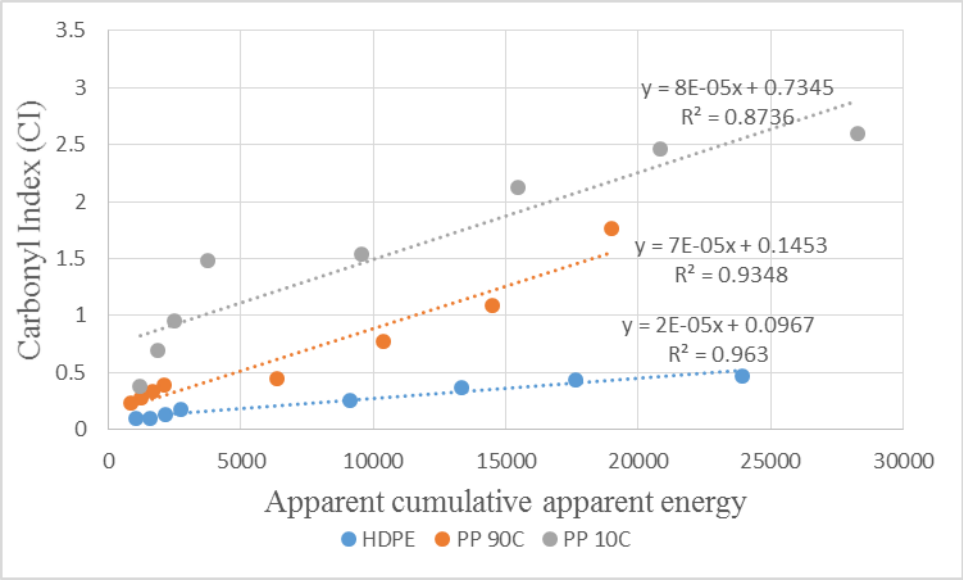

Figure 7.15. CI vs. $\dot{E}_{CA}$.

A change in σ also results from a change in $N_{1(C=O)}$. In Figure 7.16, the gradient (from low to high) is: PP aged at 90°C (0.0006), HDPE aged at 90 °C (0.0007) and PP aged at 110°C (0.0012). The higher the value of the gradient, the higher the value of σ of the sample affected by cumulative apparent energy per second $\dot{E}_{CA}$. The results show the same trend as can be seen in Figure 7.14 as both results are affected by changes in the bulk properties of the polymer.

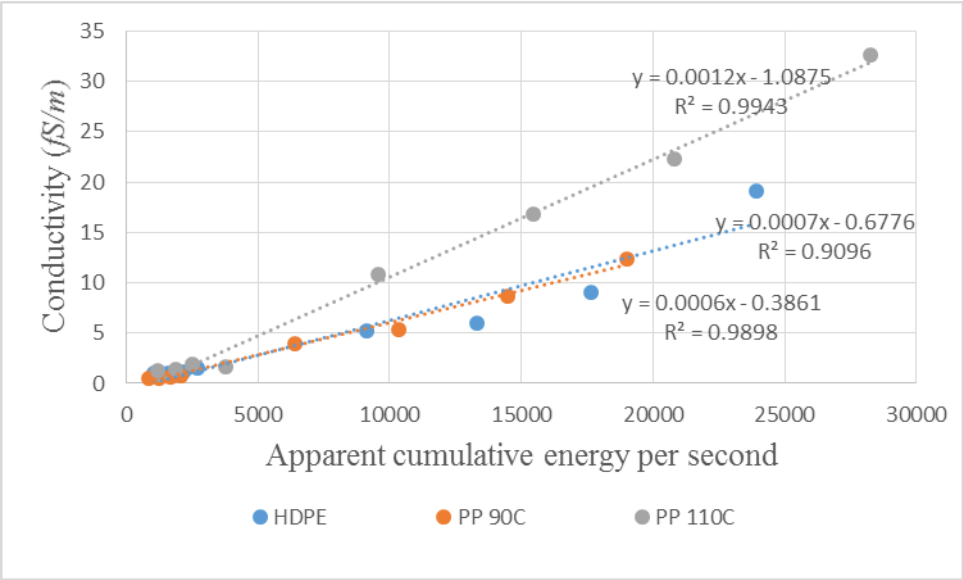

Figure 7.16. σ vs. $\dot{E}_{CA}$.

In summary, HDPE age at 90 °C and PP aged at 110 °C are at higher aging levels but PP aged at 90 °C is at lower aging level.

7.6 Conclusions

The conclusions drawn from the information in Section 7.1-7.5 are as follows:

- As expected the change in properties as a result of aging showed a dependence on temperature in PP. This agrees with Arrhenius and the other aging models introduced in Section 2.1.
- The energy provided by the partial discharges $\dot{E}_{CA}$ also showed a temperature dependence in PP.
- The energy provided by the partial discharges in the system is dependent on voltage ratios. The energy is also dependent on the superimposed frequencies.
- As the Carbonyl Index and the susceptibility index are both dependent on the number of carbonyl bonds present, there is a strong correlation at lower degrees of aging. The changes in relationship at higher aging levels can be explained in terms of the damage to the polymer starting to extend beyond scan depth of FTIR-ATR.
- The conductivity parameter associated with a different property of the system from CI and susceptibility also correlates strongly with aging.
- Most importantly there are clear and close to linear relationships between the CI conductivity and susceptibility index and the energy provided by the discharges.

7.7 References

[1] H. J. Wintle, “Charge motion in technical insulators: facts, fancies and simulations”, CEIDP 2003, pp.1-15.

[2] http://www.feynmanlectures.caltech.edu/II_11.html, [Accessed: 04 May 2016]

8. Project Achievements, Conclusions and Recommendation of Future Work

8.1 Achievements and Conclusions

In this project, HDPE and PP were chosen as the target materials to analyse. HDPE has broadly similar properties to XLPE (a common service insulation) and was available in a suitable form. The properties of HDPE were regarded as a bench-mark. As cable insulation is exposed to thermal and electrical stressing in service, in this project, thermo-electrical stress was used to age the samples. Cable insulation may have to operate at 90°C. Therefore, HDPE and PP samples were aged by 90°C. For comparison, 110°C was applied to PP to investigated reaction at higher temperature. For electrical stress, combined AC & DC voltage waveform was chosen as the applied voltage. The voltage ratio between the AC and DC components was chosen as 10%, 30% and 50%. The superimposed frequency was 1, 1.5, 2 and 2.5 kHz. PRPD was used to detect the PD activities during the aging process. FTIR-ATR and DS measurements were used to analyse and evaluate the change of chemical properties and dielectric properties of polymers after aging, respectively.

Project achievements are summarized as follows:

- The behaviour of PD activities in a triple junction when combined AC & DC voltage is applied has been characterised for certain conditions of stress. Changes in the PRPD pattern were observed as a function of the applied voltage and frequency. A mechanism has been proposed to explain the effect of the superimposed frequency on PD activity of HDPE and PP.
- A simple method to calculate the PD apparent cumulative energy per second ($\dot{E}_{CA}$) has been implemented. $\dot{E}_{CA}$ should correspond to the power delivered to the polymer as a result of PD activity. The behaviour of $\dot{E}_{CA}$ as a function of the voltage and frequency has been derived.

- From the FTIR-ATR results, the Carbonyl Index (CI) has been calculated, two other parameters affected by the ageing, the conductivity (σ) and dielectric susceptibility index (χI) of each material, have been calculated from the DS data. The behaviour of these three parameters appears to be closely correlated with the value of $\dot{E}_{CA}$ over the values of voltage and AC frequency used to age the samples. A 4th parameter related to the susceptibility index $N_{1(C=O)}$, which is related to the concentration of carbonyl groups, has been calculated to explain the correlation between CI and the susceptibility index.

8.2 Suggestions for Future Work

The results presented in this project show that a great deal of further investigation is needed in the area of combined AC and DC thermoelectric stressing. To improve our understanding of the mechanism of cable insulation under superimposed voltages and to quantify the effects the following experiments would be useful:

a) In this project the DC voltage was positive, to understand the mechanism of PD better it would be useful to perform a set of similar experiments using a negative DC voltage to see the impact of this on the partial discharge behaviour.
b) Further analysis of the partial discharge data that already exists in the project should be undertaken. The data should be plotted in an equivalent to the *n*-ϕ-*q* form and the temporal development of the partial discharge activity over the one hour aging period. It may also be possible to look at the phase angle sequences for the data.
c) In this project, to investigate how polymers degradation is affected by voltage ratios, the voltage ratio was increased to 50% (much higher than in operation). But this does not establish a relation between the experiment and the real world. Future work should establish the relationship between experimental 1 h aging under 50% voltage ratio and the lifetime of cable operation under 10% voltage ratio or below in practice. In the future, it would be of value to establish an

equation relating the aging parameters in experimental work and the real life of cable insulation. This would involve a large experimental program to look at a suitable number of aging stresses to determine the life relationships of the material. This investigation would also help to understand the observed changes in the system and the mechanisms underlying them.

d) In this project, the PD apparent cumulative energy per second was used instead of the real PD energy. Despite the good correlations observed with other parameters assumptions such as constant discharge resistance and constant discharge time were made. In the future, it may useful to establish a PD measurement system that is able to record the duration of each PD pulse so that a better approximation to real PD energy could be calculated.

e) The combined voltage stress was set by the signal generator and it was amplified by power amplifier. As the signal generator can only set the digital values, it is hard to measure the PDIV in this system. In the future, the system can be developed so that PDIV could be measured.

f) Investigations need to be carried out to look at the competing processes of higher electron emission and reduced voltage across the gap and surface. The investigation will help to establish a good understanding of mechanism of aging by combined AC/DC stress.

g) In this project, Carbonyl Index of HDPE cannot be compared with that of PP. It would be better to refine the method of calculation to allow direct comparison of the Carbonyl Index of different materials.

h) This project focuses on the change of dielectric properties and chemical properties of PP after aging, but mechanical properties were not included. Mechanical property is another important index to describe a material. Mechanical property can also provide evidence to evaluate whether a material could be a good cable insulation material in practical applications. In the future, the change of mechanical properties (such as tensile strength, compressive strength, stiffness, surface roughness, flexibility, brittleness and etc…) of PP after

aging by combined AC & DC voltages could be studied. The results will provide more information to evaluate PP as an insulation material.

Appendix

Appendix A Thermo-electrical Aging Model

1) Simoni's Model

This was based on a model proposed by Eyring. It has been difficult to find an original reference for Eyring's model for electro thermal stressing. Many authors quote [1] but examination of this book, while showing the derivation of the Eyring rate equation of temperature.

$$R(T) = A\beta(T)\exp\left(\frac{B}{kT}\right) \quad (1)$$

Where *A* and *B* are constants and $\beta(T)$ is a function of temperature depending on the form of the chemical reaction, does not show the derivation of the equation for electro-thermal ageing.

From [2-3] the general form of the Eyring rate equation for thermal and a single additional stress *S* is:

$$R(T) = A\beta(T)\exp\left(\frac{B}{kT}\right)\exp\left(\left(a+\frac{b}{T}\right)f(S)\right) \quad (2)$$

Where a and b are constants and $f(S)$ is a function of the non thermal stress applied to the system

In [4] Simoni proposed that the rate of reaction under combined electrical and thermal stressing would take the form:

$$R(T,E) = A\exp\left(-\frac{B}{T}\right)\exp\left(\left(a+\frac{b}{T}\right)f(E)\right) \quad (3)$$

Where A and B are constants as in equation 2.3 while a and b as two additional constants. $f(E)$ is an arbitrary function of the electric field. In a similar manner to the approach adopted with equation 2.3 to 2.4 the inverse of this equation gives the predicted lifetime:

$$L(T,E) = \frac{1}{A}\exp\left(\frac{B}{T}\right)\exp\left(-\left(a+\frac{b}{T}\right)f(E)\right) \quad (4)$$

If $f(E) = 0$ it can be seen that the equation takes the form for simple temperature dependent aging.

As with the Arrhenius equation the constant $1/A$ can be replaced using the expression for the lifetime L_0 when $E = 0 \Rightarrow f(E) = 0$. Again using $\Delta\left(\frac{1}{T}\right) = \frac{1}{T_0} - \frac{1}{T}$ the equation becomes:

$$L(T,E) = L_0\exp\left(-B\Delta\left(\frac{1}{T}\right)\right)\exp\left(-\left(a+\frac{b}{T_0}-b\Delta\left(\frac{1}{T}\right)\right)f(E)\right) \quad (5)$$

Simoni [4] showed that an exponential dependence on field at constant temperature could be achieved by setting $f(E) = E$

$$L(T,E) = L_0\exp\left(-B\Delta\left(\frac{1}{T}\right)\right)\exp\left(-\left(a+\frac{b}{T_0}\right)E+b\Delta\left(\frac{1}{T}\right)E\right) \quad (6)$$

And that a power dependence for E could be achieved by setting $f(E) = \ln(E/E_0)$

$$L(T,E) = L_0\exp\left(-B\Delta\left(\frac{1}{T}\right)\right)\left(\frac{E}{E_0}\right)^{-\left(a+\frac{b}{T_0}-b\Delta\left(\frac{1}{T}\right)\right)} \quad (7)$$

Based on the equation above and fitting to experimental data, Simoni then proposed [5] the model as follows, again compatible with the inverse power model for electrical aging:

$$L(T,E) = L_0 exp\left(-B\Delta\left(\frac{1}{T}\right)\right)\left(\frac{E}{E_0}\right)^{-N}, E \geq E_0 \quad (8)$$

where, L_0 is time to breakdown when $E=E_0$ under room temperature, E is the external electric field, E_0 is the value of threshold field below which the electrical stress has no

impact on the model as described above. $N = n - b\Delta\left(\frac{1}{T}\right)$, n and b are constants with based on [4] $n = a + \frac{b}{T_0}$. As before: $\Delta\left(\frac{1}{T}\right) = \frac{1}{T_0} - \frac{1}{T}$ which Simoni refers to as the *"Thermal Stress"*.

2) Ramu's Model

Ramu's model [6] is also based on Eyring's theory. In Ramu's model, threshold value was not assumed to exist.

In its first version the lifetime was assumed to take the form of:

$$L(T,E) = k(T)E^{-m(T)}\exp\left(\frac{B}{T}\right) \tag{9}$$

Where B has the same meaning as in the Simoni Model, the activation energy divided by Boltzmanns constant, and the functions $k(T)$ and $m(T)$ are given by:

$$k(T) = \exp\left(k_1 + \frac{k_2}{T}\right), \quad m(T) = m_1 + \frac{m_2}{T}$$

By dividing the lifetime $L(T,E)$ by the lifetime at ambient conditions $T_0$and a reference field E_0: $L(T_0,E_0) = L_0$ the following relationship was derived:

$$L(T,E) = L_0\frac{k(T)}{k(T_0)}\frac{E^{m(T)}}{E^{m(T_0)}}\frac{\exp\left(\frac{B}{T}\right)}{\exp\left(\frac{B}{T_0}\right)} \tag{10}$$

Substituting for the functions $k(T)$ and $m(T)$ Ramu derived the following:

$$L(T,E) = L(T_0,E_0)\exp\left(-\frac{k_2}{T_0}\frac{\Delta T}{T}\right)\left(\frac{E}{E_0}\right)^{-\left(\frac{m_2\Delta T}{T\ T}\right)}\exp\left(-\frac{B}{T_0}\frac{\Delta T}{T}\right) \tag{11}$$

Here $\Delta T = T - T_0$. Note the expressions within the exponential terms are identical to the term $\Delta\left(\frac{1}{T}\right)$ used in the Simoni Model.

$$\Delta\left(\frac{1}{T}\right) = \frac{1}{T_0} - \frac{1}{T} = \frac{T - T_0}{T_0 T} = \frac{1}{T_0}\frac{\Delta T}{T}$$

Simoni and Montanari [7] pointed out that there was an error in the derivation of Ramu's equation and that the term dealing with the dependence on E should take the form:

$$\frac{E^{m(T)}}{E^{m(T_0)}} = E^{\frac{T_0}{T}}\cdot\left(\frac{E}{E_0}\right)^{-\left(m_1+\frac{m_2}{T_0}\right)} \tag{12}$$

Leading to:

$$L(T,E) = L(T_0,E_0)\exp\left(-\frac{k_2}{T_0}\frac{\Delta T}{T}\right)E^{\frac{T_0}{T}}\left(\frac{E}{E_0}\right)^{-\left(\frac{m_2\Delta T}{T\ T}\right)}\exp\left(-\frac{B}{T_0}\frac{\Delta T}{T}\right) \quad (13)$$

The presence of the term $E^{\frac{T_0}{T}}$ comes from the difference in approach between Simoni and Ramu. Simoni uses the term E_0 to represent the threshold field below which no field driven ageing occurs, Ramu uses the term E_0 as a reference field and does not believe that a threshold field exists [7].

Later in [6] Ramu presents a simplified expression for fitting of experimental data for the lifetime based on equation 2.18 above which takes the form:

$$L(T,E) = k(T_0)\exp\left(-\frac{k_2}{T_0}\frac{\Delta T}{T}\right)\cdot\left(\frac{E}{E_0}\right)^{-\frac{b}{T_0}\frac{\Delta T}{T}}\cdot\exp\left(-\frac{B}{T_0}\frac{\Delta T}{T}\right) \quad (14)$$

Which is then rearranged to the form:

$$L(T,E) = k(T_0)\exp\left(-\frac{(k_2+B)}{T_0}\frac{\Delta T}{T}\right)\cdot\left(\frac{E}{E_0}\right)^{-\frac{b}{T_0}\frac{\Delta T}{T}} \quad (15)$$

It should be noted in this expression that $b = m_2$. Comparing this with Simoni's expression for lifetime:

$$L(T,E) = L_0\exp\left(-B\Delta\left(\frac{1}{T}\right)\right)\left(\frac{E}{E_0}\right)^{-\left(a+\frac{b}{T_0}+b\Delta\left(\frac{1}{T}\right)\right)} \quad (16)$$

And as

$$\frac{1}{T_0}\frac{\Delta T}{T} \equiv \Delta\left(\frac{1}{T}\right)$$

We can see that the two expressions are very similar as $k(T_0) \equiv L_0$. The significant differences are: Firstly in the exponential term Simoni has assumed that the effective activation energy for the thermal aging reaction is a constant while Ramu assumes that this activation energy has a dependence on temperature; Secondly there are differences in the form of the exponent for the relative field term with Simoni suggesting that a constant term $a + \frac{b}{T_0}$ should be included. This is the result of his use of the Eyring equation as a starting point for his derivation.

Simoni and Montari [7] however pointed out that a term $E^{\frac{T_0}{T}}$ should be included in the equation above.

The version of Ramu's model quoted in [8] is similar to the above though it states that

it is based on Eyring's system and inherently takes into account thresholds in both the thermal and electrical aging: the equation takes the form of:

$$L(T,E) = c(T)E^{-n(T)}exp\left(-B\Delta\left(\frac{1}{T}\right)\right) \text{ , } E>E_0 \quad (17)$$

Where, $c(T) = exp\left(c_1 - c_2\Delta\left(\frac{1}{T}\right)\right)$, $n(T) = n_1 - n_2\Delta\left(\frac{1}{T}\right)$, c_1, c_2, n_1 and n_2 are constants. $\Delta\left(\frac{1}{T}\right)$ has the same meaning as in Simoni model. It is not clear in this statement of the Ramu model why the term $\left(\frac{E}{E_0}\right)^{-n(t)}$ has been replaced by $E^{-n(t)}$ in this representation of the model. One effect of this would be to allow the possibility in a step change in the lifetime as the electric field is increased past the threshold value E_0.

3) Fallou's Model

Based on the exponential model of electrical aging, Fallou [9] raised a semi-empirical aging equation as below:

$$L = exp\left(A(E) + \frac{B(E)}{T}\right) \text{ , E>0} \quad (18)$$

Where $A(E)=A_1+A_2E$ and $B(E)=B_1+B_2E$ are determined from empirical time-to-breakdown curves under room temperature. If this expression is compared with the exponential model of aging from Simoni, described above:

$$L(T,E) = L_0 \exp\left(-B\Delta\left(\frac{1}{T}\right)\right)\exp\left(-\left(a + \frac{b}{T_0}\right)E + b\Delta\left(\frac{1}{T}\right)E\right) \quad (19)$$

This can be rearranged into a similar form:

$$L(T,E) = L_0 \exp\left(-B\Delta\left(\frac{1}{T}\right)\right)\exp\left(-\left(a + \frac{b}{T_0}\right)E + b\Delta\left(\frac{1}{T}\right)E\right) \quad (20)$$

$$L(T,E) = \exp\left(\ln L_0 - \left(a + \frac{b}{T_0}\right)E - B\Delta\left(\frac{1}{T}\right) - b\Delta\left(\frac{1}{T}\right)E\right) \quad (21)$$

$$L(T,E) = \exp\left(\ln L_0 - \left(a + \frac{b}{T_0}\right)E - B\left(\frac{1}{T_0} - \frac{1}{T}\right) - b\left(\frac{1}{T_0} - \frac{1}{T}\right)E\right) \quad (22)$$

$$L(T,E) = \exp\left(\left(\ln L_0 - \frac{B}{T_0}\right) - \left(a + \frac{2b}{T_0}\right)E + \frac{1}{T}(B + bE)\right) \quad (23)$$

Therefore the parameters for the functions $A(E)$ and $B(E)$ can be mapped directly onto the parameters in Simoni's exponential model.

$$A_1 = \ln L_0 - \frac{B}{T_0}, \qquad A_2 = -\left(a + \frac{2b}{T_0}\right), \qquad B_1 = B, \qquad B_2 = b$$

4) Crine's Model

Crine [10] approach was based on principle of reaction kinetics, rather than looking at the basic Arrhenius relationship and adding a field dependent factor, as with Simoni, Ramu and Falou. He considered the effects that the applied electric field had on the potential barrier controlling the ageing reaction. He considers that the aging reaction occurs as a result of the disruption of the relatively weak van der Waal's bonds between the polymer molecules (0.1 to 0.4 eV) [11]. If these bonds are disrupted the molecules in the polymer can rearrange, increasing crystallinity and leading to the formation of micro voids in the amorphous regions. It is assumed that the disruption is caused by the motion of electrons under the influence of the applied field. The free energy associated with the reaction path with and without stress is shown in Figure 2.1.

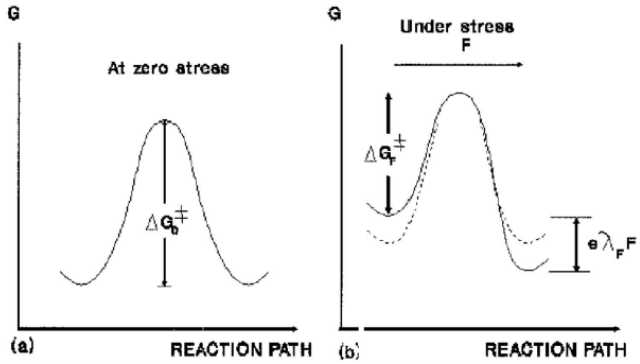

Figure A. 1 Changes in free energy barrier for the aging reaction in the presence and absence of an electric field. From [11]

The barrier height in the direction of the reaction ΔG^+ is given by:

$$\Delta G^+ = \Delta H^+ - T\Delta S^+$$

Where ΔH^+ is the activation enthalpy and ΔS^+ is the entropy of reaction for the forward process. The probability of a successful transition between the initial unaged state and the final aged state from chemical kinetics is therefore:

$$p^+ = \frac{kT}{h}\exp\left(-\frac{\Delta G^+}{kT}\right)$$

Where h is Planck constant, there is a corresponding probability for the reverse reaction, where molecular reorganization occurs and returns the system to a less aged state.

$$p^- = \frac{kT}{h}\exp\left(-\frac{\Delta G^-}{kT}\right)$$

The net probability *p* of aging occurring is therefore.

$$p = p^+ - p^- = \frac{kT}{h}\left[\exp\left(-\frac{\Delta G^+}{kT}\right) - \exp\left(-\frac{\Delta G^-}{kT}\right)\right] \quad (24)$$

If ΔG^+ is smaller than ΔG^- the net probability is positive and aging will take place. Crine defined the lifetime L of the system as being the inverse of the net probability.

$$L \simeq \frac{1}{p}$$

This approach corresponds to the Arrhenius approach adopted by Simoni and Falou for thermal aging with $\Delta G/T = B$.

When considering the effects of an electric field for simplicity and clarity Crine assumed that the barrier was symmetrical: $\Delta G^+ = \Delta G^- = \Delta G_0$. In this case in the absence of a field the probability of ageing occurring once the sample has reached its equilibrium state is zero. Reaction kinetics will cause the sample to move from an unaged state to an equilibrium aged state even if the probabilities are equal because of differences in the concentration of unaged and aged material. The presence of an electric field in the system leads to molecular distortions which have the effect of distorting the molecular structure which modify the barrier heights in the forward and reverse directions. He states that the change in energy can be calculated in terms of the charge on the electron e the value of the field E and the volume of the molecular chains affected λ corresponding to the size of micro- cavity formed during ageing.

$$W = e\lambda E \quad (25)$$

Therefore the probabilities of the forward and reverse reactions occurring become:

$$p^+ = \frac{kT}{h}\exp\left(-\frac{\Delta G_0 - e\lambda E}{kT}\right) = \exp\left(\frac{e\lambda E}{kT}\right)\frac{kT}{h}\exp\left(-\frac{\Delta G_0}{kT}\right) \quad (26)$$

$$p^- = \frac{kT}{h}\exp\left(-\frac{\Delta G_0 + e\lambda E}{kT}\right) = \exp\left(-\frac{e\lambda E}{kT}\right)\frac{kT}{h}\exp\left(-\frac{\Delta G_0}{kT}\right) \quad (27)$$

In the expression for p^+ the term $\exp(e\lambda E/kT)$ is always greater than or equal to one, while in the expression for p^- the term $\exp(-e\lambda E/kT)$ while greater than zero is always less than or equal to one. Therefore the value of $p^+ \geq p^-$.

The net probability in the presence of the electric field therefore becomes:

$$p = p^+ - p^+ = \frac{kT}{h}\exp\left(-\frac{\Delta G_0}{kT}\right)\left[\exp\left(\frac{e\lambda E}{kT}\right) - \exp\left(-\frac{e\lambda E}{kT}\right)\right] \quad (28)$$

This can be represented in a more compact form by using the $sinh$ function.

$$p = \frac{2kT}{h}\exp\left(-\frac{\Delta G_0}{kT}\right)\left[\sinh\left(\frac{e\lambda E}{kT}\right)\right] \quad (29)$$

Therefore the time to insulation failure, L, which is the inverse of the net probability, is given by

$$L \simeq \frac{h}{2kT}\exp\left(\frac{\Delta G_0}{kT}\right)\left[\operatorname{csch}\left(\frac{e\lambda E}{kT}\right)\right] \quad (30)$$

This approach predicts a different behaviour for lifetime compared to the models considered earlier in this chapter.

At electric field above critical value:

$$\operatorname{csch}\left(\frac{e\lambda E}{kT}\right) \simeq 2\exp\left(-\frac{e\lambda E}{kT}\right) \longrightarrow L \simeq \frac{h}{kT}\exp\left(\frac{\Delta G_0}{kT}\right)\exp\left(-\frac{e\lambda E}{kT}\right) \quad (31)$$

Giving an exponential model of ageing. This behavior has been reported by Montinari et al in experiments on mini cable samples insulated with XLPE at fields above 15kVmm^{-1} [12].

At electric field below critical value:

$$\operatorname{csch}\left(\frac{e\lambda E}{kT}\right) \longrightarrow 0 \implies L \longrightarrow L_0$$

Indicating that little or no electrical ageing will take place. Between these two regimes there is a transition between the two limiting behaviours.

Useful fits of this model to experimental data have been achieved [24] particularly in the high field regime. However the parameter λ is itself field dependent at lower fields which introduces complexity into the fitting process [11].

5) Montanari's Model

Montanari's model [13] is based on modifying the well-known Weibull distribution to take into account Simoni's model of insulation lifetime. The basic 2 parameter

Weibull distribution is:

$$F(t) = 1 - \exp\left(\left(\frac{t}{\alpha}\right)^{\beta}\right) \tag{32}$$

$F(t)$ is the probability of failure having occurred by time t, α is the scale parameter which gives the time at which the probability of failure is 63.2% ($F(t) = 0.632$). β is the shape parameter. Under combined thermal and electrical stresses the parameters $\propto$ and β are functions of the temperature and applied field: $\alpha(T, E)$ and $\beta(T, E)$.

As $\alpha(T, E)$ refers to a constant probability of failure, Montanari assumed that it was directly related to the expression of the lifetime. Therefore assuming that lifetime followed Simoni's expression as given in equation 2.13.

$$\propto (T, E) = \alpha_0 \exp\left(-B\Delta\left(\frac{1}{T}\right)\right)\left(\frac{E}{E_0}\right)^{-n_c(T)} \tag{33}$$

In this expression α_0 is the time for there to be a 67.3% probability of a failure to have taken place at $T = T_0, E = E_0$ and the endurance coefficient n_c takes the form of:

$$n_c(T) = n_0 - b\Delta\left(\frac{1}{T}\right) \tag{34}$$

Where n_0 is the endurance coefficient derived for room temperature $T = T_0$.

If the electrical strength E_S using a linear ramping field can be measured at the ageing temperature T_K and the time to failure t_s under a constant field of E, it is possible to use an alternative form for the scale parameter as a function of E again based on the Simoni model:

$$\alpha(E)_{T=T_K} = t_S\left(\frac{E}{E_S}\right)^{-n_c} \tag{35}$$

It can be seen that the temperature dependence of α is not explicitly stated. However the parameters t_S, E_S and n_c are all functions of temperature T, in this case evaluated at $T = T_K$.

Substituting these equations for α above into the Weibull function leads to two expressions for the Weibull distribution under combined thermal and electrical stressing. The first is based on the full Simoni expression:

$$F(t) = 1 - \exp\left(\left(\frac{t}{\alpha_0}\exp\left(B\Delta\left(\frac{1}{T}\right)\right)\left(\frac{E}{E_0}\right)^{n_c(T)}\right)^{\beta(T,E)}\right) \quad (36)$$

The second is based on data extracted at constant temperature T_K:

$$F(t) = 1 - \exp\left(\left(\frac{t}{t_S}\left(\frac{E}{E_S}\right)^{n_c(T_K)}\right)^{\beta(T,E)}\right) \quad (37)$$

To complete the probabilistic approach the behaviour of the parameter $\beta(T,E)$ must be determined. If the measurement temperature T_K is set to T_0, then $\Delta\left(\frac{1}{T}\right) = 0$. Under these conditions the expression based on the Simoni model for the Weibull distribution becomes:

$$F(t) = 1 - \exp\left(\left(\frac{t}{\alpha_0}\left(\frac{E}{E_0}\right)^{n_c(T_0)}\right)^{\beta(T_0,E)}\right) \quad (38)$$

Which can be rearranged as

$$F(t) = 1 - \exp\left(\frac{t}{\alpha_0}\left(\frac{E}{E_0}\right)\right)^{\gamma(T_0,E)} \quad (39)$$

This is another 2 parameter Weibull distribution with a shape parameter $\gamma(T_0,E)$. It can be seen that:

$$\gamma(T_0,E) = \beta(T_0,E)n_c(T_0) = \beta(T_0,E)n_0 \quad (40)$$

Therefore under these conditions:

$$\beta(T_0,E) = \frac{\gamma(T_0,E)}{n_0} \quad (41)$$

The behaviour of $\beta(T_0,E)$ can therefore be determined by performing a Weibull plot of the sample lifetime at T_0 as a function of field. The gradient of the plot corresponds to the parameter $\gamma(T_0,E)$.

From experimental data there is little variation in the value of the gradients of a Weibull plots of lifetime as a function of field for different isotherms [13].

$$\gamma(T,E) = \gamma(T_0,E) = \gamma_0 \quad (42)$$

Therefore Montinari stated that a more general expression for $\beta(T_0,E)$ can be assumed.

$$\beta(T,E) = \frac{\gamma_0}{n_C(T)} \quad (43)$$

Therefore a plot of log lifetime as a function of $\Delta\left(\frac{1}{T}\right)$ at $E = 0$ will allow the determination of the parameter B. A plot of log lifetime vs log $\Delta\left(\frac{1}{T}\right)$ at a constant field $E_K > E_0$ will allow the parameter of $n_C(T)$ to be determined. Finally a Weibull plot of lifetime as a function of applied field at ambient conditions $(T = T_0)$ allows the parameters $\alpha_0$and γ_0 to be determined. This provides sufficient data to predict the lifetime for all values of E and T having occurred after a time t is given by F (statistical calculation of Weibull distribution. The equation is shown as below:

$$F(t, E, T) = 1 - \exp\left\{-\left[\frac{t}{t_s}\left(\frac{E}{E_s}\right)^n\right]^{\beta(E,T)}\right\} \quad (44)$$

where, t_s is the time to breakdown under electric field E_s, t is time to breakdown under electric field E, $\beta(E, T)$ is the shape parameter, n is the voltage endurance coefficient at temperature T.

References

[1] Williams, J.A. Underground Transmission Systems. New York : Electrical Power Research Institute, Inc., c1992.

[2] L.A. Escobar and W.Q. Meeker, “A review of accelerated test models”, Statistical Science, Vol.21, No.4, pp.552-577, 2006。

[3] L Simoni, “A new approach to the voltage endurance test on electrical insulation”, IEEE Transactions on Electrical Insulation, Vol.EI-8, Issue.3, pp.76-86, 1973.

[4] L. Simoni, “A General Approach to the Endurance of Electrical Insulation under Temperature and Voltage”, IEEE Transactions on Electrical Insulation, Vol.EI-16, Issue.4, pp.277-289, 1981.

[5] Simoni L, “General equation of the decline in the electric strength for combined thermal and electrical stresses”, IEEE Transactions on Electrical Insulation, Vol.EI-19, Issue.1, pp.45-52, 1984.

[6] Haddad, A. and Warne, D. Advances in High Voltage Engineering. London : MPG Books Limited, c2004.

[7] Maik Koch, Michael Krueger and Markus Puetter, “Advanced Insulation Diagnostic by Dielectric Spectroscopy”, TechCon Asia Pacific, Sydney, Australia, 2009.

[8] G. L. Johnson, Solid State Thesla Coil, www.eece.kce.edu/johnson, Chapter 3-1, 2001.

[9] Kwan-Chi. Kao, “Dielectric phenomena in solids: with emphasis on physical concepts of electronic processes”, Amsterdam ; Boston : Academic Press, 2004.

[10] B. K. P. Scaife, Principles of Dielectrics (Oxford Science Publications, Oxford, 1998).

[11] H. Frohlich, Theory of Dielectrics: Permittivity and Dielectric Loss (Oxford Science Publications, Oxford, 1958.

[12] G. C. Montinari, G. Pattini and L. Simoni, "Investigation on the combined-stress behavior of XLPE insulated cables", International Conference on Properties and Applications of Dielectric Materials, pp.709-712, 1985.

[13] C. J. F. Bottcher, Theory of Electric Polarization (Elsevier Publishing Company, Amsterdam, 1952.

Appendix B - Characteristic IR absorption frequencies of organic functional groups

Table B. 1 Characteristic IR absorption frequencies of organic functional groups

Function group	Type of vibration	Characteristic wavenumber (cm^{-1})	Intensity
Alcohol			
O-H	Stretch, H-bonded	3200-3600	Strong, broad
O-H	Stretch, free	3500-3700	Strong, sharp
C-O	Stretch	1050-1150	Strong
Alkane			
C-H	Stretch	2850-3000	Strong
-C-H	Bending	1350-1480	Variable
Alkene			
=C-H	Stretch	3010-3100	Medium
=C-H	Bending	675-1000	Strong
C=C	Stretch	1620-1680	Variable
Alkyl halide			
C-F	Stretch	1000-1400	Strong
C-Cl	Stretch	600-800	Strong
C-Br	Stretch	500-600	Strong
C-I	Stretch	500	Strong
Alkyne			
C-H	Stretch	3300	Strong, sharp
C=C	Stretch	2100-2260	Variable, not present in symmetrical alkynes
Amine			
N-H	Stretch	3300-3500	Medium (primary amines have two bands; secondary have one band, often very weak)
C-N	Stretch	1080-1360	Medium-weak
N-H	Bending	1600	Medium
Aromatic			
C-H	Stretch	3000-3100	Medium
C=C	Stretch	1400-1600	Medium-weak, multiple bands
Analysis of C-H out-of-plane bending can often distinguish substitution patterns			
Carbonyl			
C=O	Stretch	1670-1820	Strong (conjugation moves

			absorptions to lower wave numbers)
Ether			
C-O	Stretch	1000-1300 (1070-1150)	Strong
Nitrile			
C-N	Stretch	2210-2260	Medium
Nitro			
N-O	Stretch	1515-1560 and 1345-1385	Strong, two bands

Appendix C - ε″ vs. 1/ω of HDPE

Table C. 1 ε'' vs. 1/ω of HDPE aged by 10% voltage ratio

Frequency [Hz]	1/ω	ε''					
		Reference	DC	DC+1k	DC+1.5k	DC+2k	DC+2.5k
1.0316	0.15428	5.01E-04	0.00243	0.00287	0.00309	0.00341	0.00345
0.42985	0.370257	6.00E-04	0.00257	0.0029	0.0031	0.00344	0.00344
0.1791	0.888637	6.59E-04	0.00272	0.00285	0.00306	0.00341	0.0034
0.07463	2.132587	7.01E-04	0.00292	0.00317	0.00312	0.00342	0.00391
0.0311	5.117522	7.31E-04	0.00311	0.00336	0.00382	0.00403	0.00431
0.01296	12.28047	8.71E-04	0.00372	0.00453	0.00444	0.00461	0.0052
0.01	15.91549	8.99E-04	0.0039	0.00465	0.00523	0.00533	0.00552

Table C. 2 ε'' vs. 1/ω of HDPE aged by 30% voltage ratio

Frequency [Hz]	1/ω	ε''					
		Reference	DC	DC+1k	DC+1.5k	DC+2k	DC+2.5k
1.0316	0.15428	5.01E-04	0.00243	0.00322	0.00365	0.00428	0.00427
0.42985	0.370257	6.00E-04	0.00257	0.00319	0.0037	0.00433	0.00434
0.1791	0.888637	6.59E-04	0.00272	0.00336	0.00372	0.00441	0.00454
0.07463	2.132587	7.01E-04	0.00292	0.00353	0.00392	0.00461	0.00467
0.0311	5.117522	7.31E-04	0.00311	0.00357	0.00409	0.0048	0.00497
0.01296	12.28047	8.71E-04	0.00372	0.00472	0.00493	0.0056	0.0062
0.01	15.91549	8.99E-04	0.0039	0.00492	0.00568	0.00635	0.0072

Table C. 3 ε'' vs. 1/ω of HDPE aged by 50% voltage ratio

Frequency [Hz]	1/ω	ε''					
		Reference	DC	DC+1k	DC+1.5k	DC+2k	DC+2.5k
1.0316	0.15428	5.01E-04	0.00243	0.0041	0.00521	0.00654	0.01045
0.42985	0.370257	6.00E-04	0.00257	0.00424	0.00582	0.00663	0.01083
0.1791	0.888637	6.59E-04	0.00272	0.00447	0.00604	0.00754	0.01275
0.07463	2.132587	7.01E-04	0.00292	0.00487	0.00653	0.00897	0.01575
0.0311	5.117522	7.31E-04	0.00311	0.00705	0.00834	0.01205	0.0223
0.01296	12.28047	8.71E-04	0.00372	0.01072	0.014	0.01834	0.03621
0.01	15.91549	8.99E-04	0.0039	0.01355	0.01598	0.0231	0.04539

Appendix D - ε″ vs. 1/ω of PP aged by 90°C

Table D. 1 ε'' vs. 1/ω of PP aged by 90°C at 10% voltage ratio

Frequency [Hz]	1/ω	ε''					
		Reference	DC	DC+1k	DC+1.5k	DC+2k	DC+2.5k
1.0316	0.15428	7.82E-04	0.00145	0.00175	0.00204	0.00228	0.00288
0.42985	0.370257	8.80E-04	0.00148	0.00177	0.00217	0.00213	0.00294
0.1791	0.888637	9.40E-04	0.00162	0.00191	0.00209	0.00222	0.00291
0.07463	2.132587	1.01E-03	0.00174	0.00197	0.00221	0.00242	0.00307
0.0311	5.117522	1.09E-03	0.00184	0.00219	0.00224	0.00261	0.0033
0.01296	12.28047	1.28E-03	0.00214	0.00266	0.00271	0.00301	0.00371
0.01	15.91549	1.32E-03	0.00227	0.00265	0.00314	0.00307	0.00376

Table D. 2 ε'' vs. 1/ω of PP aged by 90°C at 30% voltage ratio

Frequency [Hz]	1/ω	ε''					
		Reference	DC	DC+1k	DC+1.5k	DC+2k	DC+2.5k
1.0316	0.15428	7.82E-04	0.00145	0.00186	0.0022	0.00239	0.00264
0.42985	0.370257	8.80E-04	0.00148	0.00188	0.00217	0.0025	0.00267
0.1791	0.888637	9.40E-04	0.00162	0.0018	0.00223	0.00243	0.00263
0.07463	2.132587	1.01E-03	0.00174	0.00198	0.00231	0.00269	0.00267
0.0311	5.117522	1.09E-03	0.00184	0.00202	0.00233	0.00273	0.00287
0.01296	12.28047	1.28E-03	0.00214	0.00243	0.00283	0.00343	0.00351
0.01	15.91549	1.32E-03	0.00227	0.00286	0.0032	0.00357	0.00398

Table D. 3 ε'' vs. 1/ω of PP aged by 90°C at 50% voltage ratio

Frequency [Hz]	1/ω	ε''					
		Reference	DC	DC+1k	DC+1.5k	DC+2k	DC+2.5k
1.0316	0.15428	7.82E-04	0.00145	0.00374	0.0046	0.00527	0.00551
0.42985	0.370257	8.80E-04	0.00148	0.00387	0.0047	0.00547	0.00578
0.1791	0.888637	9.40E-04	0.00162	0.00386	0.00479	0.00576	0.00609
0.07463	2.132587	1.01E-03	0.00174	0.0048	0.006	0.00679	0.00745
0.0311	5.117522	1.09E-03	0.00184	0.00613	0.0079	0.00954	0.01145
0.01296	12.28047	1.28E-03	0.00214	0.0089	0.01153	0.01644	0.02142
0.01	15.91549	1.32E-03	0.00227	0.01107	0.01448	0.021	0.02773

Appendix E - ε″ vs. 1/ω of PP aged by 110°C

Table E. 1 ε'' vs. 1/ω of PP aged by 110°C at 10% voltage ratio

Frequency [Hz]	1/ω	ε''					
		Reference	DC	DC+1k	DC+1.5k	DC+2k	DC+2.5k
1.0316	0.15428	7.82E-04	0.00171	0.00295	0.00363	0.00399	0.00397
0.42985	0.370257	8.80E-04	0.00162	0.00291	0.00368	0.00403	0.00393
0.1791	0.888637	9.40E-04	0.00181	0.003	0.00357	0.00406	0.00412
0.07463	2.132587	1.01E-03	0.00164	0.00311	0.00361	0.00415	0.00435
0.0311	5.117522	1.09E-03	0.00218	0.00321	0.00403	0.00451	0.00455
0.01296	12.28047	1.28E-03	0.00271	0.00424	0.00531	0.00549	0.0056
0.01	15.91549	1.32E-03	0.00338	0.00436	0.00575	0.00644	0.00658

Table E. 2 ε'' vs. 1/ω of PP aged by 110°C at 30% voltage ratio

Frequency [Hz]	1/ω	ε''					
		Reference	DC	DC+1k	DC+1.5k	DC+2k	DC+2.5k
1.0316	0.15428	7.82E-04	0.00171	0.00278	0.00358	0.00419	0.00535
0.42985	0.370257	8.80E-04	0.00162	0.00273	0.00361	0.00433	0.00563
0.1791	0.888637	9.40E-04	0.00181	0.00281	0.00368	0.00449	0.00569
0.07463	2.132587	1.01E-03	0.00164	0.00286	0.00378	0.00446	0.00577
0.0311	5.117522	1.09E-03	0.00218	0.0032	0.00406	0.00501	0.00608
0.01296	12.28047	1.28E-03	0.00271	0.0043	0.00521	0.00662	0.0079
0.01	15.91549	1.32E-03	0.00338	0.00517	0.00609	0.00787	0.00841

Table E. 3 ε'' vs. 1/ω of PP aged by 110°C at 50% voltage ratio

Frequency [Hz]	1/ω	ε''					
		Reference	DC	DC+1k	DC+1.5k	DC+2k	DC+2.5k
1.0316	0.15428	7.82E-04	0.00171	0.00519	0.00823	0.01208	0.01521
0.42985	0.370257	8.80E-04	0.00162	0.00542	0.00859	0.01246	0.01642
0.1791	0.888637	9.40E-04	0.00181	0.00655	0.00933	0.01332	0.01834
0.07463	2.132587	1.01E-03	0.00164	0.00812	0.01035	0.01552	0.02201
0.0311	5.117522	1.09E-03	0.00218	0.0124	0.01584	0.02252	0.03438
0.01296	12.28047	1.28E-03	0.00271	0.02092	0.03051	0.04138	0.059
0.01	15.91549	1.32E-03	0.00338	0.02424	0.03799	0.05183	0.0743

Appendix F – PRPD Plot of PP Aged at 90°C

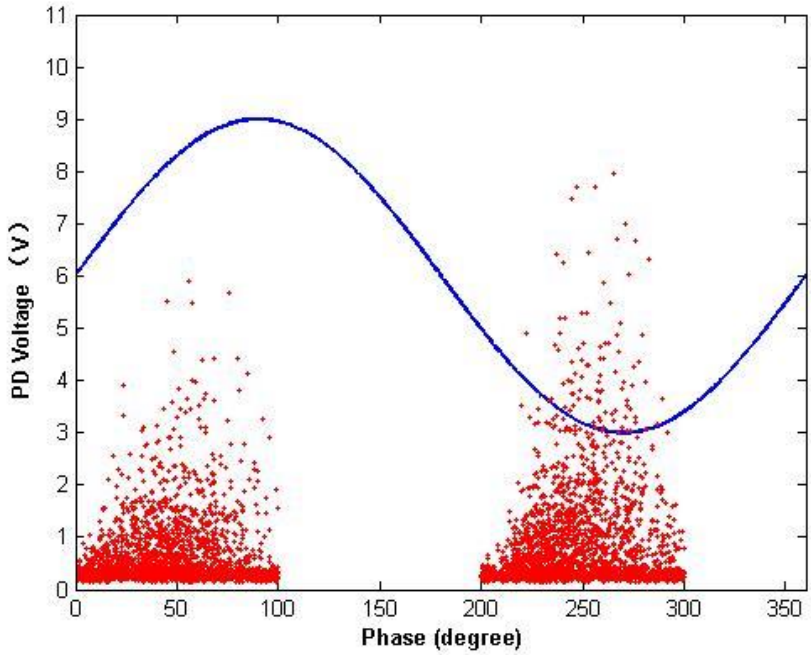

Figure F. 1 PRPD of PP aged at 90°C with 1 *kHz*, 50% voltage ratio

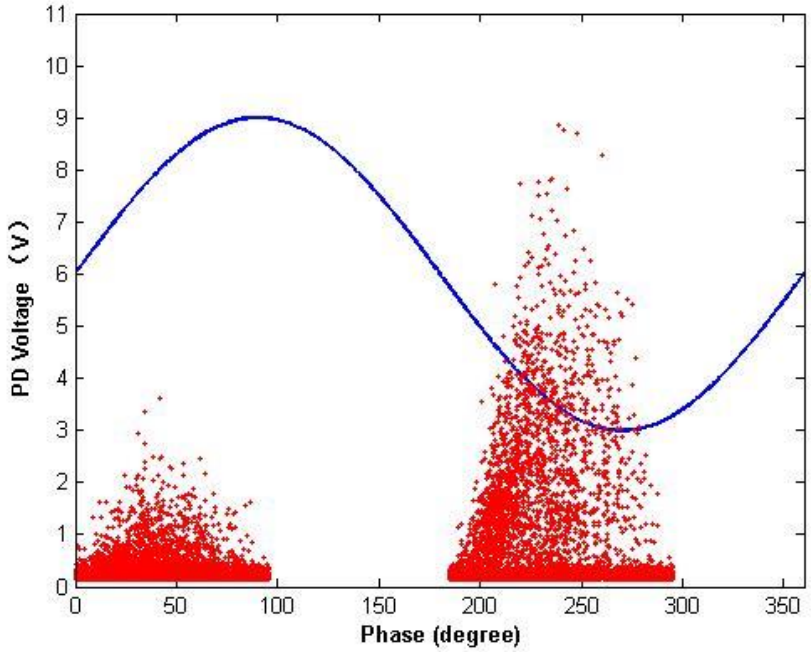

Figure F. 2 PRPD of PP aged at 90°C with 1.5 *kHz*, 50% voltage ratio

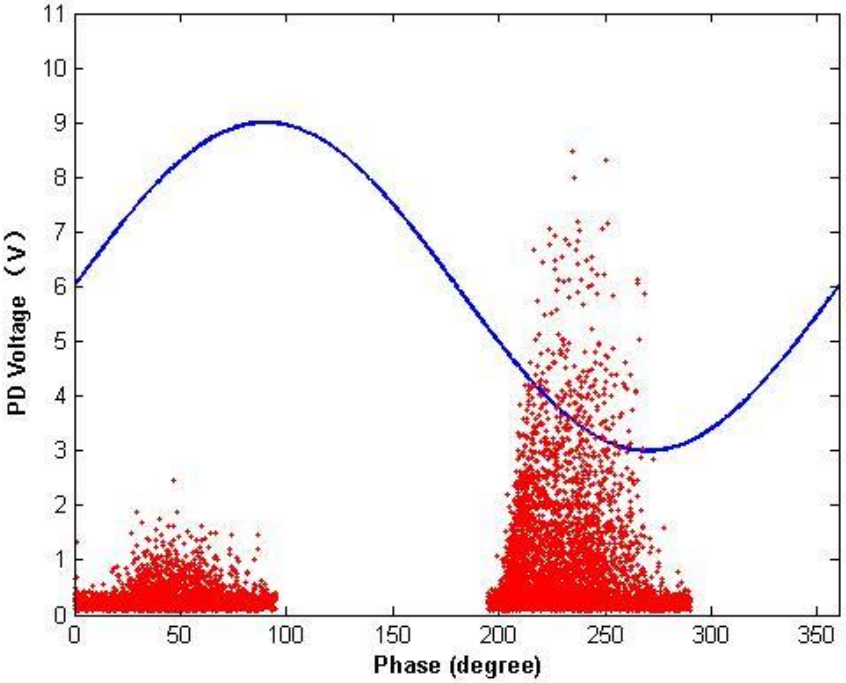

Figure F. 3 PRPD of PP aged at 90°C with 2 *kHz*, 50% voltage ratio

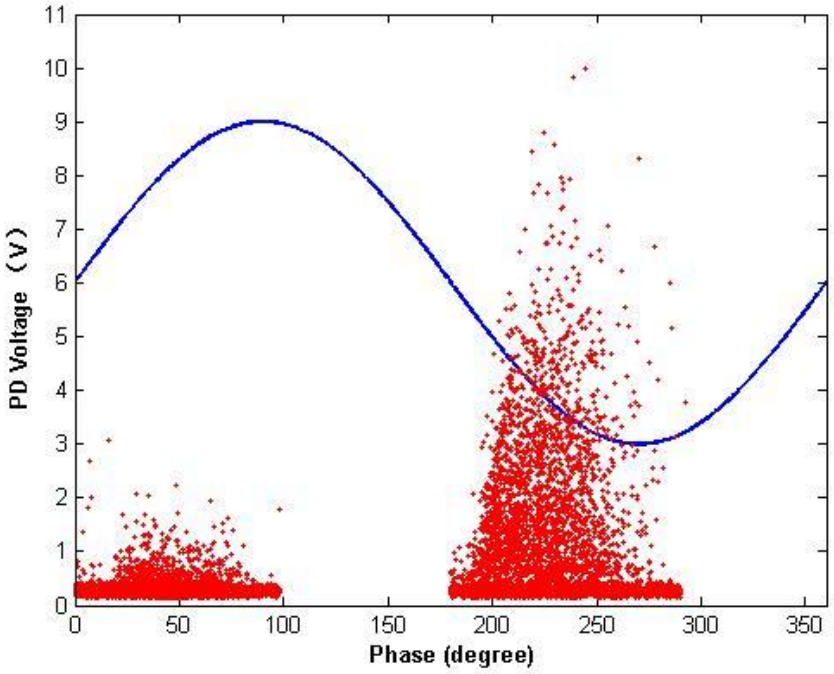

Figure F. 4 PRPD of PP aged at 90°C with 2.5 *kHz*, 50% voltage ratio

Appendix G – PRPD Plot of PP Aged at 110°C

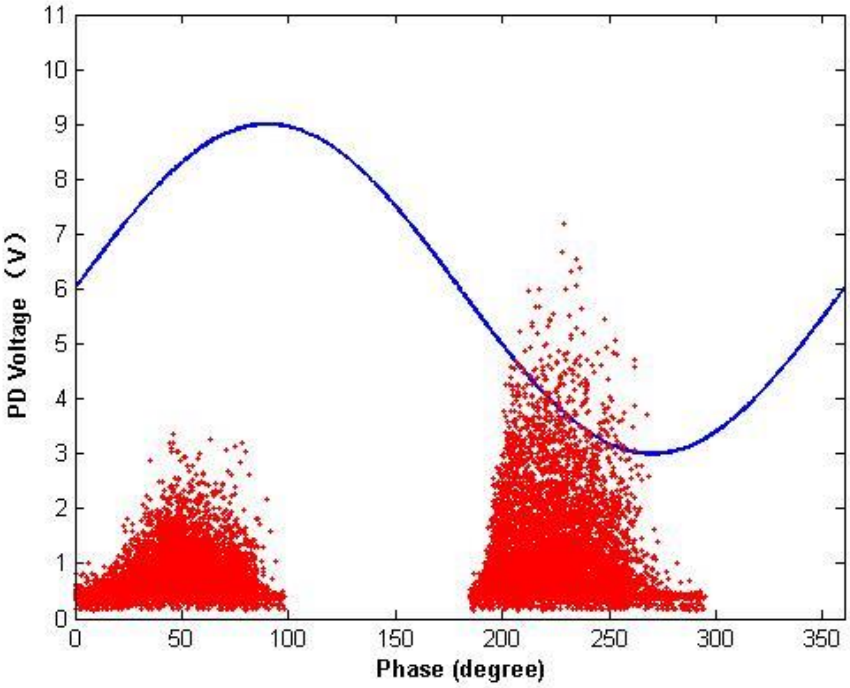

Figure G. 1 PRPD of PP aged at 110°C with 1 *kHz*, 50% voltage ratio

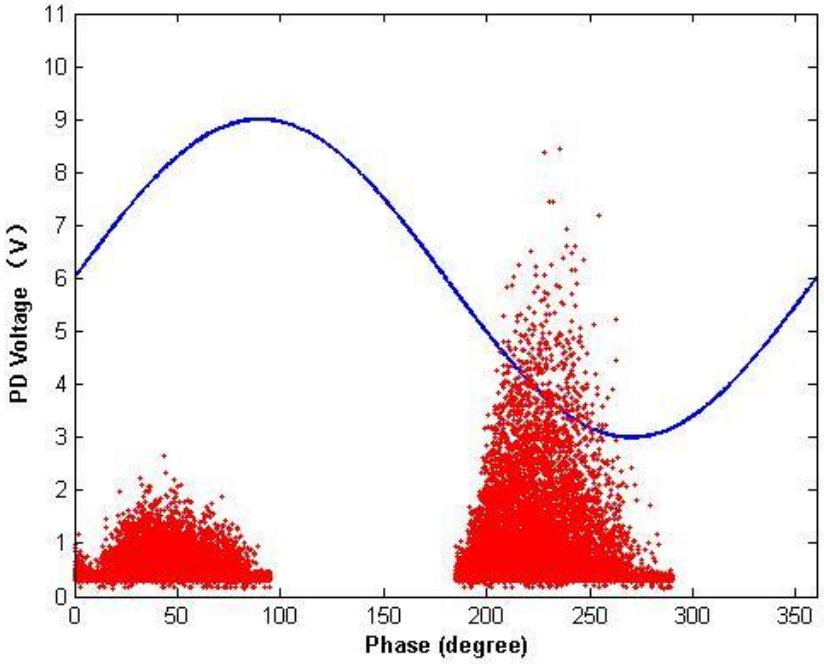

Figure G. 2 PRPD of PP aged at 110°C with 1.5 *kHz*, 50% voltage ratio

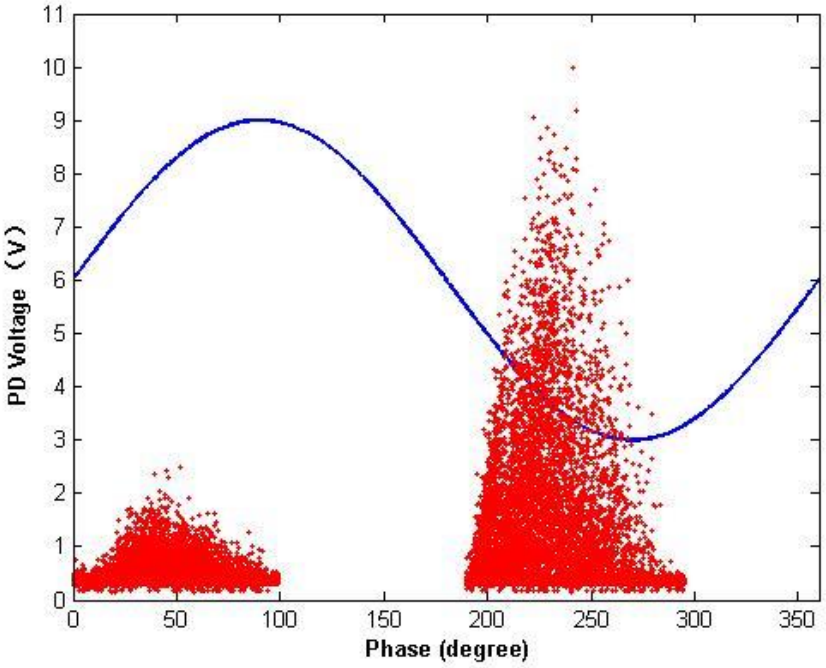

Figure G. 3 PRPD of PP aged at 110°C with 2 *kHz*, 50% voltage ratio

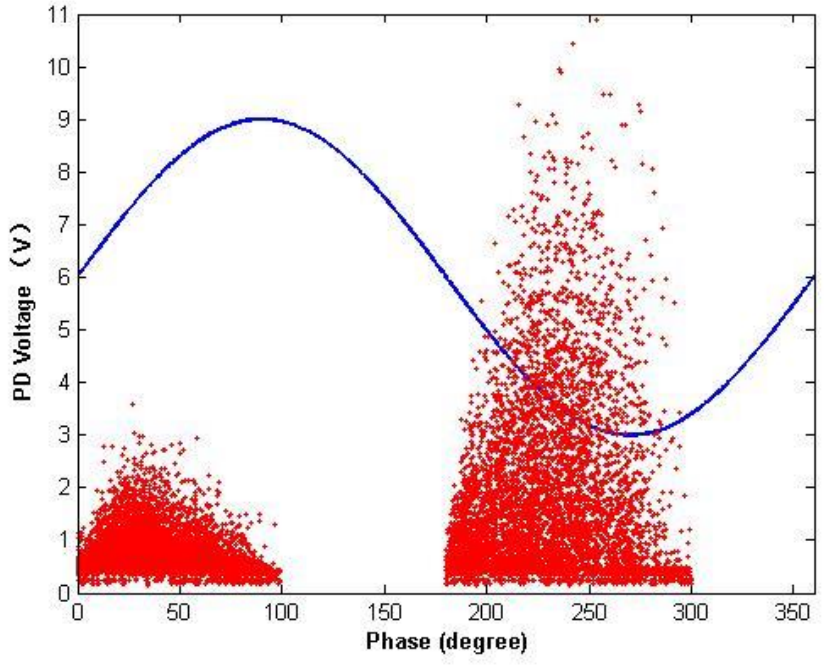

Figure G. 4 PRPD of PP aged at 110°C with 2.5 *kHz*, 50% voltage ratio